Fossil plants and environmental changes during the Permian-Triassic transition in Northwest China

Xiao Shi

Université Pierre et Marie Curie
China University of Geosciences Wuhan

Ecole doctorale GRNE

CR2P - CUG

Fossil plants and environmental changes during the Permian-Triassic transition in Northwest China

Par

SHI XIAO

Thèse de doctorat de Paléontologie

Dirigée par

Sylvie Crasquin, Jean Broutin, Tong Jinnan et Yu Jianxin

Présentée et soutenue publiquement le 9 décembre 2016

Devant un jury composé de :
François Baudin, PR UPMC, Paris, examinateur
Jean Broutin, PR émérite UPCM, Paris, directeur de thèse
Sylvie Crasquin, DR CNRS, Paris, directrice de thèse
Feng Quiglai, PR CUG, Wuhan, examinateur
Brigitte Meyer Berthaud, DR CNRS, Montpellier, examinatrice
Sun Chunlin, PR Jilin University, rapporteur
Wang Yongbiao, PR UCG, Wuhan, examinateur
Yu Jianxin, PR CUG, Wuhan, directrice de thèse

Acknowledgements

This dissertation is the result of a research initiated five years ago at the China University of Geosciences (CUG) and next continued by a PhD thesis co-supervised between Université Pierre et Marie Curie (UPMC) and CUG.

Firstly, in France, at UPMC, I would like to thank my PhD supervisors Prof. Jean Broutin and Prof. Sylvie Crasquin who offer me the opportunity to further study on my project with their scientific advice and experience. Prof. Jean Broutin spent a lot of time in helping me both in my life and my doctor project.

Also, I would like to thank Prof. Denise Pons who instructs me in fossil wood study. I gratefully acknowledge Prof. Sylvie Bourquin of Université Rennes 1 and Dr. Camille Rossignol of Université François Rabelais, Tours, who help me do field mission and instruct me in sedimentary studies. Especially, Dr. Rossignol, he helped me a lot in the sedimentary contents and gave me a lot of help when I studied in Rennes. I would like to thank Prof. Anaïs Boura for her help in identification of fossil woods. I am indebted to Colette Broutin, the wife of Prof. Jean Broutin for her kind care in France. I also thank all my colleagues in UPMC and Muséum national d'Histoire naturelle.

Secondly, in China, at CUG, I would like to thank my supervisors Prof. Tong Jinnan who give me the opportunity to finish my doctor thesis and Prof. Yu Jianxin who instructs me in both field mission and studies in lab. Prof. Yu instructs me in the study and daily life. She takes me as her child throughout the five years. She benefits me with her rich working experience and profound knowledge. I also want to thank to Prof. Huang Qisheng for his instruction in field mission and identification of fossil plants.

I am indebted to Prof. Zhang Wu and Prof. Shaolin Zheng of Shenyang Institute of Geology and Mineral Resources, Yang Xiaojun of Nanjing Institute of Geology and Palaeontology. In June 27th this year, Prof. Zhang Wu passed away. She teached all the basic knowledge of fossil woods and spent a lot of time to take care of me, when I studied in Shenyang Institute of Geology and Mineral Resources.

I thank all the members of the working team on terrestrial Permian-Triassic

boundary stratigraphy, CUG for their great help in field and lab work.

I would like to thank my parents for their unwavering emotional and financial support during all these uncertain years.

Finally, I am grateful to all of those not cited here but who helped me during this thesis on a friendly and/or scientific way.

Last, I acknowledge to China's Natural Science Fund (NO. 40972002, 41272024), China Geological Survey Grant (No. 1212011120142) and State Key Laboratory of Biogeology and Environmental Geology Grant (No. GBL11302).

Resume

Shi Xiao, male, was born in October 1987 in Xiongxian, Hebei Province, China. In September 2007, he entered China University of Geosciences, majoring in quaternary geology, was awarded Bachelor of Science in June 2011. In September 2011, he became a master-doctor student in the same university. In October 2013, he joined a co-supervised programme between China University of Geosciences and Université Pierre et Marie Curie, and became a doctor student in the "Centre de Recherche sur la Paléobiodiversité et les Paléoenvironnements", Université Pierre et Marie Curie. As a PhD student, he has accomplished 8 courses (5 for the degree and 3 selections) with an average score of 86.4.

Main publication during the master-doctor program:

Book Chapter

Shi, X.: Supplyment: New materials. An Introduction to the World's Petrified Wood, Edited by Zhang, W., Fu, X., Yi, T., Wang, S., Ding, Q., Tian, N., Yang, X., Jiang, Z., Shi, X., Cheng, Y., He, X., Zheng, S., Li, L., Wang, Y., Wang, J., Li, N., Yu, J., 04/2015: pages 615-661; Geological Publishing House, ISBN: 978-7-116-09125-2.

Journal Publications

Shi, X., Yu, J., Broutin, J., Pons, D., Camille R., Sylvie B., Li, Q., Shu, W.. Turpanopitys taoshuyuanensis gen. et sp. nov., a novel woody branch discovered in Early Triassic deposits of the Turpan Basin, Northwest China, and its palaeoecological implications. Palaeogeography, Palaeoclimatology, Palaeoecology (in review).

Shi, X., Yu, J., Broutin, J., Pons, D., 2015. *Junggaropitys,* a new gymnosperm stem from the Late Triassic of Junggar Basin, Northwest China, and its palaeoclimatic implications. Review of Palaeobotany and Palynology, 223: 10-20.

Yu, J., Broutin, J., Chen, Z. Q., **Shi, X.**, Li, H., Chu, D., Huang, Q., 2015. Vegetation changeover across the Permian–Triassic Boundary in Southwest China: Extinction, survival, recovery and palaeoclimate: A critical review. Earth-Science Reviews, 149: 203-224.

Shi, X., Zhang, W., Yu, J., Chu, D., Huang, C., 2014. The Flora from Karamay Formation in the South and North of Tianshan Mountain, Xinjiang. *Geological Science and Technology Information,* 33(1): 55-61 (In Chinese with English abstract).

Shi, X., Yu, J., Chen B., Huang, C., Li, H., Chi, H., 2014. Palynology of the Lower Permian Dazhuyuan and Liangshan Formations in Wuchuan-Zheng'an-Daozhen area, northern Guizhou Province. *Journal of Palaeogeography*, 16(2): 217-226 (In Chinese with English abstract).

Shi, X., Yu, J., Li, H., Chi, H., Zhang, W., 2014. *Xinjiangoxylon* Gen. Nov., a New Gymnosperm from the Latest Permian of China. *Acta Geologica Sinica (English Edition)*, *88*(5), 1356-1363.

Li, H., Yu, J., Huang, Q., **Shi, X.**, Huang, C., 2014, Geological significance of the lycopod megaspores from the early Triassic Kayitou Formation of the Western Guizhou and Eastern Yunnan Region. *Journal of Lanzhou University (Natural Sciences)*, 1(50), 1-10 (In Chinese with English abstract).

Conference Proceeding

Shi, X., Broutin, J., Yu, J., Crasquin, S.: Did conifers cover the Late Permian uplands of South China?. Agora Paleobotanica; 07/2016.

Résumé

La transition Permien – Trias est une période importante dans l'histoire de la Terre. L'extinction en masse de la fin du Permien est l'événement d'extinction le plus sévère de l'histoire de la vie sur Terre. Les études précédentes se sont principalement focalisées sur les événements biotiques en milieux océaniques. Récemment, de plus en plus de nouvelles recherches se sont développées sur les événements en milieu continental.

Les bassins de Junggar et de Turpan en Chine du Nord, présentent une opportunité unique d'étudier la limite Permien – Trias en milieu continental grâce à de nombreux affleurements avec des séries continues.

Les facies continentaux de la coupe de Dalongkou sur le flanc sud du bassin de Junggar et de la coupe de Taoshuyuan sur le flanc nord du basin de Turpan, ont été sélectionnés pour cette thèse. Les niveaux de l'intervalle de transition Permien – Trias correspondent aux formations "Wutonggou", "Guodikeng" et "Jiucaiyuan". D'abondants bois fossiles et empreintes de plantes ont été découverts dans ces coupes. Des logs sédimentaires détaillés ont été levés. L'approche utilisée ici est pluridisciplinaire pour reconstruire les Paléoenvironnements avec les bois fossiles et les plantes, les patrons des cernes croissance des bois et l'analyse des microfaciès sédimentaires.

Cinq genres et six espèces de bois fossiles ont été découverts. Nous établissons trois nouveaux genres: *Junggaropitys, Xinjiangoxylon* et un nouveau genre (soumis pour publication). La courbe CSDM (Cumulative Sum of the Deviation from Mean diameter) a été utilisée pour analyser les cernes de croissance dans le but de déterminer les conditions d'intersaisonnalité et la longévité des feuilles des arbres. Nous avons déterminé que *Junggaropitys dalongkouensis* est une espèce à feuilles persistantes avec les feuilles à longévité de 3 à 6 ans; le XTT-C-4 gen. et sp. nov. est également à feuilles persistantes mais avec une longévité des feuilles de 3 à 15 ans.

Septomedullopitys, Junggaropitys, Xinjiangoxylon et XTT-C-4 gen. nov. montrent tous un xylème secondaire de type *Protophyllocladoxylon.* En accord avec l'analyse paléobiogéographique, les bois de type *Protophyllocladoxylon* sont principalement

distribués dans une zone climatique tempérée froide dans l'hémisphère sud, dans des zones climatiques variables dans l'hémisphère nord et dans la zone équatoriale au Paléozoïque supérieur

Les résultats obtenus sur les bois fossiles montrent que le climat sur la région de Junggar devait être, à la limite Permien – Trias, chaud et humide, avec des températures et une humidité restant relativement stables.

Il n'existe pas de période de forte sécheresse au Trias basal. Les méga-moussons de la Paléo-Téthys n'ont pas d'influence sur la région de Junggar sur la côte est de la Pangée aux latitudes moyennes. Combiné avec les résultats précédemment obtenus, nous montrons que le climat n'a pas subit de très fortes variations entre le Permien moyen et le Trias basal.

L'analyse des plantes fossiles montre que le nombre de genres et d'espèces diminue progressivement de 26 genres et 53 espèces connues dans le Wuchiapingien à 10 genres et 15 espèces dans le Changhsingien et seulement 6 genres et 7 espèces dans l'Induen. La tendance à la réduction des assemblages floristiques dans les bassins de Junggar et Turpan semble montrer que le processus d'extinction est long et graduel et a débuté bien avant la limite Permien – Trias. Durant la période de récupération post-crise des flores, les lycopsides (*Annalepis*) et les fougères (*Neocalamites* et *Pecopteris*) ont joué un rôle d'espèces pionnières.

Trois logs stratigraphiques ont été levés pour l'analyse des facies sédimentaires. Quatre principaux environnements de dépôts ont été reconnus dans la coupe de Dalongkou. Les séries de la Formation Wutonggou se sont déposées dans un environnement de rivières en tresse et de systèmes fluviaux éphémères ou d'étangs et de plaines alluviales. Les facies associés à la partie inférieure de la formation Guodikeng se sont mis en place dans des environnements de rivières en tresse. La partie supérieure de la Formation Guodikeng correspond à une plaine alluviale et à, des environnements d'étangs ou lacs. La Formation Jiucaiyuan correspond, elle, à des environnements de rivière en tresse et de plaine alluviale.

L'analyse pétrographique des échantillons siliciclastiques montrent que les sources des particules détritiques restent constantes pendant la transition Permien – Trias. Les sources sédimentaires sont similaires pour les coupes de Dalongkou et de Taoshuyuan.

Ceci prouve que ces deux coupes correspondent à des dépôts d'un même bassin à cette période et que la surrection des Monts Bogda a été postérieure. Les sédiments carbonatés attestent d'un environnement lacustre.

L'extinction des plantes à la fin du Permien a induit une érosion plus forte des bordures de méandres et augmenté les apports détritiques sédimentaires en provenance des reliefs dans les chenaux fluviatiles. Cela a modifié les environnements de dépôts autour de la limite Wuchiapingien – Changshingien dans la région d'étude.

摘要

二叠-三叠纪之交是地球历史上的关键时期。发生在二叠纪末期的大灭绝事件是最严重的生物灭绝事件。前人对此次灭绝事件的研究主要集中于海洋生物的变化，近年来越来越多的研究开始关注于这一时期陆地生态系统的变化。

位于中国西北部的准噶尔盆地和吐鲁番盆地出露了完整的陆相二叠-三叠系界线附近地层，因此在这一研究方面具有独特的优势。前期研究中在这一个地区建立了良好的岩石地层，生物地层和旋回地层格架。本文将集中解决二叠-三叠纪之交研究区的环境变化问题。

我们选择了位于准噶尔盆地南缘的大龙口剖面和吐鲁番盆地北缘的桃树园剖面，两个陆相地层剖面作为论文的研究对象。在这一区域，二叠-三叠系之交地层是由梧桐沟组，锅底坑组和韭菜园组组成。我们在大龙口剖面和桃树园剖面二叠-三叠系地层中发现了大量木化石和植物印模化石，对剖面绘制了详细的地层柱状图。我们鉴定了木化石和植物印模化石种属,木化石年轮类型，分析了沉积相变化，进而用来识别研究区的环境变化。

我们对所采集到的130块木化石进行了切片，通过生物显微镜对其解剖结构进行研究，共发现了木化石5属6种，包括建立的三个新属：*Junggaropitys*，*Xinjiangoxylon* 和 XTT-C-4 gen. nov.（还在审稿中）。这三个属均具有内始式的初生木质部和 *Protophyllocladoxylon* 型次生木质部，其中*Junggaropitys*具有同质但异细胞的髓部；*Xinjiangoxylon*拥有具薄壁细胞和分泌管的髓部；XTT-C-4 gen. nov.的髓部中具有独特的板状支撑结构。

我们应用CSDM曲线（平均值偏差累计曲线）分析木化石的年轮用以识别其生长季的条件和叶的寿命。CSDM曲线分析表明*Junggaropitys dalongkouensis*为一种常绿植物，叶的寿命为3-6年；XTT-C-4 gen. et sp. nov.也为常绿植物，叶的寿命3-15年。

*Septomedullopitys, Junggaropitys, Xinjiangoxylon*和XTT-C-4 gen. nov.四个属的木化石均展示出*Protophyllocladoxylon*型次生木质部。我们对晚古生代全球发现的具有*Protophyllocladoxylon*型次生木质部的木化石进行了生物古地理分析，我们发现，在晚古生代，具有*Protophyllocladoxylon*型次生木质部植物，在南半球仅分布在冷温带地区；而在北半球和赤道地区，其分布在不同的气候带。

对木化石的分析显示准噶尔地块在二叠-三叠系界线附近古气候温暖湿润，温度和降雨量相对稳定；古特提斯洋巨季风没有影响到东岸的泛大陆中纬度地区。结合前人对这一地区其他木化石研究，我们认为研究区的古气候自中二叠世至早三叠世早期没有显著的变化。

植物化石分析显示，植物种属由吴家坪期的26属53种逐渐减少到长兴期的10属15种再到早三叠世印度期的6属7种。在准噶尔盆地和吐鲁番盆地，二叠-三叠系之交，植物显示了一个长时间的逐渐灭绝的过程。通过对比白垩纪-第三纪植物灭绝事件和现代恶劣环境下植物恢复的实例，我们发现石松类（脊囊属）和蕨类（新芦木属和栉羊齿属）在植物复苏阶段扮演着先驱分子的角色。

我们对大龙口剖面，桃树园A和C剖面进行了沉积相分析。在大龙口剖面我们识别出4个主要的沉积相。梧桐沟组上部主要由辫状河相，短暂的河流系统或湖和冲积平原相组成。锅底坑组为湖（或池塘）相和洪泛平原相沉积。韭菜园组主要由冲积平原和湖（或池塘）相沉积组成。在桃树园地区，梧桐沟组上部至锅底坑组底部的一套地层主要是湖（或池塘）相和洪泛平原相沉积。锅底坑组下部为一套辫状河沉积。而锅底坑组上部为冲积平原和湖（或池塘）相沉积。韭菜园组主要为辫状河和洪泛平原沉积。

对碎屑岩的样品岩相学分析显示跨越二叠-三叠系界线，沉积物物源一致。其中火山碎屑物来源于多个火山源。大龙口剖面和桃树园剖面在界线附近沉积物的物源保持一致，这说明，这两个剖面在二叠-三叠系之交时期处于同一个盆地，而博格达山隆起晚于这一时间。灰岩样品指示了湖泊环境的沉积。

二叠纪末期的植物灭绝降低了河岸的强度，增加了坡地的沉积物的提供，进而增加了河道中沉积物的卸载。这导致了研究区在吴家坪期和长兴期界线附近和早三叠世的两次沉积相的改变。

Abstract

Permian-Triassic transition is an important period in the Earth's history. The end-Permian mass extinction is the Earth's most severe known extinction event. Previous studies mainly focused on the biotic events in the ocean. Recently more and more researches on the terrestrial events during the Permian-Triassic transition attracted many attentions.

The Junggar and Turpan basins of Northwest China command a unique and significant position in the study of terrestrial Permian-Triassic boundary (PTB) events as it contains well and continuously exposed PTB sections. The lithostratigraphy, biostratigraphy, and cyclostratigraphy have been well established in the two basins. The problem we are trying to solve, based on paleobotanical studies associated with sedimentological analyses, is the environmental changes during the Permian-Triassic transition in the research area.

The terrestrial facies in the Dalongkou section on the south flank of Junggar Basin and the Taoshuyuan section on the north flank of Turpan Basin have been selected as the researching ones for this thesis. The Permian-Triassic transition strata have been included in the "Wutonggou", "Guodikeng" and "Jiucaiyuan" formations. Abundant fossil woods and plant impressions have been discovered and collected in these sections. Detailed sedimentary logs of the sections were drawn. The approach that we adopt to recognize the environmental changes is the fossil wood and plant impression species, growth-ring pattern, and sedimentary facies analysis.

Five genera and six species of fossil woods were discovered. We establish three new genera: *Junggaropitys, Xinjiangoxylon* and a new genus (submitted for publication). The CSDM (Cumulative Sum of the Deviation from Mean diameter) curve was used to analyse the growth rings to determine the intraseasonal conditions and leaf longevity patterns of the trees. We recognise that *Junggaropitys dalongkouensis* is evergreen, and the leaf longevity may be 3–6 years; XTT-C-4 gen. et sp. nov. is evergreen too, and the leaf longevity may be 3 to 15 years.

Septomedullopitys, Junggaropitys, Xinjiangoxylon and XTT-C-4 gen. nov. all show a *Protophyllocladoxylon*-type secondary xylem. According to palaeobiogeographic analysis, the *Protophyllocladoxylon*-type woods distributed mainly in the cool temperate climate zone of the southern hemisphere, various climate zones of the northern hemisphere and equatorial zone during the Late Paleozoic.

The results of fossil woods analysis obtained in this research shows the climate in the Junggar terrane around the PTB was warm and humid and the temperature and precipitation remained relatively stable. It did not exist a heavy dryness in the earliest Triassic. Meanwhile, the Palaeo-Tethys megamonsoons did not influence the Junggar terrane along the east coast of mid-latitude Pangaea. Combined with the previously reported fossil woods, it shows that the climate had no prominent change from the Middle Permian to earliest Triassic.

Plant fossil analysis show that the numbers of plant genera and species gradually decreased from 26 genera and 53 species in the Wuchiapingian, to 10 genera and 15 species in the Changhsingian, and only 6 genera and 7 species in the Induan. The trend in the plant assemblage reduction in the Junggar and Turpan basins appears to be indicative of a long, protracted extinction process that may have started well before the Permian-Triassic boundary. During the plant recovery period, the lycopsids (*Annalepis*) and ferns (*Neocalamites* and *Pecopteris*) played roles of pioneer species during the plant recovery period.

Stratigraphic logs were drawn to analyze the sedimentary facies. Four main depositional environments were recognised in the Dalongkou Section. The successions within Wutonggou Formation were deposited in braided river, and ephemeral fluvial systems or ponds and alluvial plain environments. Deposition of the Guodikeng Formation corresponds to lake or pond, and flood plain or temporary emersion. The facies associations of Jiucaiyuan Formation are interpreted to unconfined flow depositional setting and alluvial plain environment.

In the Taoshuyuan area, deposition of Wutonggou Formation and bottom of Guodikeng Formation corresponds to pond or lake, and flood plain environments. The successions of lower part of Guodikeng Formation were deposited in braided rivers

depositional setting. Deposition of the upper part of Guodikeng Formation corresponds to alluvial plain, and pond or lake environments. Deposition of Jiucaiyuan Formation corresponds to braided river and flood plain environments.

The petrographic analysis on detrital siliciclastic samples shows the sources of detrital particles remain the same in the research area across Permian-Triassic boundary. The volcaniclasts come from several distinct volcanic sources. The sedimentary sources are similar for the Dalongkou and the Taoshuyuan sections. It demonstrates that the present Dalongkou and Taoshuyuan sections belonged to the same basins at that period and the Bogda Mountains might uplift later. The limestone samples irecord a lacustrine environment.

The plant extinction at the end Permian decreased strength of channel banks and increased sediment delivery from hill slopes, and thereby would increase sediment loads in channels. It may result in the depositonal environmental changes around the Wuchiapingian -Changhsingian boundary and in the Early Triassic in the research area.

Contents

Preface

The Permian—Triassic transition is an important period for the Earth evolution from Palaeozoic to Mesozoic. A lot of work on the origin, scale, content and characteristics of this specific period has been done. Previously, major achievements have been made in the study of the changes of marine biome and geologic events (e. g. Xie et al., 2007; Payne and Clapham, 2012; Chen and Benton, 2012; Crasquin and Forel, 2014; Chen et al., 2014a, 2014b; Sun et al., 2012; Romano et al., 2012; Feng and Algeo, 2014). Recently, some achievements on the terrestrial events in South China have been made (e. g. Yu et al., 2007, 2008, 2015; Cui et al., 2015; Zhang et al., 2016; Bercovici et al., 2015, 2016). The previous studies on a Permian—Triassic boundary in terrestrial facies in South China have been concentrated on Western Guizhou—Eastern Yunnan, where the Permian-Triassic transition deposits are from marine to terrestrial. Detailed study was carried out on biostratigraphy, event-stratigraphy, sedimentation and climate changes in this area. In Northwest China, the Junggar and Turpan basins of Xinjiang Uygur Autonomous Region (Xinjiang) preserved Permian-Triassic terrestrial successions. The Dalongkou section in the Junggar Basin has even been suggested as a candidate for the global non-marine Permian–Triassic boundary reference section.

Five mass extinctions were recognized in the Phanerozoic in animal families (Jablonski, 1985), while only two major extinctions could be clearly recognized in plant families (Cascales-Miñana and Cleal, 2013). The mass extinction at the terminal Permian was the most severe biotic crisis among the “Big Five” mass extinctions (Raup and Sepkoski, 1982; Jablonski, 1991; Signor, 1994; Raup, 1994; Schubert and Bottjer, 1995; Benton and Twitchett, 2003; Bambach et al., 2004). The end-Permian mass extinction is the only one joining terrestrial plants massive extinction and a major extinction in the marine realms (Cascales-Miñana and Cleal, 2013). Many hypotheses have been proposed to account for the principle of this global change, such as volcanic events, celestial collision, anoxic deposition, environmental change, magnetic overturn and sea level changes. However, opinions vary about the origin for such “catastrophic” extinction. On such account, the research on the palaeontology and palaeoecology of this period is of great significance for the precise biologic and environmental changes across the Permian-Triassic boundary.

During the Permian to Triassic transition, the Junggar and Turpan basins in Northwest China were both located to the Northeast Kazakhstan plate. In this period, this area was in a terrestrial environment. The whole Permian-Triassic sections are well preserved with well-developed biomes, continuous strata and complete sequence, favourable for the study of the terrestrial stratigraphy and environmental changes. Hence, it can be an important area for an accurate location of the Permian-Triassic boundary in terrestrial facies and to elucidate the environmental changes during this period. Previous studies carried out were concentrated on the biostratigraphy, lithostratigraphy, biogeochemistry and palaeomagnetism in this area. For example, the Institute of Geology, Chinese Academy of Geological Science and Institute of Geology, Xinjiang Bureau of Geology and Mineral Resources investigated on the plant, spore and pollen, and

vertebrate fossils, summarizing the stratigraphy in the Dalongkou area. Cheng et al. (1993) investigate the vertebrate fossils in the Junggar and Turpan basins. Ouyang and Geoffrey (1999) researched on the earliest Triassic spores and pollen from Jiucaiyuan Formation in the Dalongkou section. Cao et al. (2008) studied on the biogeochemical disturbance indicated by the organic carbon isotopes. Metcalfe et al. (2009) studied on the stratigraphy, biostratigraphy and C-isotopes and wrote on the Permian—Triassic boundary in the Dalongkou section.

On the basis of the previous studies, this new approach covers many Permian—Triassic sections of terrestrial facies. It studies on the palaeontology, sedimentology and climatology in the area by the analysis of the wood and plant fossils collected from the outcrops and sedimentary environmental changes across the Permian—Triassic transition. It will expound the generic and specific biodiversity as well as the their implication for the palaeoecology and palaeoclimate in the Junggar and Turpan basins. This will be, on the one hand, to contributes to a better understanding of the plant palaeodiversity and, on the other hand, to enrich our knowledge on the landscape and environmental changes during Permian-Triassic transition. This may fill the blank of knowledge on the relationship between the fossil plants and sedimentary facies in this area. It is expected that this study will help the further probing of the woody plants composition and evolution, their relationship with various sedimentary facies and the environmental changes across the Permian-Triassic boundary.

This dissertation is based on the field observation and collecting of the practical sections followed by laboratory analysis, testing and processing of various samples replaced in a literature review as exhaustive as possible of related papers, published in China and other countries. The content and the innovations of this dissertation can be found as follows.

(1) Contents of the study

The focus of this dissertation is the study of the fossil woods and plants analysed in their sedimentological environments during the Permian-Triassic transition, based on abundant collected specimens and sedimentological investigation in the Xinjiang Uygur Autonomous Region (Xinjiang), Northwest China. It actually consists of the following aspects.

Field geological investigation We investigated more than 20 sections in South and North China, and selected three important terrestrial facies sections in the south and north Bogda Mountains. We observed the rock types in different areas, their structure, thickness change, spatial distribution and palaeogeographic location and collected more than 100 fossils and 32 petrographic samples.

Study of fossil woods It is necessary to work out the composition of the fossil woods and their palaeoclimatic and palaeoecologic implications. The plant compression and impression fossil assemblages in the Late Permian deposits were studied in the 1980s, but there was few analysis of any fossil woods and the palaeoclimatic information. Meanwhile, the number of the early Early Triassic plant fossils is very rare in the studied area. In recent years, with deep research, we found some new early Early Triassic plant compressions and impressions, and fossil woods. The anatomical structures of fossil woods indicate four new genera (two have been published and one has been submitted

for publication). The study of fossil woods provides evidence for the palaeoclimate during the Permian-Triassic transition in the Northwest China.

Study of sedimentary deposits. Three stratigraphic sections of a total thickness of ~570 m were measured at a centimetre scale. I analysed the sedimentological characteristics including analysis of texture, sedimentary structures, palaeosol development, palaeocurrent orientation, erosional surfaces and palaeontological contents. 32 petrographic thin sections have been made. Using these data, we analyse the sedimentary environmental changes during the Permian-Triassic transition.

(2) Innovations arising from this study

This dissertation intends to solve two problems: the floral evolution dynamics and the environmental changes in the Northwest China during Permian-Triassic transition.

The wood fossils found in the Wutonggou Formation, Guodikeng Formation and Karamay Formation reported for the first time, will fill up the blank of the fossil woods researches. Four new genera were discovered in this area. These fossils can provide more information to understand the composition of the Permian-Triassic flora and the climate changes in this period.

The field investigation on sedimentary contents and laboratory analysis on the stones allow us to recognize the sedimentary facies changes during the Permian-Triassic transitions. With the data of fossil woods and sedimentary contents, we will analyse the environmental changes in the Northwest China across the Permian-Triassic boundary. Encore des redites!

Table 0-1 lists the work done during the preparation of the dissertation.

Tab. 0-1 Main jobs completed for the dissertation

Sections	3	Petrological sthin sections	32
Fossil plant samples	130	Photos	2100
Fossil wood samples	130	Figures	70
Fossil wood thin sections	93	Tables	11
Petrological samples	32		

Chapter 1 Literature Review

Amongst the five mass extinctions recognized during the Phanerozoic in animal families (Jablonski, 1985), two major extinctions could be clearly recognized in plant families (Cascales-Miñana and Cleal, 2013). The end-Permian mass extinction is the largest mass extinction event in the earth history with the extinction of more than 90% of marine species, 70% of terrestrial vertebrates, and drastic restructuring of ecosystems (Erwin, 2006). This extinction is the only one joining a terrestrial plants massive extinction and a major extinction in the marine realms (Cascales-Miñana and Cleal, 2013).

The Global Stratotype Section and Point (GSSP) for the Permian–Triassic boundary (PTB) was defined at the Meishan section (Zhejiang province, west of Shanghai, Yin et al., 2001). After that, numerous studies have been conducted to characterize the biotic changes (Payne and Clapham, 2012; Chen and Benton, 2012; Crasquin and Forel, 2014; Chen et al., 2014a, 2014b) and environmental disturbances (Xie et al., 2007; Sun et al., 2012; Romano et al., 2012; Retallack, 2013; Cui et al., 2013; Benton and Newell, 2014; Cui and Kump, 2014; Feng and Algeo, 2014) associated with the end-Permian extinction event (Burgess et al., 2014) within marine successions.

However, the land life is more sensitive for the environmental changes. It arouses people's interests to research on the terrestrial environmental changes during the Permian-Triassic transition. The Permian-Triassic Beaufort Group of South Africa Karoo Basin yields abundant vertebrates. Thus, it is an important area for the study of terrestrial Permian-Triassic boundary and has been suggested to be a terrestrial accessory section and point for the PTB. Besides, the Permian-Triassic transition deposits were also persevered in Moscow Terrane of Russia, Ural areas of Kazakhstan, Sydney Basin and Bowen Basin of Australia, and Germany and its adjacent areas.

In China, the Junggar Basin and adjacent Turpan Basin in the north of Xinjiang Uygur Autonomous Region consist of a complete series of continental Permian-Triassic sequence with continuous depositions and fine outcrops and also contain abundant fossil fauna (e.g. ostracods, conchostracans, bivalves and vertebrates) and fossil plants across Permian-Triassic boundary. The section exposed on the south limb of Dalongkou anticline on the south flank of Junggar Basin has been suggested as a candidate for the global non-marine Permian–Triassic boundary reference section (Cheng and Lucas, 1993).

§ 1.1 Vegetational changes during the Permian-Triassic transition

During a quite long period, the evolution of floras through the Permian and Triassic was regarded as the replacement of so-called Palaeophytic floras, dominated by broad-leaved pteridosperms, cordaites, and pecopterid ferns, by Mesophytic floras largely dominated

by conifers (Knoll, 1984; Knoll and Niklas, 1987; Traverse, 1988). This transition began at the end of the Early Permian and essentially from the end of the Early Permian to the Middle Triassic. In this case, the end Permian mass extinction seems to have no significant effect on the plant evolution. It contradicts acid rain and massive erosion may have affected the land surface worldwide at the time of the PTB (Newell et al., 1999; Ward et al., 2000; Algeo and Twitchett, 2010).

DiMichele et al. (2008) recommend abandonment of the terms 'Palaeophytic' and 'Mesophytic' as they are misleading. They postulate that a complex of biome-scale species pools for the Permo-Triassic plants are necessary to reflect climate changes at many spatiotemporal scales. Therefore, they recommend that vegetational changes during the Late Palaeozoic and Early Mesozoic transition will be better understood in terms of responses of such species pools to global climate changes, at local and regional scales. That means it is necessary to conduct the study of palaeobotany and sedimentology at the scale of individual basins.

In the southern hemisphere, the PTB was marked by the extinction of glossopterid and cordaitalean gymnosperms, and by the appearance or decline of some gymnospermous and pteridophytic palynomorph groups. Peltasperms and lycophytes dominate the earliest Triassic floras (McLoughlin et al., 1997).

In the tropical area, numerous researches on the land plants have been conducted in the South China. In the western Guizhou and eastern Yunnan, 24% of megaplant species disappeared at the end-Wuchiapingian, and very few species survived into the Changhsingian mostly also decreased in abundance. At the end of the Changhsingian, about 80% of species vanished (Yu, 2008). The Permian Cathaysian *Gigantopteris* flora completely disappeared in the earliest Triassic and was replaced by the *Annalepis-Peltspermum* dominanted flora (Fig. 1-1). Microfossils show a similar pattern. From Wuchiapingian to Induan the palynomorphs decreased in abundance in a stepwise pattern and most extincted before the Induan (Yu, 2008).

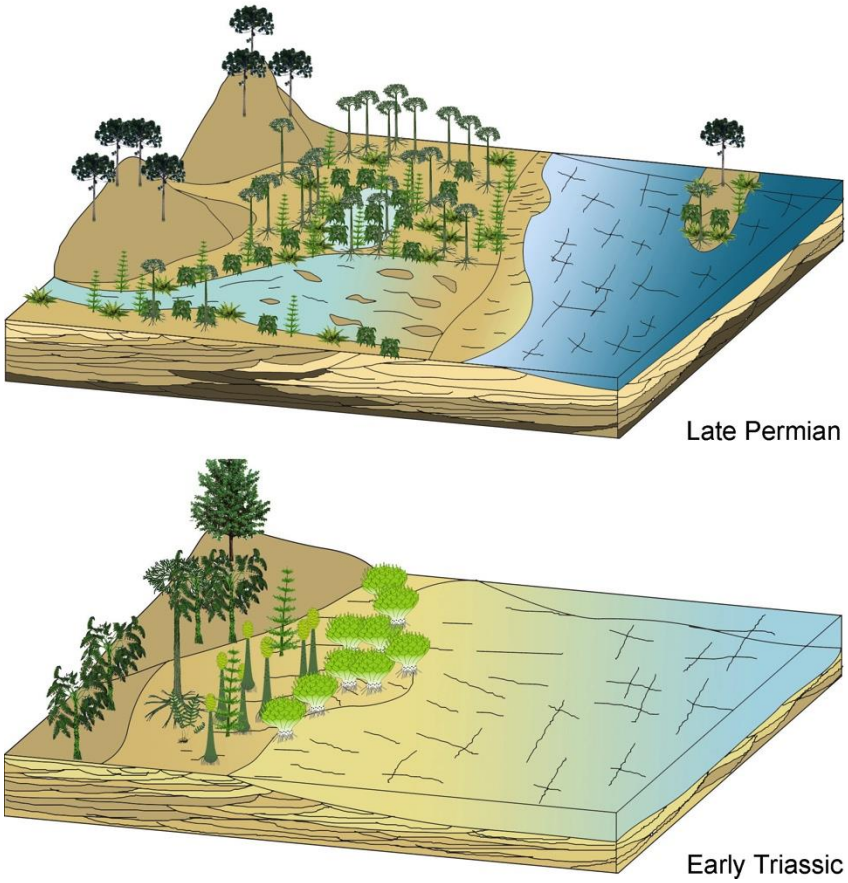

Figure 1-1 The landscape across the PTB in the South China. The Late Permian Cathaysian *Gigantopteris* flora was replaced by the *Annalepis-Peltspermum* dominanted flora in the early Triassic (according to Yu, 2008 and Bercovici et al., 2015).

In the northern hemisphere, lycopods and ferns replaced the gymnosperm-dominated Permian floras (Wang, 1991; Grauvogel-Stamm and Ash, 2005; Galfetti et al., 2007; Hermann et al., 2011). That resulted in the decreasing organic source in the terrestrial facies and is one of the main explanation of the Early Triassic coal gap. The changeover in floras is marked by the "spore spike" at or close to the PTB. That indicates the latest Permian gymnosperm-dominated ecosystems collapsed and the earliest Triassic lycopod-dominated ecosystems formed.

In a global study of fossil plant families, the end Permian mass extinction does stand out as a major extinction event for the plants. This event has the most severe effects on the seed-plant families, particularly conifers. Some small seedless lycopods and ferns survive to the present day (Cascales-Miñana and Cleal, 2012).

Earliest Triassic floras were dominated by the succulent low lycopod *Pleuromeia*. It is regarded as a classic disaster taxon and occupied the Eurasia and the southern continents after the extinction. Its spores (*Densoisporites*) dominated the palynological assemblages accounting for over 90% (Looy et al., 1999). The *Pleuromeia*-dominated terrestrial floras occupied the continents for 4-5 Myr. Until the earliest Middle Triassic, they were replaced by conifer *Voltzia* dominated associations (Looy et al., 1999; Hermann et al., 2011).

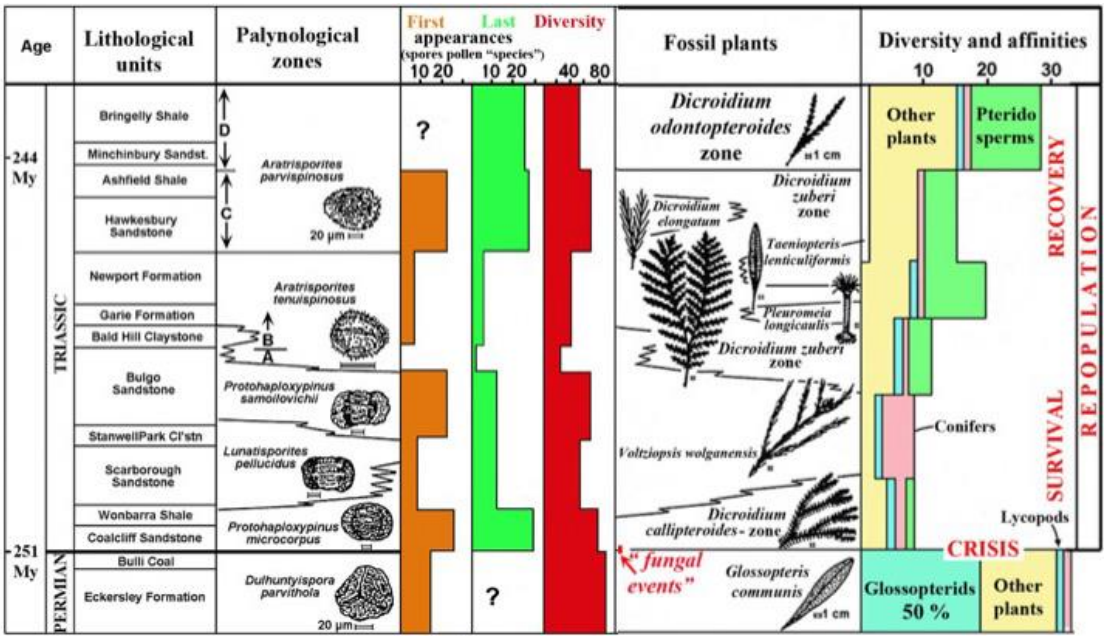

Figure 1-2 Changes in fossil floras across the Permian-Triassic boundary within the Sydney Basin, Australia, showing abrupt extinction of the peat-forming *Glossopteris* flora and replacement by a low-diversity conifer-lycopod flora that was later supplanted by adaptiveradiation of the Dicrodium flora. (After Retallack. Permian-Triassic life crisis on land. Science 267 : 77-80, 1995. Fig.1 p.78). Note the very long time necessary to reach again the same level of plant species diversity as just before the P-T extinction crisis. This duration for full recovery was similar in Gondwana as in Northern Pangea even if it was based on different floristic assemblages.

Another characteristic in the Early and early Middle Triassic is a worldwide coal gap. It is related to the decline of plant diversity through the end Permian mass extinction. Until the early Late Triassic, when the plant diversity bounded back to the pre-extinction levels (Retallack et al., 2011).

§ 1.2 Environmental changes during the Permian-Triassic transition: a review

Many extinction mechanisms for the life on land have been proposed. Evidence from stable isotopes, palaeosols, leaf stomata, and charcoal distribution indicate that the sharp increase in temperature and the reduction in the oxygen content of the atmosphere across the PTB have important roles in killing land animals and plants (Glasspool and Scott, 2010; Retallack, 2012). The interaction between life and the environment is the key to understand the end Permian mass extinction.

Wildfires events were found during the whole Permian and Permian-Triassic transition, (Veevers et al., 1994). Abundant charcoal, black carbon and carbon spherules related to the extensive wildfire have been described near the PTB from the Meishan section in south China (Shen et al., 2011). The extensive wildfires play a key role in the mass extinction of both plants and animals.

Vegetation cover has an important impact on the weathering rates of Earth surface. It not only increases the residence time of water in soil systems but also changes the concentrations of acid such as CO_2 and organic acids. Removal of land plants causes the increase in soil drainage and the flux of chemical weathering products (Goddéris et al., 2009).

Studies of strontium isotopes and biomarkers in the marine deposits indicate enhanced rates of chemical weathering during the PTB, possibly related to global warming and increased humidity (Martin and MacDougall, 1995; Algeo and Twitchett, 2010; Algeo et al., 2011). For terrestrial sedimentary basins, the palaeosols indicate the changes of weathering rates. In Antarctic, earliest Triassic palaeosols show increasing of barium relative to strontium. It may be a result of greater leaching relative to underlying coal-measure palaeosols of the latest Permian (Sheldon, 2006). In the Sydney Basin, the palaeosols show an increasing of chemical weathering (Retallack et al., 2011). An obvious "geochemical anomaly layer" exists near the PTB in South China. It was interpreted as an increase of weathering (Yu et al., 2007).

The land plants have an important effect on the erosion rates too. Smith (1995) and Ward et al. (2000) found that the rivers in the Karoo Basin, South Africa changed from the highly bended river to lowly bended river (anomaly layer) in the Late Permian to braided river deposition in the Early Triassic. They maintained that no tectonic orogeny has happened near the Permian-Triassic boundary. Thus, the change of river type should have been caused by the biologic extinction in the vegetal cover rather than the change of the slopes. They stated that the increase of the deposition load caused the bended river to change into braided river when the ground surface, especially the river bank, lost its protection from the plants because of the biologic extinction, in particular the death of plants of large rooting systems in big numbers.

Many fluvial sequences which cross the PTB, for example in the Australia, India, and the south Urals, show a marked increase in grain size across the boundary, often towards coarse pebbly material (Newell et al., 1999; Ward et al., 2000; Chakraborty and Sarkar, 2005).

In the Bowen Basin of Australia, the Late Permian deposits are characterized by large-scale, sandstone-dominated, low-sinuosity meandering river channel deposits. The overlying "Sagittarius Sandstone" unit were built up by broad shallow braided rivers (Michaelsen, 2002).

Comparable features have been observed in the rift basins of the Iberian Ranges (Arche and López-Gómez, 2005), the pull-apart Satpura Basin in India (Chakraborty and Sarkar, 2005), and the giant intracontinental Kuznetsk Basin of Siberia (Davies et al., 2010).

In the south Urals, the Late Permian metre-thick sandstone-dominated channel fills were replaced by the multi-storey gravelly, braided channels (Newell et al., 1999). In the Russian Platform, the PTB is marked by the abrupt progradation of sandy fluvial systems into former muddy lacustrine flood basins (Newell et al., 2010).

In the western Guizhou and eastern Yunnan, South China, three main formations are recognized through the terrestrial PTB successions: the Xuanwei, the Kayitou and the Dongchuan formations. The Xuanwei Formation rests unconformably on the Emeishan

basalts and is of latest Permian age (Wuchiapingian and Changhsingian) age (He, 2007).

The Xuanwei Formation consists mainly of terrigenous siliciclastic deposits with intercalations of organic-rich mudstones and coal seams. A vertical transition from alluvial plain facies to fluvial and lacustrine facies towards the top of the formation is evidenced. The Xuanwei Formation is conformably overlain by the Kayitou Formation, which is a 10–30 m massive and homogeneous silty sandstone succession. The rocks of the Kayitou Formation are finely variegated and grade from tan-green to yellow to purple-red towards the top. The monotonous succession of massive silty mudstone facies with intercalation of very fine planar lamination indicates deposition in calm, ever-flooded aqueous environments. The Kayitou Formation gradually changes to facies typical of the overlying Dongchuan Formation represented by a thick succession of purple-red terrigenous siliciclastic sandstones and mudstones. Deposits of Dongchuan Formation show a progressive change in depositional environment to braided rivers within semi-arid alluvial floodplains (Bercovici et al., 2015).

In North China, comparable features can be observed. The upper member of the Sunjiagou Formation represents lake successions. They were overrun by Early Triassic sandy braided river deposits of the Liujiagou Formation.

Lacustrine environments remaining across the PTB are few. The North German Basin is one of the rare locations where lacustrine environments persist across the PTB. Hiete et al (2006) documented that the boundary succession changed from sabkha to playa lacustrine facies around the PTB.

Chapter 2 Stratigraphy of non-marine Permian-Triassic in the Junggar and Turpan basins

§2.1 Junggar and Turpan basins

The Xinjiang Uygur Autonomous Region is the largest Chinese administrative division, spanning over 1.6 million km2. It borders the countries of Mongolia, Russia, Kazakhstan, Kyrgyzstan, Tajikistan, Afghanistan, Pakistan and India. The massive Karakorum, Kunlun, Altai and Tian Shan mountains ranges occupy much of the Xinjiang's periphery. It also borders the Tibet Autonomous Region and the provinces of Gansu and Qinghai (Fig. 2—1). In recent decades, abundant oil and mineral reserves have been found in Xinjiang, oil and petrochemicals now accounting for about 60 per cent of the gross domestic product (GDP). The capital of Xinjiang Uygur Autonomous Region is Urumqi.

Figure 2-1 Location of the Junggar and Turpan basins in the Xinjiang Uygur Autonomous Region (Modified after http://www.chinamaps.org/china/provincemaps/xinjiang.html)

§2.2 Locations of Dalongkou anticline

The Junggar Basin (Fig.2—1) is one of the three largest sedimentary basins in the Xinjiang Uygur Autonomous Region of Northwest China. It is bounded by the Tianshan Mountains range to the south and the Altai Mountains to the North. It covers an area of ca. 380, 000 km^2.

Dalongkou anticline is located on the southern flank of the Junggar Basin in the foothills of the Bogda Mountain, about 20 kilometres southwest of Jimsar County (Fig. 2-2; 2-3). As globally important non-marine P-T transitional sequences, the section exposed on the south limb of Dalongkou anticline has been suggested as a candidate for the global non-marine Permian-Triassic boundary reference section (Cheng and Lucas, 1993). In the dissertation, we mainly research on the north limb of Dalongkou anticline.

§2.3 Location of Taoshuyuan syncline

The Turpan basin covers about 53, 500 km^2, and was regarded as the third lowest exposed terrestrial point on the earth's surface. The present boundaries of the basin are the Bogda Mountains and Haerlike Mountains to the north, and Juluotage Mountains to the south. It is known as the hottest and driest area in China.

The Taoshuyuan syncline is located about 12 kilometres northeast of Daheyan town (Fig. 2-2; 2-4). It is on the northern flank of the Turpan basin in the foothills of the Bogda Mountain. We investigated three sections, respectively Taoshuyuan A, B, C sections, in this area.

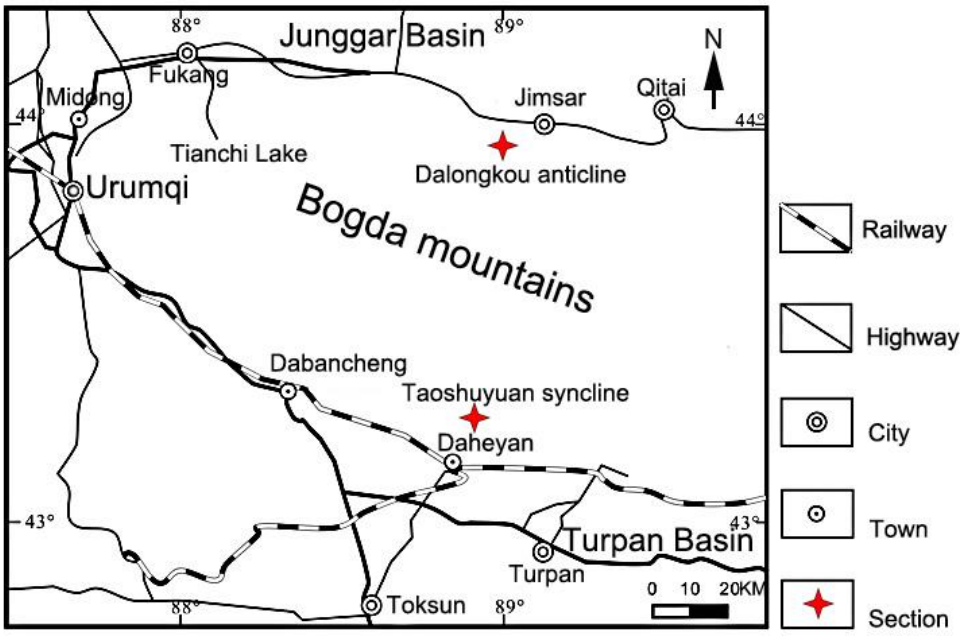

Figure 2-2 Precise location of the Dalongkou anticline (Junggar Basin) and Taoshuyuan syncline (Turpan Basin)

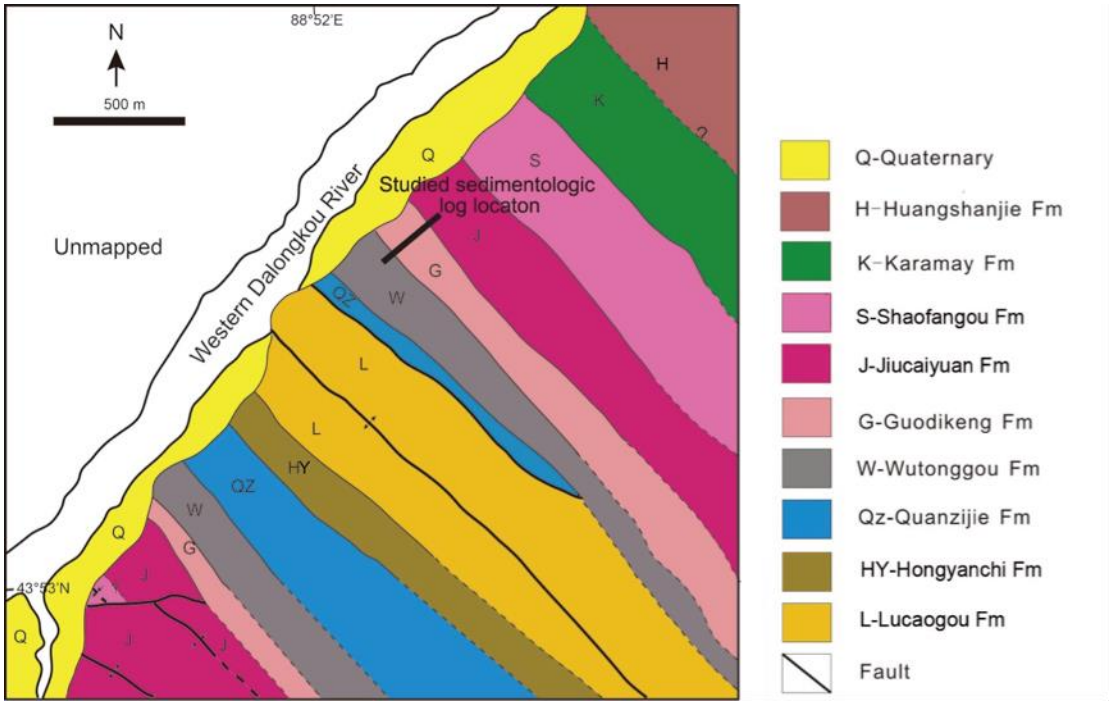

Fig 2-3 Geological map of the Dalongkou anticline

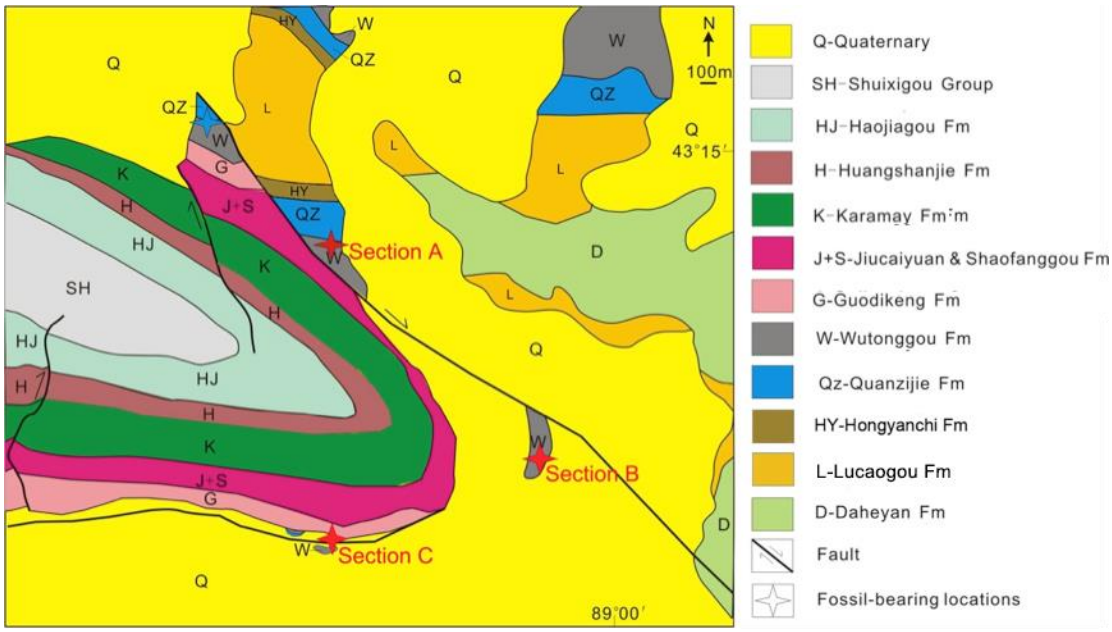

Fig 2-4 Geological map of the Taoshuyuan syncline

§2.4 Geological background

The present Junggar and Turpan basins are composed of three parts: Junggar terrane, West Junggar and East Junggar. Junggar and Turpan basins are located on the Junggar terrane. Junggar terrane consists of Late Proterozoic metamorphic basement rocks unconformably overlain by Early Palaeozoic marine sediments with Sinian tillites. It was previously considered to be integrated and connected with the Tarim craton, but the recent palaeomagnetic, geological, and geochemical data indicate that they were

independent with oceans between them in the Palaeozoic (Choulet et al. 2012, Xiao et al. 2008, Yang et al. 2012). The terranes of the Altai and Junggar regions were fully amalgamated into an orogen by the end of Early Carboniferous to the Middle—Late Carboniferous. Since then, Junggar regions became a part of the Siberia Craton. Junggar terrane and West Junggar were amalgamated during Late Carboniferous to Late Permian times and accompanied by closure of the Balkhash-Junggar Ocean. The Junggar regions uplifted and became an intra-continental basin in the latest Carboniferous (Yang et al., 2010, Fig. 2-7).

The Bogda Mountains are the northern branch of Tianshan Range. The giant anticline contains Devonian to Quaternary sedimentary and igneous rocks. Prior to the Triassic period, the Junggar Basin and Turpan Basin were connected. Since the Early Mesozoic, the Bogda Mountains were uplifted and separated the Junggar Basin to the north-northwest and Turpan-Hami basin to the south. Permian-Triassic fluvial and lacustrine deposits are exposed along the foothills of the Bogda Mountains. They were deposited in the greater Turpan-Junggar rift basin on the Late Carboniferous marine limestone and clastic stones.

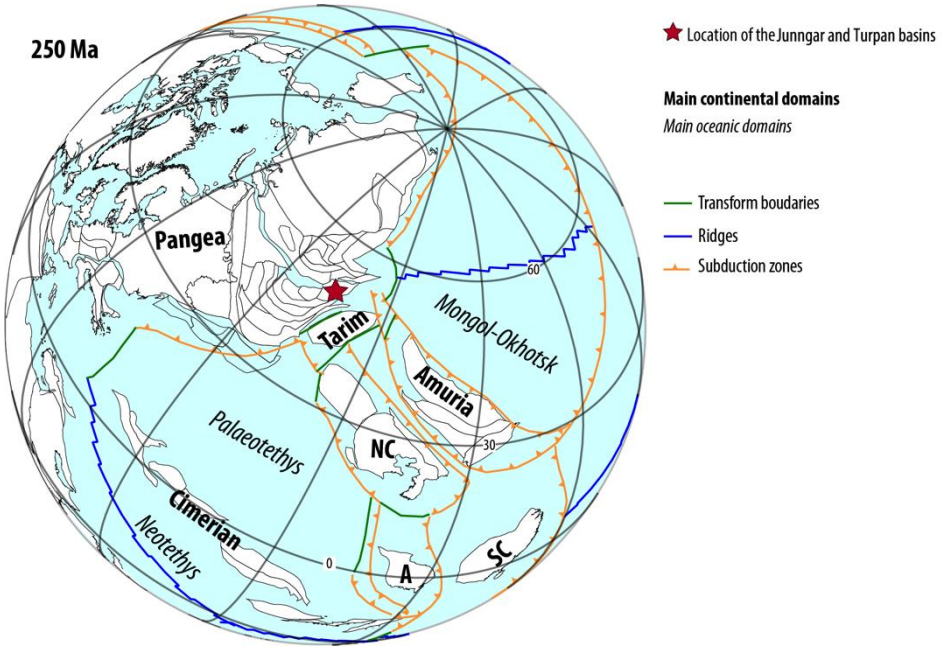

Figure 2-5 Simplified palaeogeographic reconstruction showing the location of the Junggar and Turpan basins at 250 Ma.

A: Anamia; NC: North China; SC: South China. Modified after Domeier and Torsvick, 2014. Reconstruction generated using GPlates software (http://gplates.org).

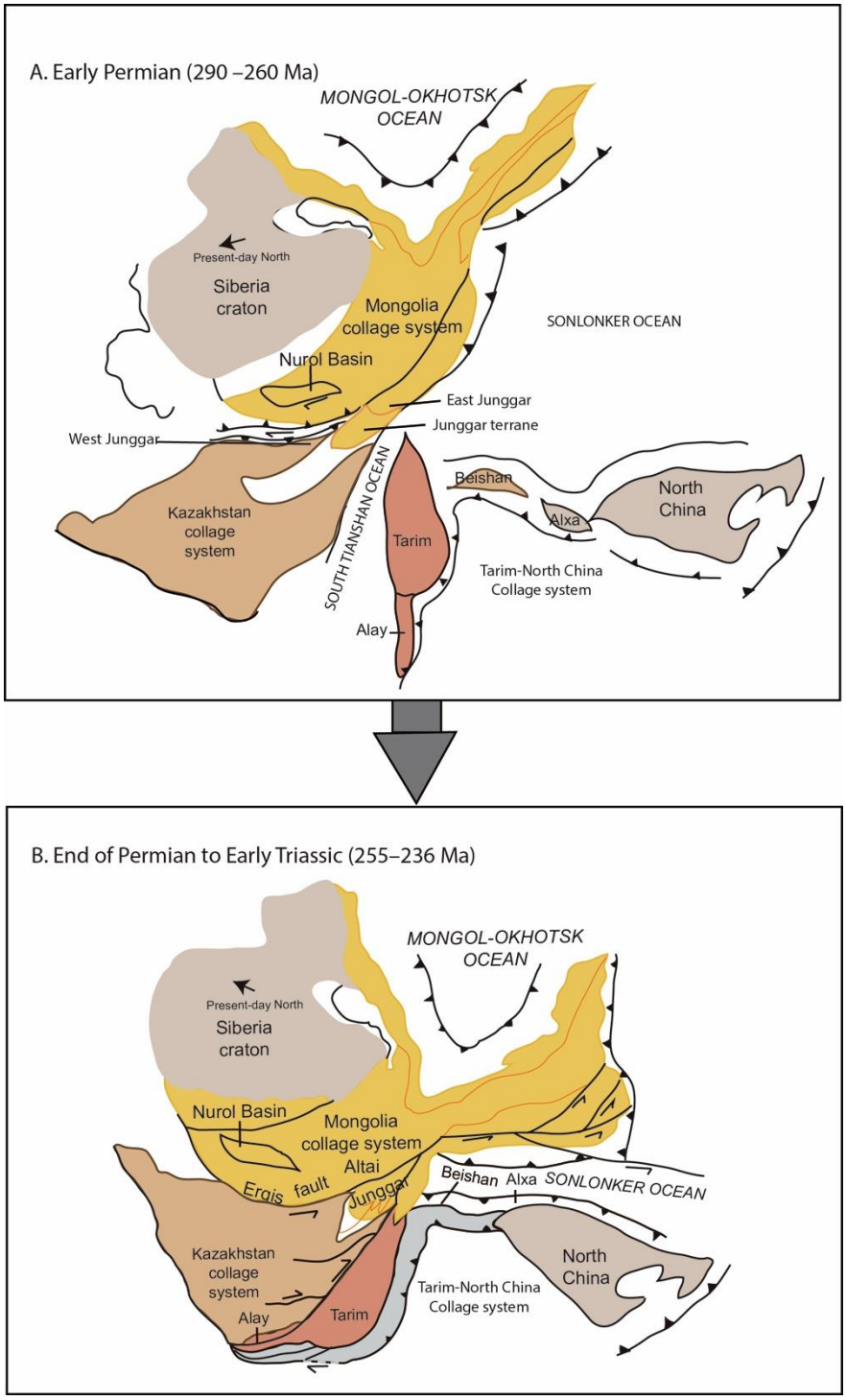

Fig.2.6 Palaeogeographic reconstructions showing simplified plate boundaries and labels of some major features of the Central Asian Orogenic Belt. Modifid after Xiao et al., 2015. (A) Early Permian (290–260 Ma) and (B) End-Permian to Early Triassic (255–246 Ma)

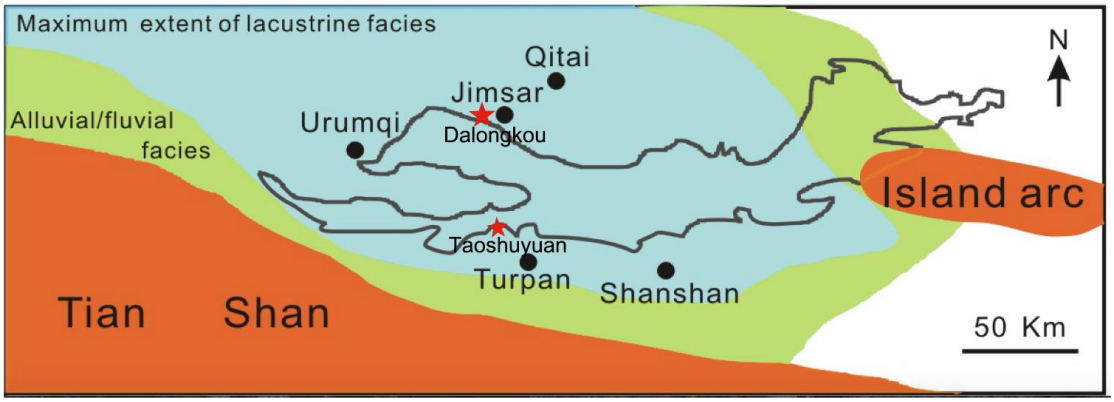

Figure 2-7 Palaeogeographic map in the Late Permian Xinjiang (According to Greene et al., 2001, 2005)

§2.5 Lithostratigraphic units across Permian—Triassic boundary in the research area

The lithostratigraphy across the terrestrial Permian—Triassic boundary used in this dissertation, include Late Permian Wutonggou Formation, Late Permian-Early Triassic Guodikeng Formation, Early Triassic Jiucaiyuan and Shaofanggou Formation and Middle-Late Triassic Karamay Formation (Table 2-1). The detailed characteristics of the formations will be discussed in Chapter 4.

Table 2-1 Lithostratigraphy of Permian–Triassic strata in the Junggar and Turpan basins

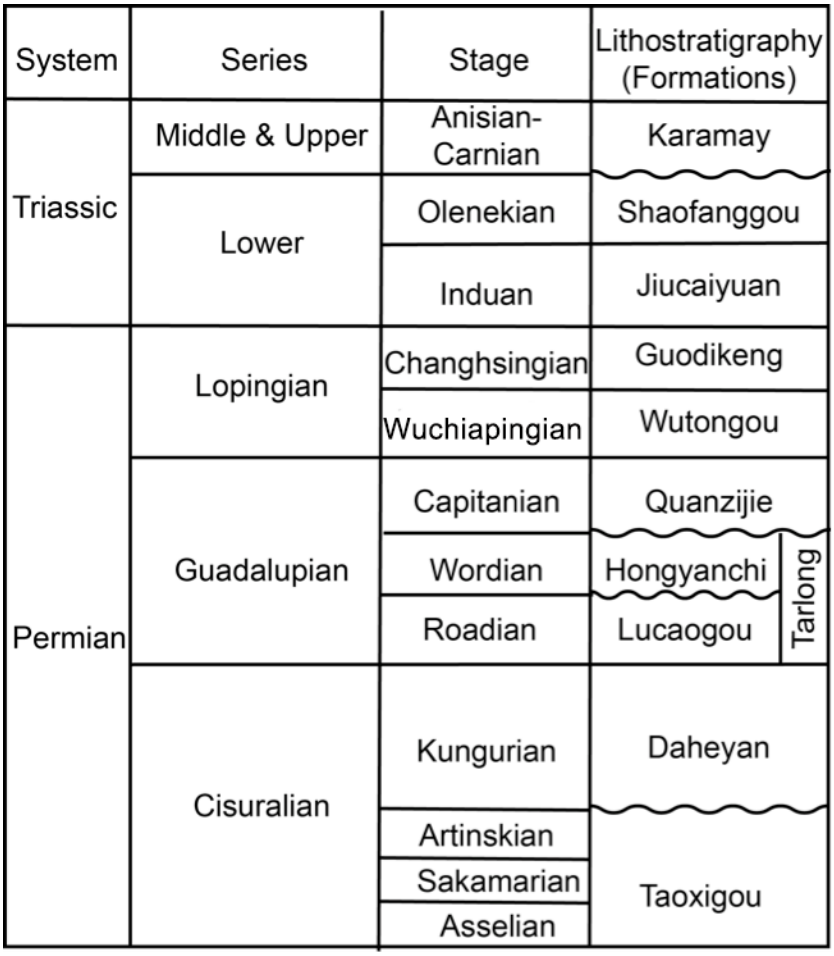

§2.6 The Permian—Triassic boundary in Xinjiang

2.6.1 The Permian-Triassic boundary at Dalongkou Section

The previous biostratigraphic investigations on the Permian—Triassic Boundary (PTB) were concentrated on the south limb of Dalongkou anticline. Based on the vertebrate, spores and pollen, and ostracod fossils, the Permian–Triassic Boundary Stratigraphic Set was assigned to a ~31 m interval of Guodikeng Formation (Cheng et al., 1997; Zhou et al., 1997; Foster and Afonin, 2005; Pang and Jin, 2004; Hou, 2004). The $\delta^{13}C_{org}$ data indicate the PTB locate at 53 m below the basal coarse sandstone in the overlying Triassic Jiucaiyuan Formation (Cao et al., 2008).

Our research team worked on the biostratigraphy of the north limb of Dalongkou anticline. Palynomorphs gathered from the upper Guodikeng Formation of the Dalongkou section, which is the most likely interval to plot the P-T boundary according to previous studies. Four palynofloral assemblages were defined, based on 61 statistically significant

samples picked out from 99 continuously collected samples. In stratigraphic order, oldest to youngest, they are:

Assemblage 1: *Limatulasporites-Alisporites-Lueckisporites* (nine samples: 31 to 39, 133-136.5 m in Fig. 4-1). The amount of gymnosperm pollen grains is much more than that of pteridophyte spores. The three eponymous taxa, as well as *laevigate azonotriletes*, are generally common. *Lundbladispora willmotii*, the widely used marker for the Early Triassic, was found in two samples, pointing to the transitional nature of the palynofloras.

Assemblage 2: *Leiotriletes-Limatulasporites-Alisporites* (ten samples: 40 to 49, 136.5-142.2 m in Fig. 4-1). Pteridophyte spores, dominated by a significant increase of laevigate and apiculate azonotriletes, exceed gymnosperm pollen grains in quantity. The latter are mainly non-taeniate bisaccate pollen grains. Another obvious change compared with the older assemblage is the decrease of *Limatulasporites* and the absence of *Lundbladispora*. In addition, the species diversity of this assemblage distinctly dropped by nearly fifty percent.

Assemblage 3: *Limatulasporites-Lundbladispora-Sulcatisporites* (twelve samples: 50 to 63, 142.2-150 m in Fig. 4-1). Similarly to assemblage 1, *Limatulasporites* returned to the leading position among pteridophyte spores. While, laevigate and apiculate azonotriletes went back to secondary place after their remarkable rise. Moreover, several species of *Lundbladispora* occurred more frequently and evenly in a sudden. As to gymnosperm pollen grains, the number dominating again over pteridophyte spores, non-taeniate bisaccate pollen grains being still the majority. Taeniate bisaccate pollen grains are more abundant than in assemblage 2, but didn't reach the richness of assemblage 1.

Assemblage 4: *Punctatisporites- Limatulasporites-Alisporites* (thirty samples: 64 to 132, 150-179.8 m in Fig. 4-1). The abundance of pteridophyte spores in this assemblage reached an unprecedented high domination among all assemblages, far more than that of gymnosperm pollen. *Limatulasporites*, *Kraeuselisporites*, *Lundbladispora* and some taxa of Laevigate and apiculate azonotriletes are all common components. Non-taeniate bisaccate pollen grains maintained a dominant position among gymnosperm pollen grains, although their percentage reduced to the lowest level. The proportion of taeniate bisaccate pollen grains is as low as that of assemblage 2.

According to relevant researches worldwide, the characteristics of plant microfossil assemblages of Late Permian and Early Triassic are more and more clear, some of which have become reasonable basis when discussing the position of P-T boundary. The upper Permian strata is characterized by abundant taeniate bisaccate pollen grains and large increasing of *Limatulasporites* and *Alisporites*, while the first Triassic strata are distinguished by the ascending ratio of pteridophyte spores relatively to gymnosperm pollen grains, correlated with a decline of taeniate bisaccate pollen grains (particularly of the genus *Lueckisporites*) and the sudden appearance of *Aratrisporites* associated with *Lundbladispora*.

In this study, the ratio of pteridophyte spores to gymnosperm pollens shows global increaseing tendency in spite of the slight fluctuation in assemblage 3. The changes of the typical genera also conform to the above characteristics. Therefore, we place the P-T boundary in the Dalongkou section below sample 50, between assemblage 2 and 3, where *Lundbladispora* and *Kraeuselisporites* increased abruptly. Besides, we found the fossil

plants *Annalepis* sp. at the 143 m of the log. *Annalepis* is widely distributed in the Early Triassic strata. With those data, we assign a ~0.33 m (142.27-142.6 m in the log) interval to the PTBST (Fig. 4-1).

2.6.2 The Permian-Triassic boundary at Taoshuyuan Section

Some works on the PTB have been done in the north limb of the Taoshuyuan syncline (Taoshuyuan A Section). Based on the bivalves and plant fossils, a Late Permian age was assigned to the Wutonggou Formation (Sun, 1989; Fu and Deng, 1997). The fossil plants found in the upper part of Guodikeng Formation show similarities to Late Permian (Sun, 1989). The bed with those fossil plants equal to 71.5 m in our log (Fig. 4-6). The spores and pollen assemblages indicate that the age of the upper part (roughly equal to 126-140 m in our log, Fig. 4-6) of the Guodikeng Formation is Early Triassic (Liu, 2010). The palaeomagnetism data suggest that the PTB is located 41 m above the base of the Guodikeng Formation (roughly equal to 74 m in our log, Fig. 4-6; Li et al., 2004). Based on the $\delta^{13}C_{org}$ data, the PTB could be placed 77 m above the base of the Guodikeng Formation (roughly equal to 79 m in our log, Fig. 4-6; Cao et al., 2008). As mentioned above, we assigned the 74 m to 77 m in our log of Taoshuyuan A Section to the Permian–Triassic Boundary Stratigraphic Set (PTBSS, Fig. 4-6).

The accurate Permian-Triassic boundary (PTB) at Taoshuyuan C Section has not been precisely located yet. The first occurrence of the Early Triassic vertebrate *Lystrosaurus* has been suggested as a major marker of the terrestrial basalmost Early Triassic (e.g., Lucas, 1998; Lucas, 2009). The vertebrate *Lystrosaurus* first occurred in the upper part of Guodikeng Formation, at 110.5 m of our log (Fig. 4-7).

Chapter 3 Fossil woods

§3.1 Materials and methods of study

One hundred and thirty permineralized wood samples were collected from the Wutonggou, Guodikeng and Karamay formations of Junggar and Turpan basins, Xinjiang, northwestern China. Fossil woods are classified into the manoxylic and the pycnoxylic. Manoxylic wood is the non-compact wood with large amount of parenchyma, large pith and cortex mixed with fewer amounts of xylem tracheids. Two specimens belong to manoxylic woods. Pycnoxylic wood is the compact strong wood with large amount of xylem tracheids and small amount of cortex and pith with fewer parenchymas. Most of our samples are pycnoxylic woods.

3.1.1 Methods for systematic palaeobotany

Microscopic thin sections of the transverse, radial and tangential wood sections were made following the traditional techniques for permineralized woods (Fig. 3—1; 3—2): First, the samples were cut into appropriate sizes using a diamond saw and the top surface polished using a grinding wheel with carborundum grades of #240, #800 and #1200 in turn. The smooth top surface was then glued onto a glass slide with epoxy resin and the bottom surface ground down to a thickness of about 30 μm. The thin section was covered with abienic balsam. With those slides, we can analyse the characteristics of the fossil woods. To identify these homoxylic woods, the anatomical features are important (Fig. 3—3), as follows:

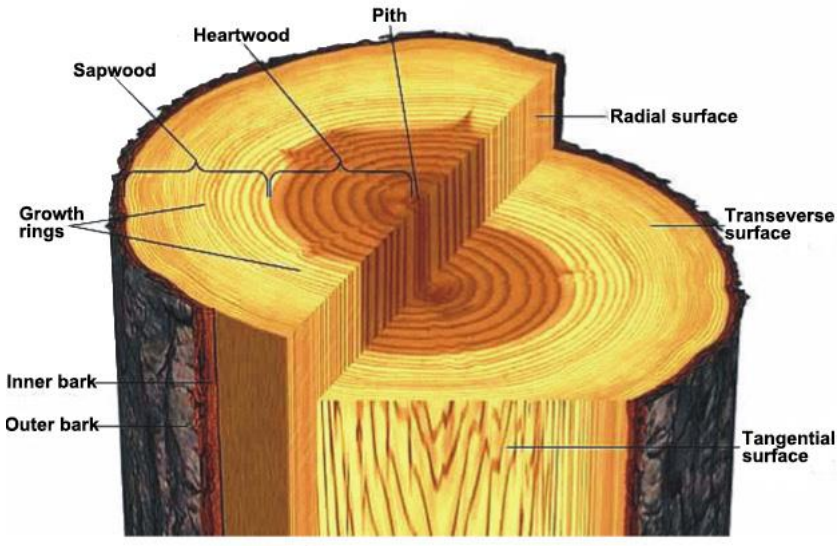

Figure 3—1 Anatomy of wood trunk (modified after https://global.britannica.com/plant/tree/Tree-structure-and-growth)

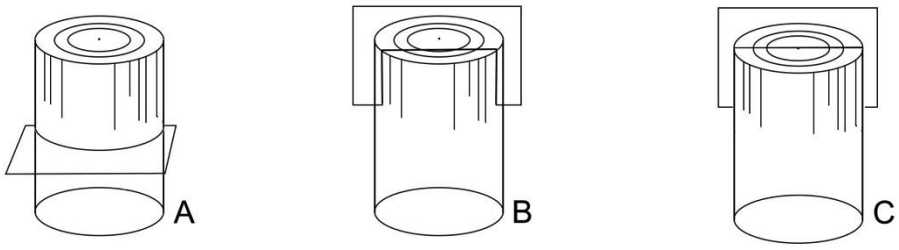

Figure 3—2 Three sections of the wood
A. Transverse section B. Tangential section C. Radial section

Transverse section

In the transverse section some typical characters can be recognized, such as shape and size of the pith, medullary cells, the presence or absence of growth rings, distinct or indistinct, axial resin canals, traumatic resin canals, distribution and size of tracheids and density of wood rays.

Radial section

In the radial section, bordered pits and their pattern on the radial walls of tracheids are important characters. The pattern of thickening on walls of tracheids also deserves attention. Another important character is the cross-field pitting, it can be divided into 5 basic types: the fenestriform (window-like), the pinoid, the piceoid, the taxdioid, the Araucarioid and the cupressoid (Fig. 3—4). Characters of ray tracheids, pinoid small pores on horizontal walls of ray cells, and nodular end wall of ray cells also need to be observed.

Tangential section

In the tangential section, characters of rays (such as rows, height, density, thickness of cell walls, form and size of ray cells), presence or absence of transverse resin canals frequently seen in fusiform rays, and pits on tangential walls of tracheids, as well as arrangement and abundance of axial wood parenchyma are important to note for classification.

3.1.2 Methods for reconstruction of the palaeoecologic significance of the wood anatomy contents

Growth-ring patterns provide efficient informations to determine the tree habit. Falcon-Lang (2000) developed the CSDM curve (Cumulative Sum of the Deviation from Mean diameter) to determine the intraseasonal conditions and leaf longevity patterns of the tree.

To construct the CSDM curve, radial diameters of individual cells across each ring increment were measured. Five adjacent files of cells were measured for each ring increment, and these data were averaged to give the final plots. A slightly different number of cells were present in each growth rings, measured file. Therefore to create meaningful average plots, data from the shorter sequences are stretched out by adding spaces into the spreadsheet, so that data from the ring boundaries matched up exactly. Two different

ring boundary markedness parameters are calculated: percentage latewood and percentage diminution. The cumulative algebraic sum of each cell's deviation from the mean radial cell diameter is calculated and plotted as a curve (the CSDM curve). The position of the earlywood/latewood boundary is taken as the point where the CSDM curve turns towards zero for the last time. The percentage diminution is derived by calculating the difference between the maximum and minimum radial cell diameter in each ring increment and dividing it by the maximum cell diameter. *Junggaropitys dalongkouensis* and XTT-C-4 gen. et sp. nov. preserved enough growth rings to analyse the tree habit.

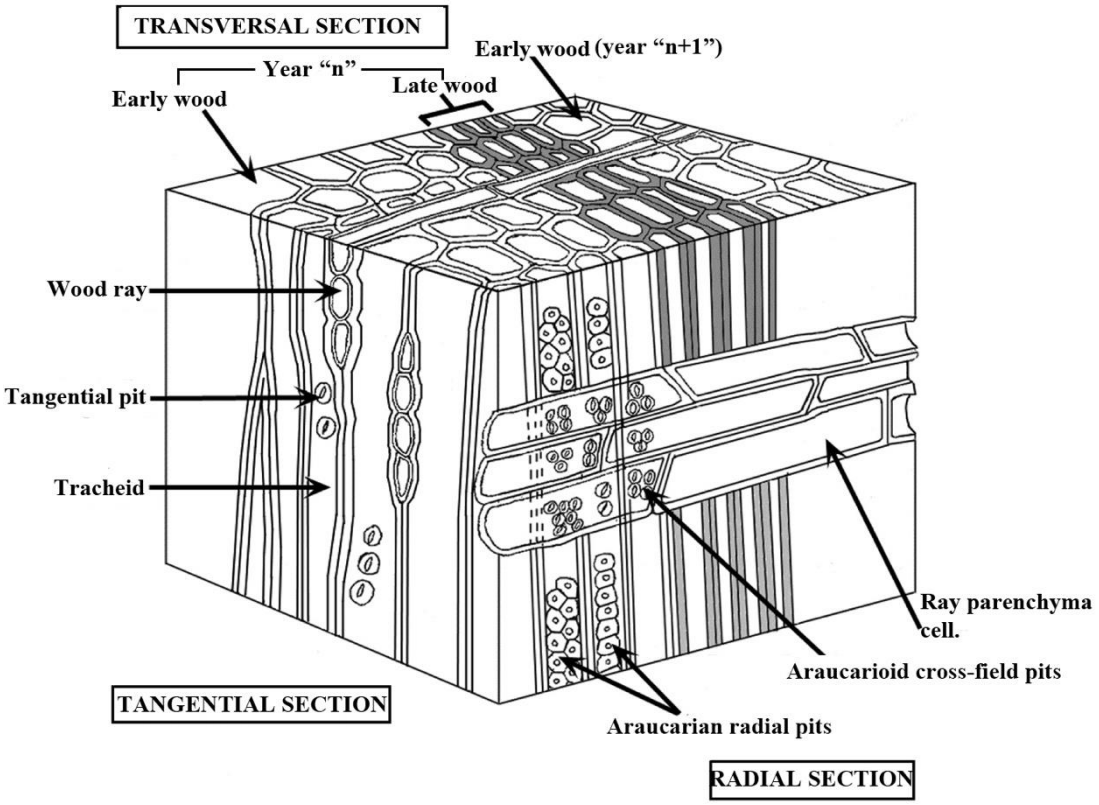

Figure 3—3 Anatomy of *Araucaria* wood

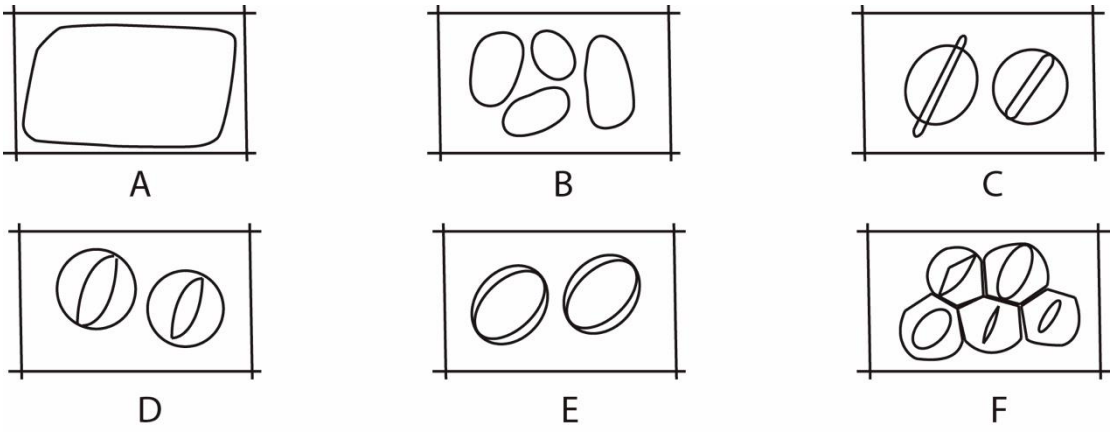

Figure 3—4 Cross-field pitting type

A."Window-like", fenestriform. *Pinus sylvestris*. B. Pinoid. *Pinus ponderosa*. C. Piceoid. *Picea abies*. D. Cupressoid. *Juniperus communis*. E. Taxodioid. *Taxodium distichum*. F. Araucarioid. *Araucaria araucana.*

§3.2 Descriptions

3.2.1 Arthrophyta

Division Arthrophyta
Class: Sphenopsida
Order: Equisetales
Family: Calamitaceae
Genus: *Arthropitys* Goeppert, 1864-65

Type species: *Arthropitys bistriata* (Cotta) Goeppert emend. Rößler, Feng and Noll, 2012

***Arthropitys* cf. *communis* (Binney) Hirmer and Knoell, 1935**

Description: The specimen possesses pith, primary and manoxylic secondary vascular tissues. The pith area is made of a large central "medullar" cavity, surrounded by a narrow perimedullary zone in internodal region and of diaphragms in nodal zone. Carinal canals are circular and lined metaxylem tracheids. The metaxylem tracheids are not well preserved. The only space where metaxylem tracheids are visible is a single layer of cells. Secondary xylem consists of interfascicular rays and fascicular wedges. The fascicular wedges comprise thick-walled tracheids and thin-walled fascicular rays. Interfascicular rays are not well preserved. The only space where interfascicular rays are visible shows they are initially 4 to 5 cells wide, gradually diminishing distally. Radial tracheid walls have uniseriate or biseriate circular pits, or scalariform pits. Fascicular parenchymatous rays vary from five to more than 45 cells high and from one up to seven cells wide in the middle of the secondary xylem. Fascicular ray cells are rectangular in transverse section, polygonal in tangential section.

The specimen XTT-C-11 is 250 mm long and 58 mm in diameter. It is composed of

pith, primary xylem and secondary xylem.

The medullar cavity surrounded by pith cells of this specimen is elliptical in outline, which is likely the consequence of partial compression (Fig. 3—4A a close up focused on this area is needed). The diameter is about 17×11 mm. The medullar cavity is filled with calcite contents. The pith diaphragms are poorly or most often not preserved, but the protuberances at the nodes are visible (Fig. 4B). At the internodes, the pith area constitutes a large cavity surrounded by a narrow perimedullary zone (Figs. 3—4C, D, black arrows).

A discrete ring of primary xylem strands surrounds the pith (Fig. 3—4D and 3—5). There are approximately 55 primary xylem strands. The carinal canals are lined surrounded by a single layer of metaxylem tracheids (Fig. 3—4C, 3—4D and 3—5). These tracheids are 16-34 μm in diameter. The secondary xylem of the specimen is between 13 and 25 mm wide in transverse section. It consists of interfascicular parenchymatous rays and fascicular wedges. Interfascicular rays are not well preserved. The only space preserved shows they may start at the outer periphery of the pith at a width of four to five cells (ca. 0.3 mm) (Fig. 3—4D and 3—5). After a short distance, they gradually diminished. In the radial section, the interfascicular rays are hard to distinguish, as they are poorly preserved. The fascicular wedges start from the external side of the primary xylem at a width of four to six rows of tracheids and rays. The widths of the fascicular wedges rapidly increase as new files of tracheids and rays are added. In the inner part of the secondary xylem the tracheids and the ray cells are both rectangular in the transverse section and the tracheids are smaller in dimension. In the outer part of the secondary xylem, the fascicular and interfascicular ray cells are both always rectangular, 29×47-49×97 μm. Tracheids are nearly square and smaller than ray cells, 31×38-48×57 μm. In radial section the ray cells are rectangular, 76-117 μm high (Fig. 3—4F). The radial walls of the tracheids possess uniseriate or biseriate circular pits and scalariform pits (Figs. 3—4E and 3—4G). In the tangential section, the ray cells are polygonal with smooth walls (Figs. 3—4H and 3—4I). The rays vary from five to more than 45 cells high (400-3125 μm) and one to seven cells (~500 μm) wide.

Comparisons: The nature of interfascicular rays is used to distinguish the three morphogeneras classically defined within the group of anatomically preserved calamitean stems, namely: *Arthropitys* Goeppert, *Arthroxylon* Reed and *Calamodendron* Brongniart (Andrews, 1952; Eggert, 1962; Cichan and Taylor, 1983, Boureau, 1964). The studied specimen shows the characteristic of *Arthropitys*: interfascicular ray cells only parenchymatous, more or less isodiametric in shape.

For the delimitation of the different species of *Arthropitys*, the constant characteristics such as interfascicular rays, nature of tracheid pitting, size of carinal canals and development patterns in the primary and secondary xylem are to be taken into account (Andrews, 1952; Wang et al., 2003; Rößler and Noll, 2007). The secondary xylem contains most of the features considered to be important for classifying the anatomically preserved calamitean axes (Wang et al., 2003).

Twenty-seven species of *Arthropitys* have previously been reported as far as we know. Of these species, *A. jongmangsi* Hirmer, 1927, *A. renaulti* Hirmer and Knoell 1935, *A. herbacea* Hirmer and Knoell 1935, *A. bistriatoides* Hirmer and Knoell 1935 and *A. renaultii*

Boureau 1964 either lack or have very thin secondary xylem (Knoell, 1935; Boureau, 1964). That makes it difficult to compare with other species. *A. hirmeri* Knoell is a unique species in *Arthropitys*, with a secondary xylem showing a homogeneous aspect due to the absence of interfascicular rays (Anderson, 1954).

Arthropitys kansana Andrews, *A. versifoveata* Anderson, *A. felixi* Hirmer and Knoell, *A. bisriata* (Cotta) Goeppert emend. Rößler and Noll, 2012, *A. gallica* Renault, 1896, *A. deltoides* Cichan and Taylor, 1983, *A. yunnanensis* (Tian and Gu) ex Wang, Hilton, Galtier and Tian, 2006, *A. isoramis* Neregato, Rößler, and Noll, 2015 and *A. iannuzzii* Neregato, Rößler, and Noll, 2015 possess well-developed interfascicular rays. Their interfascicular rays extended throughout the secondary xylem. *Arthropitys major* (Weiss) Renault, 1896 and *A. approximata* (Schlotheim) Renault, 1896 have very broad interfascicular rays. The interfasicular rays of the present specimen are visible only on some areas, only 4 to 5 cell width.

The tracheid radial walls of our specimen possess uniseriate or biseriate circular pits or scalariform pits. But *A. lineata* Renault 1896 and *A. rochei* Renault, 1896 are characterized by elongate bordered pits on its tracheid walls; *A. gigas* (Brongniart) Renault, 1896 and *A. cacundensis* Mussa, 1984 have round pits (Coimbra and Mussa, 1984); in *A. illinoensis* Anderson, 1954, the pits are multiseriate oval to elongate ~~pits~~; *A. sterzelii* Rößler and Noll, 2010 shows equally spaced reticulate wall thickenings. The tracheid radial walls of *A. porosa* Renault, 1896 are composed of circular reticulate, elongate reticulate and scalariform thickenings. *A. junlianensis* Wang, Hilton, Li and Galtier, 2003 has only elongate scalariform pits. These pitting patterns are all different from those of the present sample.

The present sample possesses multiseriate fascicular rays, similar with those of *A. medullata* Renault 1896. While the pith of *A. medullata* Renault, 1896 is weakly developed, when *Arthropitys* sp.1 has a large pith. The secondary rays of *Arthropitys ezonata* Goeppert, 1864-65 are only two cells wide.

Arthropitys communis (Binney) Hirmer and Knoell, 1935 is a broad morphospecies. The present sample resembles *Arthropitys communis* (Binney) Hirmer and Knoell, 1935. They both show similar pith and interfascicular rays. But in *A. communis* (Binney) Hirmer and Knoell, 1935 the carinal canal and metaxylem tracheids are surrounded by an arch of multiple layers of isodiametric cells. But in our specimen, this part is not well preserved enough to determine that it is fully in accordance with the diagnosis of *Arthropitys communis*. Therefore, we determine this specimen as *Arthropitys* cf. *communis,* it may correspond to a new subspecies or even new species if new better preserved material was collected.

Locality and Horizon

Taoshuyuan C Section, Turpan, Xinjiang; Late Permian Wutonggou Formation.

Sample Number

XTT-C-11

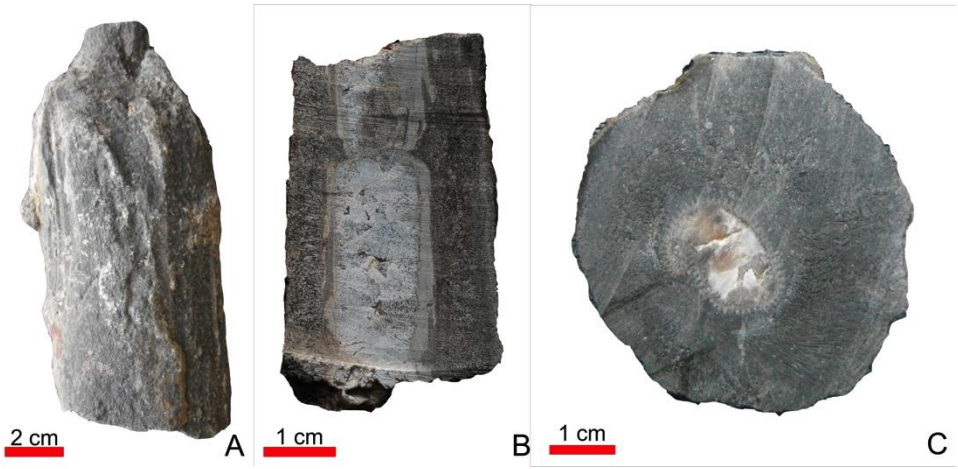

Figure 3-3 *Arthropitys* cf. *communis* A. General view of a part of XTT-C-11; B. Radial polish section showing the overview of the medullar cavity fulfilled be calcite, primary xylem and secondary xylem; C. Transverse polish section showing the overview of the "calcitic geode-like" medullar cavity, primary xylem and secondary xylem.

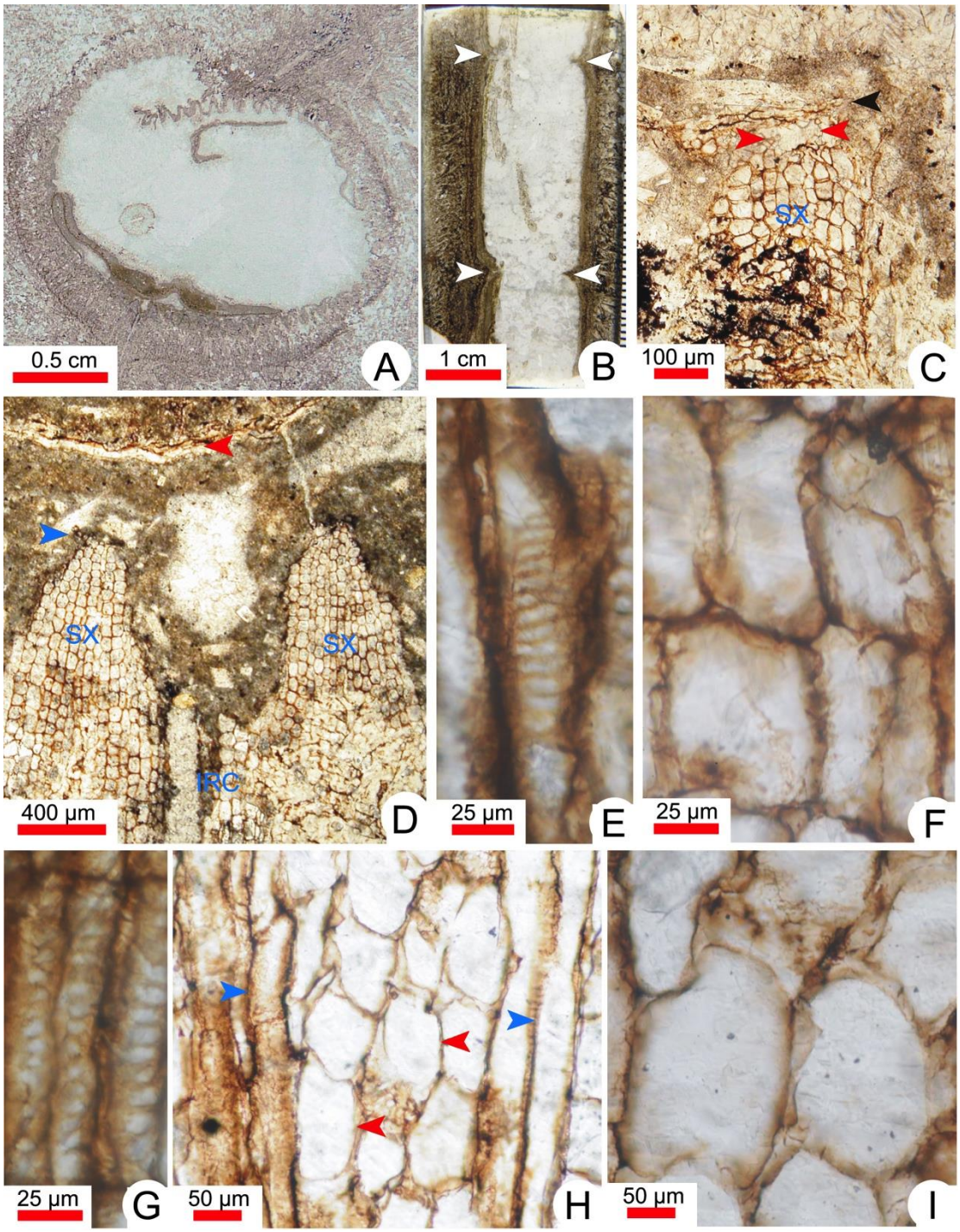

Figure 3-4 *Arthropitys* cf. *communis* A. Transverse section (TS) showing the overview of the medullar cavity, pith, primary xylem and secondary xylem. Slide no. XTT-C-11a1; B. Radial section (RS) showing the overview of the medullar cavity bordered by pith cells, primary xylem and the internal part of the secondary xylem, the white arrows indicate the relict diaphragms, at the node. Slide no. XTT-C-11b1; C. TS showing the layer of perimedullary cells (red arrow), the carinal canal with possible metaxylem tracheids (blue arrows) and the secondary xylem strand (SX). Slide no. XTT-C-11a1; D. TS showing the layer of perimedullary cells (red arrow), the single layer of metaxylem tracheids (blue arrow), the secondary xylem strands (SX) and interfascicular ray cells (IRC). Slide no. XTT-C-11a1; E. RS showing the scalariform pits of the

tracheids. Slide no. XTT-C-11b2; F. RS showing the secondary ray cells. Slide no. XTT-C-11b2; G. RS showing the circular pits of the tracheids. Slide no. XTT-C-11b2; H. Tangential section (Tg.S) showing the ray cells (red arrows) and tracheids (blue arrows). Slide no. XTT-C-11c2; I. TGS showing the close-up of the ray cells. Slide no. XTT-C-11c2.

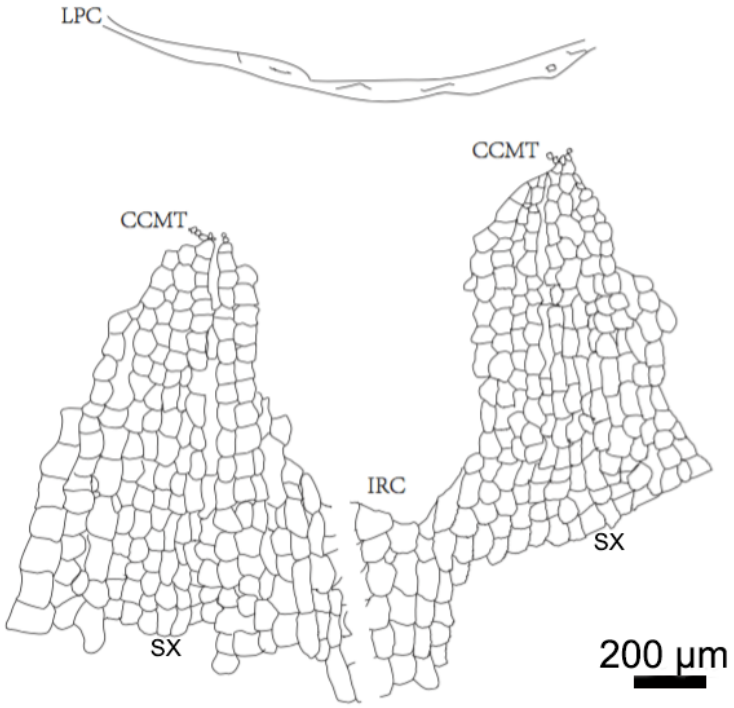

Figure 3-5. Schematic drawing of Figure 3-4D showing the layer of perimedullary cells (LPC), the carinal canal and metaxylem tracheids (CCMT), interfascicular ray cells (IRC) and the secondary xylem strands (SX).

Arthropitys sp.

Description: The specimen "XTT-BW-04" is 84 mm long, unfortunately only the manoxylic secondary xylem was preserved, but its excellent state preservation deserve by itself a description. In cross section, the outline is rectangular, 59.5×42.3 mm (Fig. 3-6).

In cross section, the fascicular ray cells are rectangular, 53×102-85×169 μm (Fig. 3-7A). The tracheids are small, rectangular or square, 22×49-70×101 μm (Fig. 3-7A). In radial section, the fascicular ray cells are rectangular, 60-142 μm high (Fig. 3-7B). The radial walls of tracheids possess reticulate or scalariform thickenings (Fig. 3-7C, D; Fig. 3-8). There are many simple pits in the cross-field units (Fig. 3-7E; Fig. 3-9). In tangential section, the ray cells are polygonal, with smooth walls (Figs. 3-7F,G). The rays vary from three to more than 39 cells (350-3225 μm) high and up to seven cells (~425 μm) wide.

Comparisons: As nor pith, nor primary xylem are preserved, it is impossible to determine which species the specimen belongs to. Although the width and height of fascicular rays are similar to that of the specimen *Arthropitys* cf. *communis*, the tracheid-pitting pattern of this specimen is different. Besides, the cross-fields show many simple pits in the present specimen. That is also different from those of the specimen *Arthropitys* cf. *communis*.

The tracheid radial walls of *A. porosa* Renault, 1896 are composed of circular reticulate, elongate reticulate and scalariform thickenings. The rays are 1 to 28 cells and 1 to 3 cells wide. These characteristics are similar to the present specimen.

Locality and Horizon

Taoshuyuan B Section, Turpan, Xinjiang; Late Permian Wutonggou Formation.

Sample Number

XTT-BW-04

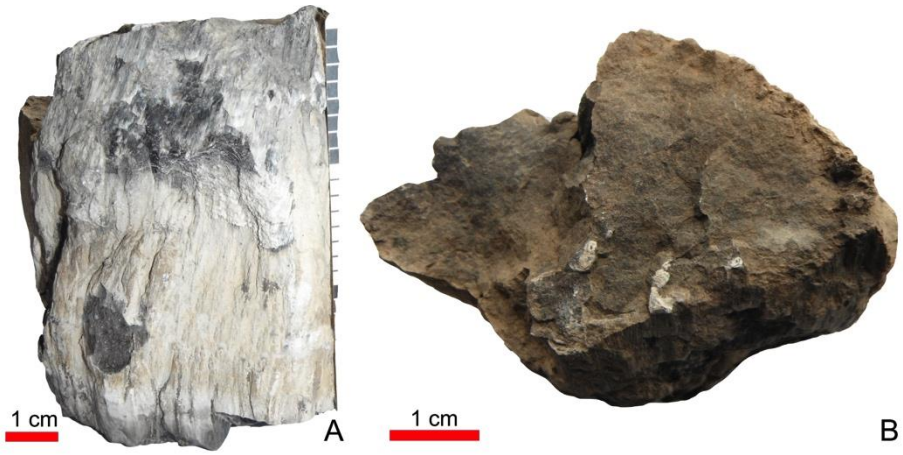

Figure 3-6 General views of the specimen XTT-BW-04 (A: Longitude view; B: Transvers view)

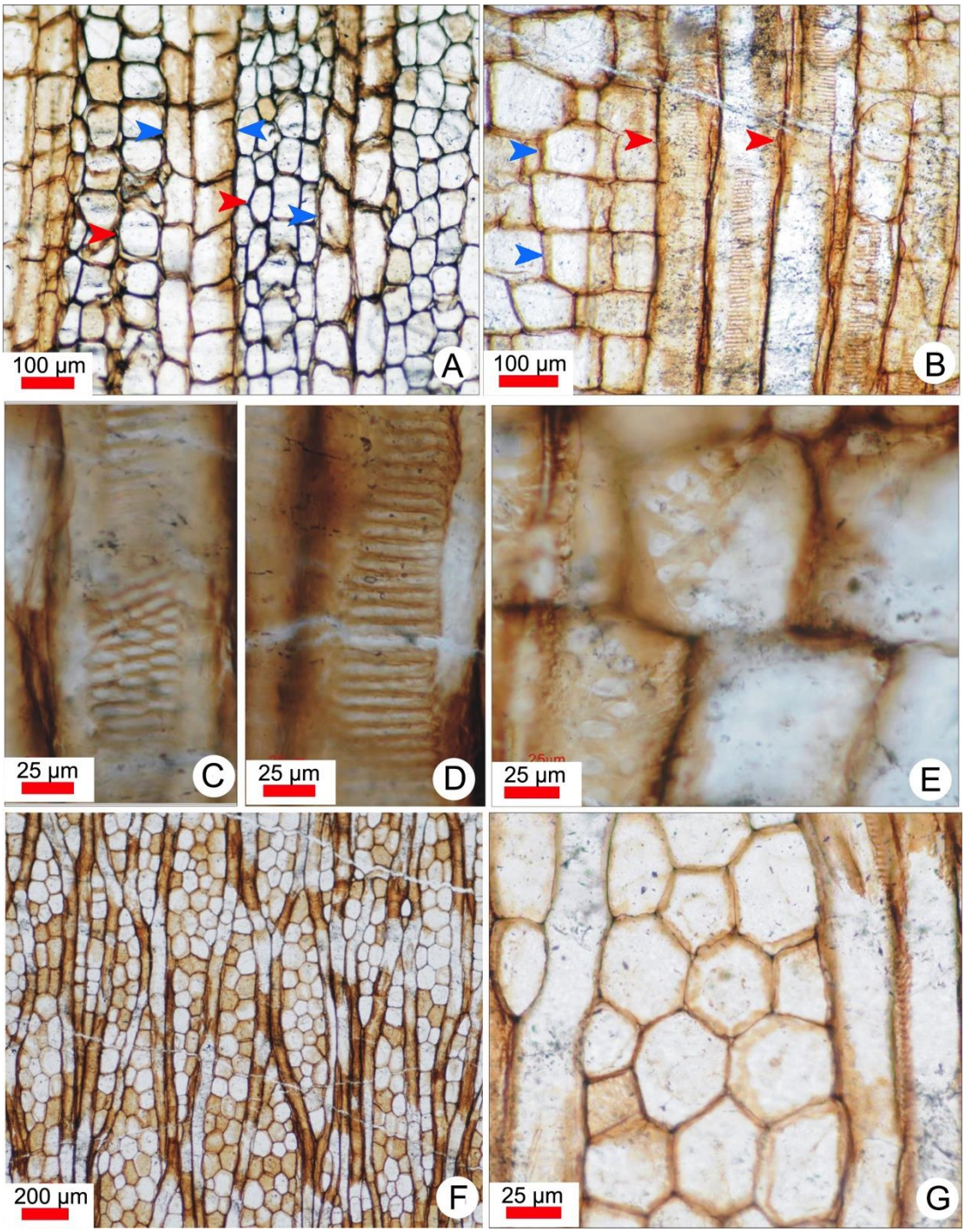

Figure 3-7 *Arthropitys* sp. A. Transverse section (TS) showing the tracheids (Red arrows) and ray cells (blue arrows). Slide no. XTT-BW-04a1; B. Radial section (RS) showing the tracheids (Red arrows) and ray cells (blue arrows). Slide no. XTT-BW-04b1; C. RS showing the reticulate thickening of the tracheids. Slide no. XTT-BW-04b1; D. RS showing the scalariform thickening of the tracheids. Slide no. XTT-BW-04b1; E. RS showing the simple pits in the cross-field units. Slide no. XTT-BW-04b1; F. Tangential section (Tg.S) showing the ray cells and tracheids. Slide no. XTT-BW-04c1; G. Tg.S: close-up of the ray cells. Slide no. XTT-BW-04c1.

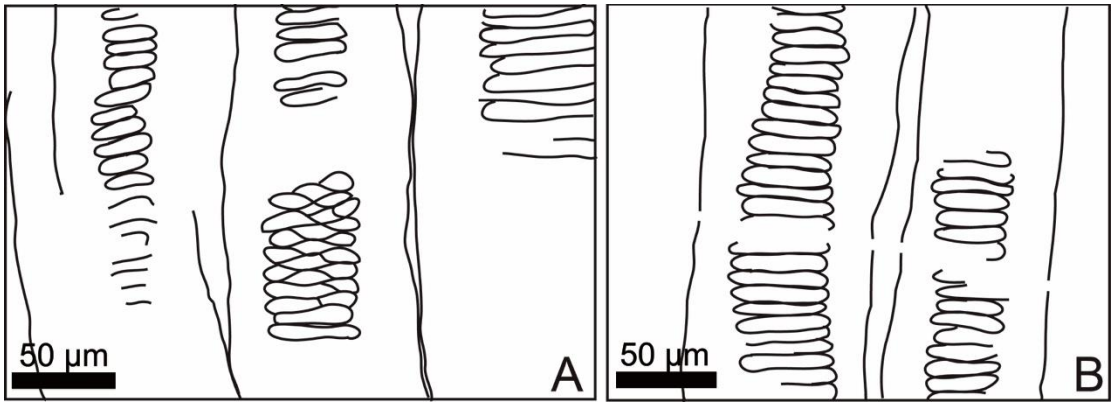

Figure 3-8 Drawings of *Arthropitys* sp. A: Reticulate and scalariform thickening of the tracheids walls; B: Scalariform thickening of the tracheids walls.

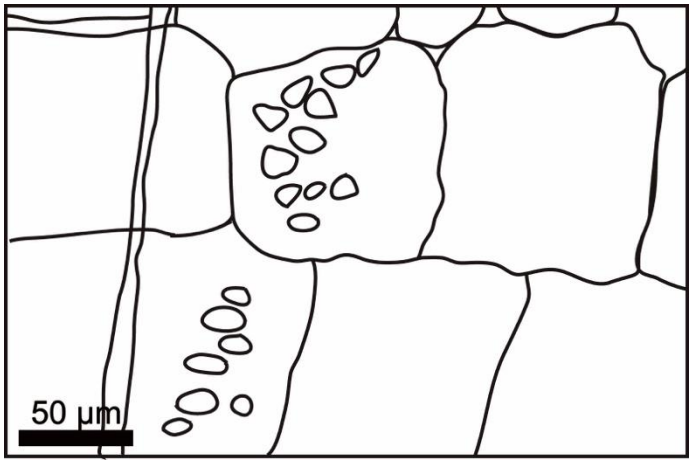

Figure 3-9 Drawing of *Arthropitys* sp. showing the multiple simple pits in the cross-field units.

3.2.2. Gymnosperms

Class: Coniferopsida
Order: Coniferales
Family: Incertae sedis
Genus: *Junggaropitys* Shi, Yu, Broutin and Pons, 2015
***Junggaropitys dalongkouensis* Shi, Yu, Broutin and Pons, 2015**

This part has been published on the journal Review of Palaeobotany and Palynology. The genus *Junggaropitys* was established on the basis of samples from the Middle-Late Triassic Karamay Formation of Dalongkou section (Shi et al., 2015). The *Junggaropitys dalongkouensis* were found in the Guodikeng Formation of Taoshuyuan C section and the Karamay Formation of Dalongkou section.

Genus diagnosis: Pith small, homogeneous but heterocellular. Primary xylem endarch. Secondary xylem homoxylic, with growth rings, and uni- to biseriate araucarioid pits. Xylem rays uniseriate, homogeneous, low. Cross-field pits rectangular to oblique oval, partially circular, simple, sometimes slightly areolate. Vertical parenchyma cells and secretory cells absent.

Specific diagnosis: Pith small, homogeneous, heterocellular with variable diameter

parenchyma cells. Primary xylem endarch. Tracheids in primary xylem with annular and helical thickening. Secondary xylem homoxylic, with growth rings. Radial pitting, uniseriate, contiguous and flattened; rarely biseriate, alternate. Xylem rays uniseriate, homogeneous, low (1-7 cells high). Cross-fields with 1, rarely 2, rectangular to oblique oval, partially circular, simple, sometimes slightly areolate pits. Vertical parenchyma cells and secretory cells absent.

Description:

The description here is mainly based on specimen XJD-3, as it is much easier to get the radial section of pith. The specimen XJD-3 is elliptical in transverse section, 3.3×5.7-4.6×8.7 cm in diameter and 42.5 cm long (Plate3-10, 1).

Pith

The pith of specimen XJD-3 is small, oval and homogeneous but heterocellular (Plate3-10, 2). It is often broken due to crystallization. The parenchyma cells in the pith are crowded, smooth and circular to polygonal. The thickness of the walls is irregular, around 10 μm, up to 30 μm. Such an irregularity is due to white rot effect and/or by maceration in water. The diameters of parenchyma cells are variable, ranging from 25 to 125 μm (n=100, mean=57.7 μm) in transverse section (Plate 3-10, 3). In the radial section, these cells are sub-rectangular or polygonal and vertically aligned, and range from 35 to 515 μm (n=100, mean=122.65 μm) in height (Plate 3-11, 5). The parenchyma pith cells display lining-like structures inside the cell lumens, and these structures are comparable with cell wall separations caused by white rot (Plate 3-10, 3; Plate 3-11, 1).

Primary xylem

The primary strands show endarch maturation (Plate 3-11, 2). Primary xylem tracheids, with annular and helical thickenings, are 15 to 35 μm (n=50, mean=21.75 μm) in diameter (Plate 3-11, 6).

Secondary xylem

The diameter of the pycnoxylic secondary xylem is up to 8.7 cm in transverse section. Twenty-five growth rings are present (Plate 3-10, 1; Plate 3-11, 3, 4). The tracheid lumens are circular, polygonal or rectangular, and 15 to 60 μm (n=50, mean=33.6 μm) in diameter. Helical cracks often occur on the tracheid walls. In some areas, tracheids show wide spaces between each other, corresponding to the removal of middle lamellae caused by white rot (Plate 3-11, 3, 4).

Radial bordered pits are almost uniseriate (98.5%), rarely biseriate (1.5%). When uniseriate, the pits are contiguous, often flattened (flattening index=0.56-0.90); when biseriate, pits are alternate, crowded hexagonal (flattening index=0.63-0.94). They are 12.5 to 22.5 μm in radial diameter with circular or elliptical apertures (Plate 3-12, 1, 2). The margins from the pits to the tracheid internal walls are 2.5 to 15 μm in width.

Rays are homogeneous, uniseriate and very low. In tangential view, ray cells are triangular, rectangular or elliptical, 17.5 to 30 μm × 10 to 15 μm (height × width) (Plate 3-12, 6, 7). In radial view, they are rectangular, 35 to 400 μm long. Ray height is from 1 to 7 cells, 40 to 240 μm (Plate 3-12, 5; Fig. 3).

Cross-field pits are rectangular to oblique oval, sometimes circular. They are simple, sometimes slightly areolate. There is 1, rarely 2 pits in each cross-field unit (Plate III, 3, 4). In the late wood, the pits are more oblique. The pits are 15 to 27.5 μm × 10 to 22.5 μm

(height × width).

Vertical parenchyma cells and secretory canals are absent.

Comparisons

Junggaropitys possesses a small parenchymatous pith, an endarch primary xylem and a thick pycnoxylic secondary xylem. These features closely resemble some extinct and extant conifers. Thus, we consider *Junggaropitys* to be a coniferophyte of uncertain systematic affinity. The anatomy of the pith and primary xylem is always regarded as a critical criterion for the classification of gymnospermous woods (Lepekhina, 1972; Pant and Singh, 1987; Feng et al., 2011). Its secondary xylem shows close affinities to the genus *Protophyllocladoxylon* Kräusel.

Four morphogenera of coniferous fossil woods with a *Protophyllocladoxylon*-type secondary xylem and different structures of pith and primary xylem have been documented as far as we know (Table 3-1).

Kräusel described *Phyllocladopitys* based on the specimens collected from southwestern Africa (Kräusel, 1928), which possess a *Protophyllocladoxylon*-type secondary xylem and homocellular or heterocellular pith. However, the primary xylem of *Phyllocladopitys* is mesarch or exarch, compared to the endarch primary xylem of *Junggaropitys*.

Medullopitys Kräusel 1928, *Megaporoxylon* Kräusel 1956 and *Septomedullopitys* Lepekhina 1972 are characterized by a heterogenous pith. *Medullopitys* Kräusel and *Megaporoxylon* Kräusel were found in the Early Permian sequences in Southwest Africa. They both possess large piths, but the pith in *Medullopitys* is composed of parenchyma and sclerenchyma cells, and the one in *Megaporoxylon* consists of parenchyma cells and secretory canals. These are all different from the homogeneous pith in *Junggaropitys*.

Septomedullopitys Lepekhina was first documented in Russia, and also discovered in the Late Permian of Turpan-Hami Basin, North China (Wan et al., 2014). It is characterized by the large septate pith. The pith is composed of parenchyma cells and secretory canals. That is different from *Junggaropitys*.

To date, about 5 genera and 6 species of fossil woods were reported from the whole Triassic in China: *Tianoxylon duanmutougouense* Zhang and Zheng (in Zhang et al. 2006), *Scalaroxylon jalaidqiense* Zhang and Zheng (in Zhang et al. 2006), *S. multiforium* Zhang and Zheng (in Zhang et al. 2006), *Liaoningoxylon chaoyangensis* Zhang and Zheng (in Zhang et al. 2006), *Protophyllocladoxylon* szei Wang (1991a), *Xenoxylon ellipticum* Schultze-Motel (Wang, 1991b). Of these, *Tianoxylon duanmutougouense*, *Scalaroxylon jalaidqiense* and *S. multiforium* all possess a manoxylic secondary xylem, which is different from conifers (Table 3-2).

The secondary xylem of *Liaoningoxylon chaoyangensis* Zhang and Zheng (in Zhang et al., 2006) is similar to that of *Protophyllocladoxylon*. However, it possesses a large pith with parenchyma cells and secretory canals, that differs from *Junggaropitys dalongkousensis*. Besides, its rays are heterogeneous.

Protophyllocladoxylon szei Wang (1991a) was established from the Upper Triassic of Guangdong Province, South China. The secondary xylem of our new genus shares the greatest similarities with the one of the species P. szei, which shows an araucarian type of pitting, simple large oval cross-field pits and low rays (1-10 cells high). But the pith and

the primary xylem of *Protophyllocladoxylon szei* are still unknown.

Xenoxylon ellipticum Schultze-Motel is only based on its secondary xylem as well (Wang, 1991b). It possesses vertical parenchymas. That is different from *Junggaropitys*.

We compare also our new genus with the Late Palaeozoic fossil woods displaying as well preserved pith and primary xylem: 12 species in 10 genera have been reported in China (Table 3-3).

Xinjiangoxylon turpanense Shi, Yu, Li, Chi and Zhang was described in the Late Permian sequences in Turpan-Hami Basin (Shi et al., 2014). Its secondary xylem is similar to *Protophyllocladoxylon*. The pith of *Xinjiangoxylon turpanense* is heterocellular with parenchyma and secretory canals. It differs from *Septomedullopitys szei* Wan, Yang and Wang (2014) in the absence of parenchymatous bands in the pith and axial parenchyma cells. The pith is also different from that of *Junggaropitys*.

Chapmanoxylon xiuqienense Zhang and Zheng (1984), *Chapmanoxylon*? *taiyuanense* (Li 1986) Wang (2000) and *Chapmanoxylon*? *teilhardii* (Sze 1934) Wang (2000) were described in the Permian North China. Their piths are of homocellular and composed of parenchyma cells. Their types of cross-field pits differ from that of our new genus. *Chapmanoxylon xiuqienense* possesses 4-12 bordered pits in each cross-field unit. The cross-fields of *Chapmanoxylon*? *taiyuanense* have 1-2 taxodioid pits. *Chapmanoxylon xiuqienense* has 3-6 non-bordered pits in each cross-field unit. They all differ from those of the genus.

The secondary xylem of *Guizhouoxylon dahebianense* Tian and Li (1992) shows many affinities to *Protophyllocladoxylon*. But it possessed multiple simple pits in its cross-field unit. Its pith is heterocellular with parenchyma, sclerenchyma and secretory cells.

As to the other fossil conifer woods with pith and primary xylem from the Late Palaeozoic in China, the cross-filed pits of *Ningxiaites specialis* Feng (2012), *Plyophyllioxylon hulstaiense* Feng, Wang, Liu and Röβler (2012), *Shenoxylon mirabile* Feng, Wang and Röβler (2011), *Sclerospiroxylon neimongolense* Zhang, Zheng, Wang, Yang, Li, Fu and Li (2006) and *Walchiopremnon gaoi* Tian, Hu and Zhao (1996) are all of cupressoid type; the cross-filed pits of *Damudoxylon zhoui* Zhang and Zheng (2006) are of araucarian type. These are all different from that of our genus.

Besides, the rays of *Junggaropitys* are very low: only 1-5 cells high, occasionally 6 or 7 cells high (Fig. 3-12). Within the already known species from the Late Palaeozoic or Triassic of China, only *Chapmanoxylon*? *teilhardii* (1-6 cells high) and *Damudoxylon zhoui* (1-5, up to 9 cells high) show low rays as that in *Junggaropitys*. As mentioned above, based on other characters, they are clearly different from our genus.

Locality and Horizon

Dalongkou north limb Section, Jimsar, Xinjiang; Middle-Late Triassic Karamay Formation；Taoshuyuan C Section, Turpan, Early Triassic Guodikeng Formation.

Sample Number

XJD-1; XJD-2; XJD-3; XJD-4; XTT-C-16

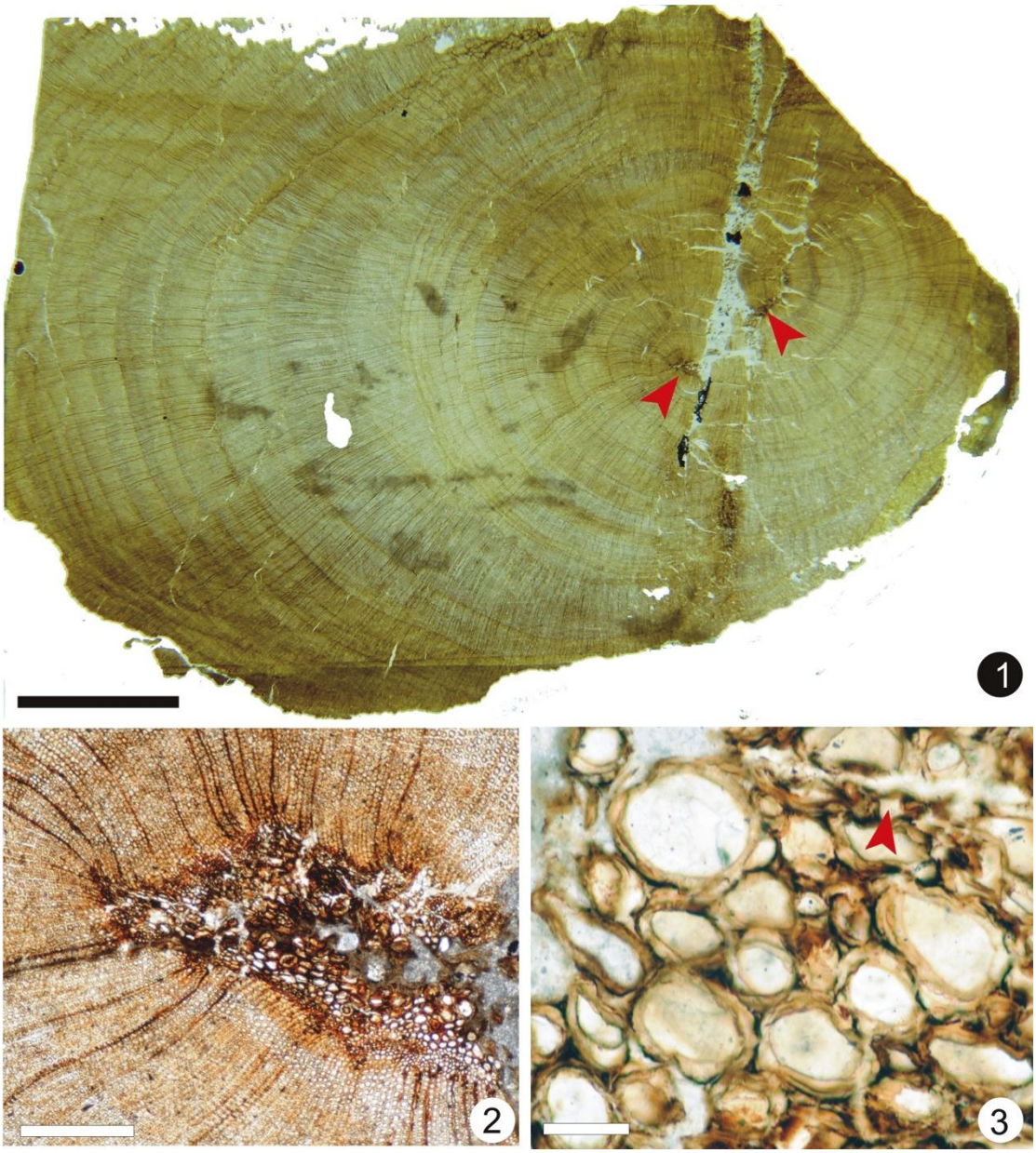

Figure 3-10 *Junggaropitys dalongkouensis* 1. Transverse section (TS) showing an overview of the pith (red arrows), primary xylem and secondary xylem, scale bar =1 cm. Slide number: XJD-3a3; 2. TS showing the close-up of the pith and the primary xylem, scale bar =100 μm. Slide number: XJD-3a3; 3. TS showing the parenchyma cells with variable diameters in the heterocelluar pith; the red arrow indicates cell wall separations caused by white rot, scale bar =100 μm. Slide number: XJD-3a3.

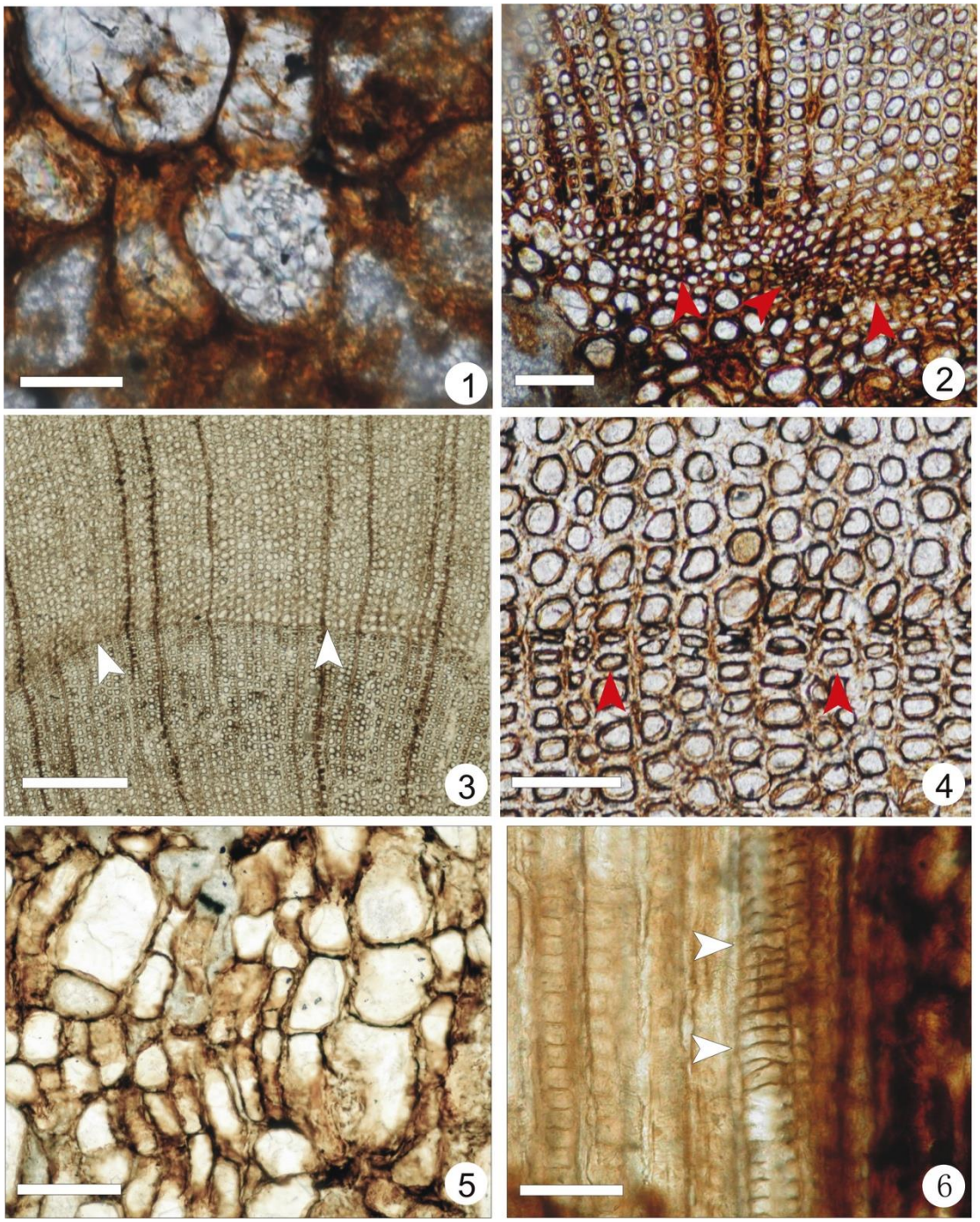

Figure 3-11 *Junggaropitys dalongkouensis* 1. Transverse section (TS) showing lining-like structures inside the pith cell lumens, scale bar =50 μm. Slide number: XJD-3a3; 2. TS showing the endarch primary xylem (red arrows) in the pith periphery, scale bar =100 μm. Slide number: XJD-3a3; 3. TS showing a limit between two growth rings (white arrows), scale bar =500 μm. Slide number: XJD-3a3; 4. TS showing the close-up of the transition from late wood to early wood of the next growth ring; the red arrows indicate two tracheids in the late wood, scale bar =100 μm. Slide number: XJD-3a3; 5. Radial section (RS) showing the parenchyma cells with variable heights in the heterocelluar pith, scale bar =100 μm. Slide number: XJD-3b3; 6. RS showing the helical thickenings of primary xylem (white arrows), scale bar =50 μm. Slide number: XJD-3b3.

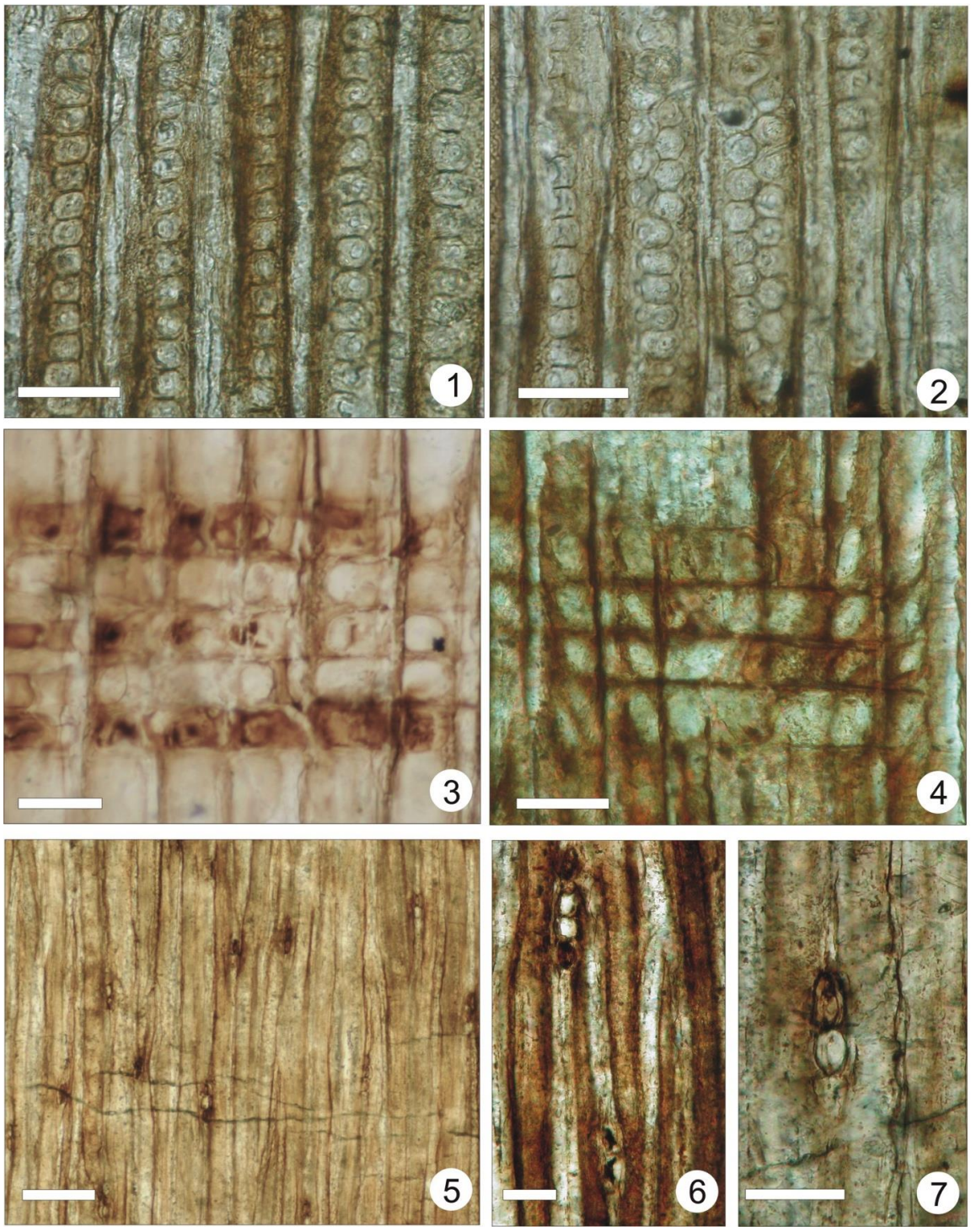

Figure 3-12 *Junggaropitys dalongkouensis* 1. Radial section (RS) showing uniseriate araucarioid bordered pits with circular or elliptical apertures on the radial walls of wood tracheids, scale bar =100 μm. Slide number: XJD-3b3; 2. RS showing uniseriate or biseriate bordered pits with circular or elliptical apertures on the radial walls of wood tracheids, scale bar =100 μm. Slide number: XJD-3b3; 3. RS showing 1, occasionally 2 window-like pits in each cross-field, scale bar =50 μm. Slide number: XJD-3b3; 4. RS showing the oblique-oval, occasionally partially bordered cross-field pits, scale bar =50 μm. Slide number: XJD-3b2; 5. Tangential longitudinal section (TLS) showing the homogeneous, uniseriate, low rays, scale bar =100 μm. Slide number: XJD-3c2; 6, 7. TLS showing the details of the ray cells, scale bar =50 μm. Slide number: XJD-3c2.

Table 3-1 Comparative features of pith and primary xylem with *Protophyllocladoxylon*-type secondary xylem.

Genus	Pith	Primary xylem	Type locality and age	References
Junggaropitys Shi et al. 2015	Small, homogenous but heterocellular	Endarch	Xinjiang, China; Late Triassic	The present paper
Phyllocladopitys Kräusel 1928	Variable, homo- or heterocellular	Mesarch	South-West Africa; Early Permian. Argentina, South America; Early Late Carboniferous.	Kräusel (1928, 1961), Lepekhina (1972), Brea and Césari (1995)
Medullopitys Kräusel 1928	Large, heterogenous with parenchyma cells and sclerenchyma cells	Endarch	South-West Africa; Early Permian	Kräusel (1928, 1961), Lepekhina (1972)
Megaporoxylon Kräusel 1956	Large, heterogenous with parenchyma cells and secretory canals	Endarch	South-West Africa; Early Permian. Antarctica	Kräusel (1956, 1961), Lepekhina (1972), Maheshwari (1972)
Septomedullopitys Lepekhina 1969	Large, septate, heterogenous with branched secretory canals	Endarch	Russia and China; Late Permian	Lepekhina (1969, 1972), Wan et al., (2014)

Table 3-2 Comparison among fossil conifer woods from the Triassic in China.

Species	Pith	Primary xylem	Secondary xylem			Type locality and age	References
			Tracheid pits	Cross–field pits	Xylem rays		
Junggaropitys dalongkouensis Shi et al. 2015	Small, homogenous but heterocellular	Endarch	Araucarian type: uniseriate, contiguous and flattened; biseriate, alternate	1 (rarely 2); rectangular to oblique oval, partially circular; simple, sometimes slightly areolate pits	Uniseriate, homocellular, 1–7 cells high	Xinjiang, China; Late Triassic	The present paper
Liaoningoxylon chaoyangensis Zhang and Zheng 2006	Large, heterogenous with parenchyma cells and secretory canals	Endarch	Mixed-type: uniseriate or biseriate, contiguous or separated	1, oblique oval or circular large pits	Uniseriate, rarely biseriate, 2-24 (up to 55) cells high; heterogeneous	Liaoning, China; Early Triassic	Zhang et al., 2006
Protophyllocladoxylon szei Wang 1991	Unknown	Unknown	Araucarian type: uniseriate, contiguous and flattened or sometimes separated	1 (rarely 2); simple, broad, large, oblique and oval or elliptical pits	Uniseriate, 1–10 cells high	Guangdong, China; Late Triassic	Wang (1991a)
Xenoxylon ellipticum Schultze-Motel 1988	Unknown	Unknown	Araucarian type: uniseriate, contiguous and flattened (Flattening index = 1:1.5); rarely biseriate, alternate	1, rectangular, rarely oblique oval or circular large pits	Uniseriate or biseriate, 2-9 (up to 37) cells high	Guangdong, China; Late Triassic	Wang (1991b)

Table 3-3 Comparison among fossil conifer woods with pith and primary xylem from the Late Palaeozoic in China.

Species	Pith	Primary xylem	Secondary xylem			Type locality and age	References
			Tracheid pits	Cross–field pits	Xylem rays		
Junggaropitys dalongkouensis	Small, homogenous but heterocellular	Endarch	Araucarian type: uniseriate,rarely biseriate	1, rarely 2; rectangular to oblique oval, partially circular; simple, sometimes slightly areolate pits	Uniseriate, homocellular, 1–7 cells high	Xinjiang, China; Late Triassic.	The present paper
Xinjiangoxylon turpanense Shi, Yu, Li, Chi and Zhang 2014	Solid, heterogenous with parenchyma and secretory canals	Endarch	Araucarian type: uniseriate to triseriate	1, partly 2; window–like simple pits	Uniseriate, homocellular, 1–16 cells high	Xinjiang, China; Late Permian	Shi et al. (2014)
Septomedullopitys szei Wan, Yang and Wang 2014	Solid and heterocellular, with parenchyma, secretory canals and parenchymatous bands	Endarch	Araucarian type: uniseriate to biseriate, rarely triseriate	1–2 simple pits	Uniseriate to biseriate, up to 50 cells high	Xinjiang, China; Late Permian	Wan et al. (2014)
Ningxiaites specialis Feng 2012	Solid and homocelluar, with parenchyma cells, radial cell walls commonly pitted	Endarch	Araucarian type: uniseriate, partially biseriate or triseriate	1–2 cupressoid pits	Uniseriate, partially biseriate, up to 21 cells high	Ningxia, China; Late Permian	Feng (2012)
Plyophyllioxylon hulstaiense Feng, Wang, Liu and Röβler 2012	Septate and homocellular with parenchyma cells	Endarch	Araucarian type: uniseriate or biseriate,	1–2 cupressoid pits	Uniseriate, partially biseriate or triseriate; 1–22 cells high	Inner Mongolia, China; Middle Permian	Feng et al. (2012)

Shenoxylon mirabile Feng, Wang and Röβler 2011	Sclerenchyma, parenchyma and pitted cells, intramedullary sheath consists of sclerenchyma cells	Endarch	Uniseriate, partially biseriate alternate or occasionally opposite	1–2 cupressoid pits	Uniseriate or biseriate, up to 14 cells high	Ningxia, China; Late Permian	Feng et al. (2011)
Sclerospiroxylon neimongolense Zhang, Zheng , Wang, Yang, Li, Fu and Li 2006	Solid, rounded or polygonal sclerotic cells grouped in parenchyma cells	Endarch	Araucarian type: uniseriate, partially biseriate	2–5 cupressoid pits	Uniseriate, 1–25 cells high	Inner Mongolia, China; Middle Permian	Zhang et al. (2006)
Chapmanoxylon xiuqiense (Zhang and Zheng) Zhang, Zheng, Wang, Yang, Li, Fu and Li 2006	Homocellular with parenchyma cells	Endarch	Araucarian type: uniseriate to pentaseriate	4–12 araucariod pits	Uniseriate, 1–10 cells high	Inner Mongolia, China; Middle Permian	Zhang and Zheng (1984); Zhang et al. (2006)
Chapmanoxylon? *teilhardii* (Sze) Wang 2000	Homocellular with parenchyma cells	Endarch	Araucarian type: uniseriate to triseriate	3–6 pinoid pits	Uniseriate, 1–6 cells high	Xinjiang, China; Middle Permian	Sze (1934); Wang (2000)
Chapmanoxylon? *taiyuanense* (Li) Wang 2000	Homocellular with parenchyma cells	Endarch	Araucarian type: uniseriate to biseriate	1-2 taxodioid pits	Uniseriate to biseriate, 1–14 (up to 38) cells high	Shanxi, China; Early Permian	Li (1986); Wang (2000)

Damudoxylon zhoui Zhang and Zheng 2006	Heterogenous, rounded or polygonal secretory in parenchyma cells	Endarch	Araucarian type: uniseriate to triseriate	Many araucariod pits	Uniseriate to triseriate, 1–5 (up to 9) cells high; the horizontal wall with pits	Liaoning China; Early Permian	Zhang et al. (2006)
Walchiopremnon gaoi Tian, Hu and Zhao 1996	Solid, heterogenous with parenchyma, sclerenchyma and secretory cells	Endarch	Araucarian type: uniseriate to biseriate	2–6 cupressoid pits or non-bordered pits	Uniseriate, rarely biseriate, 1-17 cells high	Guizhou, China; Late Permian	Tian et al. (1996)
Guizhouoxylon dahebianense Tian and Li 1992	Solid, heterogenous with parenchyma, sclerenchyma and secretory cells	Endarch	Araucarian type: uniseriate to tetraseriate	3-5 scalariform or oval simple pits; or 6-8 oval simple pits	Uniseriate, 1–11 (up to 15) cells high	Guizhou, China; Late Permian	Tian and Li (1992)

Chapmanoxylon? *teilhardii* (Sze) Wang 2000	Homocellular with parenchyma cells	Endarch	Araucarian type: uniseriate to triseriate	3–6 pinoid pits	Uniseriate, 1–6 cells high	Xinjiang, China; Middle Permian	Sze (1934); Wang (2000)
Chapmanoxylon? *taiyuanense* (Li) Wang 2000	Homocellular with parenchyma cells	Endarch	Araucarian type: uniseriate to biseriate	1-2 taxodioid pits	Uniseriate to biseriate, 1–14 (up to 38) cells high	Shanxi, China; Early Permian	Li (1986); Wang (2000)
Damudoxylon zhoui Zhang and Zheng 2006	Heterogenous, rounded or polygonal secretory in parenchyma cells	Endarch	Araucarian type: uniseriate to triseriate	Many araucariod pits	Uniseriate to triseriate, 1–5 (up to 9) cells high; the horizontal wall with pits	Liaoning China; Early Permian	Zhang et al. (2006)
Walchiopremnon gaoi Tian, Hu and Zhao 1996	Solid, heterogenous with parenchyma, sclerenchyma and secretory cells	Endarch	Araucarian type: uniseriate to biseriate	2–6 cupressoid pits or non-bordered pits	Uniseriate, rarely biseriate, 1-17 cells high	Guizhou, China; Late Permian	Tian et al. (1996)
Guizhouoxylon dahebianense Tian and Li 1992	Solid, heterogenous with parenchyma, sclerenchyma and secretory cells	Endarch	Araucarian type: uniseriate to tetraseriate	3-5 scalariform or oval simple pits; or 6-8 oval simple pits	Uniseriate, 1–11 (up to 15) cells high	Guizhou, China; Late Permian	Tian and Li (1992)

Additional informations

The calcified specimen from in the Guodikeng Formation of Taoshuyuan C section is a young branch, of 4.8 cm in diameter and 10 cm high. It is characterized by (1) a small homogenous pith; (2) endarch primary xylems strands; (3) a *Protophyllocladoxylon*-type secondary xylem (Fig. 3-13, 3-14). Therefore, the sample can be assigned to *Junggaropitys dalongkouensis.* As the specimen is very thin, the secondary xylem has false rings but no growth ring.

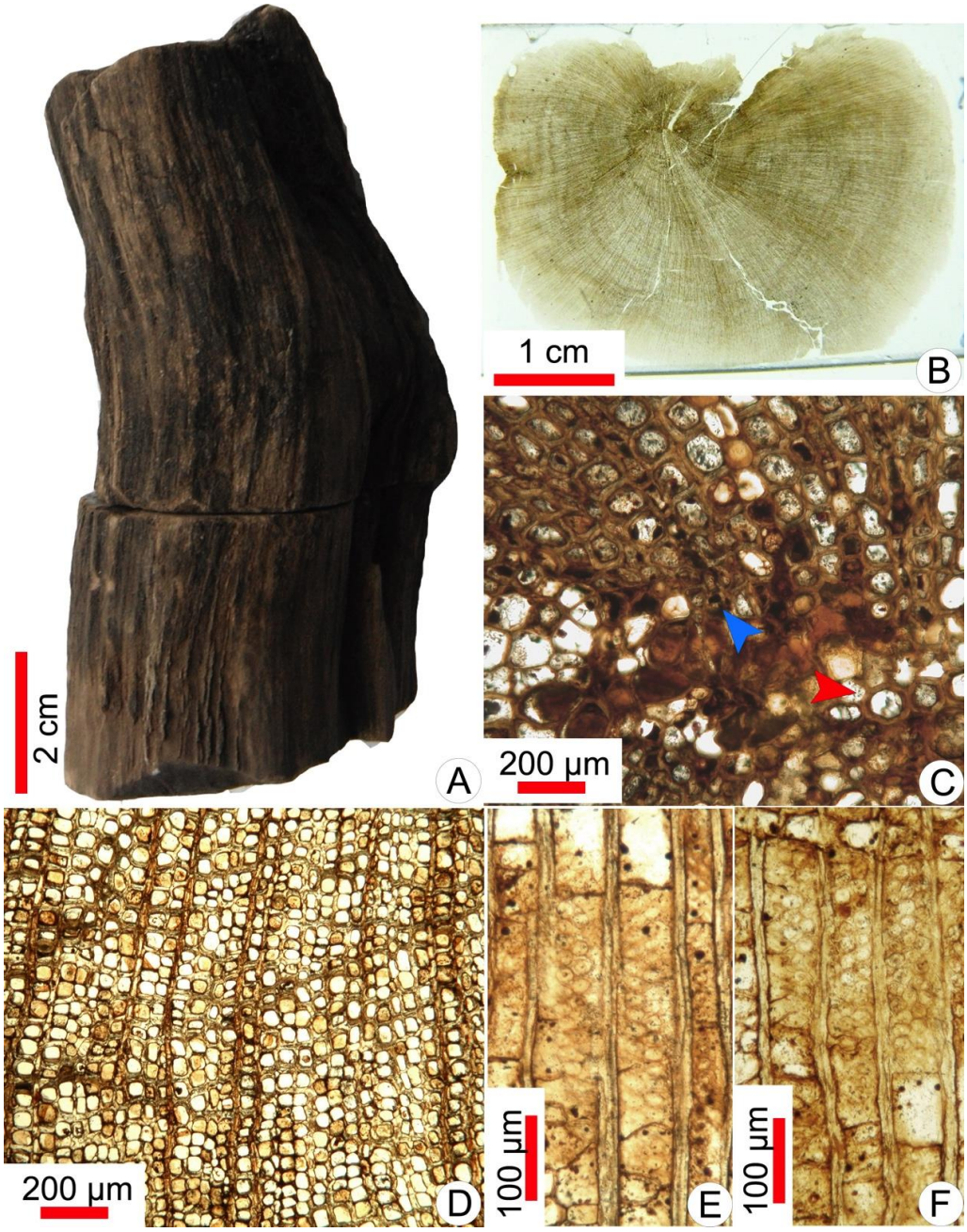

Figure 3-13 *Junggaropitys dalongkouensis* from the Guodikeng Formation A. General view of the specimen XTT-C-16; B. Transverse section (TS) showing the overview of the pith, primary xylem and secondary xylem. Slide no. XTT-C-16a1; C. TS showing the homogenous pith and the endarch primary xylem (red arrows) in the pith periphery. Slide no. XTT-C-16a1; D. TS showing the tracheids in the secondary xylem. Slide no. XTT-C-16a1; E, F: Radial section showing the uniseriate

to triseriate araucarian pits on the tracheid wall. Slide no. XTT-C-16b1.

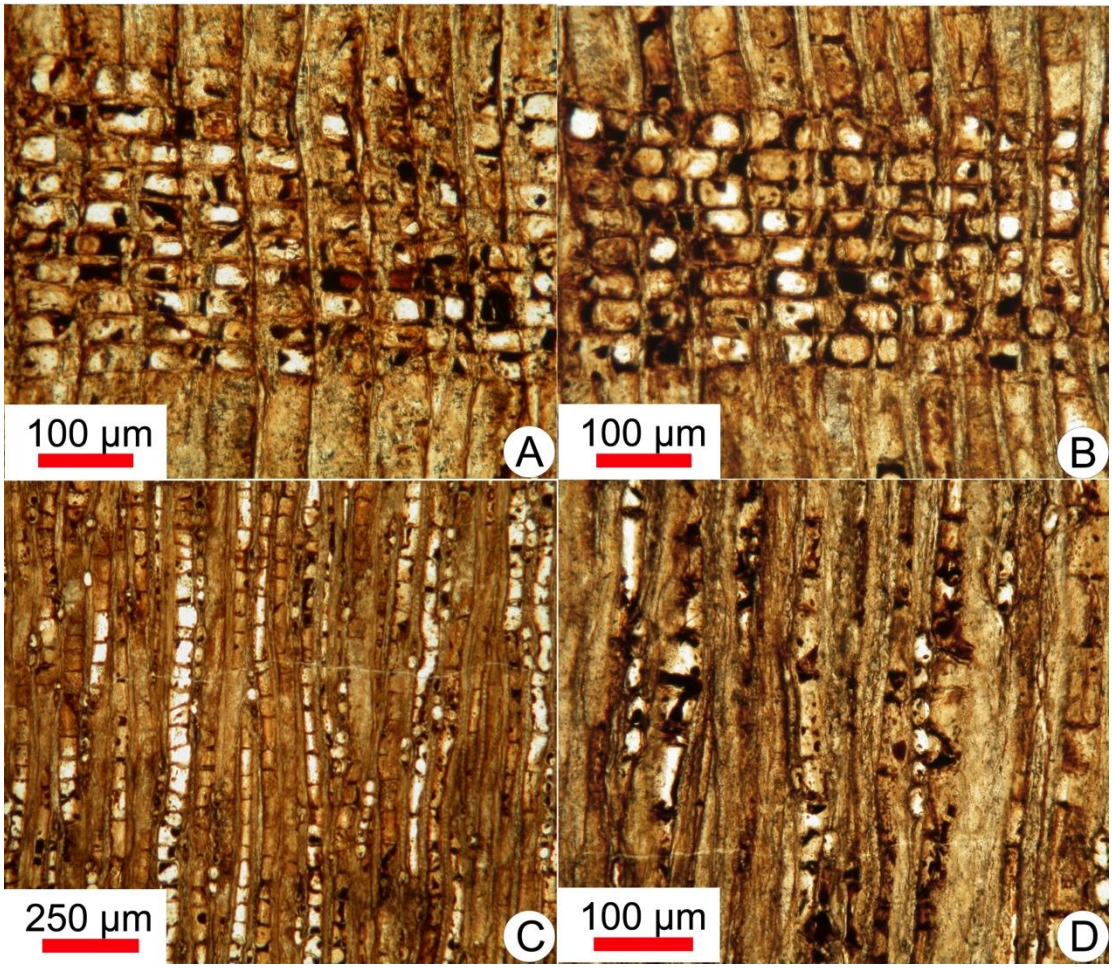

Figure 3-14 *Junggaropitys dalongkouensis* A, B. Radial section showing 1, occasionally 2 oblique oval or window-like pits in each cross-field. Slide no. XTT-C-16b1. C. Tangential longitudinal section (TLS) showing the homogeneous, uniseriate, low rays. Slide no. XTT-C-16c1. TLS showing the details of the ray cells. Slide no. XTT-C-16c1.

In this specimen, abundant tyloses were preserved in the tracheids. A tylosis is a growth from a neighbouring wood ray cell or, more rarely, a parenchyma cell through the pit of a tracheid (or vessel) wall, which causes the partial or entire obstruction of the tracheid (or vessel) lumen. Tyloses may occur in small numbers or, due to division, they may be numerous, thin-walled or thick-walled, with pits or without. They may contain starch, crystals, resin or gum (Zürcher et al., 1985).

In the secondary xylem, tylose-filled tracheids mainly occur along ray cells (Fig. 3-15A). Some tylose-filled tracheids are irregularly present among the ray cells. The zones of tylose-free tracheid appear much brighter in transmitted light than the intercalated tracheid zones that are filled with tyloses. Within the tracheids, single tyloses are observed in the transverse section; they show more or less rounded outlines, with 1 to 3 μm thick walls. In most cases, they occupy the entire tracheid liminae. Sometimes they are balloon-shaped and protrude from the ray cells through the pits (Fig. 3-15B, C, D).

Longitudinal sections of the secondary xylem show tyloses in the tracheids in both the radial and tangential views. The well-developed tyloses occupy the entire width of the tracheids. The walls of tyloses are septum-like inside the tracheids. They are very thin membrane-like structures, dividing the tracheid lumen into irregular chambers (Fig. 3-15E, F; Fig. 3-16D). Fungal remains can be observed in the chambers. These may represent various types of fungi. They are mostly fragmentary, probably tubular, and range from 0.5 to 5 μm in diameter. In most cases they are opaque and dark in colour. They are commonly characterised by repeatedly branched hyphae. These hyphae develop in one chamber (Fig. 3-15E, F; Fig. 3-16B, D) or penetrate the tylosis walls, develop in different chambers (Fig. 3-16A, C, D).

The walls of tyloses are in horizontal, oblique, convex or concave forms. Tangential sections also show that tyloses protruding from the ray cells (Fig. 3-16E, F). Ray cells and tyloses commonly contain amorphous black substances. The dimension and shape of the ray cells that produce tylose are no different from the non-tylose-producing ray cells.

Abundant tylosis formations were found in the secondary xylem of the fossil woods from Late Permian Turpan Basin, not only in *Junggaropitys*, but also in *Septmedullopitys* and XTT-C-4 gen. nov..

The tylosis formation may be trigged by various kinds of heterogeneity in both abiotic and biotic stimuli, including mechanical injuries, infection by pathogenic microorganisms (Biggs, 1987; Pearce, 1990), natural senescence (Dute et al., 1999), heartwood formation (Chattaway, 1949; Meyer, 1967; Panshin and DeZeeuw, 1980; Parameswaran et al., 1985; Wilson and White, 1986), frost (Cochard and Tyree, 1990) and flooding (Davison and Tay, 1985).

The development of tyloses has been regarded as a normal physiological process marking the transformation from sapwood to heartwood in the heartwood of angiosperms (Leitch et al., 1999). But this specimen represents a young branch; the tylose-filled tracheids were widely distributed in the secondary xylem. In other specimens from Late Permian Turpan Basin, the tylose-filled tracheids occur from the innermost heartwood through the outermost of sapwood. Therefore, it is highly unlikely that the tylosis formation in our specimens corresponding to heartwood formation.

Tyloses serve to seal off damaged or infected wood areas, and to limit or retard further spreading of pathogenic agents, including wood-rotting fungi (Chrysler, 1908; Yamada, 2001). It has been shown that once a fungal pathogen has invaded the wood, tyloses can be produced in areas of wood not yet infected (Talboys, 1964). It therefore appears possible that the prominent tylosis formation in the fossil woods was a response to fungal infection of a wood-rot fungus and served to build up mechanical barriers against the advancing hyphae.

Some fungal hyphae penetrated into the tyloses. It may indicate that these fungi were capable of producing such degradational enzymes in order to break down the wall of the tyloses and thus surmount the defense mechanism of the plant.

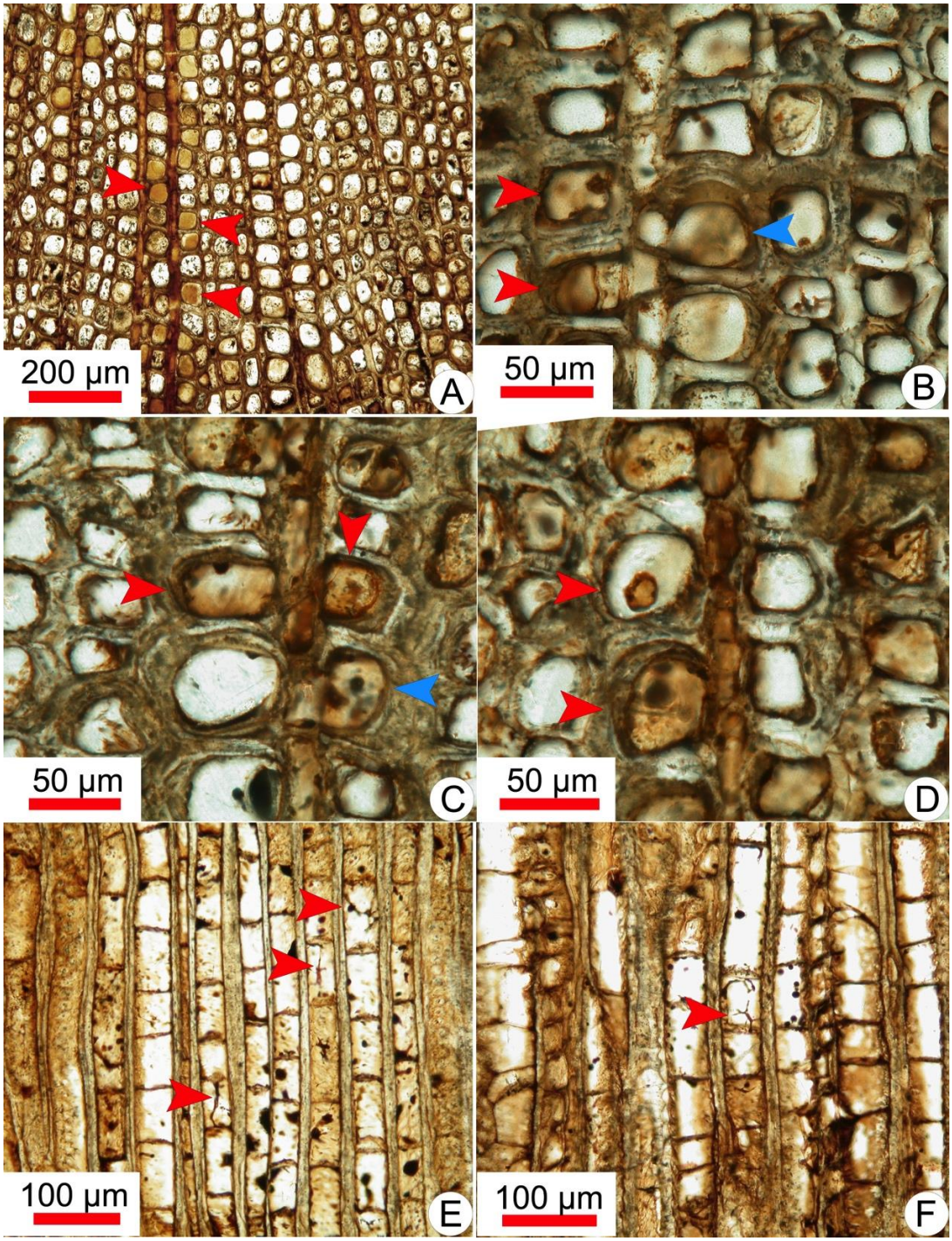

Figure 3-15 *Junggaropitys dalongkouensis* from the Guodikeng Formation A. Transverse section (TS) of the secondary xylem showing the tylose-filled tracheids occurring along ray cells (red arrows). Slide no. XTT-C-6a1. B, C, D. TS showing close-up of the tylose-filled tracheids (arrows). The blue arrows indicate the tyloses protruding from the ray cells through the pits. Slide no. XTT-C-6a1. E, F. Radial section showing the septum-like tyloses in the tracheids. The arrows indicate the fungal hyphae in chambers. Slide no. XTT-C-6b1.

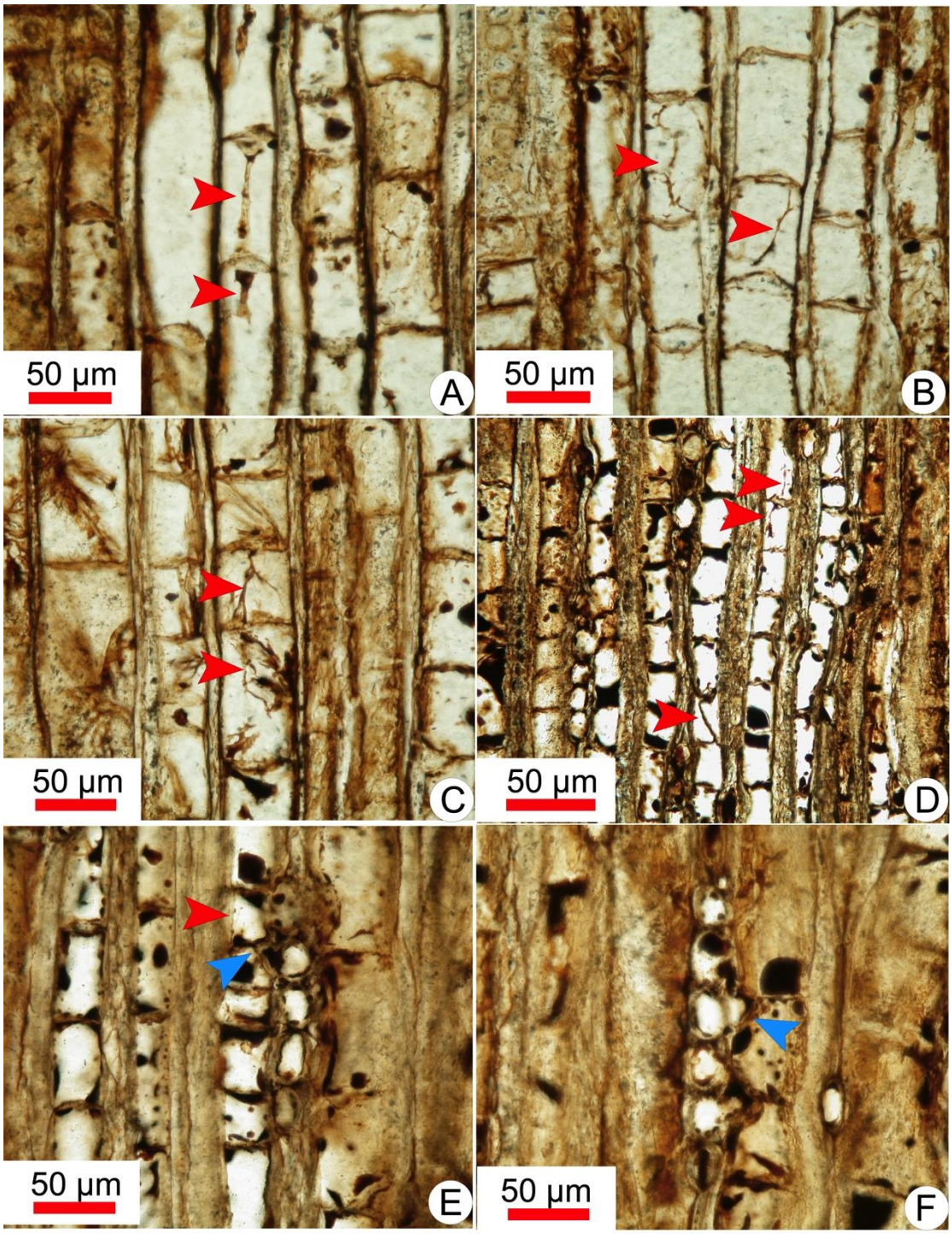

Figure 3-16 *Junggaropitys dalongkouensis* from the Late Permian-Early Triassic Guodikeng Formation A, B, C. Radial section showing the septum-like tyloses and the fungal hyphae (arrows). Some fungal hyphae penetrate the tylosis walls. Slide no. XTT-C-16b1. D. Tangential section showing the septum-like tyloses and the fungal hyphae (arrows). Slide no. XTT-C-16c1. E, F. Tangential section showing the thylosis formations protruding from the ray cells (blue arrows) and well-developed tylosis (red arrow). Slide no. XTT-C-16c1.

Genus: *Septomedullopitys* Wan, Yang et Wang, 2014

***Septomedullopitys szei* Wan, Yang et Wang, 2014**

Description:

The specimen XTT-A-2 has been broken into several pieces due to weathering. The original length was about 40 cm. A well-preserved block about 9.3 × 12.1 cm in size shows an oval outline with a large pith in the thick xylem cylinder (Fig. 3-17A). The cortex and epidermal structure are not persevered.

The specimen shows a large, septate and heterocellular pith. The sub-circular pith**,** about 2.5 cm in diameter**,** consists of parenchyma cells, sclerenchyma-like cells and secretory cells (Fig. 3-17B, 3-19A) Four slides along the transverse and radial directions of the pith were made. In transverse views, the parenchyma cells are circular or polygonal, 60 to 175 μm (mean = 117.5 μm) in diameter (Fig. 3-19B). Intercellular spaces are visible (Fig. 3-19B). In radial section, the parenchyma cells are rectangular to polygonal, regularly arrange, 30 to 145 μm (mean = 78.9 μm) in height (Fig. 3-19E). The pith is separated by horizontally distributed septa. They are 25 to 200 μm high (Fig. 3-18A). In some areas, the parenchyma cells are solid (Fig. 3-18B, 3-20B).

In the transverse section, the sclerenchyma-like cells are sub-rectangular, 22.5 × 35 to 60 × 70 μm (height × width) in size (Fig. 3-19C). They regularly arrange and form irregular bands. In the slides, one or two bands can be observed. The width of the bands is 0.25 to 0.6 mm and reduces on the periphery of the pith. The bands disappear in the primary xylem or the initial secondary xylem (Fig. 3-17B). Sometimes, they are branched (Fig. 3-19A). In the radial section, the bands are nearly vertical (Fig. 3-18A). The sclerenchyma-like cells are rectangular with 2.5 to 5 μm thick walls (Fig. 3-20A).

In the transverse section, the circular or polygonal secretory cells consist of two layers–the light coloured external and the darker inner. The cell wall is transparent. The diameter is 60 to 135 μm (mean = 88.5 μm) (Fig. 3-19D). In the radial section, they are linear, 0.98 to 1.56 mm long (Fig. 3-19F).

Some lining-like structures, corresponding to the white rot, are in the parenchyma cells or cavities.

The primary strands show endarch maturation (Fig. 3-20C). The primary xylem tracheids with annual, helical, scalariform or reticulate thickenings are 8 to 22 μm in diameter (Fig. 3-20D).

The secondary xylem consists of tracheids and parenchymatous rays. Growth rings are indistinct (Fig. 3-20E). Tracheids are circular or oval, diameter 16 to 38 μm in transverse section. The pits on the tracheid walls are of araucarioid type. The pits are usually uniseriate to triseriate, when close to the pith, up to pentaseriate. When uniseriate, the pits are contiguous, circular or flattened (flattening index ≥ 0.47), ca. 5 μm from the tracheid internal walls; when multiseriate, pits are alternate, crowded hexagonal or oval (flattening index = 0.43–0.69), close to the internal wall of tracheid. They are 10 to 22.5 μm (mean = 15.7 μm) in diameter, with circular apertures (Fig. 3-20F, 3-21A). Helical cracks often occur on the tracheid walls.

Cross-field pits are rectangular to oblique oval, sometimes circular. They are simple, sometimes slightly areolate, and 12 × 15 to 32 × 45 μm in size. There is 1, partly 2 pits in each cross-field unit (Fig. 3-21B). When close to the pith, more units have 2 pits.

In tangential views, the uniseriate rays consist of circular, elliptical or rectangular parenchyma cells. They are 1–15 (> 90%), up to 29, cells high (20-900 μm). Ray cells are

15.5 × 20 to 27.5 × 37.5 μm in size in tangential views (Fig. 3-21C). The tracheids are septate with numerous tylosis. These tylosis originate from ray cells (Fig. 3-21D).

Axial parenchyma cells and resin canals are absent.

Locality and Horizon

Taoshuyuan A Section, Turpan, Xinjiang; Late Permian Wutonggou Formation.

Sample Number

XTT–A–2

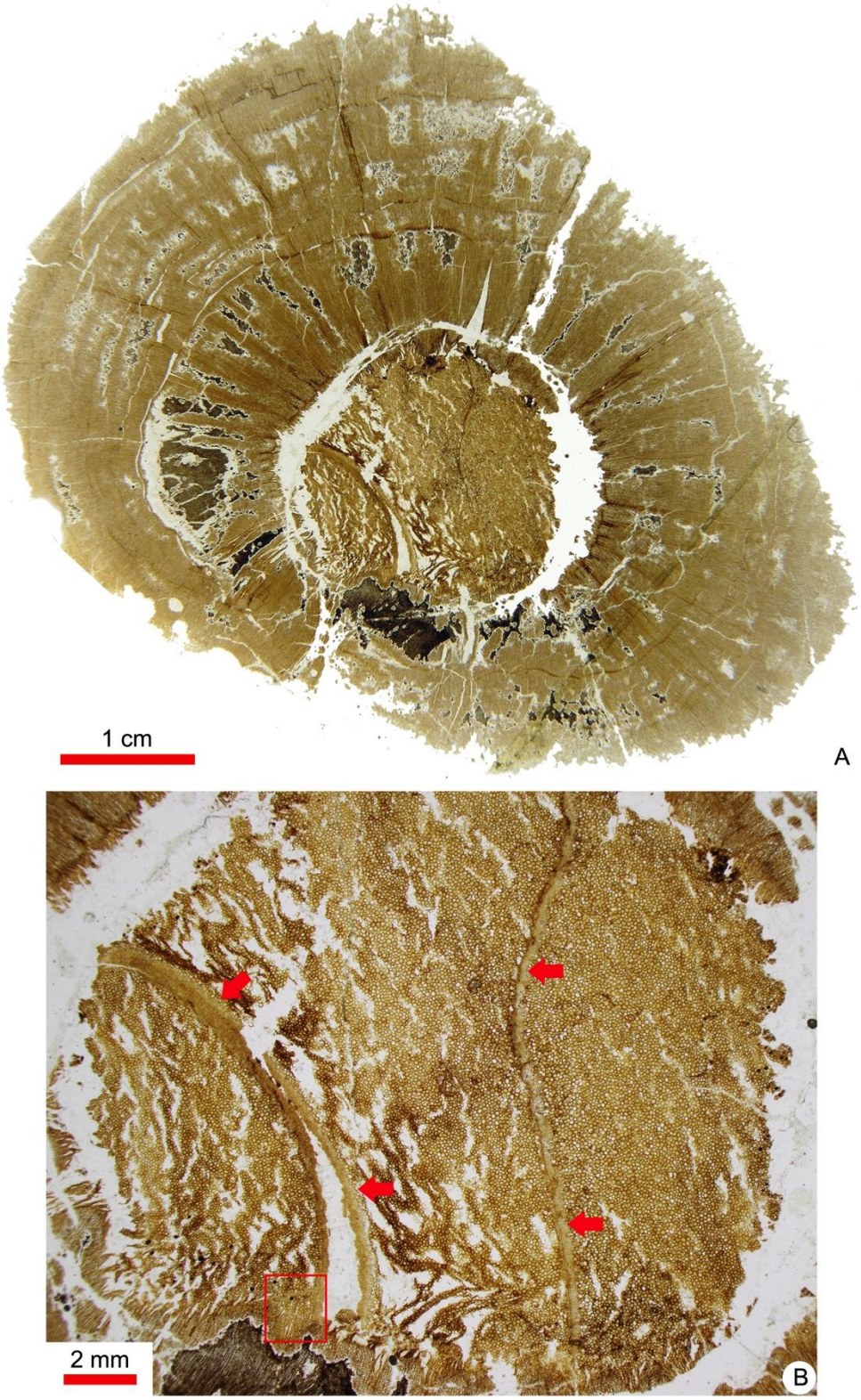

Figure 3-17 *Septomedullopitys szei* A. Transverse section (TS) showing the overview of the pith, primary xylem and secondary xylem. Slide no. XTT–A–2a1. B. Close-up of the pith. Arrows indicate the bands in the pith. Slide no. XTT–A–2a1.

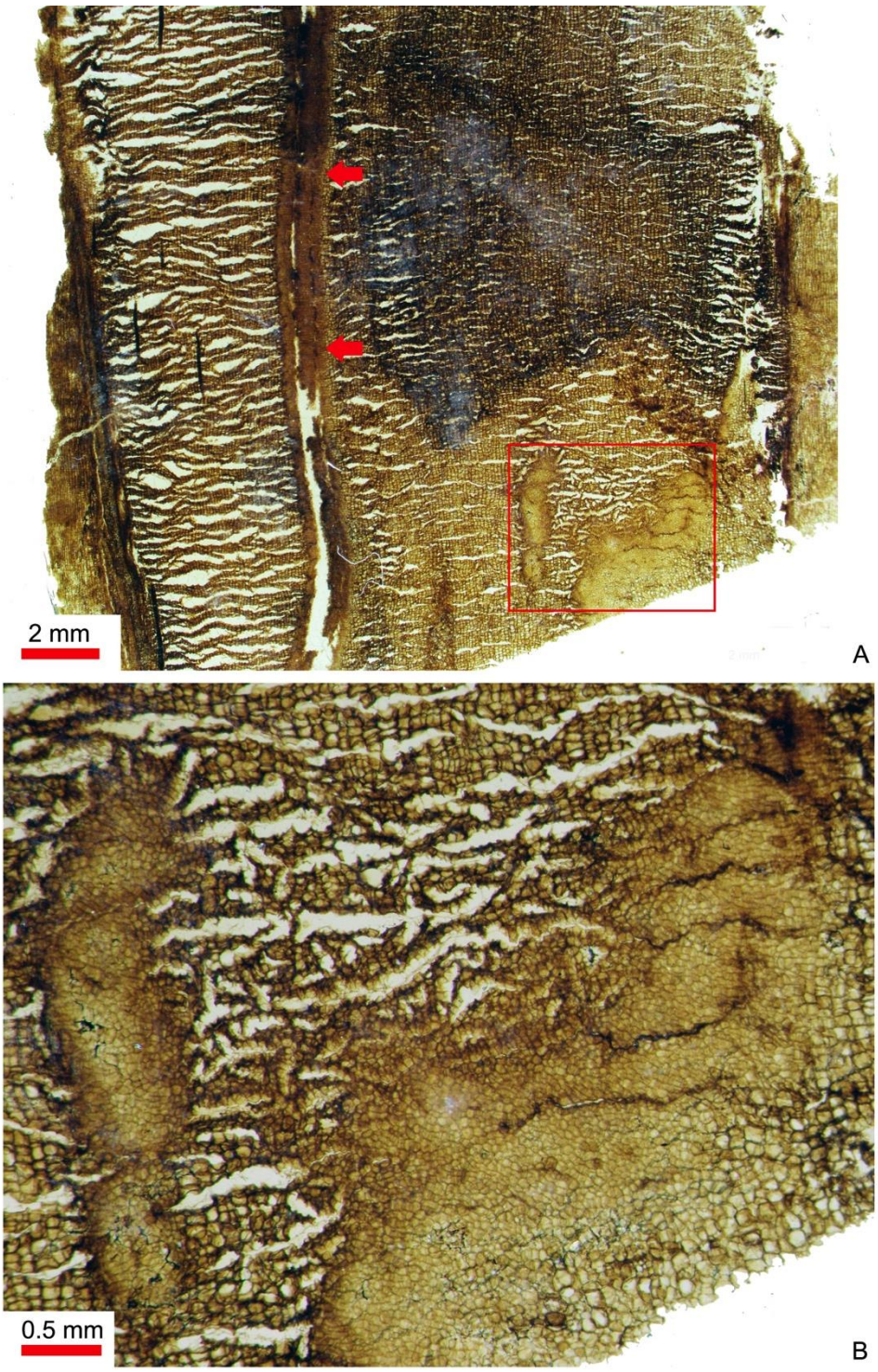

Figure 3-18 *Septomedullopitys szei* A. Radial section showing the overview of the pith. Slide no. XTT–A–2b1. B. Close-up of the box in the picture A (Radial section). The solid parenchyma cells in the pith. Slide no. XTT–A–2b1.

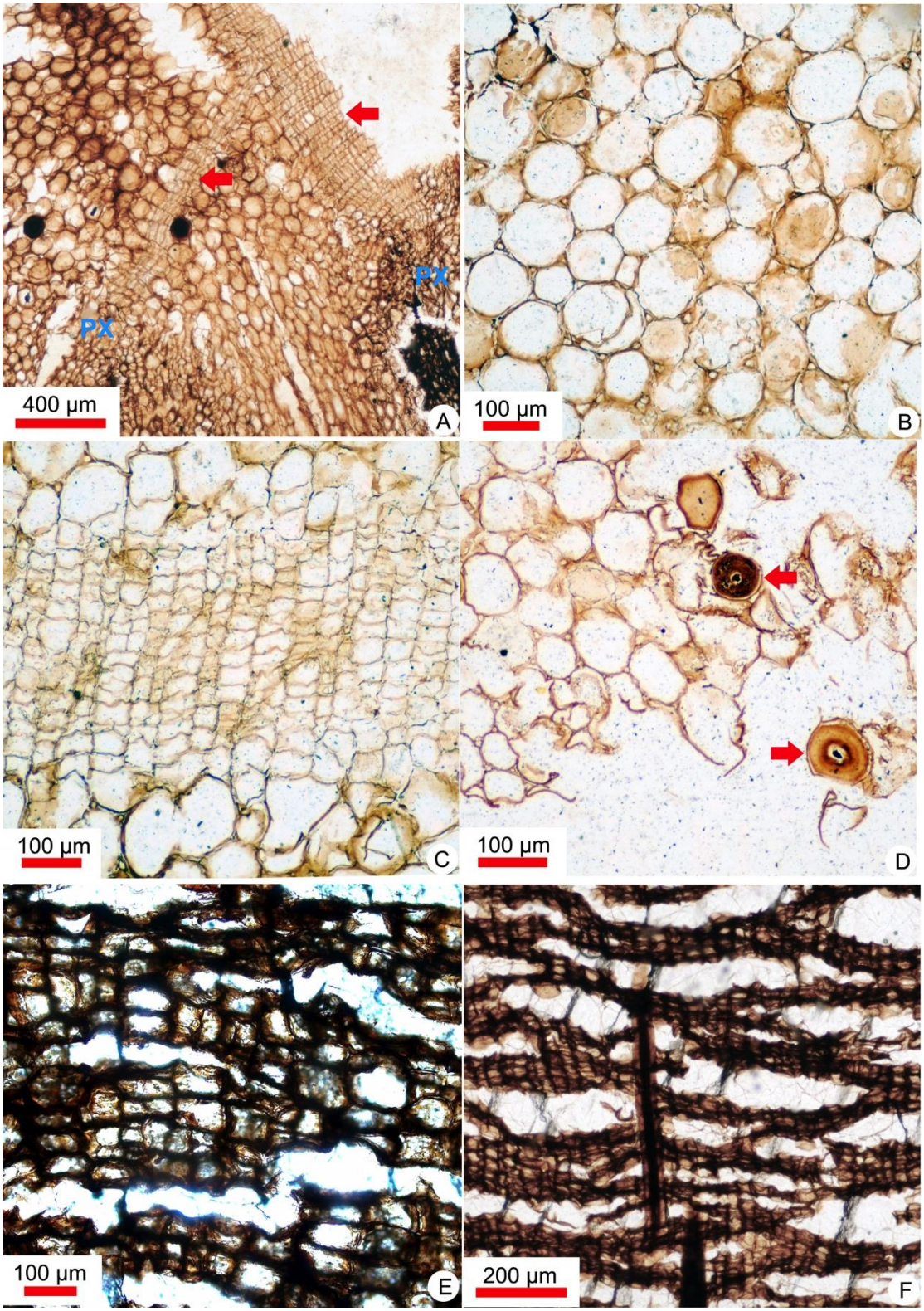

Figure 3-19 *Septomedullopitys szei* A. Close-up of the pith and primary xylem (PX). Arrows indicate the bands in the pith (Transverse section (TS)). Slide no. XTT–A–2a1. B. TS showing the parenchyma cells and intercellular spaces in the pith. Slide no. XTT–A–2a2. C. The close-up of the band in the pith. Slide no. XTT–A–2a2. D. TS showing the secretory ducts in the pith (arrows). Slide no. XTT–A–2a2. E. Radial section (RS) showing the parenchyma cells in the pith. Slide no. XTT–A–2b1. F. RS showing the secretory ducts in the pith. Slide no. XTT–A–2b1.

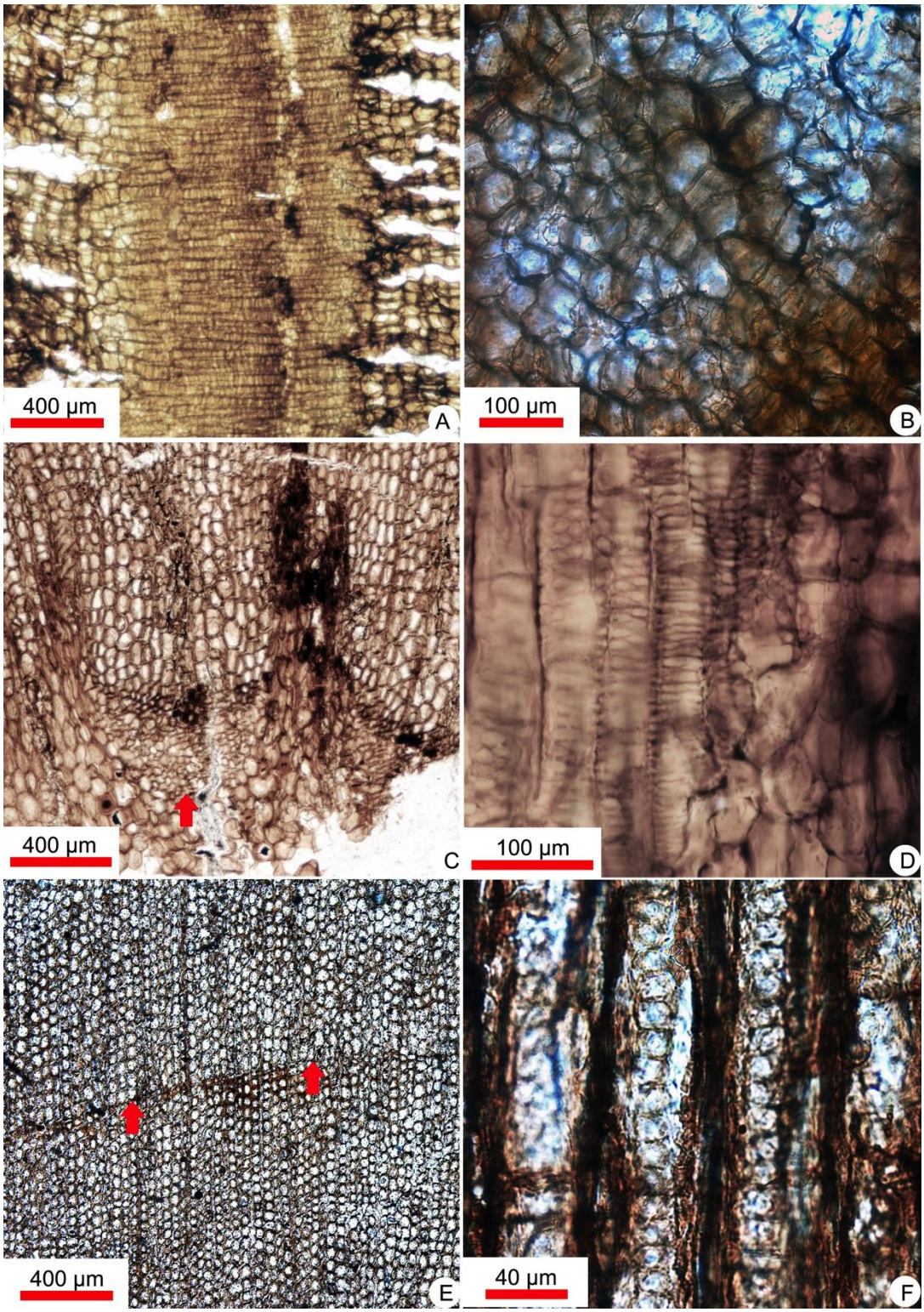

Figure 3-20 *Septomedullopitys szei* A. Close-up of the bands in the pith (radial section (RS)). Slide number: XTT–A–2b1. B. The parenchyma cells in the area without septa (RS). Slide number: XTT–A–2b1. C. Transverse section (TS) showing the endarch primary xylem (arrow) on the pith periphery. Slide number: XTT-A-2a1. D. RS showing the helical and reticulate thickenings of the tracheids of primary xylem. Slide number: XTT-A–2b1. E. TS showing the growth-ring boundary (arrows) in the secondary xylem. Slide number: XTT-A-2a1. F. RS showing the uniseriate radial pits on the tracheid walls. Slide number: XTT-A–2b1.

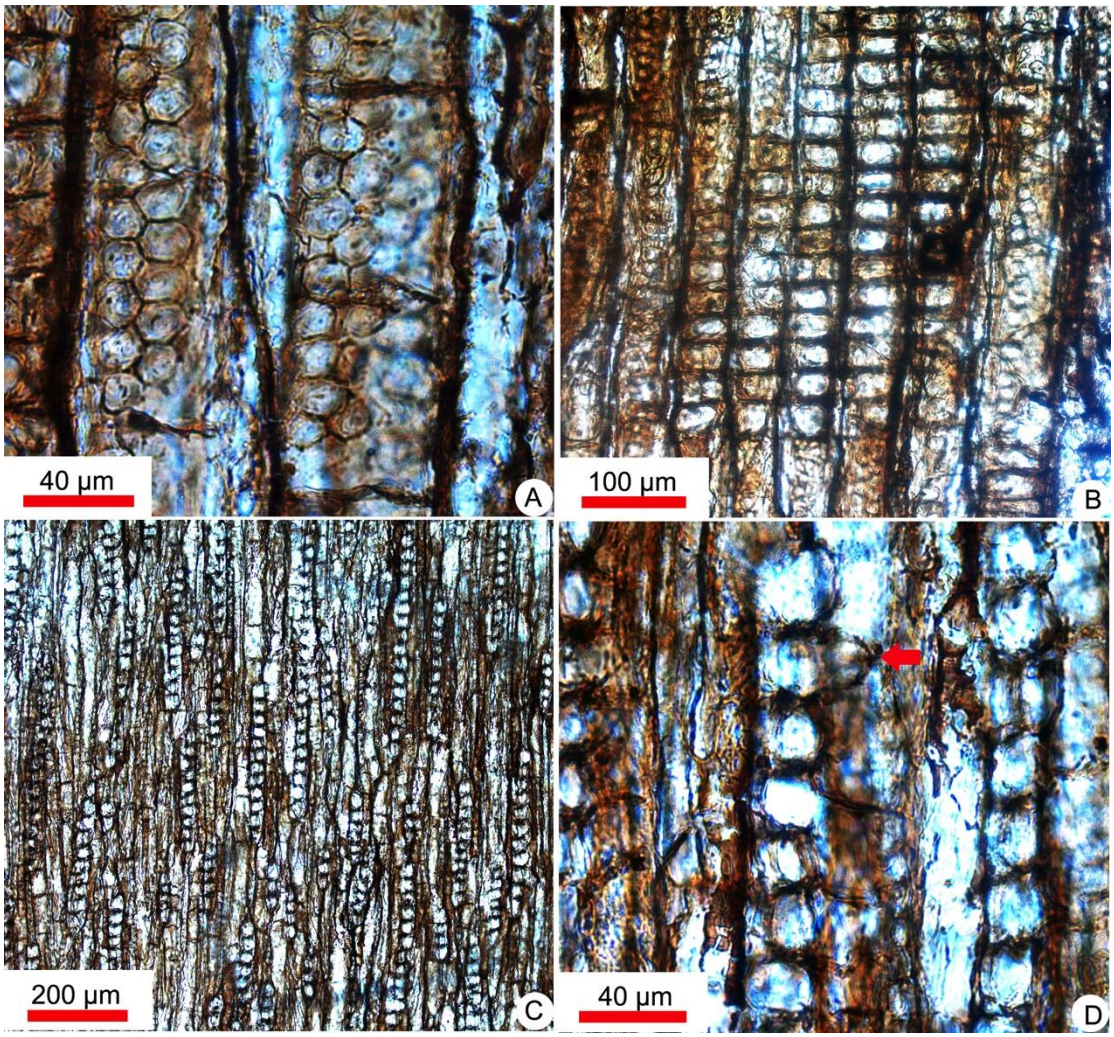

Figure 3-21 *Septomedullopitys szei* A. Radial section (RS) showing the biseriate and triseriate radial pits on the tracheid walls. Slide no. XTT–A–2b1. B. RS showing one rectangular, ovoid or round simple cross-field pits in the branchlet. Slide no. XTT–A–2b3. C. Tangential section (TGS) showing the homogeneous, uniseriate or biseriate rays. Slide number: XTT–A–2c1. D. TGS showing the homogeneous rays. The red arrows indicate the tylosis protruding in the lumen of tracheids. Slide number: XTT–A–2c1.

Genus: *Xinjiangoxylon* Shi, Yu, Li, Chi et Zhang, 2014

This part has been published on the journal Acta Geologica Sinica (English Edition).

Diagnosis: Woody stem with pith, primary xylem and secondary xylem. Pith solid, nonseptate, heterocellular, with parenchyma cells and sclerenchyma cells. Primary xylem endarch. Secondary xylem pycnoxylic. Growth rings present. Tracheids with uni- to triseriate araucarioid pits. Cross-field pits window-like, simple. Ray cells homogeneous, parenchymatous. Axial parenchyma cells present. Resin canals absent.

***Xinjiangoxylon turpanense* Shi, Yu, Li, Chi et Zhang, 2014**

Diagnosis: Woody stem with pith, primary xylem and secondary xylem. Pith solid, nonseptate, heterocellular, with parenchyma cells, sclerenchyma cells. Sclerenchyma cells circular or polygonal in transverse section, longitudinal extension. Primary xylem endarch

with scalariform thickenings. Tracheids of the primary xylem with scalariform thickenings. Secondary xylem pycnoxylic. Growth rings present. Tracheids with uni- to triseriate araucarioid pits. Cross-fields with 1, partly 2 window-like simple pits. Rays homogeneous, parenchymatous and uniseriate, ranging from 1 to 16 cells in height. Longitudinally elongated axial parenchyma cells are irregularly distributed among the xylem tracheids. Resin canals absent.

Description:

General features

The stem piece with a piece of a branch is about 12 cm long, and a maximum diameter of 6cm. As not well preserved, it is deformed. It composes of the pith, primary xylem, secondary xylem and a branch trace (Fig. 3-22, A).

Pith

The pith is approximately oval in outline, about 3.0×1.0–3.7×1.2 cm in diameter, and consists of parenchyma cells and sclerenchyma cells (Fig. 3-22, B). In transverse section, parenchyma cells are circular or polygonal, diameter 12.5 to 150 μm (n=100, mean=91.5 μm) (Fig. 3-22, C). Sclerenchyma cells are circular or polygonal, 45 to 155 μm (n=100, mean=93.5 μm) in diameter (Fig. 3-22, C). They have thick brown walls with dark contents in their centers.

In radial view, the parenchyma cells are flat, sub-rectangular and horizontally aligned, high 27.5 to 80 μm (n=100, mean=47.6 μm) (Fig. 3-22, E). And the sclerenchyma cells are very long, 175 μm to 4.95 mm in length (Fig. 3-22, D).

Primary xylem

The primary strands show endarch maturation (Fig. 3-22, F). The tracheids of the primary xylem are scalariformly thickened (Fig. 3-23, B).

Secondary xylem

The secondary xylem is pycnoxylic. Growth rings are distinct (Fig. 3-23, A). Tracheids are rectangular or polygonal in transverse views, 12.5×15–37.5×62.5 μm in diameter (Fig. 3-23, A). In longitude section, the ends of the tracheids are blunt and erect. Araucarioid-type bordered pits are uni- to triseriate on radial walls of the tracheids. When uniseriate, the pits are contiguous, circular or elliptical; when biseriate, pits are alternate, crowded hexagonal (Fig. 3-23, C&D). The pits are 10 to 15 μm in diameter, with circular apertures.

Rays are homogeneous, parenchymatous and uniseriate. Ray parenchyma cells are circular, oval or rectangular, uniseriate, high 5 to 37.5 μm, and wide 5 to 25 μm in tangential views (Fig. 3-23, H). Ray height is from 1 to 16 cells (P95≤9, n=200, mean=4.65) (Fig. 3-24).

Cross-field pits are windows-like. There is 1, partly 2 pits in each cross-field unit (Fig. 3-23, F&G). Isolated or vertically aligned axial parenchyma cells are longitudinally elongated and distributed among the xylem tracheids (Fig. 3-23, E).

Discussion: This petrified stem shares anatomical features with fossil and extant gymnospermous. The taxa cordaitalean always possess septate pith, that is different from *Xingjiangoxylon* (Falcon-Lang and Scott, 2000). Fossil ginkgophyte woods have complex piths and abundant axial parenchyma cells in the secondary xylem. The ends of the ginkgophyte tracheids are always bent, which is not seen in present specimen. Therefore, we tentatively attribute *Xingjiangoxylon* to a possible coniferous affinity.

In China, several previously documented fossil gymnospermous woods show a heterogeneous pith, such as *Guizhouoxylon dahebianense* Tian et Li, 1992 (Tian and Li, 1992), *Walchiopremnon gaoi* Tian, Hu et Zhao, 1996 (Tian et al., 1996), *Damudoxylon zhoui* Zhang et Zheng, 2006 (Zhang et al., 2006a)， *Liaoningoxylon chaoyangense* Zhang et Zheng, 2006 (Zhang et al., 2006a), *Sclerospiroxylon neimongolense* Zhang, Zheng,Wang, Yang, Li, Fu et Li, 2007 (Zhang et al., 2007), *Shenoxylon mirabile* Feng, Wang et Rößler, 2011 (Feng et al.， 2011).

The pith of *Guizhouoxylon dahebianense* consists of parenchyma cells, sclerenchyma cells and secretory cells. And all the cells in pith are longitudinal, which is different from the present wood. Besides, each cross-field unit has 3 to 8 pits and tracheids in the early wood zones are scalariformly thickened (Tian and Li, 1992), these all differ from *Xingjiangoxylon* .

The pith of *Walchiopremnon gaoi*, 1996 is similar to the new genus. But pits on the walls of secondary xylem tracheids are uniseriate (occasionally biseriate), and the 1 to 3 or more simple or cupressiod pits are in each cross-field unit, which are different from *Xingjiangoxylon* (Tian et al., 1996).

Liaoningoxylon chaoyangense possesses parenchyma cells and secretory ducts in its pith as well. Without axial parenchyma cells in the secondary xylem (Zhang et al., 2006a), *Liaoningoxylon* is different from the present specimen. Another important feature that rays in *Liaoningoxylon* are heterocellular cannot be seen in *Xingjiangoxylon.*

The pith of *Damudoxylon* consists of parenchyma cells and secretory cells. However, the pits in each cross-field unit are small and many (Maheshwari, 1966; Zhang et al., 2006a). That are different from *Xingjiangoxylon*.

Sclerospiroxylon neimongolense differs from *Xingjiangoxylon* the tertiary spiral thickening on its secondary xylem tracheids and cupressiod cross-field pits(Zhang et al., 2007).

Shenoxylon mirabile is characterized by the intramedullary sheath, and its cross-field pits are cupressoid (Feng et al., 2011). These make it different from *Xingjiangoxylon.*

Medullopitys, *Phyllocladopitys*, *Medulloxylon*, *Septomedullopitys* were established from the Permian of Africa, for the woods with *Phyllocladoxylon*-type secondary xylem and heterogeneous pith (Lepekhina, 1972). The secondary xylem of *Xingjiangoxylon* is similar to *Phyllocladoxylon*, but *Xingjiangoxylon* possesses abundant axial parenchyma cells. Besides, *Medullopitys* and *Medulloxylon* have special short secretory canals in their pith, which differs from *Xingjiangoxylon*. The pith of *Septomedullopitys* possesses branched secretory canals, and *Phyllocladopitys* is mesarch or exarch. They are different from *Xingjiangoxylon* as well.

The pith of *Megaporoxylon* is homogeneous or heterogeneous. One or two simple pits are in each cross-field unit, which is similar to *Xingjiangoxylon.* However there are multiseriate pits on the walls of secondary xylem tracheids and rays are multiseriate (Maheshwari, 1972). These make *Megaporoxylon* different from the new genus (Maheshwari, 1972).

Locality and Horizon

Taoshuyuan C Section, Turpan, Xinjiang; Early Triassic Guodikeng Formation. (The age was revised, section 2.6.2)

Sample Number

XTT-C-5

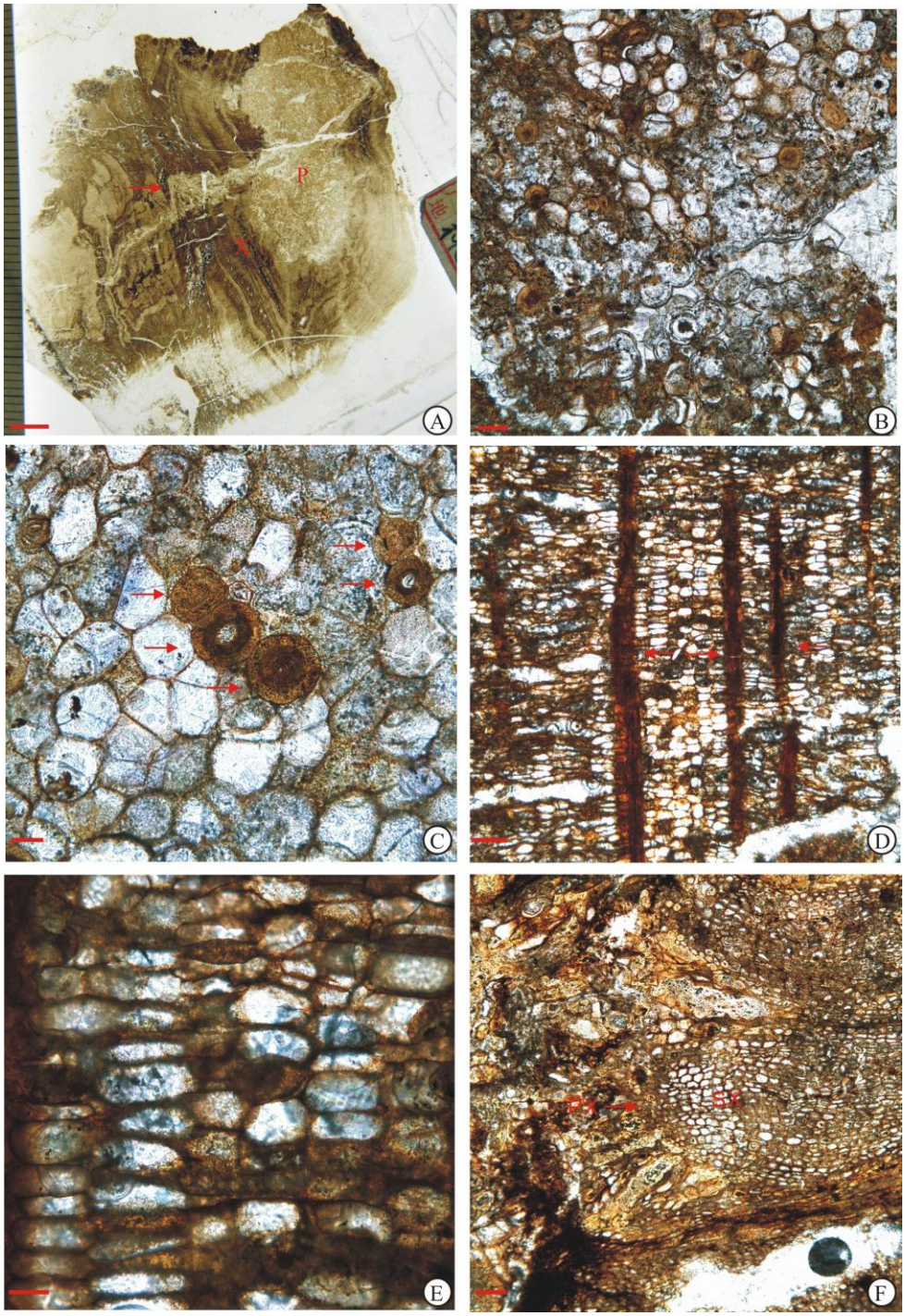

Figure 3-22 *Xinjiangoxylon turpanense* A. Transverse section (TS), showing the pith (P), xylem cylinder (X) and a branch trace (arrow), scale bar =0.5 cm; B. TS, showing the parenchyma cells and sclerenchyma cells, scale bar =100 μm; C. Radial longitudinal section (RLS), showing the sclerenchyma cells (arrows), scale bar =50 μm; D. TS, showing the sclerenchyma cells (arrows), scale bar =50 μm; E.RLS, showing the parenchyma cells of the pith, scale bar =50 μm; F. TS, showing the primary xylem (PX) and secondary xylem (SX), scale bar =100 μm;

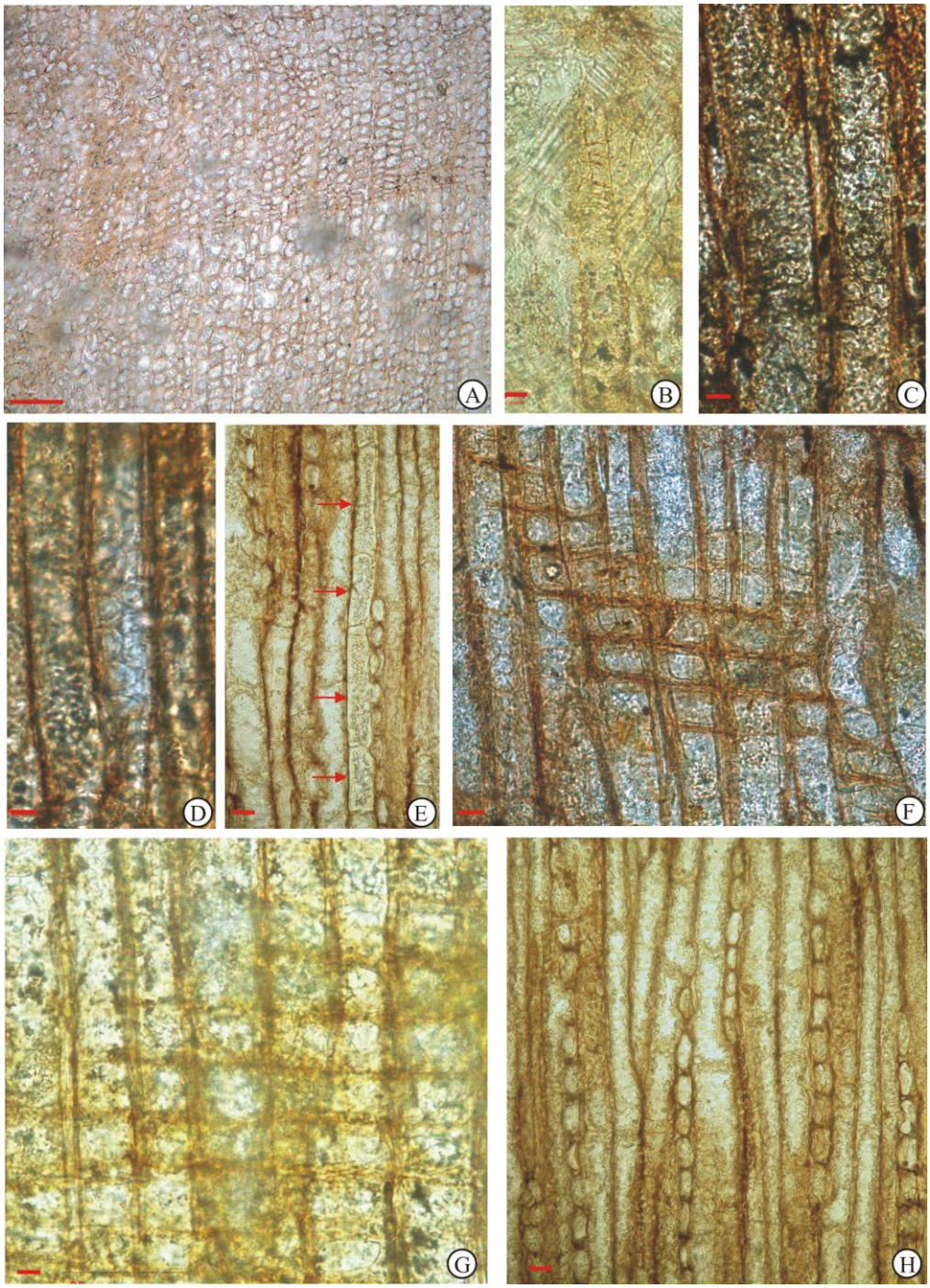

Figure 3-23 *Xinjiangoxylon turpanense* A. Transverse section (TS), showing a growth ring, scale bar =100 μm; B. Radial longitudinal section (RLS), showing the scalariform thickenings of the primary xylem tracheid, scale bar =10 μm; C. RLS, showing the biseriate or triseriate bordered pits on the radial wall of tracheids, scale bar =10 μm; D. RLS, showing the biseriate bordered pits on the radial wall of tracheids, scale bar =10 μm; E. Tangential longitudinal section (TLS), showing vertically aligned axial parenchyma cells (arrows), scale bar =20 μm; F&G. RLS, showing the window-like cross-field pits, scale bar =10 μm; H. TLS, showing the unseriate rays, scale bar =20 μm.

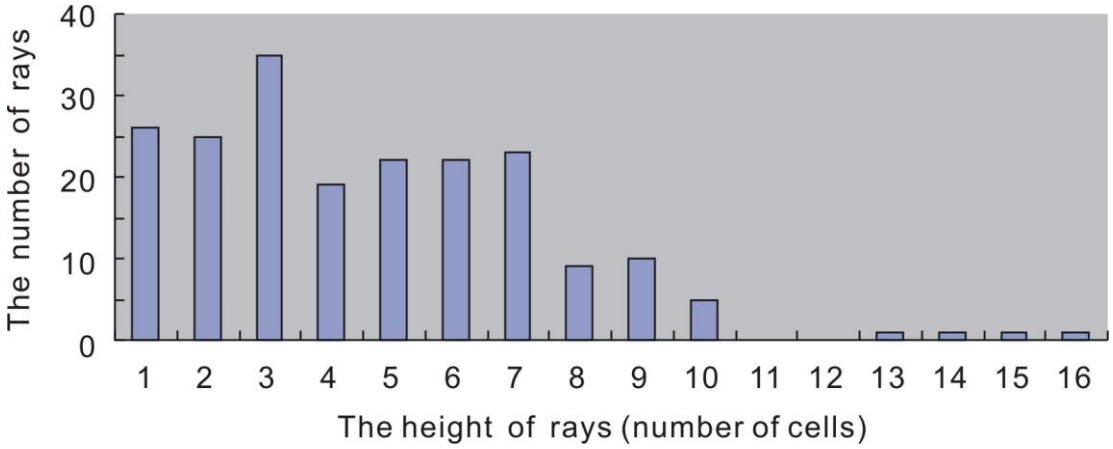

Figure 3-24 Histogram showing the height-frequency distribution of 200 rays in tangential longitudinal section of Xinjiangoxylon turpanense

Genus: XTT-C-4 gen. nov.

The manuscript that described these new genus and species has been submitted to the journal Palaeogeography, Palaeoclimatology, Palaeogeography (Elsevier) for validation of these taxa, but it is still "under editor's evaluation".

Diagnosis: Pith heterogeneous with parenchyma cells and supporting diaphragms. Primary xylem endarch. Tracheids in primary xylem with annular, helical and reticulate thickenings. Secondary xylem homoxylic, with indistinct growth rings. Tracheids with araucarian pits. Xylem rays uniseriate or biseriate, homogeneous. Cross-fields with rectangular, oval or round, simple, sometimes slightly areolate pits. Vertical parenchyma cells and secretory cells absent.

XTT-C-4 gen. et sp. nov.

Diagnosis: Pith heterogeneous with parenchyma cells and supporting diaphragms. Diaphragms consist of brick-like sclerenchyma cells. Sclerenchyma cells vertically regularly aligned. Primary xylem endarch. Tracheids in primary xylem with annular, helical and reticulate thickenings. Secondary xylem homoxylic, with indistinct growth rings. Tracheids with uni- to triseriate araucarian pits. Xylem rays uniseriate (rarely biseriate), homogeneous, 1–40 cells high. Cross-fields with 1 (up to 3), rectangular, oval or round, simple, sometimes slightly areolate pits. Vertical parenchyma cells and secretory cells absent.

Description:

The calcified fossil wood piece is about 12.5 cm long with a maximum diameter of 9.0 cm (Fig. 3-25A). Interestingly, a young lateral branchlet emerges horizontally from the main branch (Fig. 3-25B, C). No cortical tissues are preserved. The pith was preserved only in the branchlet. In the branch, it is impossible to get any slides of the pith. Several leaf traces, helically arranged, occur in the secondary xylem of the branchlet (Fig. 3-25C, E). This leave phyllotaxy is consistent with an evergreen characteristic for this species.

Pith

The pith is circular in outline. Along the direction of the branchlet extension, the pith diameter increases from 0.6 to 1.65 cm (L=5.5 cm) (Fig. 3-26A). Two slides along the

transversal direction and two slides along the radial direction were made. The pith of the branchlet is heterogeneous. It consists of parenchyma cells and diaphragms made of sclerenchyma-like cells. The parenchyma cells are isodiametric, circular or polygonal in transverse section, diameter 25 to 152.5 μm (Fig. 3-25D). The wall is mean 2.4 μm thick. Some cell walls are dark brown. Intercellular spaces are visible.

Seven complete diaphragms can be observed in the present specimen (Fig. 3-26A). In the radial section, the diaphragms are lense-like (Fig. 3-26A, B). Two perpendicular radial sections of the pith indicate that these diaphragms are true platforms (Fig. 3-26C, D). The intact diaphragms are horizontal or slightly curved, but three incomplete diaphragms at the top of the branchlet appear bent (Fig. 3-26A). Their thickness decreases gradually from the middle part of the pith to the periphery and reduces to one or two cells at the contact with the primary xylem or the initial secondary xylem (Fig. 3-26E, F). The middle part of the diaphragm is 0.32 to 1.24 mm thick and only one or two cells thick at the peripheral ends.

The sclerenchyma cells of the diaphragms are brick-like. In radial section, the sclerenchyma cells are very close and vertically regularly arranged in lines. The intercellular spaces are absent. The sclerenchyma cells are ca. 7.5×29 to 40×76 μm in size with 2.5 to 15 μm thick walls (Fig. 3-27A). The pith cells display lining-like structures inside the cell lumens and the cell walls are separated in some area. These artifact structures are caused by white rot.

Primary xylem

The primary xylem shows endarch maturation (Fig. 3-27B). The primary xylem tracheids are ca. 17.5 to 25 μm wide and show annular, helical and reticulate thickenings (Fig. 3-27C).

Secondary xylem

The secondary xylem is pycnoxylic, with tracheids and parenchymatous rays. Eight growth rings were preserved in the transverse section of the main branch (Fig. 3-27D). Early wood tracheids are circular or polygonal, while late wood ones are elliptical or rectangular. The percentage of late wood is 8.79-19.57%. The tracheids are 16 to 66 μm in diameter. The lumens of some tracheids are fully filled by tyloses.

In the radial section, pits on the tracheid walls are of araucarian type. In the branchlet, they are uniseriate (24%) or biseriate (74%), occasionally triseriate (2%) (Fig. 6E, F), while in the main branch, they are uniseriate (60%) or biseriate (40%) (Fig. 3-28A). When uniseriate, the pits are contiguous, circular or flattened, 5-15 μm from the tracheid internal walls, and the flattening index is 0.58-0.95; when biseriate or triseriate, the pits are alternate, crowded hexagonal, close to the internal wall of the tracheids, and the flattening index is 0.63-0.96. Near to the pith, some opposite pits can be observed (<1%). The pits are 7.5 to 20 μm in diameter, with circular or elliptical apertures.

Cross-field pits are rectangular, oval or round. They are simple, sometimes slightly areolate. In the branchlet, there is 1 or 2, rarely 3, pits in each cross-field unit (Fig. 3-28B, C). In the main branch there is only one pit in each cross-field unit (Fig. 3-28D). The pits are 9×12 μm to 28×35 μm (width × height).

The information for the tangential view is based only on the main branch. The lumens of tracheids are secondarily septate by numerous tyloses originating from ray cells (Fig.

3-28F). The homogeneous rays consist of elliptical or sub-rectangular parenchyma cells. The horizontal and tangential ray walls are smooth. They are uniseriate, or very rarely biseriate (< 1%). Rays are constituted by 1–15 (> 90%), up to 40, cells (30–1110 μm) high (Fig. 3-28E). There are 35 rays per square millimetre. Ray cells are 12.5 to 27.5 μm wide, and 17.5 to 32.5 μm high. Vertical parenchyma cells and secretory canals are absent.

Locality and Horizon

Taoshuyuan C Section, Turpan, Xinjiang; Early Triassic Guodikeng Formation.

Sample Number

XTT-C-4

Comparisons

The anatomical features of XTT-C-4 gen. nov. closely resemble some extinct and extant conifers that also display a heterogeneous pith, endarch primary xylem and thick pycnoxylic secondary xylem. As the anatomy of the pith and primary xylem consitutes a critical criterion for the classification of gymnosperms woods (Lepekhina, 1972; Pant and Singh, 1987; Feng et al., 2011), we thus consider XTT-C-4 gen. nov. as a coniferophyte of uncertain systematic affinity.

XTT-C-4 gen. nov. possesses unique solid lenticular diaphragms in the pith. All the sclerenchyma cells of the diaphragms are morphologically different and smaller than the parenchyma cells and closely arranged without intercellular space. The sclerenchyma cell walls are thicker than that of parenchyma cell. Based on these characters, these diaphragms play clearly a role of support to the pith.

The secondary xylem of XTT-C-4 gen. nov. is identical to *Protophyllocladoxylon* Kräusel: (1) the presence of growth rings, (2) araucarian radial pitting of tracheids, (3) simple large oval or round cross-field pits, (4) the absence of axial parenchyma and resin canals, (5) unpitted ray walls. Five morphogenera of fossil woods with a *Protophyllocladoxylon*-type secondary xylem and different structures of pith and primary xylem have been documented as far as we know (Table 1). Among them, the pith of *Junggaropitys* Shi, Yu, Broutin and Pons, 2015 is homogeneous that is different from XTT-C-4 gen. nov.

Septomedullopitys Lepekhina 1972 was first found documented in Russia. *S. szei* Wan, Yang and Wang 2014 was first described in the Late Permian deposition of Turpan Basin. In the pith of *S. szei*, parenchymatous bands composed of closely arranged brick-like cells are observed. However, these bands are irregularly distributed in the pith,of *S. szei* which is different from the lenses-like diaphragms in the present specimen. Besides, the pith of *S. szei* is septate and heterocellular, long secretory ducts with dark contents being distributed throughout the pith. It differs from the pith of XTT-C-4 gen. nov. , which is solid and lacks secretory ducts.

Phyllocladopitys Kräusel, 1928 was first collected from southwest Africa. It possesses a *Protophyllocladoxylon*-type secondary xylem and homogeneous pith. However, the primary xylem of *Phyllocladopitys* is mesarch or exarch, compared to the endarch primary xylem of *Junggaropitys*.

Medullopitys Kräusel, 1928 and *Megaporoxylon* (Kräusel, 1956) were found in the Early Permian sequences in southwest Africa. They both possess large heterogeneous piths but without diaphragms, contrary to XTT-C-4 gen. nov.

Cordaixylon andresii Césari, Álvarez-Vázquez, Méndez-Bedia, Álvarez-Laó, Turrero and Arbizu, 2015 were documented from Pennsylvanian (Stephanian) outcrops at Arnao beach, Spain. It has a *Protophyllocladoxylon*-type secondary xylem, but its pith is homogeneous with isodiametric parenchyma cells and differs from the pith in XTT-C-4 gen. nov.

Austroscleromedulloxylon (Mussa, 1980) was erected as a genus based on samples from the Early Permian of Brazil (Mussa, 1980, 1986; Crisafulli, 1998). In its pith, the supporting sclerenchymatous diaphragms are present and display a very similar morphology to those of XTT-C-4 gen. nov. However, the secondary xylem of *Austroscleromedulloxylon* is of *Australoxylon*-type instead of *Protophyllocladoxylon*.

Nandorioxylon saksenae, described by Biradar and Bonde (1981) based on specimens collected from the Late Permian of India, and *Xuanweioxylon* He, Wang, Hilton and Shao, 2013 was discovered in strata from the Late Permian of South China, display some similarities with those of XTT-C-4 gen. nov.. In the piths of *Nandorioxylon saksenae* and *Xuanweioxylon*, sclerenchymatous sheaths form peripheral annuli in radial direction that is different from the diaphragms in XTT-C-4 gen. nov. Additionally, the secondary xylem of *Nandorioxylon* is also of *Araucarioxylon*-type that is different from XTT-C-4 gen. nov. *Xuanweioxylon* also contrast with XTT-C-4 gen. nov., because the tracheids of the latter display scalariform bordered pits.

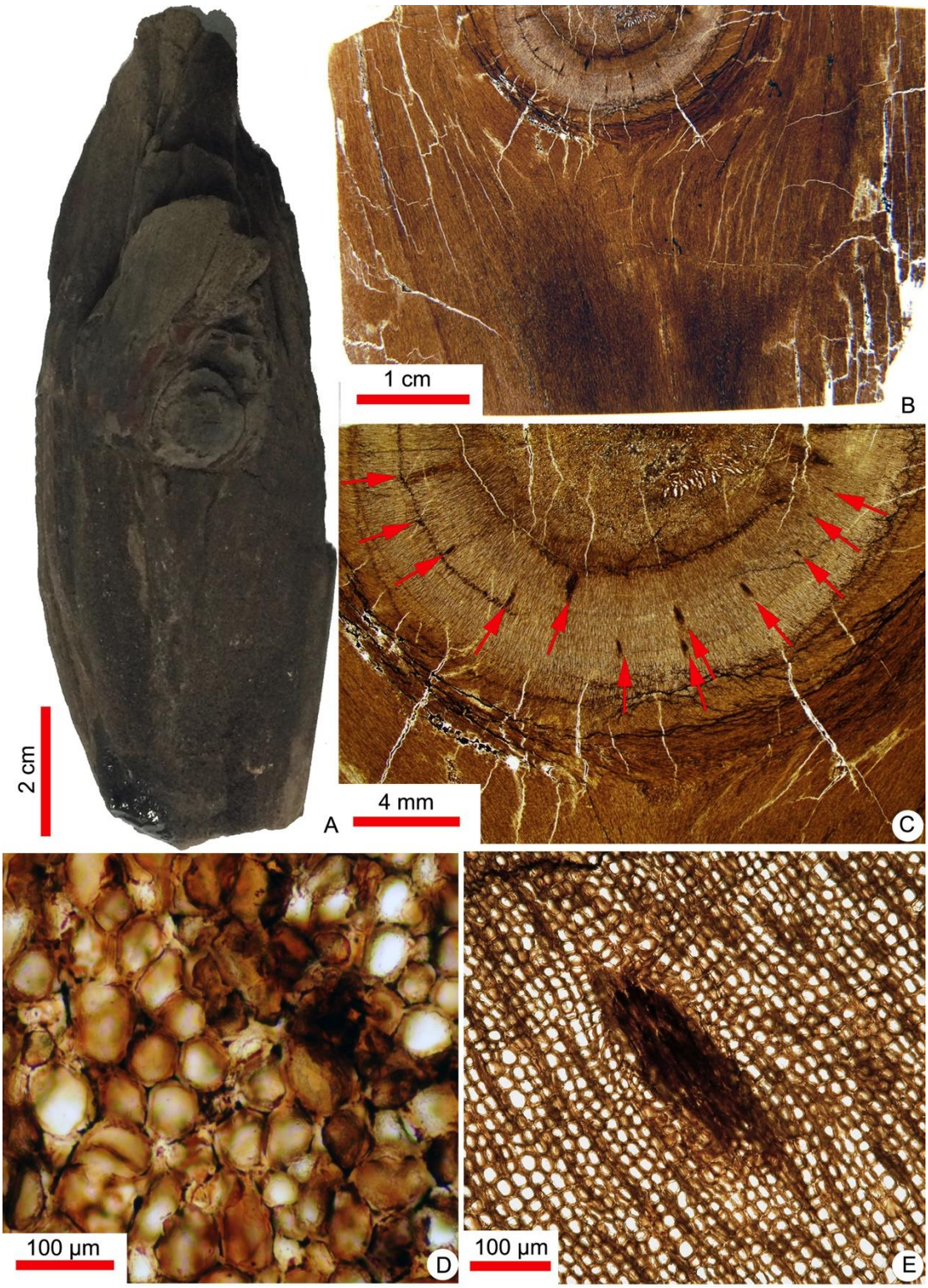

Figure 3-25: XTT-C-4 gen. et sp. nov. A. General view of the specimen XTT-C-4. B. Overview of the pith and the primary xylem of the branchlet (transverse section) and the secondary xylem of the branch (tangential section). Slide number: XTT-C-4a1. C. Close-up of the pith with cracked cavities and the primary xylem of the branchlet (transverse section). Slide number: XTT-C-4a1. D. Transverse section showing the isodiametric parenchyma cells in the pith. Slide number: XTT-C-4a1. E. A leaf trace in the secondary xylem. Slide number: XTT-C-4a1.

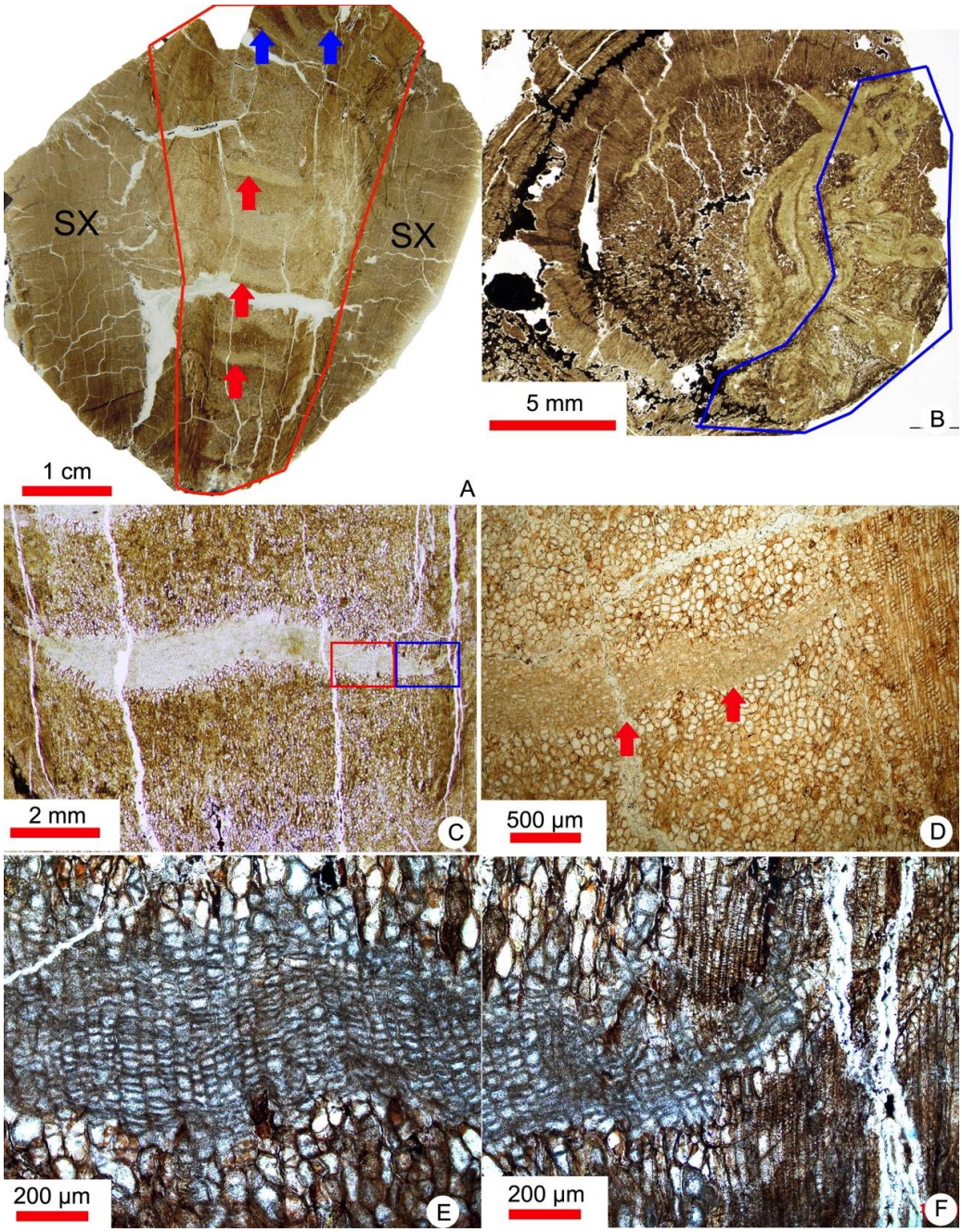

Figure 3-26: XTT-C-4 gen. et sp. nov. A. Overview of the pith and the primary xylem of the branchlet (radial section; in the red box) and the secondary xylem (SX) of the main branch (transverse section). The red arrows indicate the lense-like diaphragms and the blue arrows indicate the curved diaphragms in the pith. Slide number: XTT-C-4b1. B. Overview of the pith, primary xylem and secondary xylem of the branchlet (transverse section). The area in the blue box is disturbed due to a local maceration during decay. Slide number: XTT-C-4a2. C. Radial section showing one diaphragm in the pith. Slide number: XTT-C-4b1. D. Radial section showing one diaphragm in the pith. Slide number: XTT-C-4b2. The slides XTT-C-4b1 and XTT-C-4b2 are perpendicular. E. Radial section showing the small brick-like supporting cells of the diaphragm (the red box in picture C). Slide number: XTT-C-4b1. F. Radial section showing the close-up of the diaphragm (the blue box in picture C). The thickness of the diaphragm reduces on the periphery of the pith. The diaphragm

disappears at the contact with the initial of the secondary xylem. Slide number: XTT-C-4b1.

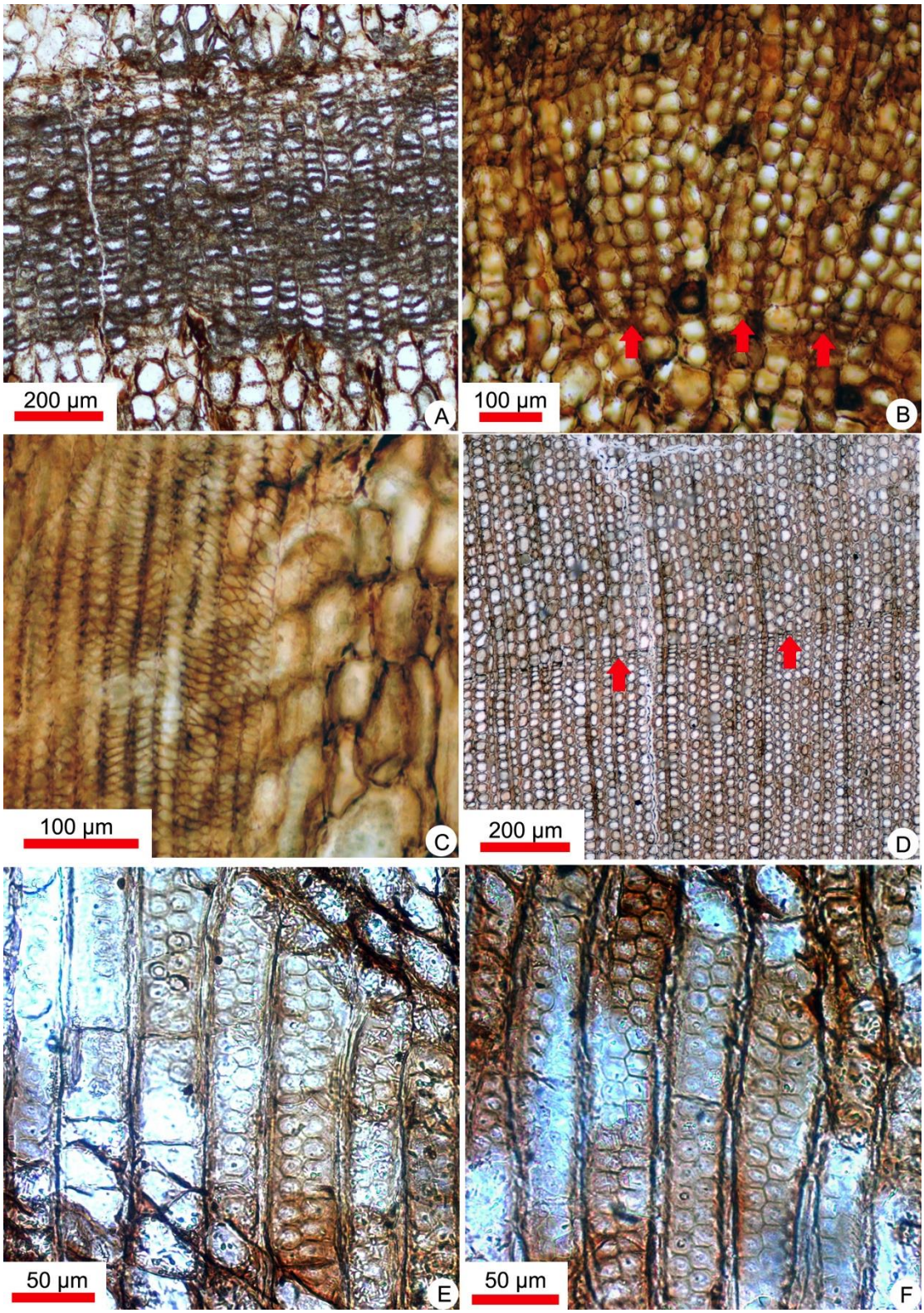

Figure 3-27: XTT-C-4 gen. et sp. nov. A. Close-up of the diaphragm cells. Slide number: XTT-C-4b1. B. Transverse section showing the endarch primary xylem (arrows) on the pith periphery. Slide number: XTT-C-4a1. C. Radial section showing the helical and reticulate thickenings of the tracheids of primary xylem. Slide number: XTT-C-4b1. D. Transverse section showing the subtle

growth-ring boundary, characteristic of “indistinct growth rings” (arrows) in the secondary xylem of the main branch. Slide number: XTT-C-4b1. E, F. Radial section showing the uniseriate and biseriate radial pits on the tracheid walls in the branchlet. The biseriate pits are alternate or rarely opposite. Slide number: XTT-C-4b1.

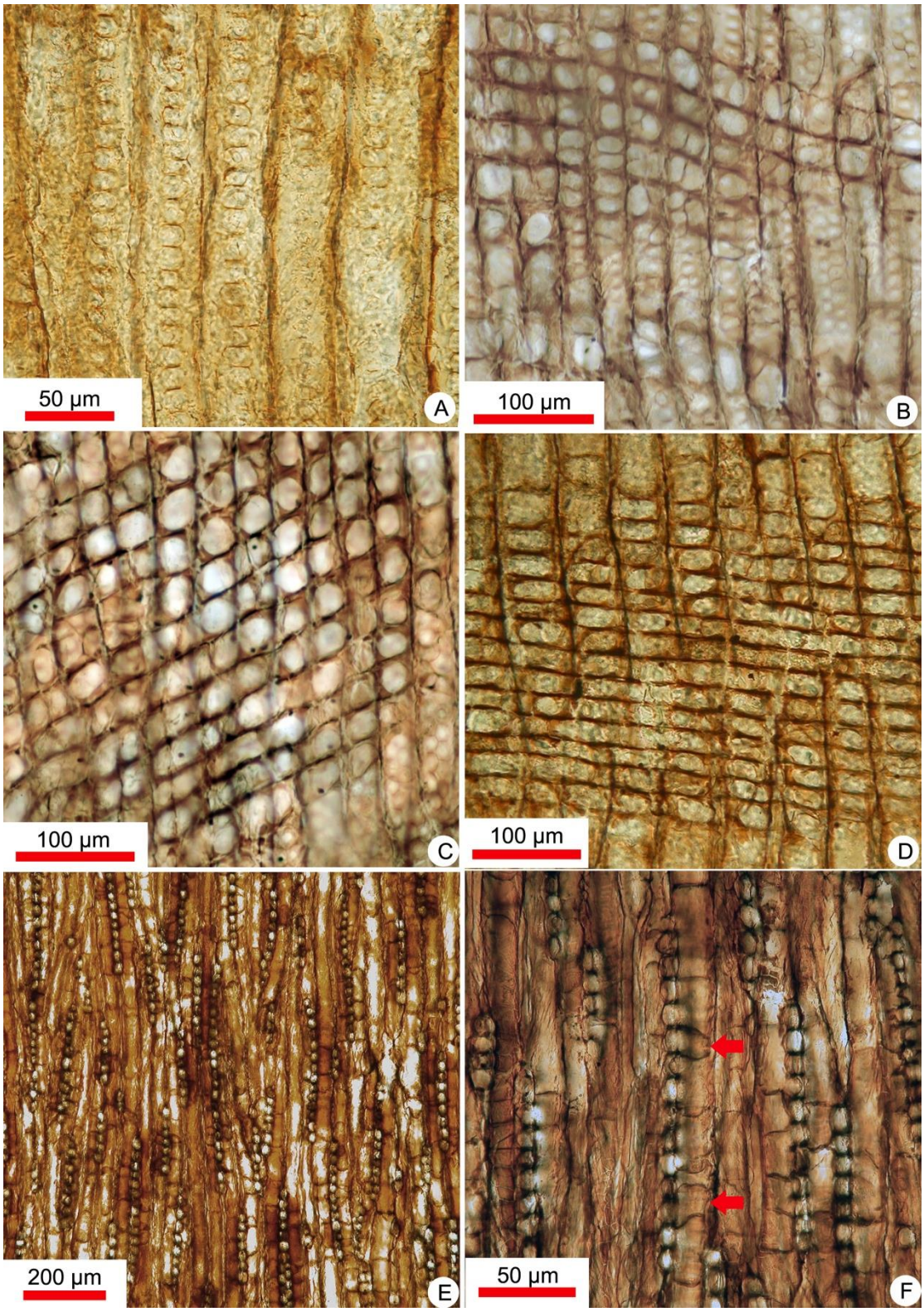

Figure 3-28: XTT-C-4 gen. et sp. nov. A. Radial section showing the uniseriate radial pits on the

tracheid walls in the main branch. Slide number: XTT-C-4b2. B, C. Radial section showing 1 to 3 rectangular, ovoid or round simple cross-field pits in the branchlet. Slide number: XTT-C-4b1. D. Radial section showing 1 to 3 rectangular, ovoid or round simple cross-field pits in the main branch. Slide number: XTT-C-4b2. E. Tangential section showing the homogeneous, uniseriate or biseriate rays. Slide number: XTT-C-4a1. F. Tangential section showing the homogeneous rays; the red arrows indicate tyloses protruding in the lumen of tracheids. Slide number: XTT-C-4a1.

Genus: *Agathoxylon*

***Agathoxylon* cf. *leei* Szei, 1952**

Description:

The specimen "XTT-BW-04" is 75 mm long. In cross section, the outline is rectangular, 75 × 45 mm.

Transverse section—Growth rings and frost rings are present (Fig. 3-29A, B). Resin duct and axial parenchyma are absent. Axial tracheids are rectangular or oval. The diameter of radial traicheid is 6–26 μm and that of tangential tracheid is 9-33 μm (average 20 μm) (Figure 2B, 2C). Xylem rays usually consist of uniseriate cells. There are 2-9 seriates of traicheids between each two rays. The frequency of the ray is 6-8 in number in each millimetre.

Radial section—The pits on the tracheid walls are bordered and circular or oblate in shape (flattening index≥0.42). They are arranged in uniseriate contiguously, occationally, partically biseriate, ca. 9 μm from the tracheid internal walls (Fig. 3-29C). They are 15×13 to 23×15 μm in size. Pores are circular or oblique oval. The ray cells are brick-like and usually span 65.5 to 203.5 μm. The horizontal and end walls of ray cells are both smooth. There is 1, rarely 2 or 3 (<1%) oculipores in each cross-field unit. Oculipores are of cupressoid-type, with elliptic apertures, 2 to 4 μm in diameter (Fig. 3-29D, E).

Tangential section—Xylem rays are homogenous, uniseriate. They consist of circular or elliptical parenchyma cells. Rays 1 to 25 (Mean=7.44) cells high and 23-29 per mm^2 (Fig. 3-29F), 5-8 per mm. Ray cells are circular to rectangular, 1×16-16×33 μm in size.

Locality and Horizon

Taoshuyuan B Section, Turpan, Xinjiang; Late Permian Wutonggou Formation.

Sample Number

XTT-BW-03

Discussion:

The cross-field pitting is crucial to the identification of coniferous woods. Cross-field pit features include frequency, arrangement, form, size and/or position of the apertures relative to the border of the pits. Six types of cross-field pitting are proposed for description and identification of coniferous woods.

The woods with the extant Araucariaceae characteristics were assigned to *Dadoxylon* Endlicher 1847, *Agathoxylon* Hartig 1848, and *Araucarioxylon* Kraus 1870. But both *Dadoxylon* Endlicher and *Araucarioxylon* Kraus are illegitimate. *Agathoxylon* Hartig can be used legitimately and is the most appropriate name for the woods similar to that of the extant Araucariaceae (Rößler et al., 2014). Philippe (1995) provides more complete diagnosis for *Agathoxylon*, namely: "tracheidoxyls without resin canals; bordered pits araucaroid; cross-field araucaroid; xylem rays mostly uniseriate, horizontal and

tangential walls of ray cells un-pitted. Axial parenchyma is present or absent".

Our fossil wood resembles to the former species *Agathoxylon leei,* 1952. As mentioned above, we temporarily name it *Agathoxylon* cf. *leei*. The species "*Agathoxylon leei* 1952" was erected by Sze, based on only one specimen from Shihchienfeng Formation (= Sunjiagou Formation), Yaoxian, Shaanxi Province. It is characterized by (1) uniseriate, rarely biseriate Araucarian radial pitting; (2) one cupressoid pits in each cross-field unit; (3) uniseriate ray cells; (4) absence of resin canals and axial parenchyma.

However, the araucaroid cross-field pits mean "the individual pits are predominantly cupressoid, but their arrangement in the cross-field is distinctive. The pits are arranged in alternate rows of usually three or more with a tendency for crowding; individual pits often have a polygonal outline similar to the alternate intertracheary pitting in Araucariaceae."

Only one cupressoid cross-field pit in each cross-field unit can be found in "*Agathoxylon leei*", instead of three or more like that in extant Araucariaceae. As a result, we consider that *Agathoxylon* (or *Araucarioxylon*) is not suitable for these specimens.

So far, there is no reasonable name for the present specimen. A new genus is needed to accommodate tracheidoxyls with Araucarian radial tracheid pitting and cupressoid cross-fields.

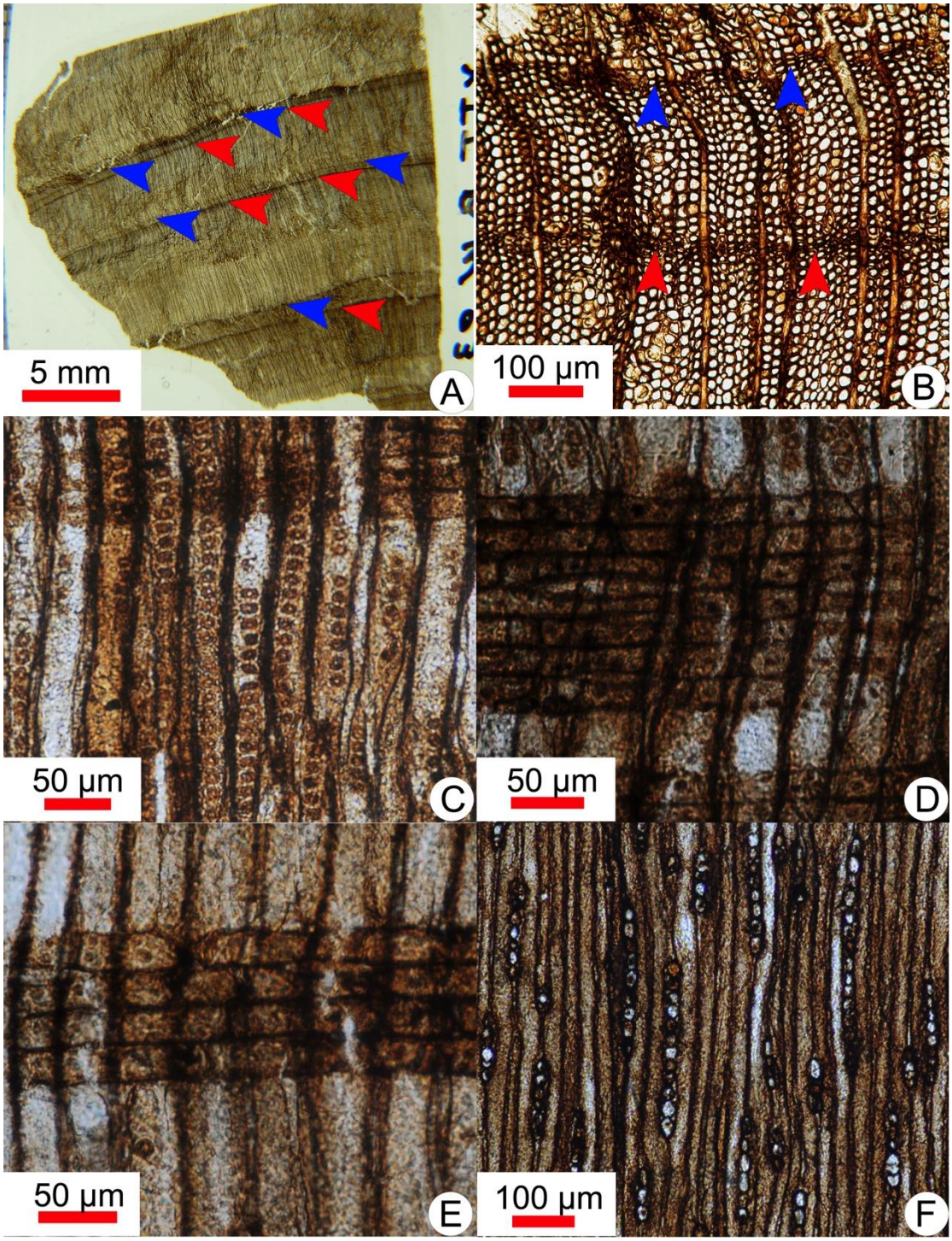

Figure 3-29 *Agathoxylon* cf. *leei* A. Transverse section (TS) showing two adjacent growth rings (red and blue arrows). Slide number: XTT-BW-03a. B. Close-up of two adjacent growth rings (red and blue arrows). Slide number: XTT-BW-03a. C. Radial section (RS) showing the uniseriate radial pits on the tracheid walls. Slide number: XTT-BW-03b. D, E. RS showing one to two cupressoid-type pits in each cross-field unit. Slide number: XTT-BW-03b. F. Tangential section showing the homogeneous, uniseriate rays. Slide number: XTT-BW-03c.

Other gymnosperm fossil woods

Material: XTT-C-11

The original stem is about 5 cm long, and shows a maximum diameter of 5.5 cm, gray. The specimen is composed of pith, primary xylem and secondary xylem (Fig. 3-30A, B).

Pith-The pith is small and homogeneous, about 0.3 mm in diameter. Most of the parenchyma cells are not preserved well. In transverse section, the parenchyma cells are circular or polygonal, diameter 11 to 55.5 μm. In radial section, the parenchyma cells are rectangular, 32 to 65 μm high.

Primary xylem-The primary strands show endarch maturation (Fig. 3-30B). The primary xylem tracheids are with annual and helical thickenings.

Secondary xylem-The secondary xylem is pycnoxylic. Growth rings are absent. In transverse section, the tracheids are polygonal, 13-47 μm (Fig. 3-30C). In longitude section, radial pits on the tracheid walls are uniseriate or biseriate, araucaroid type. When uniseriate, the pits are contiguous, circular or slightly flattened, 5-15 μm from the tracheid internal walls; when biseriate, pits are alternate, crowded hexagonal, close to the internal wall of tracheid (Fig. 3-30D). Rays are uniseriate, 1-14 cells (16-265 μm) high (Fig. 3-30E). Ray cells are not preserved. Cross-field pits are not clear.

Locality and Horizon

Taoshuyuan C Section, Turpan, Xinjiang; Late Permian-Early Triassic Guodikeng Formation.

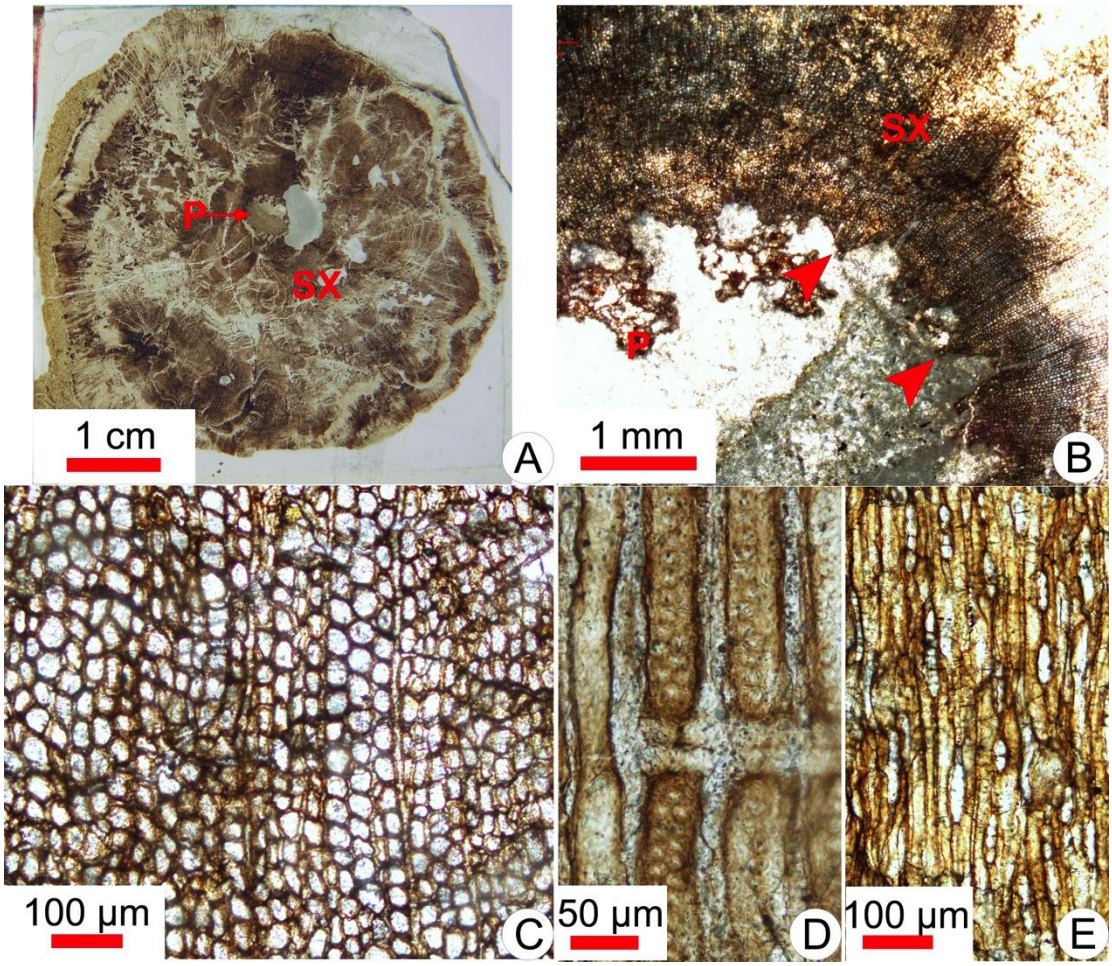

Figure 3-30 XTT-C-11 A. Transverse section (TS) showing the overview of the pith (P), primary xylem and secondary xylem (SX). Slide no. XTT-C-11a. B. TS showing the pith (P), endarch primary xylem and secondary xylem (SX). Slide no. XTT-C-11a. C TS showing the close-up of the tracheids. Slide no. XTT-C-11a. D. Radial section showing the uniseriate or biseriate radial pits on the tracheid

walls. Slide no. XTT-C-11b. E. Tangential section showing the uniseriate rays. Slide no. XTT-C-11c.

Material: XTT-C-6

The original stem is about 40 cm long, and shows a maximum diameter of 7.5 cm, gray. The specimen is composed of pith, primary xylem and secondary xylem (Fig. 3-31A).

Pith-Most cells in the pith are not preserved. The remnant part shows a homogeneous small pith. The parenchyma cell is about 50-135 μm.

Primary xylem-The primary strands show endarch maturation (Fig. 3-31B).

Secondary xylem-The secondary xylem is pycnoxylic. Growth rings are indistinct (Fig. 3-31C). In transverse section, the tracheids are polygonal, up to 50 μm in diameter. In longitude section, radial pits on the tracheid walls are uniseriate, 14-20 μm in diameter (Fig. 3-31D). Rays are uniseriate, 2-24 cells (50-600 μm) high (Fig. 3-31E). Ray cells are Ray cells are not preserved. Cross-field pits are not clear.

Discussions: The two samples XTT-C-6 and XTT-C-11 are not well preserved. That makes it hard to identify and to compare with other samples.

Locality and Horizon

Taoshuyuan C Section, Turpan, Xinjiang; Late Permian-Early Triassic Guodikeng Formation.

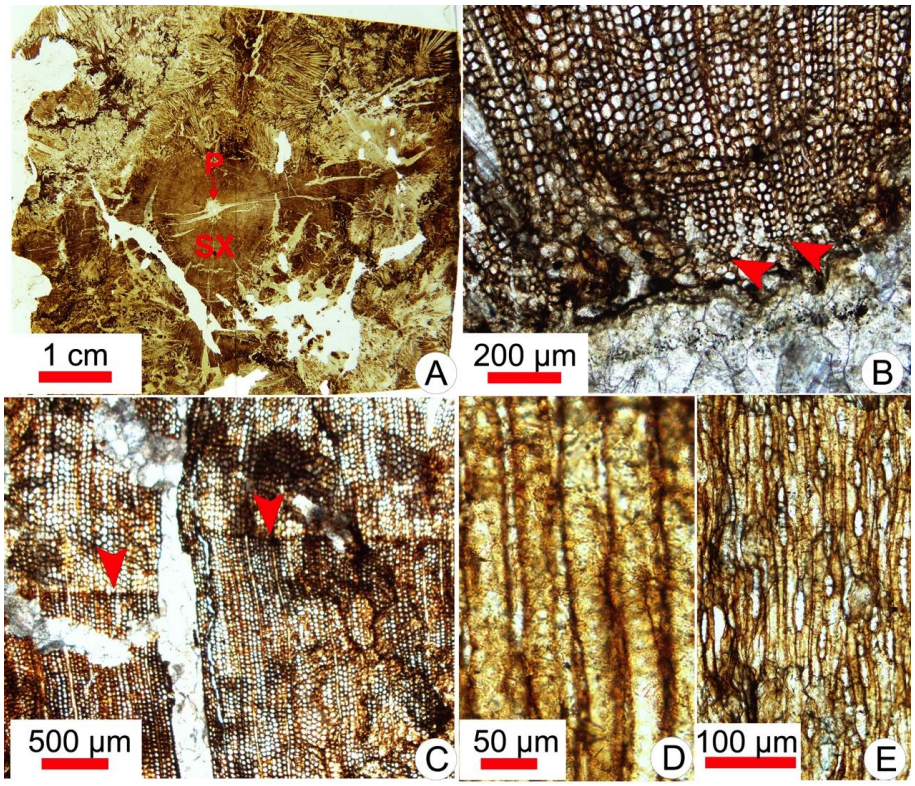

Figure 3-31 XTT-C-6 A. Transverse section (TS) showing the overview of the pith (P) and secondary xylem (SX). Slide no. XTT-C-6a. B. TS showing the endarch primary xylem. Slide no. XTT-C-6a. C TS showing the close-up of the tracheids and the growth ring boundary (arrows). Slide no. XTT-C-6a. D. Radial section showing the uniseriate radial pits on the tracheid walls. Slide no. XTT-C-6b. E. Tangential section showing the uniseriate rays. Slide no. XTT-C-6c.

Note: The fossil woods from Taoshuyuan A and C sections are ploted on the Fig. 4-6 and

4-7. Taoshuyuan B section is a small outcrop of Wutonggou Formation (Fig. 2-4). The location of fossil woods from Dalongkou section was ploted on the Fig. 2 in the annexes Shi et al. 2015. The accurate Permian-Triassic boundary is unknown in Taoshuyuan C section. Abundant fossils of vertebrate Lystrosaurus have been found in the upper part of Guodikeng Formation, just above the bed we collected the fossil woods (Cheng et al., 1996). The first occurrence of the vertebrate *Lystrosaurus* has been suggested as a major marker of the terrestrial Permian-Triassic boundary. Based on the *Lystrosaurus,* the age of the fossil woods may be the earliest Triassic.

§3.3 Palaeoecologic implication of fossil woods

Junggaropitys dalongkouensis and XTT-C-4 gen. et sp. nov. preserve distinct growth rings. That provides good materials to detect their habits.

Junggaropitys dalongkouensis

(This part has been published in the journal Review of Palaeobotany and Palynology.)

The growth rings of the conifer *Junggaropitys dalongkouensis* were analyzed quantitatively using this technique. To construct the CSDM curve, four parameters were calculated: (1) skew of CSDM curves, (2) percentage of late wood, (3) percentage of cell diminution in a ring increment and (4) Ring Markedness Index (RMI).

Deciduous conifers have dominantly left-skewed CSDM or symmetrical curves, whereas evergreen conifers have dominantly right-skewed CSDM curves. The CSDM curves of *Junggaropitys dalongkouensis* are from +6.67% to +27.27% (mean percentage of skew +13.37), right-skewed, suggesting that this species was evergreen.

The late wood development in conifer woods could be related to foliar retention (Falcon-Lang, 2000a, b). The percentage of late wood may be strongly influenced by both leaf longevity and the intensity of climate seasonality. The percentage of late wood in *Junggaropitys dalongkouensis* is 20.00-43.75%, with a mean of 32.87%. The percentage of cell diminution ranges from 60.00% to 72.00%, with an average of 66.68%.

The RMI for *Junggaropitys dalongkouensis* varies between 14.40% and 26.25%, with a mean of 21.63% (Fig. 3-32, Table 3-4). For the group of extant conifers, it shows a strong inverse linear relationship between the leaf retention and the different quantitative parameters of growth rings (percentage of skew, late wood, cell diminution and RMI values) (Falcon-Lang, 2000a). The lower values of percentage of late wood and RMI correlate with the highest foliar retention in evergreen plants, whereas higher values relate to shorter periods of leaf retention. The results indicate that the foliar retention of *Junggaropitys dalongkouensis* is similar to those extant conifers with 3-6 years of foliar retention (Table 3-5).

Four ring sequences ranging from 3 to 29 rings in length were measured for four samples of *Junggaropitys dalongkouensis*, with a total of 67 rings measured for the whole assemblages. These growth rings provide information on seasonal conditions. The mean ring width for *Junggaropitys dalongkouensis* is 2.036 mm; the mean minimum ring width is 0.835 mm; the mean maximum ring width is 3.975 mm. The narrowest ring is 0.375 mm wide and the broadest is 6.5 mm. The variability in ring width may reflect either fluctuations in annual water supply or other environmental changes in the growth environment (Table 3-6).

Annual sensitivity (AS) and mean sensitivity (MS) were calculated to determine the degree of variability between years (Fritts, 1976). The AS of *Junggaropitys dalongkouensi* varies between 0 and 1.494. The largest values of AS indicate extreme climatic events. The strong fluctuations of AS of the samples show variations in ring thickness between adjacent years. MS values range between 0.332 and 0.397, with an average of 0.367 (Table

3-6). These data indicate that the growing environment was not uniform. Possible extreme climatic events may have stressed the growth of *Junggaropitys dalongkouensis*.

Table 3-4 Results of the quantification of Ring Markedness parameters for *Junggaropitys dalongkouensis.*

Ring number	Percentage latewood	Percentage diminution	Ring Markedness Index (RMI)	Percentage skews
Ring A	20.00%	72.00%	14.40%	+11.11%
Ring B	38.24%	68.18%	26.07%	+27.27%
Ring C	35.71%	65.22%	23.29%	+11.11%
Ring D	43.75%	60.00%	26.25%	+12.50%
Ring E	26.67%	68.00%	18.14%	+6.67%
Averages	32.87%	66.68%	21.63%	+13.37%

Table 3-5 Comparison of the quantification of Ring Markedness parameters for *Junggaropitys dalongkouensis* with the five extant taxa taken from the data of Falcon-Lang (2000a, b)

Species	Percentage latewood (%)	Percentage diminution (%)	Ring Markedness Index (RMI) (%)	Range of percentage skews (mean value) (%)
Deciduous conifer				
Larix decidua	50.00–54.83	71.55–85.91	35.77–44.36	-40.0 to +7.7 (-6.8)
Evergreen conifers (LRT in years)				
Pinus sylvestris (1–3 years)	41.03-50.00	70.53-77.28	31.56-35.26	-9.1 to +17.9 (+5.2)
Picea abies (3–5 years)	25.93-44.19	74.02-84.03	19.90-35.42	0.0 to +38.2 (+12.0)
***Junggaropitys dalongkouensis* (? years)**	**20.00-43.75**	**60.00-72.00**	**14.40-26.25**	**+6.67 to +27.27 (+13.37)**
Cedrus libani (3–6 years)	30.77-39.58	62.33-72.06	20.22-24.68	+35.7 to +42.9 (+39.0)
Araucaria araucana (3–15 years)	10.00-22.50	28.67-51.79	3.17-10.35	+55.0 to +80.0 (66.7)

Table 3-6 Summary of the growth-ring data for *Junggaropitys dalongkouensis* (a, only conspicuous intact rings were calculated; b, the rings are too few for mean sensitivity and annual sensitivity).

Sample number	Number of rings[a]	Minimum ring width (mm)	Maximum ring width (mm)	Mean ring width (mm)	Mean sensitivity	Minimum annual sensitivity	Maximum annual sensitivity
XJD-1	29	0.375	4.425	1.816	0.397	0	1.185
XJD-2[b]	3	1.7	6.5	3.992	-	-	-
XJD-3	23	0.5	4.675	1.787	0.332	0	1.494
XJD-4	12	1.6	4.275	2.585	0.371	0.014	0.934
Total	67						
Average		0.835	3.975	2.036	0.367	0.005	1.204

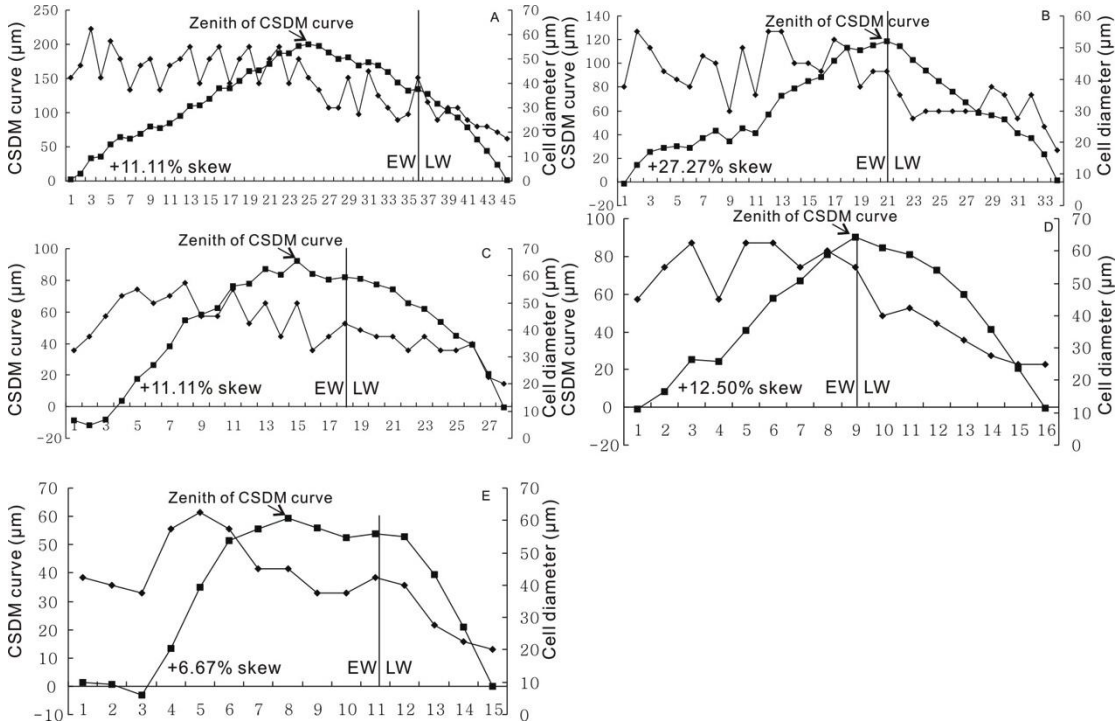

Figure 3-32 Right-skewed CSDM curves of five growth rings and cell diameters of growth ring increment. For each ring increment, the percentage of skew for CSDM curves was calculated using Falcon-Lang's (2000a) method. The position at which the CSDM curve reaches the zenith represents the percentage of skew in relation to the total distance between the centre of the CSDM curve to the right of the plot. EW: Early wood; LW Late wood.

XTT-C-4 gen. et sp. nov.

This part has been contributed to the journal Palaeo-3. It is in review now.

To construct the CSDM curve, we selected five adjacent growth rings and measured the radial diameter of five adjacent rows of cells for each growth ring (Fig. 3-33). The radial diameters of the cells were then averaged using the method of Falcon-Lang (1999) (Fig. 3-33). The mean cell diameters of XTT-C-4 gen. et sp. nov. in a growth ring are fluctuant. Variability in mean cell diameters may result from fluctuations in water supply or other environmental changes.

We calculated four parameters: (1) skew of CSDM curves, (2) percentage of late wood, (3) percentage of cell diminution in a ring increment and (4) Ring Markedness Index (RMI). Deciduous conifers have dominantly left-skewed CSDM or symmetrical curves, whereas evergreen conifers have dominantly right-skewed CSDM curves. The CSDM curves of XTT-C-4 gen. et sp. nov. are from + 4.92% to + 82.41% (mean percentage of skew + 38.18%), right-skewed, suggesting that this species was evergreen (Fig. 3-34). This result is consistent with the phyllotaxy of XTT-C-4 gen. et sp. nov.

The percentage of late wood in conifer woods could be related to foliar retention (Falcon-Lang, 2000a, 2000b). The late wood development may be strongly influenced by both leaf longevity and the intensity of climate seasonality. The percentage of late wood in XTT-C-4 gen. et sp. nov. is 8.79-19.57%, with a mean of 13.66%. The percentage of cell diminution ranges from 60.61% to 72.00%, with an average of 73.02%. The RMI varies between 5.86% and 14.12%, with a mean of 9.48% (Table 3-7). Falcon-Lang (2000a) found a strong inverse linear relationship between the leaf retention and the different quantitative parameters of growth rings (percentage of skew, late wood, cell diminution and RMI values) in the group of extant conifers. The results show that the foliar retention of XTT-C-4 gen. et sp. nov. is similar to those of extant conifers with 3–15 years of foliar retention (Table 3-8).

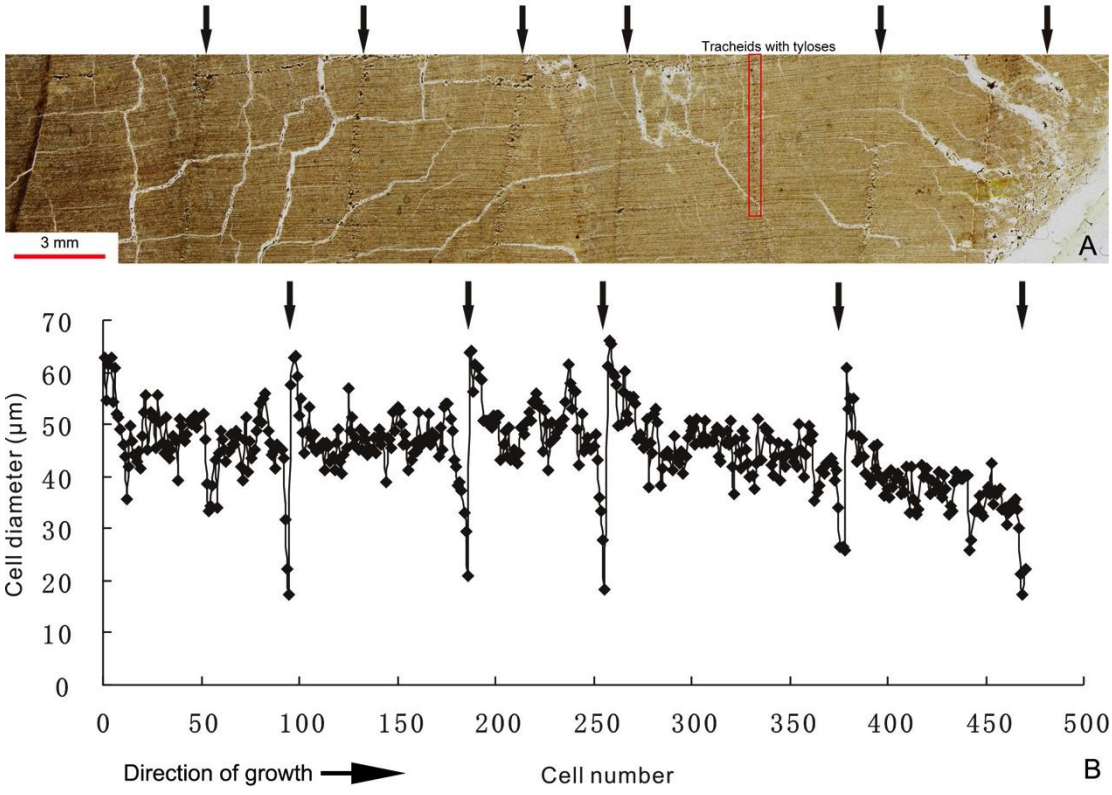

Figure 3-33: A. The growth rings with the subtle growth-ring boundary, in the main branch; B. Variation in cell radial diameter across growth rings. Growth is left to right. Arrows indicate the growth-ring boundaries.

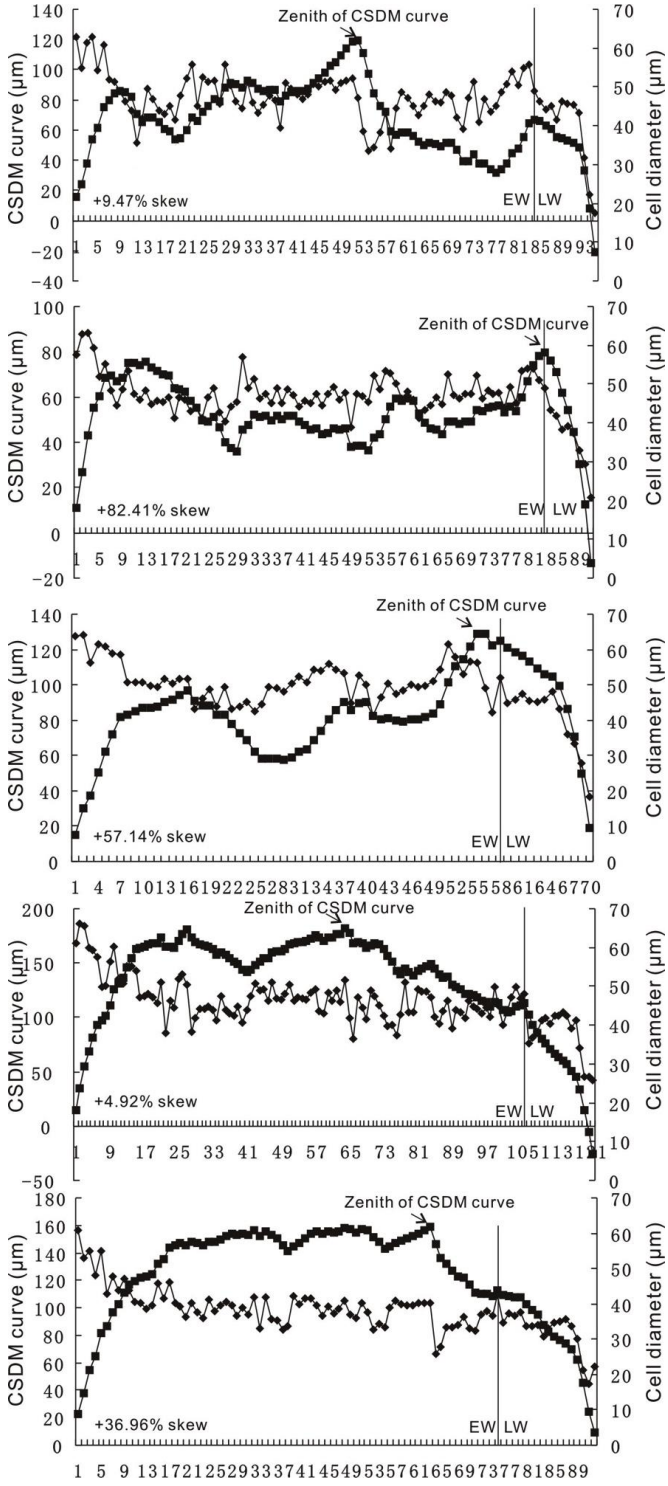

Figure 3-34 Right-skewed CSDM curves of five growth rings and cell diameters of growth ring increment. For each ring increment, the percentage of skew for CSDM curves was calculated using Falcon-Lang's (2000a) method. The position at which the CSDM curve reaches the zenith represents the percentage of skew in relation to the total distance between the centres of the CSDM curve to the right of the plot. EW: Early wood, LW Late wood.

Table 3-7 Results of the quantification of ring markedness parameters for XTT-C-4 gen. et sp. nov.

Ring number	Percentage latewood	Percentage diminution	Ring Markedness Index (RMI)	Percentage skews
Ring A	10.5%	73.02%	7.67%	+9.47%
Ring B	8.79%	66.67%	5.86%	+82.41%
Ring C	17.14%	71.88%	12.32%	+57.14%
Ring D	12.30%	60.61%	7.46%	+4.92%
Ring E	19.57%	72.13%	14.12%	+36.96%
Averages	13.66%	68.86%	9.48%	+38.18%

Table 3-8 Comparison of the quantification of ring markedness parameters for XTT-C-4 gen. et sp. nov. with the five extant taxa taken from the data-base of Falcon-Lang (2000a, b).

Species	Percentage latewood (%)	Percentage diminution (%)	Ring Markedness Index (RMI) (%)	Range of percentage skews (mean value) (%)
Deciduous conifer				
Larix decidua	50.00–54.83	71.55–85.91	35.77–44.36	-40.0 to +7.7 (-6.8)
Evergreen conifers (LRT in years)				
Pinus sylvestris (1–3 years)	41.03-50.00	70.53-77.28	31.56-35.26	-9.1 to +17.9 (+5.2)
Picea abies (3–5 years)	25.93-44.19	74.02-84.03	19.90-35.42	0.0 to +38.2 (+12.0)
Cedrus libani (3–6 years)	30.77-39.58	62.33-72.06	20.22-24.68	+35.7 to +42.9 (+39.0)
XTT-C-4 gen. et sp. nov. (? years)	**8.79-19.57**	**60.61-73.02**	**5.86-14.12**	**+4.92 to +82.41 (+38.18)**
Araucaria araucana (3–15 years)	10.00-22.50	28.67-51.79	3.17-10.35	+55.0 to +80.0 (66.7)

Chapter 4 Sedimentology and facies analysis

This study is focused on sedimentological study of the north limb of the Dalongkou, Taoshuyuan A and Taoshuyuan C sections. Sedimentological analysis (facies analysis, paleocurrent measurements), identification of unconformities and of preserved elements (fossils, ichnites and palaeosols), were used for the characterization and the reconstruction of each depositional environment. The study included the logging of 3 vertical profiles (scale 1/100) and the establishment of detailed sedimentological profiles. We took samples to analyze the petrographic nature of different selected rocks in the sandstone units. Vertical sedimentological profiles for each section were used to establish correlations based on sequence stratigraphy at the scale of the study area. Parts of this work are still in progress and prepared for publications.

§4.1 Dalongkou North limb Section

In the Dalongkou area, because of present day weathering, trenches have been dug to expose sufficiently fresh exposure for observation, measurement and sampling. Along the studied section, strike of the beds where comprised between N127 and N174, and dip between 54 and 71° to the NE. Apart from a tectonic tilting of the series, no fault have been observed, allowing for continuous logging from the upper part of the Wutonggou Formation to the lower part of the Jiucaiyuan Formation.

Only the uppermost 44 m of this formation have been investigated (Fig. 4-1). A ca. 17 m thick part, located between 20 and 37 m on the measured section, has not been investigated because weathering were too intense to access fresh rock.

This formation comprises five main facies consisting of conglomerates, sandstones and siltstones. Conglomeratic levels (0.2 to 1 meter thick) constitute only a minor constituent of the uppermost part of the Wutonggou Formation and comprise only the Gt facies (Fig. 4-2A, Table 4-1). This conglomerate is clast-supported and is made up of rounded to sub-rounded, polygenic gravel and pebbles. The conglomerate display through cross stratification, characteristic of 3D megaripples migration (Miall, 1996).

Sandstones facies, represented by the Sh and St facies (All the abbreviations of facies are explained in Table 4-1) are dominant throughout the Wutonggou Formation, and are represented by 0.3 to 3 meters thick units. St facies sandstones display 3D megaripples, and occasional erosive base. Sh facies are composed of fine to coarse sandstones with faint horizontal laminations, and sometimes display parting lineation (Fig. 4-2B).

Deposition of the Sh facies corresponds to tractive current or repeated sediment discharges within aqueous environments (Miall, 1978; Einsele, 2000). These facies show common evidence of bioturbation, such as burrows (Fig. 4-3C), and contain abundant minute sized plant remains.

Petrographic investigations reveal these sandstones consist of lithic arenite, sometimes cemented by secondary calcite (Table 4-2). Lithic elements are commonly strongly weathered and display rounded to sub-rounded shapes. They are constituted by rock fragments of igneous origins (volcaniclasts, microgranular, granular and microcrystalline rock fragments) and elements of sedimentary origin, such as silty lithic fragments (Fig. 4-3). Individual crystals are constituted mainly by quartz grains displaying angular to rounded shapes, and altered feldspar (plagioclase, microcline and a few alkaline feldspar). Accessory minerals comprise biotite flakes, chlorite, epidote and zircon grains. Some samples also contain calcite coating around detrital elements, a typical feature of paleosols. The combination of grains displaying shapes ranging from angular to rounded points toward various sources proximal to distal sources and/or multiple reworking for the grains displaying the most rounded shapes. Sources rocks include magmatic rocks (both plutonic, hypovolcanic and volcanic rocks). The diversity of textures displayed by the volcaniclasts, their roundness and weathering reflect their reworking from a distant area and/or that a long duration spanned between their production and their final deposition within the Wutonggou Formation The grains found in the Wutonggou Formation also originate from the dismantling of various sedimentary rocks.

The conglomeratic and sandstones layers alternate with finer facies, less abundant, which are made up of silts rich in organic matter displaying planar laminations (Fl, Table 4-1) or coal seams (C, Table 4-1).

4.1.2 Guodikeng Formation

The Guodikeng Formation comprises various rock types, including red, green, brown, to grey and dark grey mudstone, siltstones, fine sandstones and limestone. The total thickness of this formation reaches 193 m in the Dalongkou area. This measured thickness is in good agreement with the 197 m thickness measured by Metcalfe et al. (2009) in the same area. Because of intense present day weathering, trenches did not allow in some places to observe fresh rock, reported as missing part in the sedimentological section (Fig. 4-1). Six different facies have been documented in this formation.

Fl and Fm facies (Table 4-1) are dominant throughout the Guodikeng Formation and are represented by 0.1 to 5 meters thick units (Fig. 4-1). They comprise mudstones to siltstones laminated with sub-centimeter-scale sets (Fl facies) or more rarely, massive to crudely laminated and heterolithic packages (Fm facies), and are interpreted as deposition within calm aqueous environments (Miall, 1978; Einsele, 2000). Large

burrow sometimes crosscut the lamination (Fig. 4-2C).

Slightly coarser levels are made up of very fine to fine sandstones commonly display small asymmetrical ripples (Sr facies, Table 4-1, Fig. 4-2D). Numerous beds yielded abundant ostracods, conchostracans, bivalves, plant remains (Fig. 4-2E), and bioturbations frequently occur in the Fm, Fl and Sr facies. Nodules made up of calcite (L facies, Tables 4-1) occur locally within siltstones. These facies, made up of terrigenous material that locally contains limestone nodules, alternate with limestone layers containing numerous bioclasts and displaying a mudstone texture (Fig. 4-4).

Petrographic analyses (Table 4-2) showed that detrital elements are essentially similar to those occurring in the underlying Wutonggou Formation. The main petrographic feature for the Guodikeng Formation at the Dalongkou section is the occurrence of limestone layers. Particularly, limestone layers displaying mudstone texture imply a quiet depositional environment and a reduced amount of detrital particles input. These petrographic features, as well as biological remains enclosed within the limestone layers, are consistent with a lacustrine depositional environment.

Some levels constituted by claystone to siltstone locally display small polished surfaces, interpreted as slickenslides. Such features are common in clay-rich soils where shrink-swell processes dominate. Pedogenic processes are consequently inferred to have affected part of the Guodikeng Formation Paleosols (P facies, Table 4-1) are developed in 10 to 50 cm thick units evident only at three stratigraphical positions in the lower part of Guodikeng Formation. A few layers, containing pods rich in organic matter (C facies) possibly represent paleosol facies.

4.1.3 Lower part of the Jiucaiyuan Formation

To take avantage of better outcrop exposure, the Jiucaiyuan Formation was investigated a few hundred of meters to the West of the area where the Wuttonggou and Guodikeng formations, have been measured (West bank of the Dalongkou river, Fig. 2-3). The emplacement selected for logging was chosen after careful consideration of structural continuity between these two areas. Despite the attempt to access the best-exposed outcrops, some parts of the Jiucaiyuan Formation were masked by small landslide that locally prevented logging. These areas are reported missing on the Fig. 4-1. The Jiucaiyuan Formation comprises red siltstones, sandstones and conglomerates. Due to the upper part did not crop out well, only the lowermost 34 m part of the Jiucaiyuan Formation has been measured.

The investigated part of the Jiucaiyuan Formation comprises mainly two sandstone facies and a finer siltstone facies. Sandstones consists of Sh and St facies (Table 4-1). They are composed of fine to coarse sandstones with horizontal laminations (Sh facies, Fig. 4-2G) and display parting lineation, while sporadic small-scale current ripples or 3D mega ripples, and occasional erosive

base characterizes the St facies (Fig. 4-2F). Coarse-grained, well-rounded elements, up to a few cm in diameter and mud clasts underline the basis of through cross bedding. Plant stems and micro-fragments occur in the St facies (Fig. 4-2H). Horizontal and vertical bioturbations can be found throughout this part. Deposition of the Sh facies corresponds to tractive current or repeated sediment discharges within aqueous environments (Miall, 1978; Einsele, 2000). Deposition of the St facies corresponds to fluvial channel bedforms.

Small exposure of finer layers, made up of reddish to greenish siltstones, show numerous nodules within the siltstones, possibly indicative of pegodenic processes (P facies?). Poor outcrop exposure does not allow further characterization of these levels and potential pedogenic layers could have occurred immediately after deposition but could also be related to present day pedogenesis.

Petrographic investigations (two samples, Table 4-2 and Fig. 4-5) show that the sandstones are mainly made up of feldspar grains, but also contain quartz, volcaniclasts and accessory minerals. The shapes displayed by the particles suggest a moderate reworking, implying a relatively proximal source constituted predominantly by magmatic (plutonic and volcanic) rocks.

4.1.4 Paleoenvironmental interpretation

Wutonggou Formation. Two facies associations characterize the upper part of this formation. The first association comprises the Gt, and the St facies forming fining upwards sequences. This facies association corresponds to sinuous crested 3D megaripples, typical of braided river deposits (Best and Bristow, 1993; Miall, 1996, Fig. 4-1).

The above-mentioned facies association alternates with a second facies association consisting of Sh, Fl and C facies, attributed to ephemeral fluvial systems or ponds and alluvial plain deposits (Fig. 4-1).

Guodikeng Formation. Two facies associations are identified within the Guodikeng Formation. The first facies association corresponds to the monotonous succession of massive mudstones and siltstones (Fm and Fl facies), fine sandstones (Sr facies) with intercalation of limestone layers (L facies). This facies association additionally displays abundant fossil remains (e.g., bivalves) and bioturbation (such as large burrows). This association is consequently interpreted to correspond to perennial freshwater lake or pond environments (Fig. 4-1).

The second facies association comprises the C, P, Sr and Fl facies. Such association, comprising paleosols, attests sub-aerial environments, possibly related to flood-plain environment or to temporary emersion due to changes of the lake level (Fig. 4-1).

Jiucaiyuan Formation. The investigated part of the Jiucaiyuan Formation is composed of fining-upward sequences of Sh facies displaying parting lineation and St facies, each

stack being 0.5 to 3.5 m thick. The numerous mud clasts occurring within the Sh facies are interpreted to result from the reworking of mud chips produced by mud craks formation. This facies association is interpreted to correspond to fluvio-lacustrine environments (Fig. 4-1) and unconfined flow depositional setting (i.e., sheetflood, tabular beds) within shallow lakes or ponds. The finer, silty facies could correspond to alluvial plain environment but the poor outcrop exposure unfortunately impedes precise interpretation.

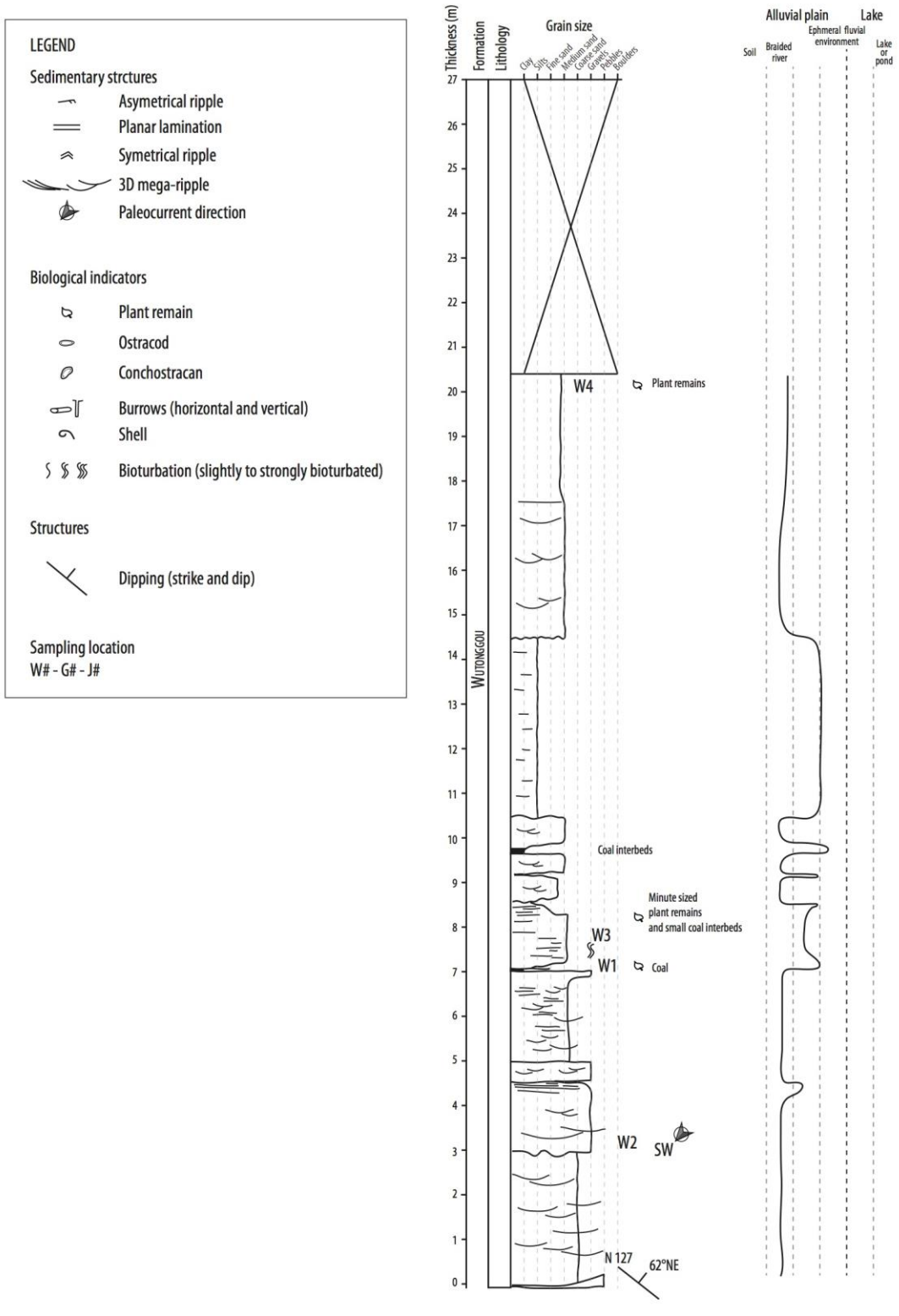

Figure 4-1 Sedimentological log along with depositional environment interpretation for the Dalongkou north limb section. Logging of the uppermost part of the Wuttonggou Formation and the Guodikeng Formation have been performed between the coordinates N43°57’45.4”; E88°52’07.8” and N43°57’40.0”; E88°52’29.2”. To access better exposed outcrops, and after careful consideration of structural continuity, the lowermost part of the Jiucaiyuan Formation have been

logged a few hundred meters away, at the coordinate N43°57’59.6”; E88°52’02.2”.
The location of the sampling site for petrographic and paleontological investigation is reported along the measured section.

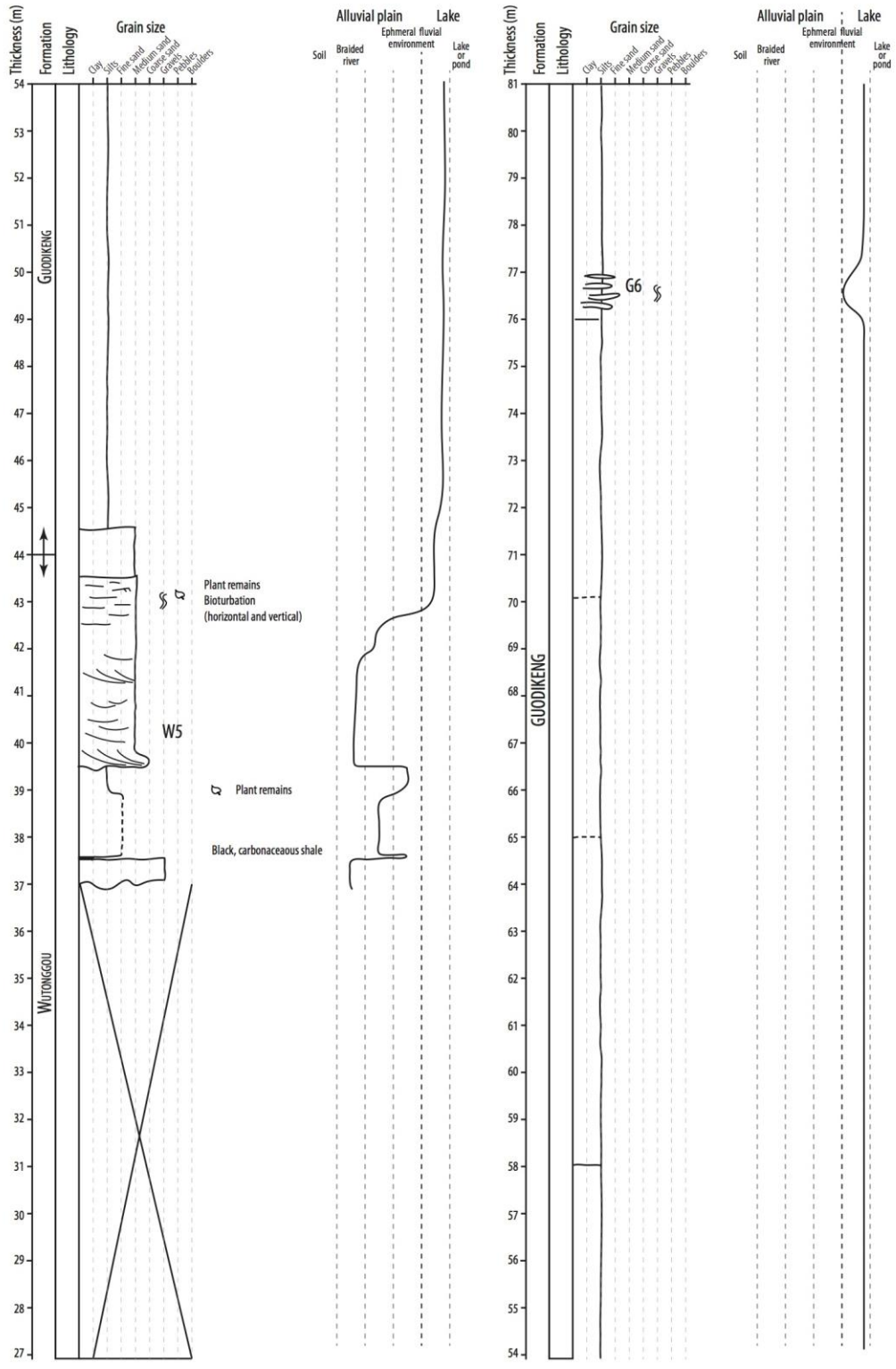

Figure 4-1 (continued) Sedimentological log along with depositional environment interpretation for the Dalongkou north limb section.

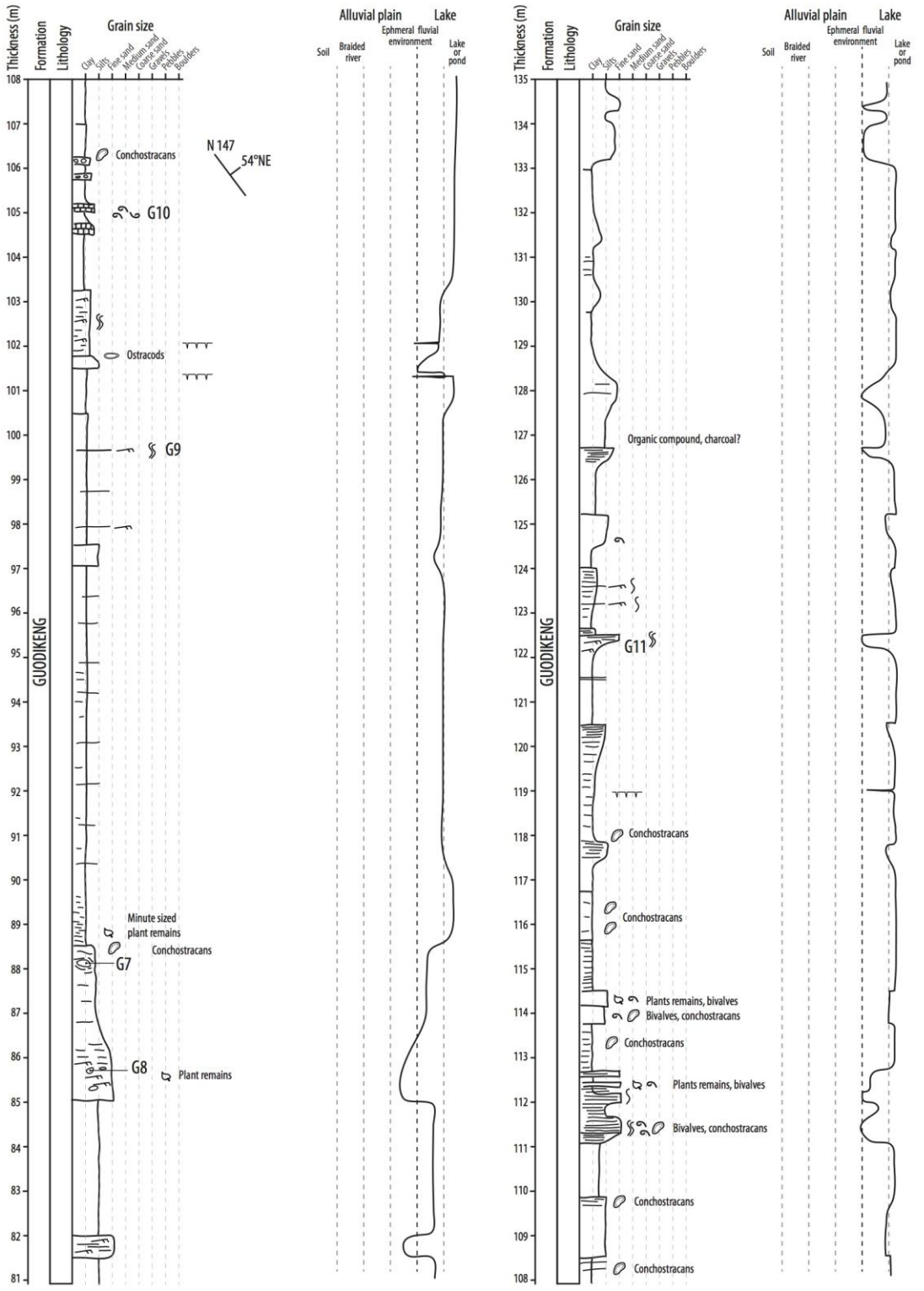

Figure 4-1 (continued) Sedimentological log along with depositional environment interpretation for the Dalongkou north limb section.

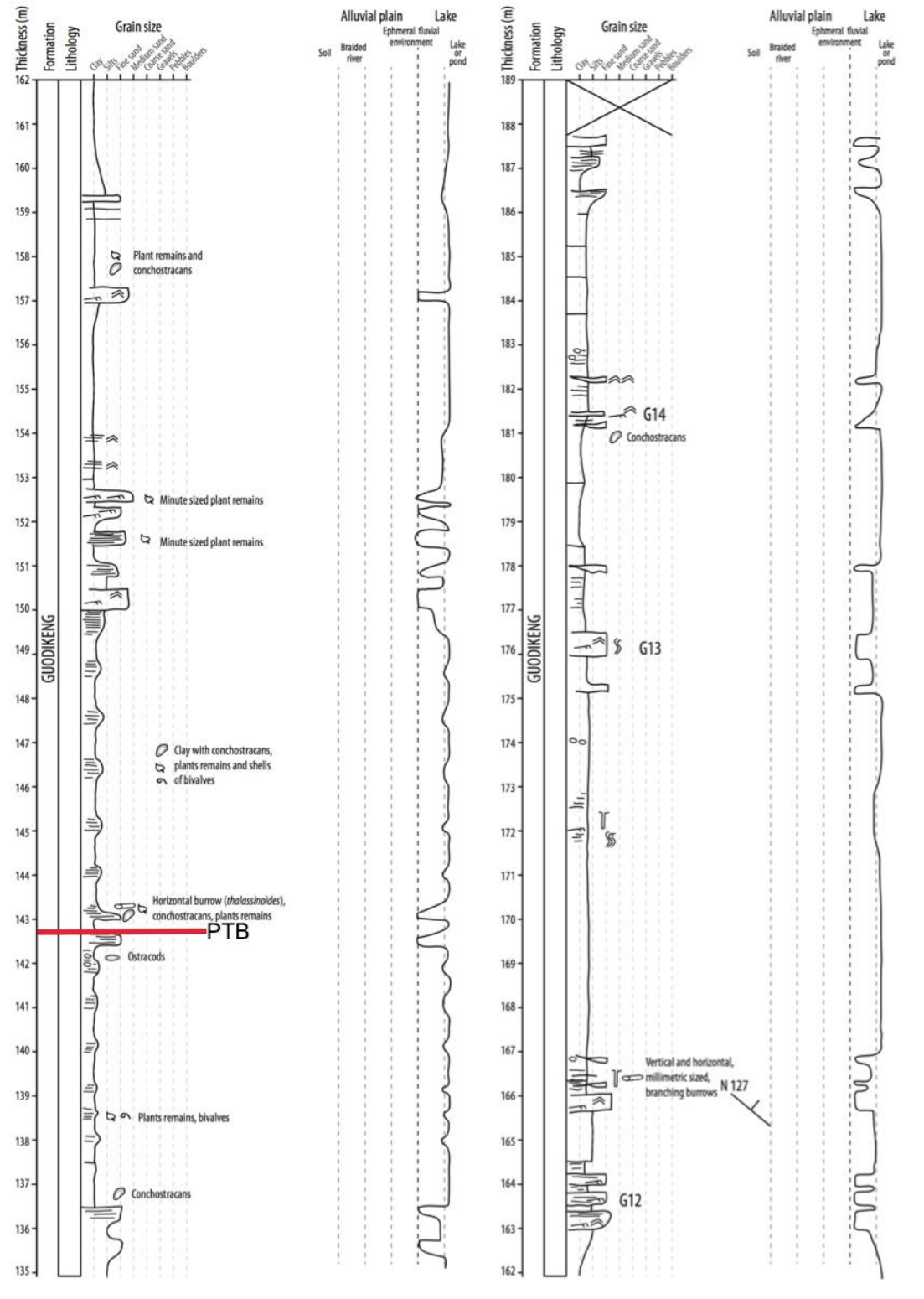

Figure 4-1 (continued) Sedimentological log along with depositional environment interpretation for the Dalongkou north limb section.

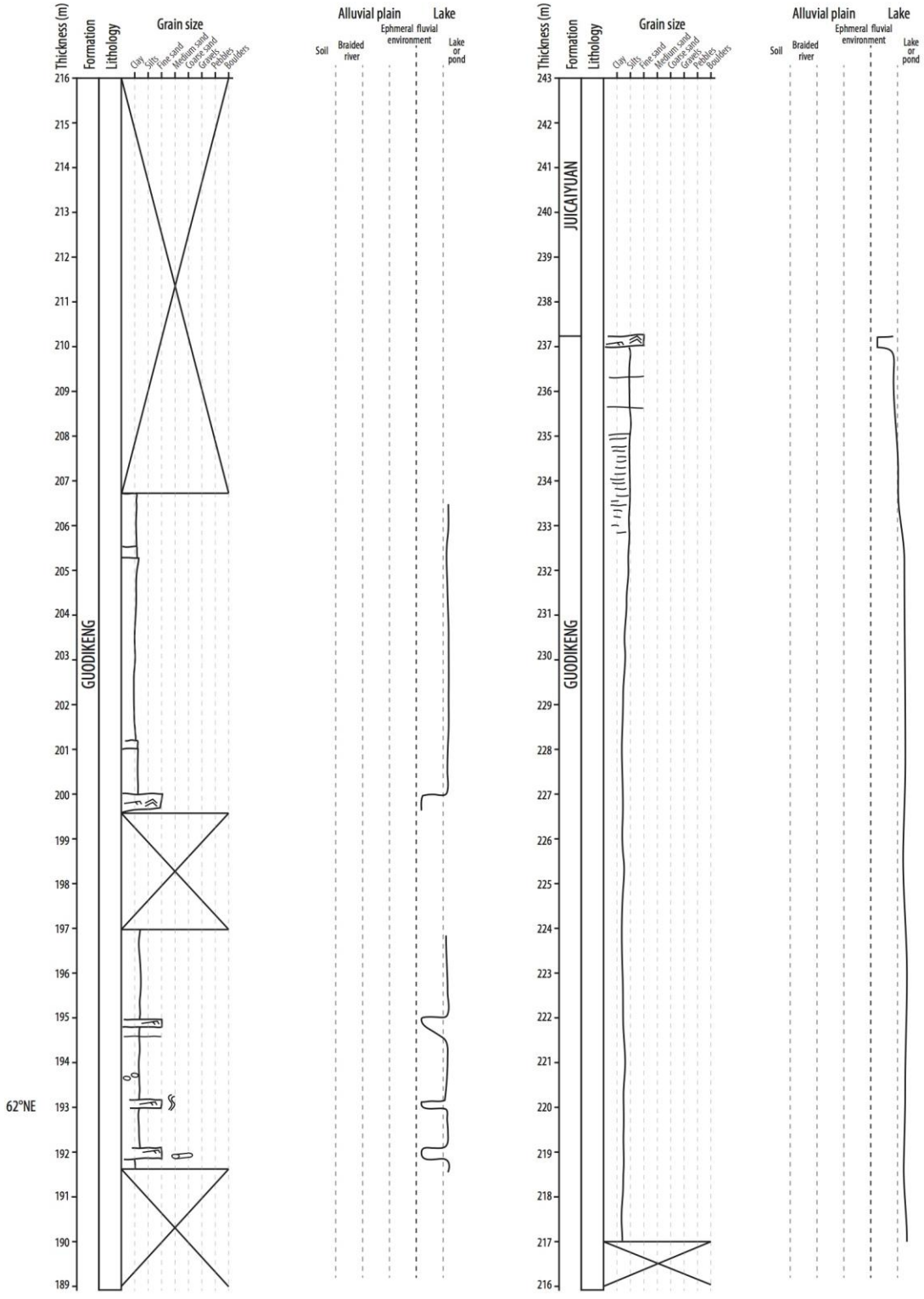

Figure 4-1 (continued) Sedimentological log along with depositional environment interpretation for the Dalongkou north limb section.

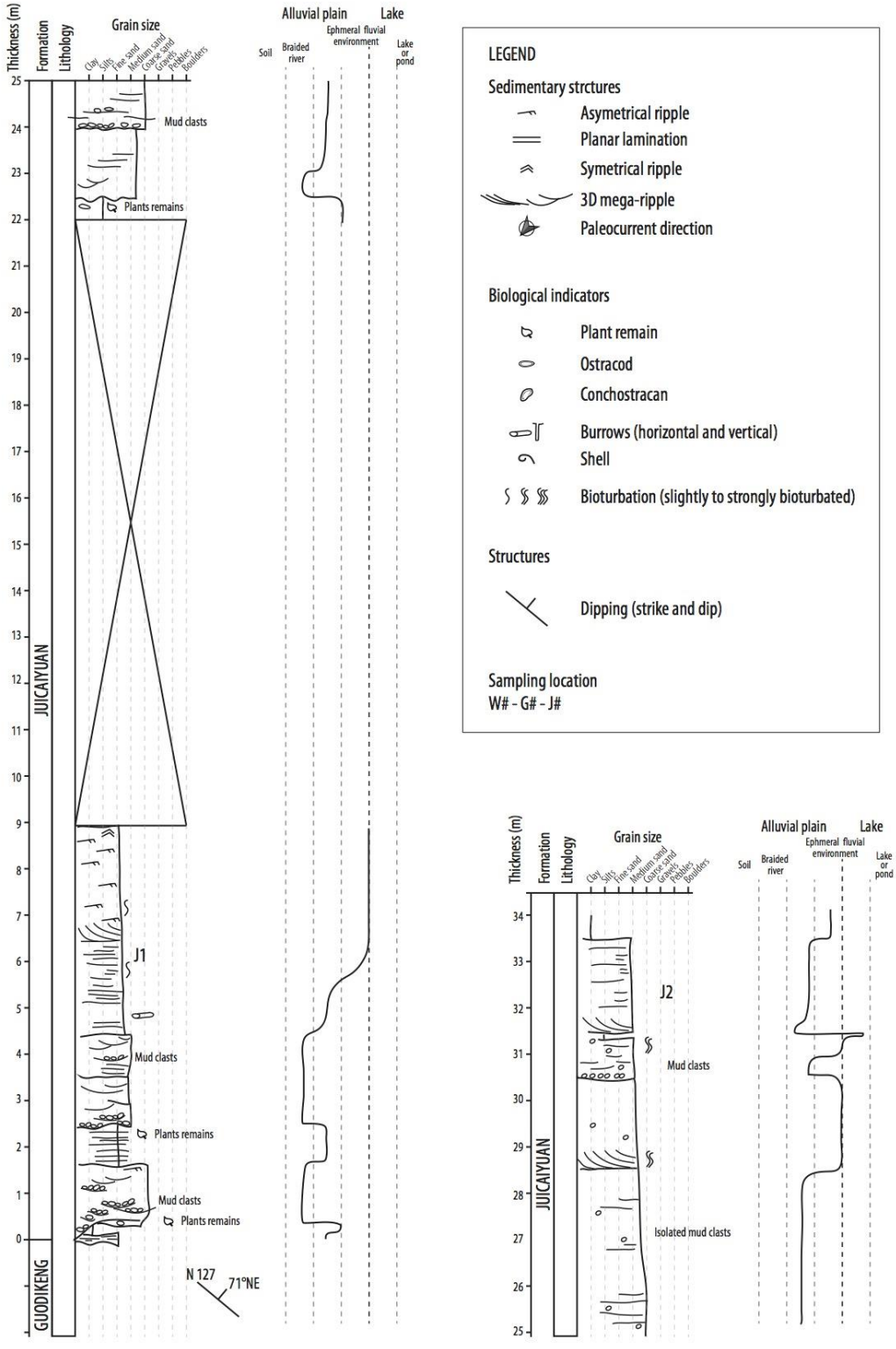

Figure 4-1 (continued) Sedimentological log along with depositional environment interpretation for the Dalongkou north limb section.

Figure 4-2 Representative sedimentary facies of the Wuttonggou, Guodikeng and Jiucaiyuan formations of the Dalongkou area.

A. Conglomeratic layer displaying through cross bedding (Gt facies, Table 4.1), Wuttonggou Formation Hammer for scale (40 cm).

B. Sandstone layer (Sh facies) displaying parting lineation (underlined by the dotted line), Wuttonggou Formation.

C. Large burrow crosscutting siltstones (Fl facies), Guodikeng Formation.

D. Fine sandstone displaying ripple cross lamination (Sr facies), Guodikeng Formation Hammer for scale (30 cm).

E. Bivalve fossils and plant remains fossilized together, Guodikeng Formation.

F. Large scale through cross bedding (St facies) underlined by mud clasts, Jiucaiyuan Formation Hammer for scale (40 cm).

G. Sandstone displaying planar lamination (Sh facies), Jiucaiyuan Formation. Hammer for scale (40 cm).

H. Plant stem fossil within the sandstones of the Jiucaiyuan Formation.

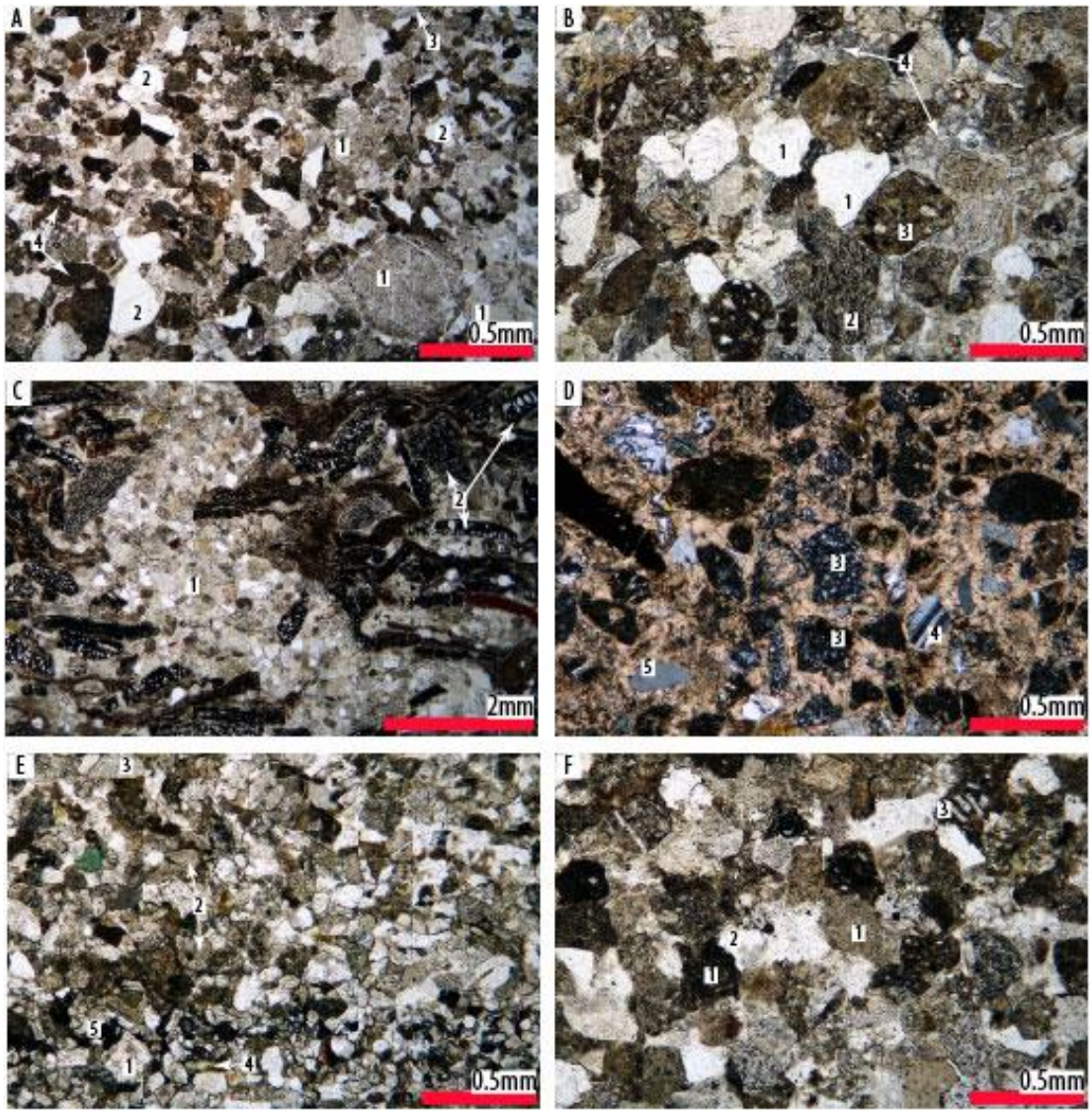

Figure 4-3 Thin section photographs of representative samples from the Wutonggou Formation, Dalongkou section.

A. Lithic arenite (sample W2), plane polarized light. 1: rounded cryptocrystalline lithic fragments. 2: rounded to sub-angular quartz grains. 3: weathered alkaline feldspar. 4: rounded silty rock fragments.

B. Calcite cemented lithic arenite (sample W1), plane polarized light. 1: sub-angular, monocrystalline quartz grains. 2: rounded trachytic volcaniclast. 3: silty lithic fragment. 4: sparitic calcite cement.

C, D. Calcite cemented lithic arenite (sample W3), plane polarized light (B) and cross-polarized light (C). 1: burrow filled up by material similar to those presented in D. 2: Reworked wood fragments. 3: sub-rounded cryptocrystalline lithic fragments. 4: sub-angular plagioclase. 5: sub-

angular quartz grain.

E. Laminated, well-sorted lithic arenite (sample W4), plane polarized light. 1: microgranular lithic fragment. 2: slity rock fragments. 3: weathered sub-angular feldspar. 4: biotite flake and 5: rounded opaque minerals underlining a lamina.

F. Fine grained, well-sorted lithic arenite (sample W5), plane polarized light. 1: sub-rounded slity rock fragments. 2: polycrystalline quartz grain. 3: weathered, rounded volcaniclast displaying a microlithic texture.

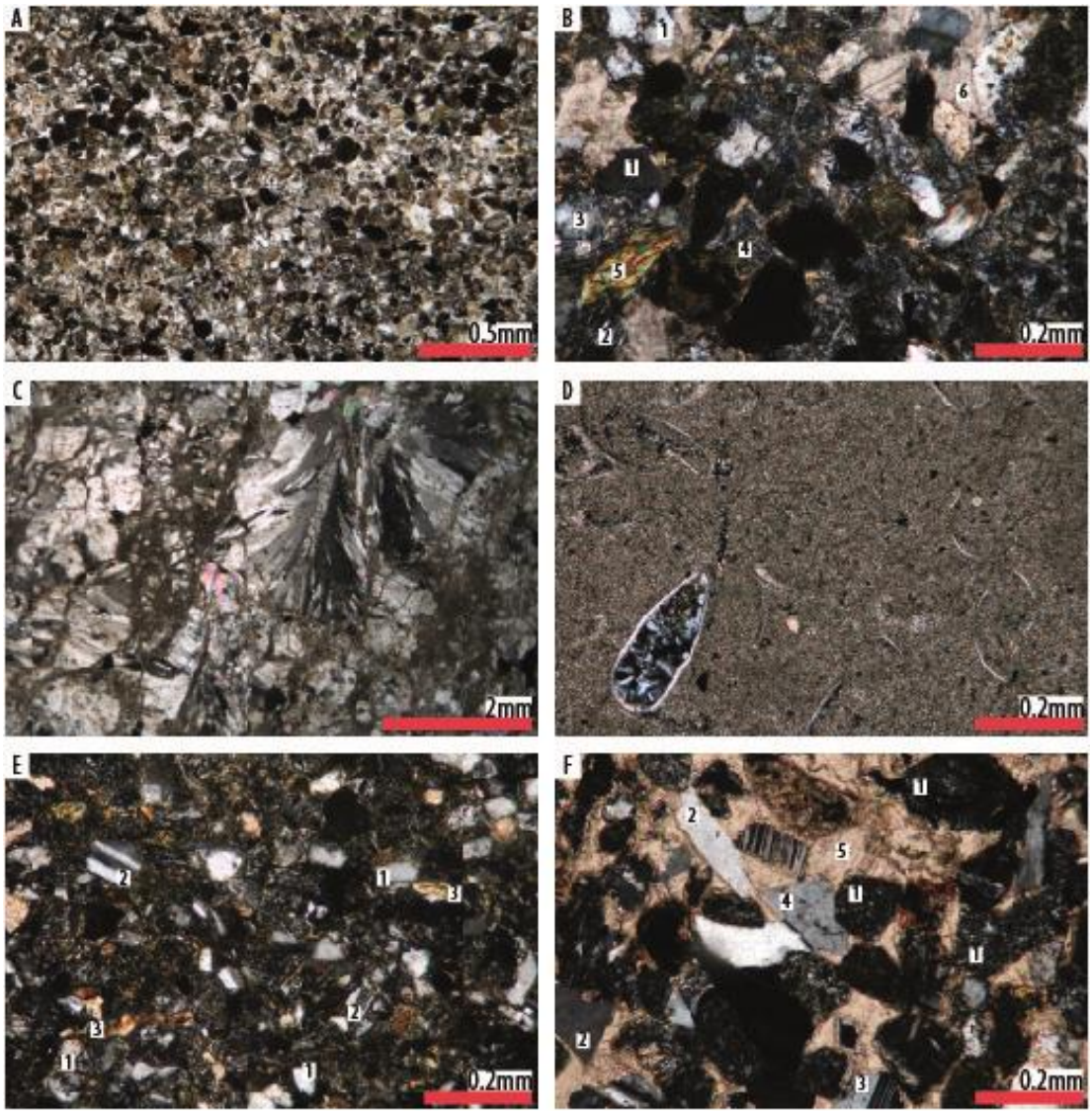

Figure 4-4 Thin section photographs of representative samples from the Guodikeng Formation, Dalongkou section, Xinjiang.

A. Packstone limestone (sample G6), plane polarized light. This limestone is made up pelloidals (dark, rounded elements) and detrital minerals enclosed within a micritic matrix.

B. Fine grained quartz arenite constituting the matrix of calcareous nodules (sample G8), cross-polarized light. 1: quartz grains. 2: plagioclase. 3: seritized alkaline feldspar. 4: cryptocrystalline lithic element. 5: biotite. 6: sparitic calcite.

C. Limestone (sample G7), cross-polarized light. This limestone is composed of radial fibrous calcite within a micritic matrix.

D. Limestone (sample G10), cross-polarized light. Mudstone containing small bioclasts.

E. Quartz wacke (sample G11), cross-polarized light. 1: quartz grains. 2: plagioclase. 3: biotite flakes.

F. Fine grained, calcite cemented, lithic arenite (sample G14), cross-polarized light. 1: cryptocrystalline lithic fragments. 2: sub-rounded to sub-angular quartz grains. 3: plagioclase. 4: alkaline feldspar. 5: sparitic cement enclosing the various detrital elements contained within this lithic arenite.

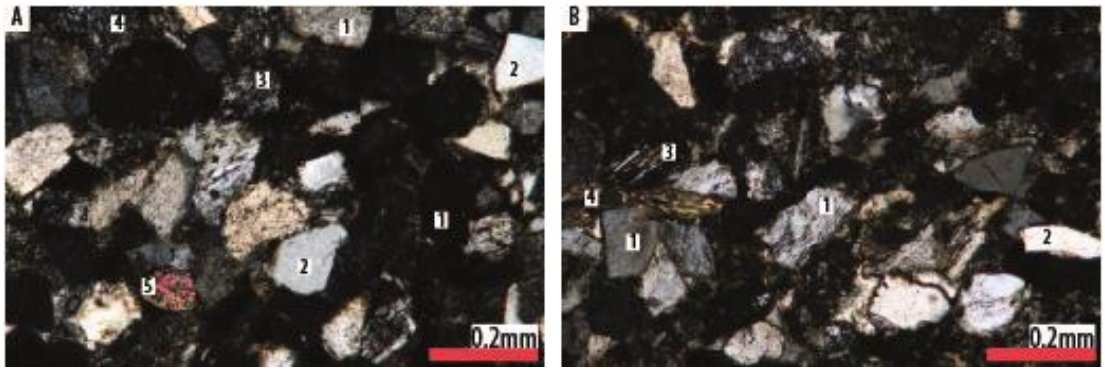

Figure 4-5 Thin section photographs of representative samples from the Jiucaiyuan Formation, Dalongkou section, Xinjiang.

Cross-polarized light.

A. Feldspathic arenite (sample J1). 1: sub-angular to sub-rounded, weathered alkaline feldspar. 2: sub-angular quartz grains. 3: trachytic volcaniclast. 4: cryptocrystalline lithic fragment. 5: zircon grain.

B. Feldspathic arenite (sample J2). 1: seritized to strongly weathered feldspar grains. 2: quartz grain. 3: microlithic volcaniclast. 4: biotite flake.

§4.2 Taoshuyuan area

Two distinct sections, called the Taoshuyan A (Fig. 4-6) and the Taoshuyuan C (Fig. 4-7) sections, have been investigated in the Taoshuyuan area. As these two sections are distant by only 1.5 km and display essentially similar characteristics, they are presented together. Some faults have been observed in this area and sections selected for logging have been carefully evaluated to avoid measurements in area that underwent tectonic deformation (except a tilting of the series). The bedding displays consistent WNW-ESE strike (between 108 and 109°N) and subvertical dipping in the Taoshuyuan A section. In the Taoshuyuan C section, beds display a NW-SW strike, comprised between 123 and 136°N, and dip toward the NE with a dipping angle of 50 to 53°.

4.2.1 Upper part of the Wutonggou Formation

In the Taoshuyuan area, the upper part of Wutonggou Formation comprises mudstone, siltstones and sandstones. As for the Wuttonggou Formation in the Dalonkgou area, only

the uppermost part of this formation has been measured. A 36 m thick section has been logged in the Taoshuyuan A section (Fig. 4-6). For the Taoshuyuan C section (Fig. 4-7), only a very limited part (ca. 3 m thick) of the Wuttonggou Formation was available for logging. Remaining part of this formation, as well as the boundary with the stratigraphically overlying Guodikeng Formation and the lower part of the Guodikeng Formation was hidden by the alluvium of a small temporary stream. The thickness non available for logging was measured using a Jacob's staff. In the Taoshuyuan sections, a total of six facies have been identified in the Wutonggou Formation

The sediments of the upper part of Wutonggou Formation are rather homogeneous and the Fl and Fm facies dominate throughout the section. Coarser sandstones constitute a minor component of the Wuttonggou Formation in the Taoshuyuan sections. Fl and Fm facies are characterized by 0.1 to 3 m thick units made up of yellowish, grey to black mudstone to siltstones with frequent interbedding of very thin (cm thick) layers made up of very fine sandstones underlying planar lamination (Fl facies, Table 4-1). The Fl and Fm facies are interpreted to represent deposition from suspension, in a perennial, shallow water body.

Fine to medium sandstones (Sr facies, Table 4-1) commonly display small-scale current ripples. Plant leaves and leafy stems were preserved (Fig. 4.8B), and a few coal seams (C facies, Table 4-1) have also been identified. Numerous beds with abundant ostracods, conchostracans, bivalves (Fig. 4.8A) and plant remains frequently occur in fine sandstones displaying horizontal laminations (Sh facies, Table 4-1). Plant leaves sometimes underline these laminations.

Petrographic investigations (Table 4-2, Fig. 4-9) indicate that the sandstone levels from the Taoshuyuan sections display overall similar features than those displayed by the samples from the Dalongkou section. However, both lithic and monocrystalline elements display a more rounded shape in the Taoshuyuan sections than in the Dalongkou section, suggesting a longer transportation (either longer in time and/or in space).

4.2.2 Guodikeng Formation

The Guodikeng Formation comprises detrital terrigenous red, green, yellow, to grey and dark grey mudstones, siltstones, sandstones and conglomerates as well as limestone layers. In the Taoshuyuan A section, the whole Guodikeng Formation has been measured except a small part disturbed by faults (Fig. 4-6). In the Taoshuyuan C section (Fig. 4-7), the basal part of the Guodikeng Formation is hidden by recent alluvial deposits and has consequently not been measured. This formation comprises mainly siltstone to fine sandstone facies, but also contains subordinate conglomerates and limestone facies. A total of 8 distinct facies have been identified in the Guodikeng Formation

Conglomeratic facies are represented by the Gt facies (Table 4-1). These conglomerates are characterized by polygenic, mixed angular to rounded clasts,

displaying a grain size ranging from gravels to pebbles (Fig. 4.8C and D).

The sandstone facies comprise a variety of grain size, ranging from microconglomeratic levels (very coarse sandstones) to fine sandstones. These sandstones display either planar laminations (Sh facies, Table 4-1), sometimes underlined by plant leaves, or cross-laminated ripples (Sr facies, Table 4-1) to megaripples, generally underlined by grain size changes (St facies, Tables 4-1) and erosive base. These sandstone facies sometimes constitute meter thick units, but are more frequently interbedded within finer facies (siltstones to mudstones) as centimeter to 0.5 thick units.

Siltstones to mudstones facies correspond to the Fl and Fm facies (Table 4-1). The succession comprises 0.1 to 1.5 meter thick units. The Fl facies (Fig. 4-8C) shows horizontal laminations and sporadic small scale current ripples. Fm facies are well developed and constitute pluri-meters thick units.

Siltstone facies also comprise reddish silts containing carbonated nodules and sporadically displaying small polished surfaces, interpreted as slickenslides. These features are interpreted to result from pedogenic processes and indicate the occurrence of P facies within the Guodikeng Formation vertebrate fossil remains have been excavated from these levels.

A few limestone layers, ca. 0.1 m thick (L facies, Tables 4-1 and 4-2) also occur within the Guodikeng Formation. They display wackestone to mudstone textures and contain bioclast remains. They are interpreted as deposition from suspension in a permanently flooded shallow water body or lake.

Petrographic analyses (Table 4-2, Fig. 4-10) indicate that the samples composed mainly by siliceous detrital elements contain volcaniclasts displaying various textures. These samples also contain clinopyroxene and olivine, sometime embedded within volcaniclasts. This attests the contribution of a mafic volcanic source to the detrital particles that composes these arenites. The weathering and roundness displayed by the volcaniclasts suggest a distal volcanic source, and/or that the volcanism is not coeval with the sedimentation.

4.2.3 Lower part of the Jiucaiyuan Formation

As in the Daglonkou area, we have only investigated the lower part of the Jiucaiyuan Formation in the Taoshuyuan area. The basal part of Jiucaiyuan Formation comprises a few limestone layers, silty mudsones, siltstones and sandstones (Figs. 4-6 and 4-7). The investigated part of the Jiucaiyuan Formation exhibits 5 distinct facies.

Coarse-grained facies are represented by a conglomeratic facies displaying trough cross bedding (Gt facies, Table 4-1) and two sandstones facies. Coarse-grained sandstones forming normally graded, 1 to 1.5 m thick units and displaying 3D megaripples correspond to the St facies (Fig. 4-8E, Table 4-1). A few sandstone units display finer grain-size (medium sand grain-size) and are characterized by horizontal

lamination (Sh facies, Table 4-1). These conglomeratric and sandstone units alternate with reddish siltstones with erosive basis.

The Fm facies is the dominant facies of the investigated part of the Jiucaiyuan Formation in the Taoshuyuan area. This facies comprises homogenous siltstones to silty mudstones. The Fm facies is interpreted as deposition within calm aqueous environments.

Subordinate limestone layers (L facies, Table 4-1) also occur within the Jiucaiyuan Formation

Petrographic analyses (Fig. 4-11, Table 4-2) indicate that the limestone displays a mudstone texture (Fig. 4-11A). It attests a quiet, sub-aqueous depositional environment. Sandstones (lithic arenite, Fig. 4-11B) are made up of volcaniclasts displaying various textures and mafic mineral, implying a mafic volcanic source.

4.2.4 Paleoenvironmental interpretation

Wutonggou Formation. Two facies associations characterize this formation. The first association comprises the Fm, Fl and Sr facies. This facies association corresponds to calm, ever-flooded lake or pond environments (Figs. 4-6 and 4-7).

The second facies association is made up of Fl, Sh and C facies, and is interpreted to represent flood plain depositional environment, in which unconfined and temporary fluvial environment occurs (Figs. 4-6 and 4-7).

Guodikeng Formation. Three distinct facies association are present in this formation. As for the Wutonggou Formation, the Fm, Fl, Sr and L (where present) facies association represents calm, ever-flooded freshwater pond or lake environments (Figs 4-6 and 4-7).

A second facies association, represented by the Gt and St facies, constitutes a minor component of the Guodikeng Formation This facies association is interpreted as braided rivers depositional setting (Figs 4-6 and 4-7).

The third facies association includes the P, Fl, Fm and Sh facies. This association is indicative of unconfined and ephemeral fluvial environments, such as waning flood and overbank deposits within an alluvial plain where soils locally develop (Figs 4-6 and 4-7). Specifically, 1 to 4 meters thick sequences comprising Sh facies fining upwards to the Fl and Fm facies are interpreted as flash discharges leading to the deposition of sand-sheets within alluvial plain settings.

Jiucaiyuan Formation. Two facies associations characterize this formation. The Gt and St facies association corresponds to braided rivers depositional environment (Figs 4-6 and 4-7).

The Fm, Sh and L (where present) facies association is characteristic of ephemeral fluvial environments that temporarily flow through a flood plain. The development of limestone layers suggests that lake or ponds could have occurred within this flood plain.

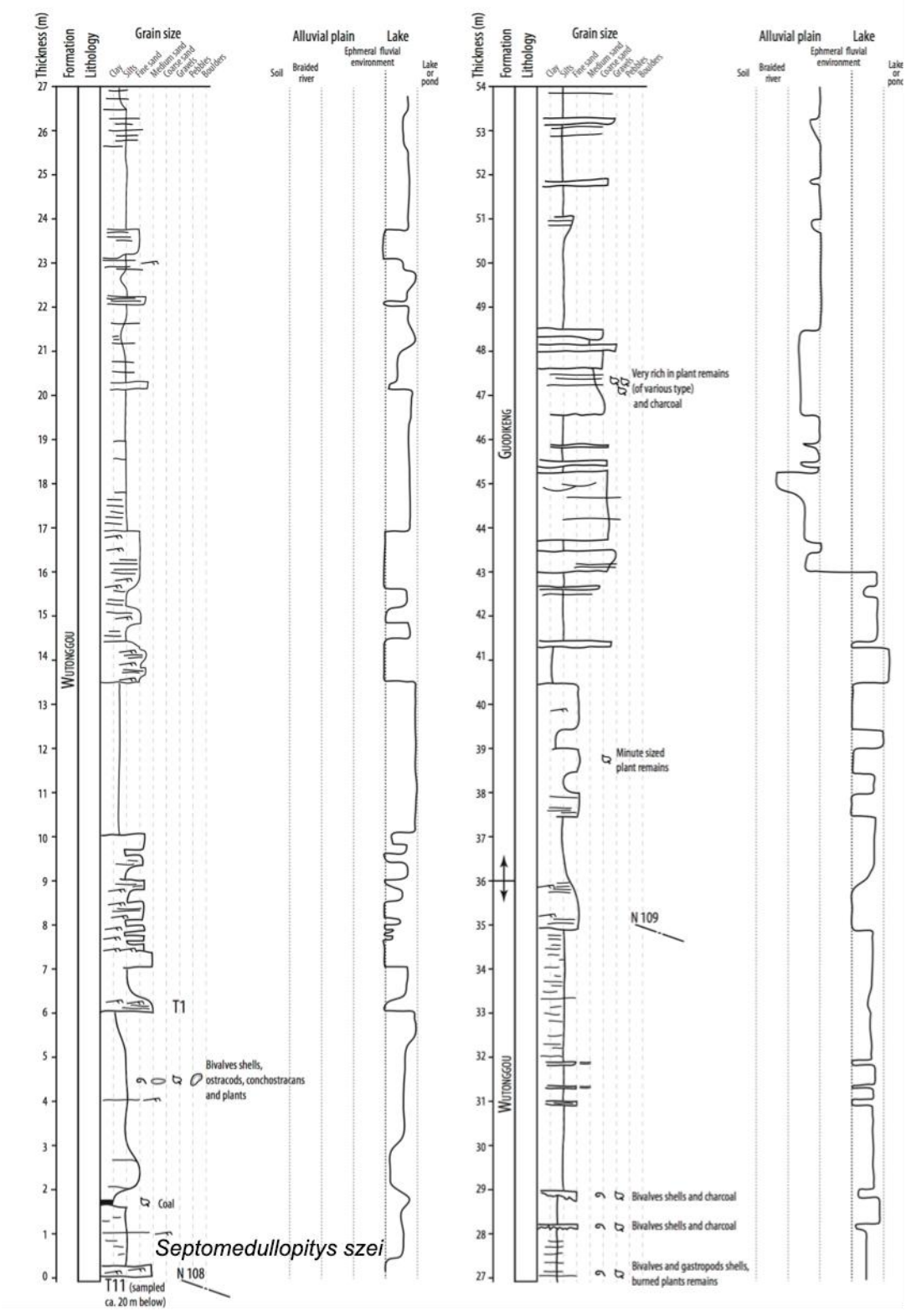

Figure 4-6 Sedimentological log along with depositional environment interpretation for the Taoshuyuan A section.

Logging have been performed between the coordinates N43°15'06.2"; E88°58'08.0" and N43°15'00.8"; E88°58'08.5". The location of the sampling site for petrographic and paleontological investigation is reported along the measured section. See Fig. 4-1 for legend.

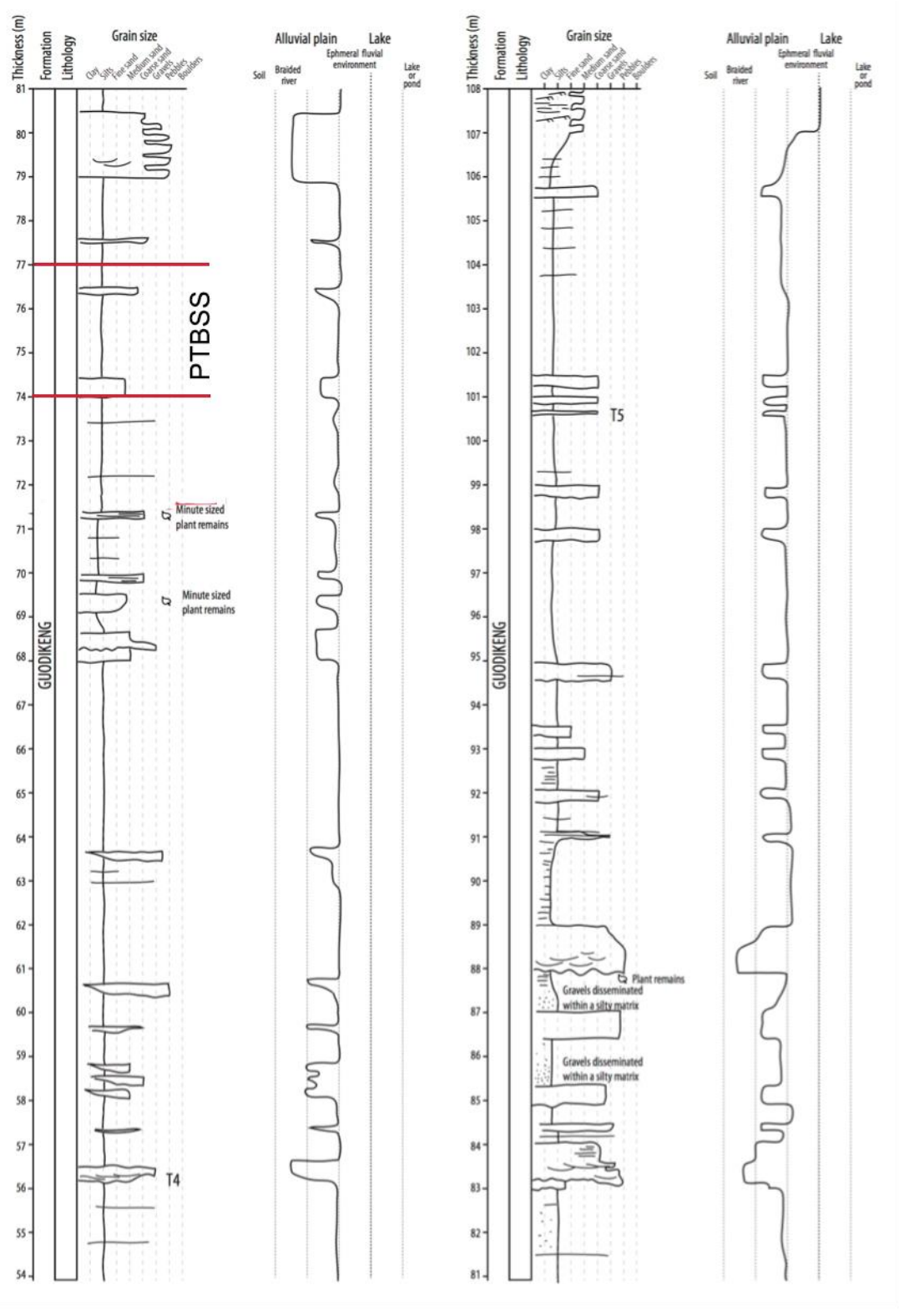

Figure 4-6 (continued) Sedimentological log along with depositional environment interpretation for the Taoshuyuan A section.

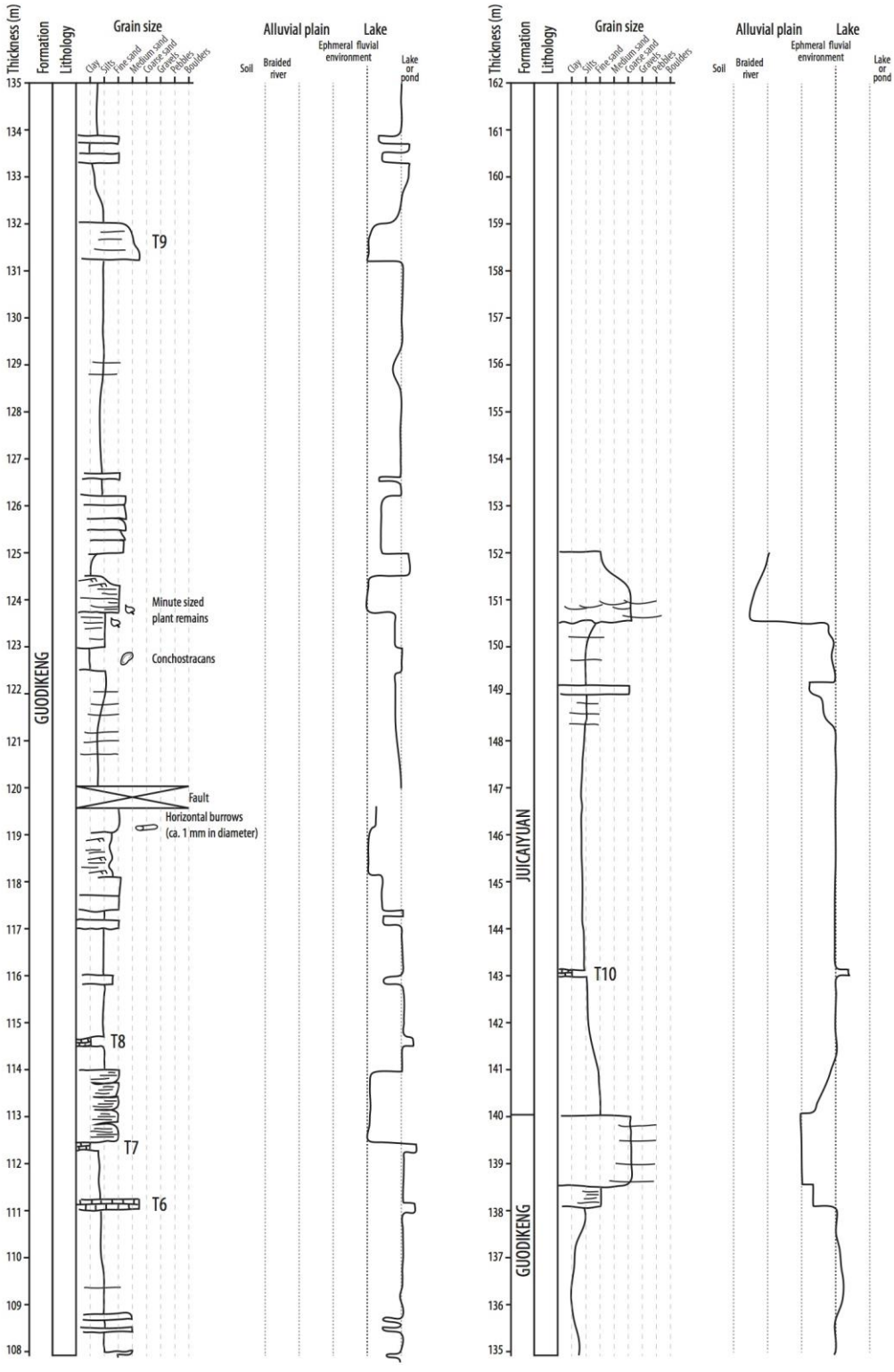

Figure 4-6 (continued) Sedimentological log along with depositional environment interpretation for the Taoshuyuan A section.

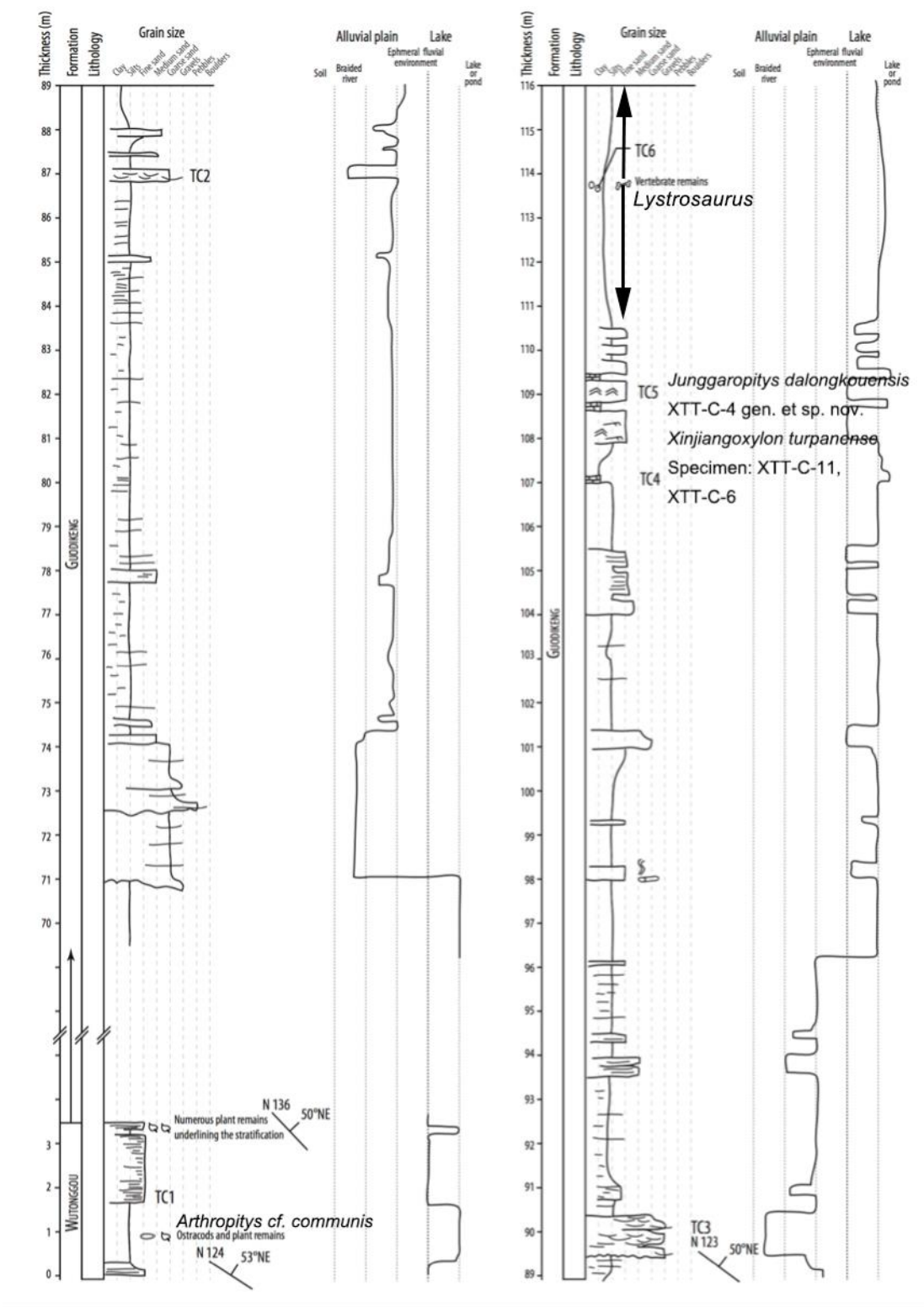

Figure 4-7. Sedimentological log for the Taoshuyuan C section.

Logging have been performed at the coordinate N43°13'54.7"; E88°58'17.6". The location of the sampling site for petrographic and paleontological investigation is reported along the measured section.

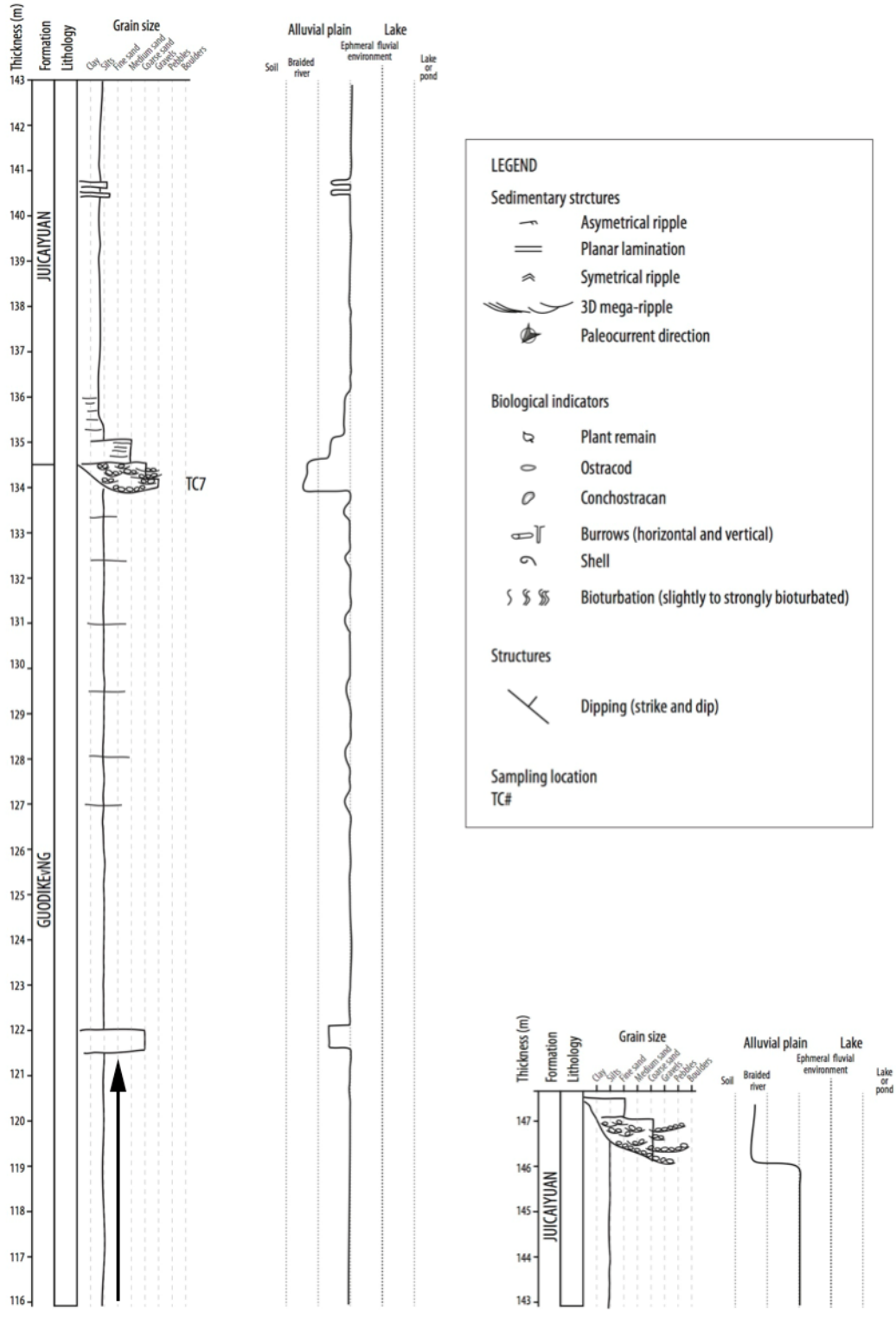

Figure 4-7 (continued) Sedimentological log for the Taoshuyuan C section.

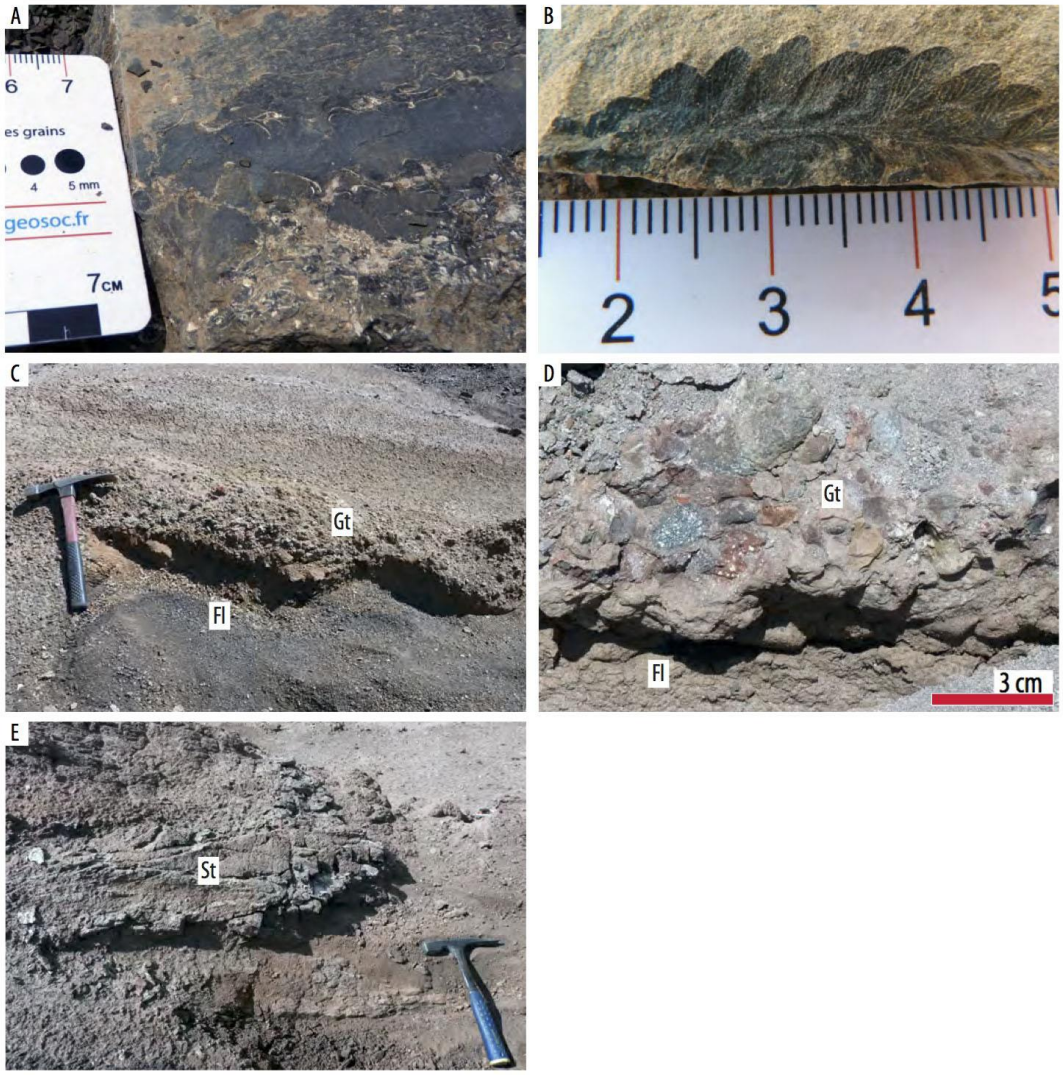

Figure 4-8 Representative sedimentary facies of the Wuttonggou, Guodikeng and Jiucaiyuan formations of the Taoshuyuan area.

A. Bivalve shells within black silts. Wutonggou Formation, Taoshuyuan A section.

B. Plant leave "*Callipteris*" sp. underlying the planar lamination within fine sandstones. Wuttonggou Formation, Taoshuyuan C section.

C, D. Conglomeratic layer displaying through cross bedding (Gt facies, Table 4-1) overlying siltstones (Fl facies, Table 4-1) with erosional base. Conglomerates are made up rounded to sub-rounded, polygenic clasts. C: hammer for scale (40 cm). Guodikeng Formation, Taoshuyuan A (picture C) and Taoshuyuan C (picture D) sections.

E. Sandstone facies displaying 3D megaripples (St facies, Table 4-1). Jiucaiyuan Formation, Taoshuyuan A section.

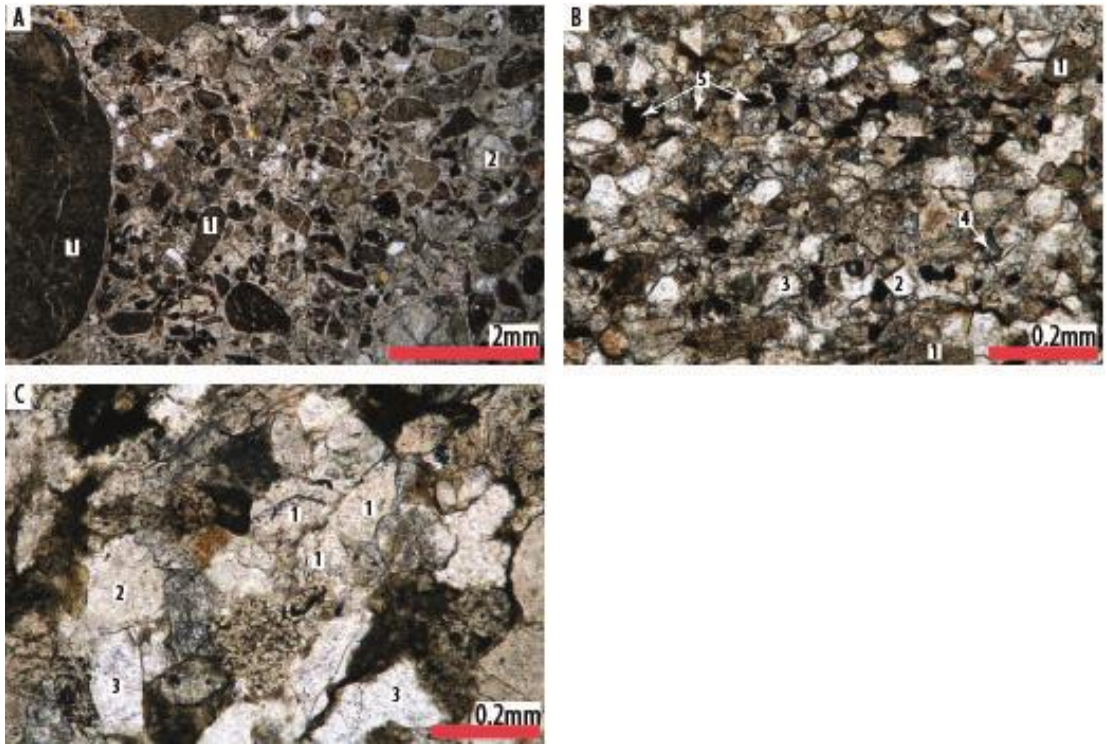

Figure 4-9 Thin section photographs of representative samples from the Wutonggou Formation, Taoshuyuan A and C sections, Xinjiang.

A. Coarse grained calcite cemented lithic arenite (sample T11, Taoshuyuan A section), plane polarized light. 1: variously sized rounded silty lithic fragments. 2: volcaniclast displaying a microlithic texture.

B. Fine grained, laminated calcite cemented lithic arenite (sample T1, Taoshuyuan A section), plane polarized light. 1: silty lithic fragments. 2: sub-angular quartz grains. 3: seritized feldspar. 4: zircon grain. 5: rounded opaque minerals underlining the laminae.

C. Fine grained calcite cemented lithic arenite (sample T1, Taoshuyuan C section), plane polarized light. 1: rounded cryptocrystalline lithic fragments. 2: microgranular lithic fragment. 3: seritized alkaline feldspar.

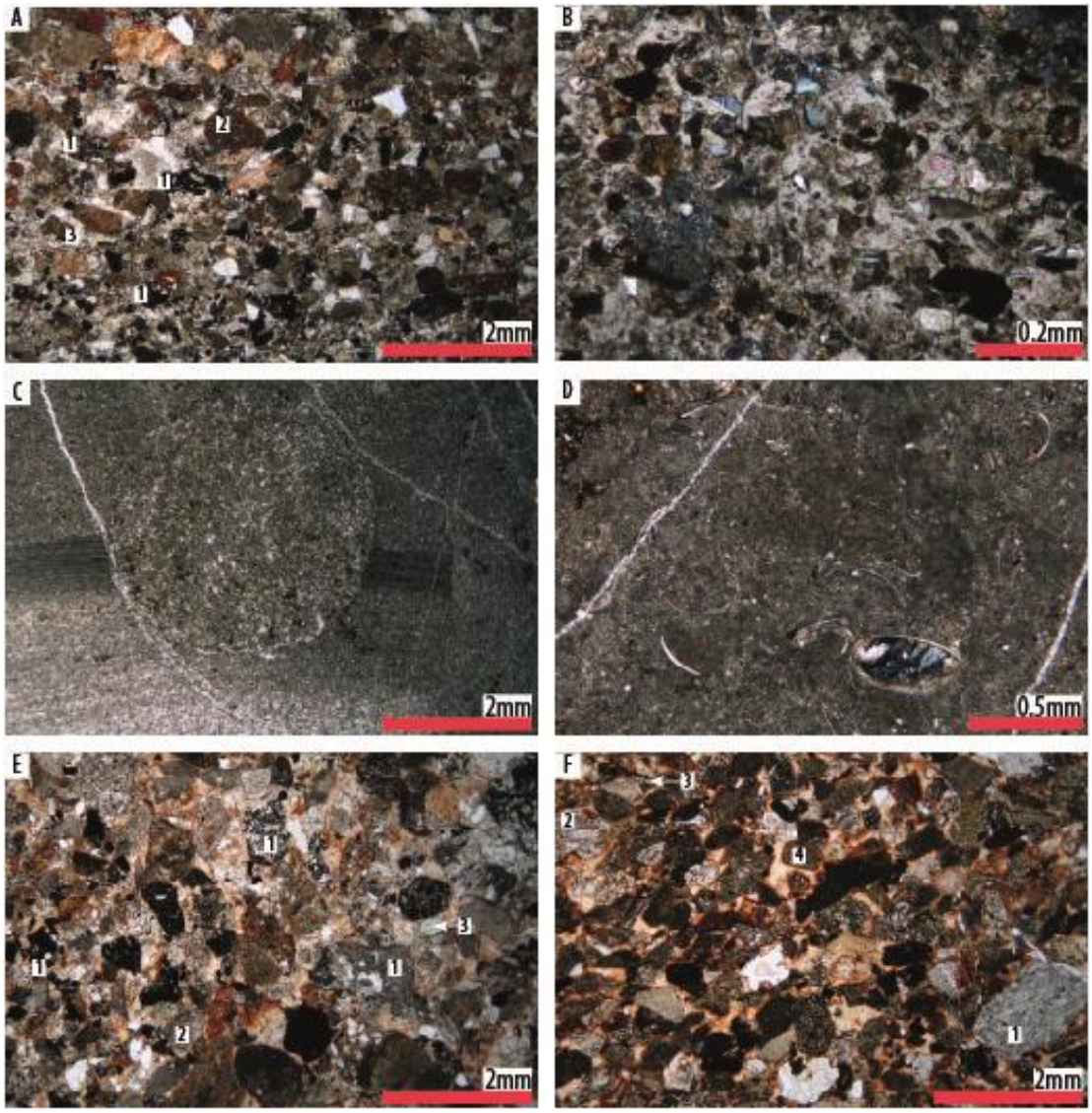

Figure 4-10 Thin section photographs of representative samples from the Guodikeng Formation, Taoshuyuan A and C sections, Xinjiang.

A. Calcite cemented lithic arenite (sample T5, Taoshuyuan A section), plane polarized light. 1: rounded volcaniclasts displaying microlithic textures. 2: rounded silty lithic fragments. 3: sparitic calcite cement.

B. Limestone (sample T6, Taoshuyuan A section), cross-polarized light. Wackestone texture with micritic calcite enclosing very fine-grained detrital and pelloidals elements.

C. Limestone (sample T7, Taoshuyuan A section), plane polarized light. Mudstone texture with laminae disturbed by bioturbation.

D. Limestone (sample T8, Taoshuyuan A section), cross-polarized light. Mudstone texture. Bioclasts.

E. Lithic arenite (sample T9, Taoshuyuan A section), plane polarized light. 1: rounded volcaniclasts displaying various textures ranging from glass-rich, microlithic to trachytic textures. 2: rounded cryptocrystalline lithic fragments. 3: sub-rounded monocrystalline clinopyroxene.

F. Lithic arenite (sample TC3, Taoshuyuan C section), plane polarized light. 1: volcaniclast displaying a trachytic texture. 2: volcaniclast displaying a porphyritic texture. 3: volcaniclast

displaying a microlitic texture. 4: silty lithic fragment.

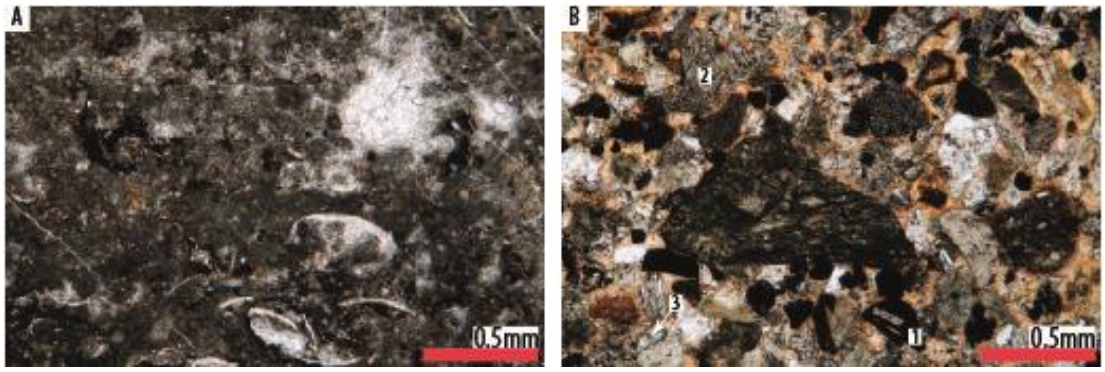

Figure 4-11 Thin section photographs of representative samples from the Jiucaiyuan Formation, Taoshuyuan A and C sections, Xinjiang.

A. Limestone (sample T10, Taoshuyuan A section), cross-polarized light. This limestone displays a mudstone texture and contains bioclasts.

B. Lithic arenite (sample TC7, Taoshuyuan C section), plane polarized light. 1: volcaniclast displaying a microlithic texture. 2: volcaniclast displaying a trachytic texture. 3: pyroxene.

§4.3 Discussion

The depositional environments evidenced in this work refine previous interpretations proposed for the Wutonggou, Guodikeng and Jiucaiyuan formations in both Dalongkou and Taoshuyuan areas. Indeed, the Wutonggou Formation have been interpreted to corresponds to “fluvial, meandering streams, and lacustrine systems” in the Dalongkou area (Metcalfe et al., 2009). In this area, the Guodikeng Formation is supposed to represent lacustrine setting (Metcalfe et al., 2009). The present study corroborates these interpretations and allow for precise and accurate paleoenvironments setting for each fossil sampling site. Such paleoenvironmental study constitutes a prerequisite condition to interpret the fossil record evolution in these sections that have been suggested as candidates for the global non-marine Permian-Triassic boundary reference section (e.g., Metcalfe et al., 2009; Chu et al., 2015).

Additionally to the sedimentary facies analysis, these sections (or geographically closely located section within the Junggar and Turpan basins) have been studied for petrography (e.g., Carroll et al., 1995; Hendrix, 2000; Greene et al., 2005). These petrographic analyses intended notably to assess the sandstone provenance to document paleogeographic and tectonic evolution of this area. The paleoevironmental, paleogeographic and tectonic implications of the composition of sandstone and limestone samples studied in this work are briefly considered below.

Detrital siliciclastic samples. The three investigated formations (Wutonggou, Guodikeng and Jiucaiyuan formations) comprise detrital siliciclastic samples, sometimes with calcareous cement. These samples consist mainly in lithic arenite, with a minor

amount of feldspathic arenite and quartz wacke. These general petrographic features are in good agreement with previous petrographic observations made in these 3 formations (Greene et al., 2005).

The shapes displayed by particles of the same lithology (notably quartz grains and feldspar grains) suggest the contribution of relatively proximal sources. The co-occurrence of angular and rounded grains within the same sample implies either the combined contribution of proximal and more distal sources or the reworking of particles previously reworked particles.

The lithology displayed by the detrital siliciclastic particles within each formation does not show marked changes through time, implying that the sources of detrital particles remains essentially the same. The textures displayed by the lithic fragments as well as the nature of the monocrystalline elements suggests that the dismantling of various types of sedimentary (silty and microcrystalline lithic fragments lithic fragment) and magmatic rocks (plutonic, hypovolcanic and volcanic rocks) contributed to the sedimentary input of these formations.

The volcaniclasts occurring within these three formations display various textures, implying the contribution of at least several distinct volcanic sources. The volcaniclasts are commonly weathered and rounded, suggesting a long transportation of the volcaniclastic particles and/or that the volcanic activity was not coeval with the sedimentation (e.g., the volcaniclasts experienced multiple sedimentation-reworking episodes). This corroborates the interpretation of Hendrix (2000) who suggested that volcaniclasts found within the Mesozoic volcaniclastic rocks of the Junggar and Turpan basins resulted from erosion of Devonian through Carboniferous volcanic arcs that cropped out along the northern flank of the Bogda mountains, with a distribution assumed to be similar to the recent ones. However, some samples display a relatively high content of volcaniclasts. Late Permian to Early Triassic magmatic activity has been reported in this area (e.g., Greene et al., 2005). Based on petrographic and geochronological evidences, Tang et al. (2014) argued for a volcanic activity coeval to the sedimentation during the early to middle Permian in the Junggar and Turpan basins, while the volcaniclasts appear to be of reworked origin during the Triassic. Further investigations (geochemical, geochronology) about the volcaniclastic material contained in these formations could potentially be useful to provide additional constrains on the tectonic setting for the volcanism, the provenance of the volcanic material and the depositional age of these formations.

The sources (both sedimentary and magmatic rocks) appear to be similar for the Dalongkou and the Taoshuyuan sections. A noticeable difference lies in the occurrence of mafic (volcanic and/or plutonic) sources (e.g., pyroxene, olivine) material within the detrital siliciclastic particles that compose the rocks of the Taoshuyuan section. Except this difference (that could be link to preferential weathering of the mafic materials, small differences in the sources between the Dalongkou and the Taoshuyuan sections or to sampling bias, for instance), the material is nearly the same. This supports the interpretation that the present Dalongkou and Taoshuyuan sections belonged to the same

basins during the deposition of the Wutonggou, Guodikeng and Jiucaiyuan formations, as already put forward by several authors (e.g. Greene et al., 2005; Bian et al., 2010). Thus, the uplift of the Bogda Mountains probably took place later (during the Early Jurassic according to Greene et al., 2005).

Limestone samples. The Guodikeng Formation (both in Dalongkou and Taoshuyuan sections) and the Jiucaiyuan Formation (only in the Taoshuyuan section) comprise limestone samples. These limestones display packstone, wackestone and mudstone textures and commonly contain evidence of biological activity (bioturbation, pelloid elements) and/or biological remains (e.g., shells). These fossils attest a sub-aqueous depositional environment. The textures displayed by these limestone rocks also imply a quiet, low energetic depositional environment with a moderate (packstone and wackestone) to very limited (mudstone) siliciclastic detrital input. These observations are consistent with a lacustrine setting.

Similar limestones (i.e., “mixed siliciclastic sandstone and carbonate mudstone, peloidal packstone to grainstone”; Carroll et al., 1995) interbedded within siliciclastic conglomerates and sandstones have also been reported in the Late Permian formations (including the Wutonggou Formation) located between the cities of Urumqi and Jimsar (Carroll et al., 1995). These limestone beds are also interpreted as fresh-water carbonates (Carroll et al., 1995).

Table 4-1. Description of the main sedimentological facies and associated abbreviations.

Code	Lithofacies	Sedimentary structures	Depositional processes
Siltstone and mudstone			
Fl	Homogeneous black silt, locally rich in organic matter.	Planar lamination.	Deposition from suspension.
Fm	Black, reddish and greenish mudstone to siltstone.	Massive.	Deposition from suspension.
Sandstone			
Sr	Very fine to fine sand.	Asymmetrical, cross-laminated ripples or symmetrical ripples.	Current ripples (asymmetrical), lower part of the lower flow regime (Miall, 1996) and wave generated ripples (symmetrical).
St	Fine to coarse to sand.	Through cross-stratifications underlined by grain-size variations. Erosive basal boundary.	Tractive current, upper part of the lower flow regime, 3D megaripple migration (Miall, 1996).
Sh	Fine to coarse to sand.	Planar or sub-planar lamination.	Tractive current, upper flow regime (Miall, 1996).
Conglomerate			
Gt	Polygenic, with angular to rounded clasts with a grain size ranging from gravel to pebbles (cm), sometimes containing plant remains.	Through cross stratification.	Tractive current, upper part of the lower flow regime (Miall, 1996).
Other facies			
P	Small polished surfaces occurring within mudstone rich layers.		Shrink-swell processes in clay rich paleosols.
C	Coal seams with detrital terrigenous particles.	Reworked plant fragments.	Reworking of plant remains and mixing with detrital particles.
L	Limestone layers or nodules, displaying mudstone to packstone textures and containing a various amount of siliciclastic particles and fossils (mainly bivalves).	Laminated with occasional bioturbation (e.g., burrows).	Deposition from freshwater lake.

Table 4-2 Main petrographic features for the Wutonggou, Guodikeng and Jiucaiyuan formations in Dalongkou and Taoshuyuan sections.

Sample	Petrography
	Dalonkgou section
Wutonggou Formation	
W2	Lithic arenite. Coarse grained, poorly sorted (0.1 to 2 mm in size) arenite with grain size variations underling laminae. Angular to rounded polygenic grains. Rounded to sub-rounded cryptocrystalline lithic fragments. Quartz (mainly angular, some are rounded), occurring as individual or polygenic grains. Silty lithic fragments sometimes crosscut by small veins. Trachytic volcaniclasts. Microgranular lithic fragments. Polygenic rock fragments. Weathered, mainly angular feldspar (microcline, plagioclase, a few alkaline feldspars). Biotite, epidote, chlorite, zircon, and diagenetic micritic calcite coating some quartz grains.
W1	Calcite cemented lithic arenite Very fine-grained, well-sorted arenite, mainly composed of sub-angular quartz grains, sometime displaying undulatory extinction, and rounded to sub-rounded silty fragments. Rounded to sub-rounded cryptocrystalline lithic fragments. Sub-rounded to sub-angular plagioclase. Rounded, strongly weathered volcaniclasts (microlitic to trachytic). Rounded microgranular lithic fragment. Rounded chlorite and zircon grains. Biotite. Fossil fragment? Sparitic calcite cement, with minor amount of chlorite.
W3	Calcite cemented lithic arenite. Fine-grained, well-sorted arenite. Grains are cemented by an abundant calcite cement. Rich in minute, elongated, fossil plants fragments displaying a preferred orientation underlining the laminae. Rounded silty lithic fragments. Angular to sub-angular quartz grains. Cryptocrystalline rounded to sub-angular lithic fragments. Angular microcrystalline quartz fragments. Microgranular lithic fragments. Sub-angular to angular feldspar (plagioclase, microcline). Sub-angular trachytic volcaniclasts. Rounded epidote grains. Chlorite. Biotite flakes. Bioturbation (burrow) disturbing the original lamination.
W4	Lithic arenite. Fine to very fine-grained, well sorted and laminated lithic arenite composed of rounded cryptocrystalline lithic fragments with a poorly developed silty matrix. Sub-angular to angular quartz grains. Sub-angular to rounded silty and microgranular lithic fragments. Angular to sub-angular alkaline, plagioclase and microcline feldspar. Chlorite. Epidote grains. Microlithic volcaniclasts. Biotite. Opaque minerals underlining the laminae. Zircon grains.
W5	Lithic arenite. Fine grained, well-sorted lithic arenite mainly made up of rounded silty lithic fragments, rounded, strongly weathered volcaniclasts displaying a microlitic texture, rounded to sub-angular quartz grains (sometimes with apatite needle inclusions) and weathered feldspar. Cryptocrystalline and a few granular (quartz-feldspar) lithic fragments. Rounded to sub-rounded plagioclase. Biotite flakes. Chlorite. Zircon grains.
Guodikeng Formation	
G6	Limestone. Packstone comprising pelloidal grains, rounded silty lithic fragments, sub-rounded to sub-angular quartz grains and rounded and weathered plagioclase (possibly a few alkaline feldspars). Chlorite grains. Biotite

	flakes. Some darker, patchy areas resulting from biological activity (bioturbation). Small vein filled up by calcite.
G8	Fine grained quartz arenite with embedded limestone nodules, described separately below: Quartz arenite mainly composed made up rounded to sub-rounded quartz grains enclosed within a silty matrix, locally rich or even dominated by calcite. Cryptocrystalline lithic fragments. Plagioclase, microcline. Opaque minerals. A few chlorite grains. Biotite. Some darker, patchy areas, attributed to biological activity. Limestone nodules display textural variations at the thin section scale (packstone to wackestone). Sparitic calcite grains. Rounded plagioclase. Rounded to sub-angular quartz grains. Polycrystalline grains. Crypocrystalline fragments. Rounded, weathered volcaniclasts. Chlorite. Epidote.
G7	Limestone. Divergent, radial, fibrous calcite displaying undulatory extinction ("pseudosparstone"). Micritic matrix (<10% vol.).
G9	Quartz wacke. Very fine-grained, well-sorted, rounded quartz grains embedded within a silty matrix. Rounded plagioclase grains. Calcite. Chlorite. Rounded cryptocrystalline lithic fragments. Zircon grains. Laminae underlined by opaque minerals.
G10	Limestone. Mudstone containing a few disseminated very small fine quartz grains. Biogenic elements occurring as carbonate shells, commonly displaying a single valve. Small calcite veins.
G11	Quartz wacke. Rounded to sub-angular, very fine-grained, well-sorted quartz grains, sometimes displaying undulatory extinction. Plagioclases displaying various shapes and weathering. Opaque minerals underlining laminae. Chlorite. Muscovite. Biotite. Rounded silty lithic fragments. Zircon grains.
G12	Quartz wacke. Very similar to sample G11.
G13	Quartz wacke. Essentially similar to samples G11 and G12 but displaying a slightly coarser grain-size. A rounded area, filled by pelloidal grains within micritic matrix is interpreted as the product of a biological activity (burrow?).
G14	Calcite cemented lithic arenite. Fine-grained, well-sorted arenite made up of rounded, silty lithic fragments, microgranular and cryptocrystalline lithic fragments. Strongly weathered volcaniclasts. Sub-angular to rounded quartz grains, sometimes displaying undulatory extinction. Rounded to sub-angular plagioclase. Silty chips. Chlorite. Biotite. Epidote. Opaque minerals.
Jiucaiyuan Formation	
J1	Feldspathic arenite. Fine grained and well-sorted feldspathic arenite composed of angular to rounded, nearly fresh to weathered alkaline feldspar and plagioclase. Angular quartz grains. Rounded cryptocrystalline lithic fragments. Rounded and weathered volcaniclasts. Biotite. Chlorite. Muscovite. Opaque minerals. Rounded silty fragments. Zircon grain. Silty to clayish matrix.

J2	Feldspathic arenite. Fine-grained, moderate sorted feldspathic arenite displaying a parting lineation underlined by elongated minerals and lithic fragments. Sub-rounded to sub-angular, weathered feldspar (mainly alkaline, a few plagioclase). Sub-angular to sub-rounded cryptocrystalline lithic fragments. Microgranular fragments. Angular to sub-angular quartz grains. Biotite and muscovite flakes. Chlorite. Opaque minerals. Rounded and weathered volcaniclasts with microlithic to trachytic texture.
Taoshuyuan A section	
Wutonggou Formation	
T11	Calcite cemented lithic arenite. Variously sized, poorly sorted, sub-rounded to well-rounded silty lithic fragments. Large sub-rounded polygenic lithic fragments (volcaniclasts, cryptocrystalline fragments, silty fragments). Well-rounded volcaniclasts with glassy microlithic texture. Monocrystalline minerals: feldspar, quartz, weathered pyroxene (?).
T1	Calcite cemented lithic arenite. Lithic arenite displaying laminae (underlined by well rounded opaque minerals) and composed of fine grained, well sorted and rounded cryptocrystalline, microcrystalline and silty fragments. Sub-angular quartz grains, sometimes displaying undulatory extinction. Rounded seritized plagioclase. Alkaline feldspars. Chlorite. Biotite and muscovite flakes. Apatite occurring in inclusion within other minerals. Zircon grain.
Guodikeng Formation	
T4	Calcite cemented lithic arenite. Very similar to sample T11.
T5	Calcite cemented lithic arenite. Very similar to sample T11, but finer grained.
T6	Limestone. Laminated, locally disturbed by bioturbation, very fine-grained and well-sorted limestone displaying a wackestone texture. Pelloids. Sub-angular quartz grains. A few plagioclase and seritized alkaline feldspars. Opaque minerals. Biotite. Calcite grains. Unidentified bioclasts. Cryptocrystalline lithic fragments. Small calcite veins.
T7	Limestone. Laminated and bioturbated limestone displaying a mudstone texture. Small calcite veins.
T8	Limestone. Limestone displaying a mudstone texture and containing bioclasts. Small calcite veins.
T9	Lithic arenite. Coarse grained and poorly sorted lithic arenite containing rounded to sub-rounded lithic fragments. Weathered, rounded volcaniclasts displaying various textures (porphyritic with clinopyroxene or plagioclase phenocryst, trachytic and microlitic). Some volcaniclasts contain olivine or chlorite. Rounded cryptocrystalline and microcrystalline fragments. Rounded silty fragments. Polygenic lithic fragments. Plagioclases and weathered alkaline feldspars. Sub-rounded to rounded quartz grains. Rounded opaque minerals. Zircon grain. Reworked fossils shells?
Jiucaiyuan Formation	
T10	Limestone.

	Mudstone (with micritic calcite sometime recrystallized) containing fossil shells and bioclasts. Few quartz grains. Opaque minerals. Veins filled up by sparitic calcite.
	Taoshuyuan C section
Wutonggou Formation	
TC1	Calcite cemented lithic arenite. Fine grained and well-sorted lithic arenite, mainly made up of rounded cryptocrystalline fragments. Silty lithic fragments. Microgranular lithic fragments. Quartz grains, occurring either as monocrystalline grains or within quartz granular lithic fragments. Plagioclase and alkaline feldspars, ranging from nearly fresh to strongly seritized in alteration. Muscovite. Biotite. Zircon grains. Calcite grains. Opaque minerals. A few volcaniclasts.
Guodikeng Formation	
TC2	Lithic arenite. Corse grained, poorly sorted lithic arenite, mainly composed of rounded silty fragments. Rounded volcaniclasts with trachytic or microlithic textures. Sub-rounded opaque minerals. Sub-angular quartz grains. Plagioclases and weathered alkaline feldspars. Cryptocrystalline fragments.
TC3	Lithic arenite. Weathered and rounded volcaniclasts displaying porphyritic (strongly seritized plagioclase phenocrysts), trachytic or microlitic textures. Silty, Cryptocrystalline and microgranular lithic fragments. Sub-angular to rounded quartz grains. Plagioclase and alkaline feldspars. Rounded opaque minerals. Biotite. Chlorite.
TC4	Limestone. Mudstone containing pelloidal elements and disseminated quartz grains, plagioclase and alkaline feldspars. Patches filled up by sparitic calcite. Bioturbation (?). Bioclasts. Small cryptocrystalline fragments.
TC5	Calcite cemented lithic arenite. Well-rounded silty and cryptocrystalline lithic fragments and pelloidal elements enclosed in a sparitic cement. Plagioclase and seritized alkaline feldspar. Sub-angular to sub-rounded quartz grains. Biotite. Muscovite. Sub-rounded opaque minerals. Wood fragments. Chlorite. Zircon.
TC6	Limestone. Mudstone containing a few quartz grains. Bioturbation. Veins filled up by sparitic calcite
Jiucaiyuan Formation	
TC7	Lithic arenite. Similar to sample TC3

Chapter 5 Palaeoclimate and palaeoenvironmental reconstructions

§5.1 Palaeoclimate during the Permian-Triassic transition

5.1.1 Palaeobiogeographic distribution of *Protophyllocladoxylon*-type woods in the Palaeozoic

Zhang et al. (2010) analyzed the distribution of *Protophyllocladoxylon* woods from the Early Carboniferous to the Palaeogene. Six species of *Protophyllocladoxylon* were found from the Late Palaeozoic (Table 5-1). Four of them were found in the cool temperate belt. *P. henanense* Yao, Liu and Zhang, 1994 was discovered in tropical area of Late Permian. *P. jingyuanense* Zhang, Wang, Liu and Li, 2010 lived in warm and dry conditions.

Ten species belonging to five morphogenera of coniferous fossil woods with a *Protophyllocladoxylon*-type secondary xylem from the Late Palaeozoic have been documented (Table 5-2). Almost all of them lived in the cool temperate climate zone.

In conclusion, the *Protophyllocladoxylon*-type woods were widely distributed in the southern and northern hemispheres during the Palaeozoic. The main distribution of *Protophyllocladoxylon*-type woods is cool temperate climate zone. (Fig. 5-1)

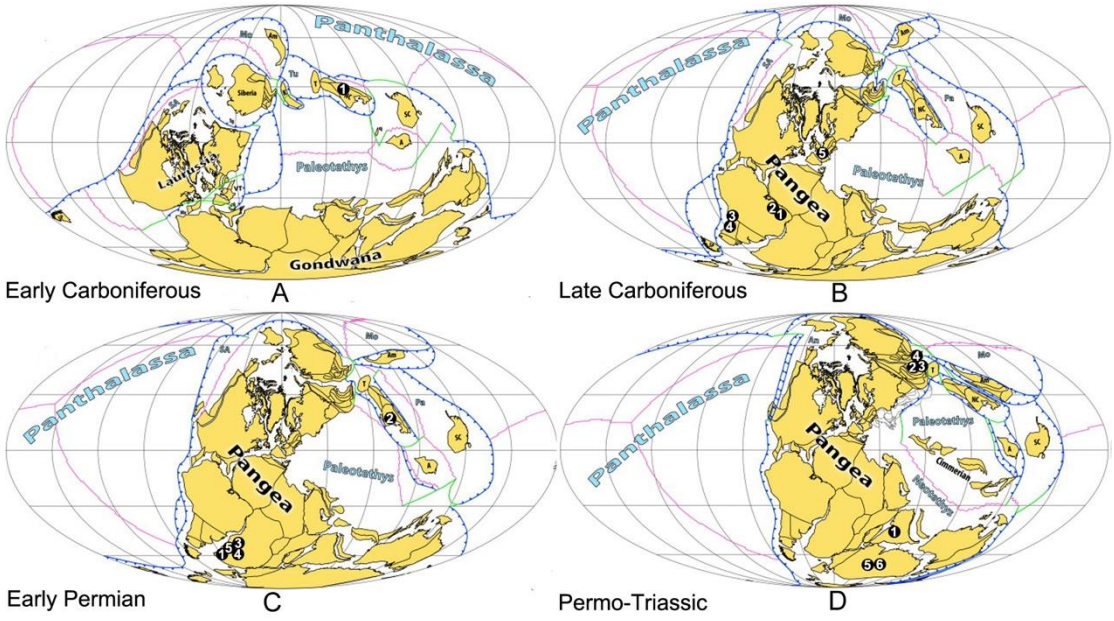

Figure 5-1 Distribution of the woods with *Protophyllocladoxylon*-type secondary xylem during the Late Palaeozoic. A. 1. *Protophyllocladoxylon jingyuanense* B. 1. *Protophyllocladoxylon dolianitii*; 2. *P. derbyi*; 3. *Medullopitys menendezii*; 4. *Phyllocladopitys petriellae*; 5. *Cordaixylon andresii*. C. 1. *Protophyllocladoxylon natalense*; 2. *P. henanense*; 3. *Phyllocladopitys capensis*; 4. *Megaporoxylon kaokense*; 5. *Medullopitys sclerotic*. D. 1. *Protophyllocladoxylon indicum*; 2. XTT-C-4 gen. et sp. nov.; 3. *Septomedullopitys szei*; 4. *Septomedullopitys sibirica*; 5. *Megaporoxylon canalosum*; 6. *M. antarcticum* (Paleogeographic maps from Domeier and Torsvick, 2014)

Table 5-1 Distribution of morphographic "species" *Protophyllocladoxylon* based only secondary xylem structure during the Palaeozoic.

Species	Type locality and age	Climatic zone	References
Protophyllocladoxylon jingyuanense Zhang, Wang, Liu and Li 2010	Gansu, China, northern hemisphere; Early Carboniferous.	Arid	Zhang et al., 2010
P. henanense Yao, Liu and Zhang 1994	Henan, China, northern hemisphere; Early Permian.	Tropical	Yao et al., 1994
P. dolianitii Mussa 1958	Brazil, southern hemisphere; Late Carboniferous.	Cool temperate	Mussa, 1958
P. derbyi (Oliveira) Maheshwari 1972	Brazil, southern hemisphere; Late Carboniferous/ Early Permian.	Cool temperate	Maheshwari, 1972
P. indicum Pant and Singh 1987	India, southern hemisphere; Late Permian	Cool temperate	Pant and Singh, 1987
P. natalense (Warren) Schultze-Motel 1961	South Africa, southern hemisphere; Early Permian	Cool temperate	Schultze-Motel, 1961

Table 5-2 Distribution of the species with *Protophyllocladoxylon*-type secondary xylem during the Late Palaeozoic.

Species	Type locality and age	Climatic zone	References
XTT-C-4 gen. et sp. nov.	Xinjiang, China, northern hemisphere; Early Triassic	Warm temperate	The present paper
Septomedullopitys sibirica Lepekhina 1969	Kuznetsk Basin, Russia, northern hemisphere; Late Permian.	Warm temperate	Lepekhina, 1969, 1972
Septomedullopitys szei Wan, Yang and Wang 2014	Xinjiang, China, northern hemisphere; Late Permian	Warm temperate	Wan et al., 2014
Cordaixylon andresii Césari et al., 2015	Spain, equator; Stephanian, Late Carboniferous	Tropical	Césari et al., 2015
Phyllocladopitys petriellae Brea and César 1995	Argentina, southern hemisphere; early Late Carboniferous	Cool temperate	Brea and Césari, 1995
Medullopitys menendezii Petriella 1982	Argentina, southern hemisphere; Late Carboniferous	Cool temperate	Petriella, 1982
Phyllocladopitys capensis Kräusel, 1928	South-West Africa, southern hemisphere; Early Permian.	Cool temperate	Kräusel, 1928; Kräusel et al., 1961; Lepekhina, 1972
Megaporoxylon kaokense Kräusel 1956	South-West Africa, southern hemisphere; Early Permian	Cool temperate	Kräusel, 1956; Kräusel et al., 1961; Lepekhina, 1972
Medullopitys sclerotic Kräusel 1928	South-West Africa, southern hemisphere; Early Permian.	Cool temperate	Kräusel, 1928; Kräusel et al., 1961; Lepekhina, 1972
Megaporoxylon canalosum Maheshwari 1972	Antarctica, southern hemisphere; Middle/Late Permian	Cool temperate	Maheshwari, 1972
Megaporoxylon antarcticum Maheshwari 1972	Antarctica, southern hemisphere; Middle/Late Permian	Cold/cool temperate	Maheshwari, 1972

5.1.2 Can the growth rings of fossil woods reflect the palaeoclimate?

As widely acknowledged, the growth rings analysis is a powerful tool to determine the tree growth habit and to deduce palaeoclimatic conditions that prevailed during the tree growth (e.g., Schweingruber, 1992, 1996; Falcon-Lang, 2000a, 2000b, 2003; Brea et al., 2008, 2011). But the factors controlling the formation of growth rings are very complex. In an environment where cambial activity can potentially occur continuously, short-term disturbances to growth may influence the patterns of wood development (Jacoby, 1989). Such disturbances are attributed to drought, flood, fire, wind damage, unusual low temperature, synchronous coning/leaf flushing, disease pathogens and insect-attack, all have potential to limit the cambial activities (Fritts, 1976; Ash, 1983; Dechamps, 1984; Schweingruber, 1992, 1996; Ash and Creber, 1992; Young et al., 1993; Falcon-Lang, 2003).

Brison et al. (2001) pointed out that the growth ring studies must include a taxonomic analysis. The fossil woods found in Junggar and Turpan basins include Arthrophyta and gymnosperms (Table 5-3). Definitely, *Arthropitys* itself is a good indicator for the palaeoclimate. It is unknown whether the growth rings of all gymnosperms can reflect the palaeoclimate. In this part, we will discuss about the relationship between the growth rings and palaeoclimate through the analysis of our material. The gymnosperms collected from Taoshuyuan and Dalongkou areas mainly contain the woods with *Protophyllocladoxylon*-type secondary xylem and *Agathoxylon*-like wood. Six growth ring types were distinguished to categorize different earlywood/latewood relationship (Fig. 5-2).

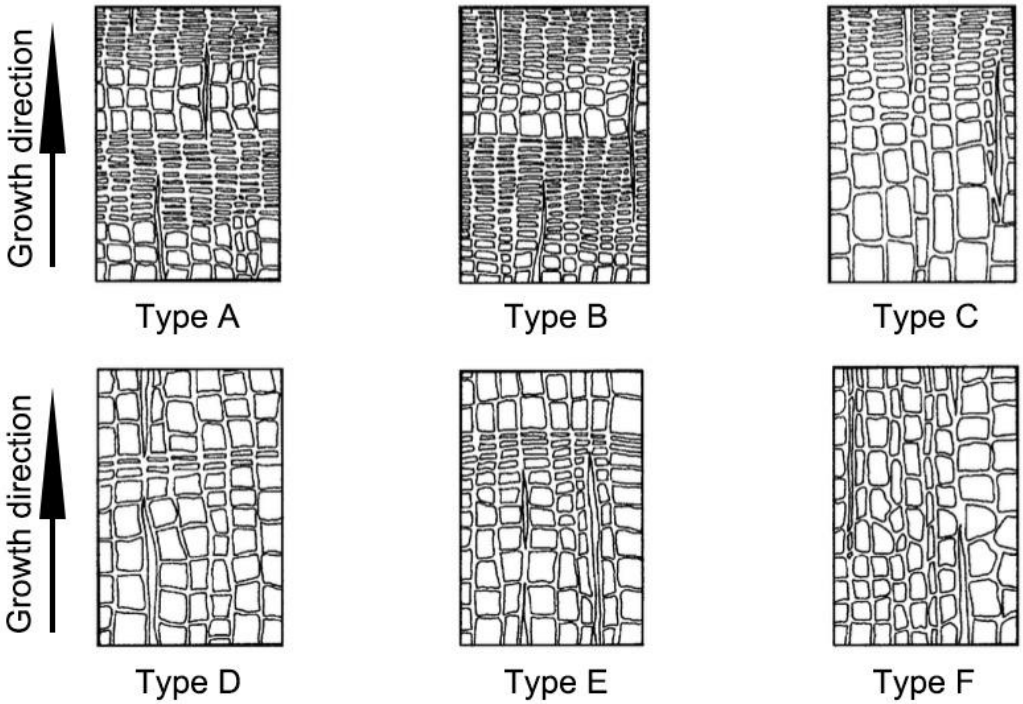

Figure 5-2 Schematic illustration of the six growth ring types defined by Creber and Chaloner (1984) to categorize different earlywood / latewood relationships. Type A: rings without much earlywood and thick latewood; sharp transitions at the earlywood / latewood boundaries. Type B: rings with a wide band of latewood; the transition to latewood is more gradual. Type C: rings with a very gradual transition from earlywood to latewood; rings indicate growth in an environment with only gradual change during the growing season. Type D: rings with a thin band of latewood; earlywood/latewood boundary well marked. Type E: rings similar to type D but the transition to latewood is not so sharp. Type F: rings resulting from a situation where all the requirements for growth are constantly present; no noticeable change in the tracheid diameter no growth-ring limits.

Table 5-3 List of the fossil woods recorded in the studied area

Formations	Fossil wood species	Age
Karamay	*Junggaropitys dalongkouensis* Shi, Yu, Broutin and Pons	Middle-Late Triassic
Guodikeng	*Junggaropitys dalongkouensis* Shi, Yu, Broutin and Pons, XTT-C-4 gen. et sp. nov. , *Xinjiangoxylon turpanense* Shi, Yu, Li, Chi and Zhang, Specimen: XTT-C-11, XTT-C-6	Early Triassic
Wutonggou	*Arthropitys* cf. *communis* (Binney) Hirmer and Knoell, *Arthropitys* sp., *Septomedullopitys szei* Wan, Yang and Wang, *Agathoxylon* cf. *leei* Szei	Late Permian

Woods with *Protophyllocladoxylon*-type secondary xylem

Five species possess a *protophyllocladoxylon*-type secondary xylem: *Septomedullopitys szei, Junggaropitys dalongkouensis,* XTT-C-4 gen. nov. *, Xinjiangoxylon turpanense,* XTT-C-11 and XTT-C-6. As demonstrated in the Chapter 3, fifteen species of Late Palaeozoic fossil woods with *Protophyllocladoxylon*-type woods have been reported. They were widely distributed in the southern and northern hemispheres during the Palaeozoic and Early

Triassic. In the southern hemisphere, they are only reported, up to now, in the cool temperature zone; while in the northern hemisphere and equatorial zone, they were found in tropical zone, arid zone, warm temperate zone and cool temperate zone.

Cordaixylon andresii Césari, Álvarez-Vázquez, Méndez-Bedia, Álvarez-Laó, Turrero and Arbizu, 2015 were documented from Late Pennsylvanian outcrops at Arnao beach, Spain. During the Pennsylvanian, Spain was located in the equatorial area. *Protophyllocladoxylon henanense* Yao, Liu and Zhang was found in the Early Permian deposits of North China block, located in the tropical area. Although recorded from two different climatic zones, two species do not show growth rings.

Maheshwari (1972) has investigated the fossil woods from the Permian Antactica where the climate was cool temperate (Boucot et al., 2009). He evdenced that *Protophyllocladoxylon dolianitii* Mussa 1958, *Magaporoxylon antarctium* Maheshwari 1972 and *Magaporoxylon canalosum* Maheshwari 1972 all possessed the *Protophyllocladoxylon*-type secondary xylem. The growth rings of *M. canalosum* and *M. antarctium* are distinct, growth ring type is hard to distinguish in Maheshwari's article. The growth ring of *P. dolianitii* belongs to type B.

Septomedullopitys szei Wan, Yang and Wang, 2014 has been found in the Tarlong area of Turpan Basin in the Late Permian deposits. The climate was considered to be humid climate with short-term, nonperiodic droughts. The growth rings of *S. szei* correspond to the D or E types**,** with a very thin band of latewood.

In consequence, the growth ring of the woods with *Protophyllocladoxylon*-type secondary xylem can be used as indicator of palaeoclimate.

***Agathoxylon* cf. *leei* Szei**

Agathoxylon is the most common wood morphogenus in the Palaeozoic and Mesozoic record. Brison et al. (2001) investigated all the *Agathoxylon* recorded from 75°S to 70°N latitude. In spite of such a wide latitudinal distribution it never displays growth rings of the (A, B, C) type. Extant Araucariaceae with *Agathoxylon*-type wood also never display these A, B, or C types (see, e.g., Seitz and Kanninen 1989), even when growing in clearly sharp seasonal climates.

For the late Palaeozoic *Agathoxylon*, the growth rings are more complex. Thirty-six species belonging to seven fossil woods genera were found from the late Carboniferous to the Late Permian of the Kuznetsk Basin (Lepkhina, 1972). During this period, the global temperature increased. In the Late Permian Kuznetsk Basin, the coal beds were more abundant and thicker, linked with a climate change to warm and humid (Davies et al., 2010). The change of the latewood width shows that the growth rings of *Agathoxylon* are related to climate change (Table 5-4).

Table 5-4 The latewood width of *Agathoxylon* from the Kuznetsk Basin

Species	Age	Width of latewood
A. monoseriale	Late Permian	~6 cells
A. conforme		1-2 cells
A. erunakovskiense		3-4 cells
A. originale	Middle Permian	1-2 cells
A. sibricum		4-5 cells
A. abashevskiense		2-3 cells
A. humiliradiale	Early Permian	More than 20 cells
A. balachonskiense	Late Carboniferous	More than 23 cells

During the Permian, the North China block was mainly located in tropical area. Four species of *Agathoxylon* were found in this area. *A*. *wudense* shows indistinct growth rings (Wang, 2000). Others do not have growth rings (Yao et al., 1994, Wang et al., 2000; Wang, 2000).

Agathoxylon africanum Bamford 1999 and *A. karooensis* Bamford 1999 were discovered in the Late Permian of the South African Karoo Basin. The climate was arid. The latewood of these two species are respectively 8-9 cells and 5-7 cells wide.

However, Maheshwari (1972) described an *Agathoxylon ningahense* (Maheshwari) Maheshwari from the Permian Antarctica. Its latewoods are very thin (0-6 cells). The growth pattern indicates a very rapid transition to seasonal dormancy, probably in response to decreasing light levels at these palaeolatitudes (Taylor and Ryberg, 2007).

Agathoxylon cf. *leei* Szei were only found in Late Permian of Shanxi, North China. That specimen does not have growth rings. But our specimen shows distinct growth rings. The latitude of studied area was higher than that of North China block in the Late Permian.

In consequence, we consider that the specimen can be an indicator a chimate indicator.

5.1.3 Palaeoclimatic implications of fossil woods

1. Late Permian

In the Wutonggou Formation, we found three genera of fossil woods. Among them, the *Arthropitys* is a good climate indicator. As a matter of fact, Palaeozoic horsetail trees preferred wetland environments as the extant *Equisetum*. They formed hygrophilous stands surrounding lakes or swamps and along sandy river banks (Scott, 1979; Pfefferkorn et al., 2001). In Euramerica, it is well-documented that the Late Carboniferous coal swamp ecosystems collapsed near the Carboniferous—Permian boundary in the euramerican floristic province (DiMichele and Hook, 1992; DiMichele et al., 2001). The geographical extinction of certain plant taxa in this event is primarily related to the rising of a more seasonal and dry climate, and the lycopsids and sphenopsids (including the calamitean plants) who cannot adapt to the climate change and, induced

palaeoenvironment change in Euramerica (DiMichele and Hook, 1992; Gastaldo et al., 1996; DiMichele et al., 2001). In Cathaysian flora, these taxa lived in the waterlogged swamp environments during the Early Permian of North China (Hilton et al., 2001, 2002) and persisted until the Late Permian in South China (Li et al., 1995; Wang et al., 2003, 2006). Accordingly, the calamitean stems found in this area indicate the presence of waterlogged environments in this region during the Late Permian in which calamitean plants lived.

Calamitean woods are manoxylic type implying that they cannot suffer cold winter-like seasons (Fig. 5-3, A).

The growth rings have been reported repeatedly among the calamitean stems of Permian age. In the *Arthropitys yunnanensis*, the growth rings are conspicuous and continuous through the entire circumference of the secondary xylem (Wang et al., 2006). The authors proposed that the growth rings in *Arthropitys yunnanensis* reflected repeated changes in environmental stress and probably related to irregularity in water availability within the growth environment (Wang et al., 2006). However, the two specimens collected from Turpan Basin have no growth ring at all. It means that the climate of this region during the early Late Permian (Wuchiapingian) was warm and humid with no or limited temperature and precipitation fluctuations.

Septomedullopitys szei were collected from Wutonggou Formation in the Taoshuyuan area. Wan et al. (2014) has already reported the same species in this area. In their sample, both growth rings and false rings (the authors explain as growth interruptions) are present. Wan et al. pointed out that the stem *S. szei* suggests weak seasonality of annual precipitation. In our specimen, the false ring is absent. The growth ring pattern is similar to that reported by Wan et al. (2014): the secondary xylem shows very thin bands of latewood (Fig. 5-3, B).

The secondary xylem of *Agathoxylon* cf. *leei* was characterized by the multiple growth rings (or false rings) appearing in a small area (Fig. 5-3, C, D). The latewood is very thin, 1-5 cells thick.

Due to the preservation of the two species, we cannot test their leaf abscission. Growth rings displaying subtle ring boundaries may be related to weakly developed climate seasonality (Falcon-Lang, 1999). For the Late Permian to Early Triassic, palaeoclimatic reconstructions show a temperate climate in this area (e.g., Fluteau et al., 2001; Kiehl and Shields, 2005; Péron et al., 2005; Boucot et al., 2009;), in accordance with the mean annual temperature of 7–15 (± 4.4)°C estimated from palaeosols proxies from the Turpan Basin (Thomas et al., 2011). Consequently, the growth rings do not appear to be related to these relatively moderate annual temperature ranges. On the contrary, Late Permian to Early Triassic palaeosols from the Turpan Basin display features indicative of variable soil moisture regimes (Thomas et al., 2011). Thus, we speculate that dry seasons trigged the formation of growth rings. Moreover, the width of growth rings is various. It indicates that the growing environment was not uniform. In conclusion, these trees developed under a warm humid climate condition with short dry periods or hydric stresses due to the irregularity of water supplies.

With the calamitean and gymnosperm woods, we speculate that the climate of Late Permian Turpan Basin was warm and humid with limited temperature and precipitation fluctuations. In the dry periods, the plants in the lowland could get enough water supplies; the cambial activities of those gymnosperm trees in the upland slowed down due to the hydric stresses. The growth disturbance triggered by dry periods was short-lived and transitory. After that, they rapidly returned to optimal growing conditions.

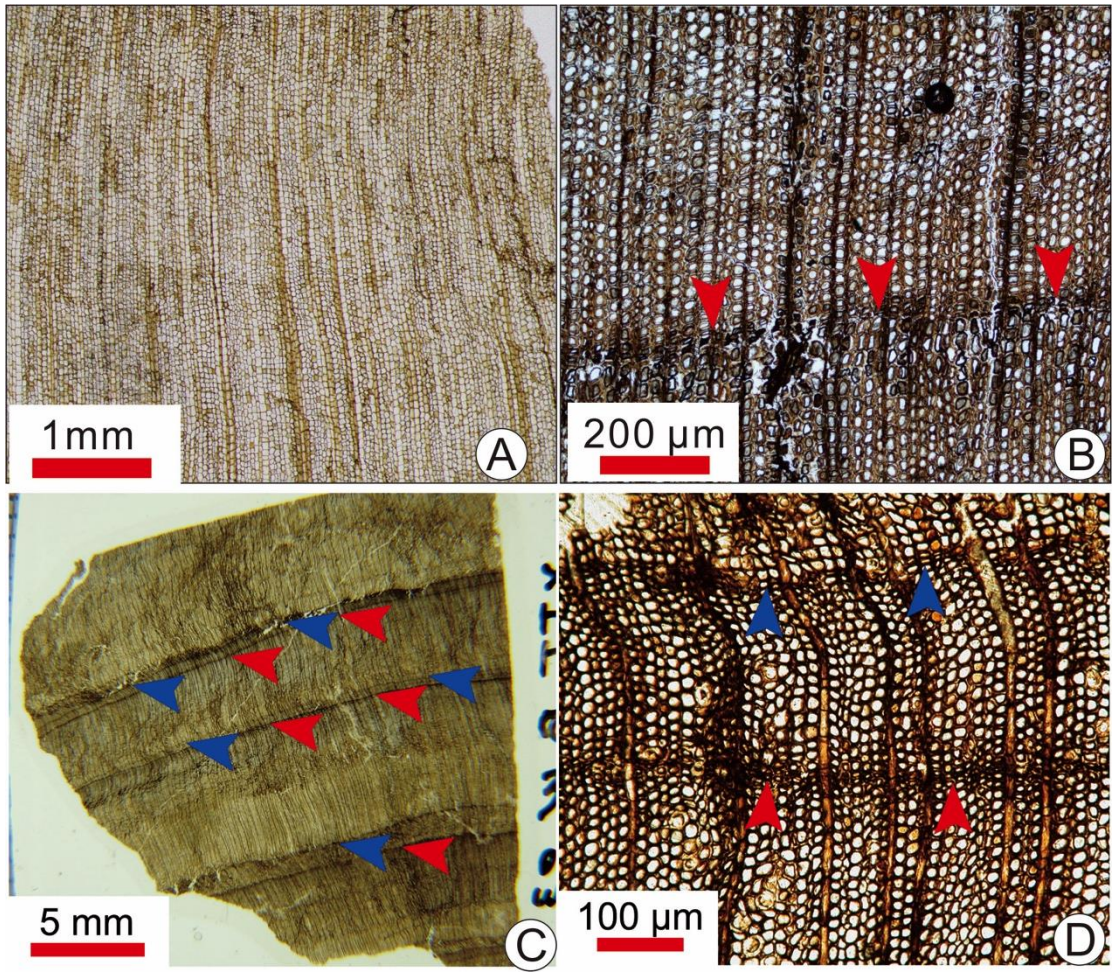

Figure 5-3 A. The secondary xylem of *Arthtopitys* sp.; B. Growth ring boundary (arrows) of *Septomedullopitys szei*; C. The secondary xylem of *Agathoxylon* cf. *leei,* arrows indicate two adjacent growth rings (red and blue arrows); D. Close-up of two growth (false) ring boundaries of *Agathoxylon* cf. *leei* (red and blue arrows).

2. Early Early Triassic

In the upper part of Guodikeng Formation, we found five well-preserved samples. In *Junggaropitys dalongkouensis*, growth rings are absent, but false rings are present. Fungal infection may be the reason for the false rings. The diameter of the *Junggaropitys dalongkouensis* collected from Early Triassic deposits is 4.8 cm. It represents the juvenile wood. The earliest formed rings in a stem generally record rapid and variable growth, so it was excluded from the analysis (e.g., Fritts, 1976; Taylor and Ryberg, 2007).

In sample XTT-C-11, the growth rings are absent (Fig. 5-4, B). That means it developed under a warm and humid conditions.

In XTT-C-4 gen. nov. (Fig. 5-4, D), *Xinjiangoxylon turpanense* (Fig. 5-4, A), and sample XTT-C-6 (Fig. 5-4, C), the growth ring boundaries are not easy to see as the late wood is very thin: 1-3 cells thick.

The growth patterns of the early Early Triassic fossil woods are similar to those from Late Permian. Thus, the early Early Triassic climate in the research area was comparable to that in the Late Permian.

Based on the data from palaeosols proxies, Thomas et al. (2011) indicated that (1) the temperature has no significant changes across the Permian-Triassic boundary; (2) the mean annual precipitation ranged from 530 to 1270 mm/year, but with most estimates >1000 mm/year in the Wutonggou lower order cycle (= Wutonggou Formation and most part of Guodikeng Formation); and above this, mean annual precipitation values show much greater variability, but are generally indicative of drier conditions. The anatomic characteristics of our fossil woods are in good agreement with the results from palaeosols.

The super Pangea was assembled by the end Permian. The great size of the exposed lands cut across almost every zonal circulation and had an extraordinary effect on global climate. The supercontinent was conducive to the establishment of the megamonsoonal circulation. The Pangeae megamonsoon system controlled the global precipitation system during the Permian and Triassic (Parrish, 1993).

During the Permian to Triassic transition, the Turpan Basin was located in the Junggar terrane at the Northeast Pangaea. According to the Community Climate System Model, during summer monsoons, the northward wind brought oceanic moisture to this area, causing abundant rainfall; while, during winter monsoons, the wind turn to east direction, causing dry conditions (Winguth and Winguth, 2013).

However, based on the data obtained from the fossil woods, we believe that it had no strong seasonality in the Junggar terrane during the Permian to Triassic transition.

In conclusion, the climate in the Junggar terrane during the Permian-Triassic transition remained warm and humid with limited temperature and precipitation fluctuations. The Palaeo-Tethys megamonsoons did not significantly influence the Junggar terrane along the east coast of mid-latitude Pangaea. It means that the climate change is not the reason of the end Permian mass extinction. It may result from that the surrounding ocean changed the climate in this area.

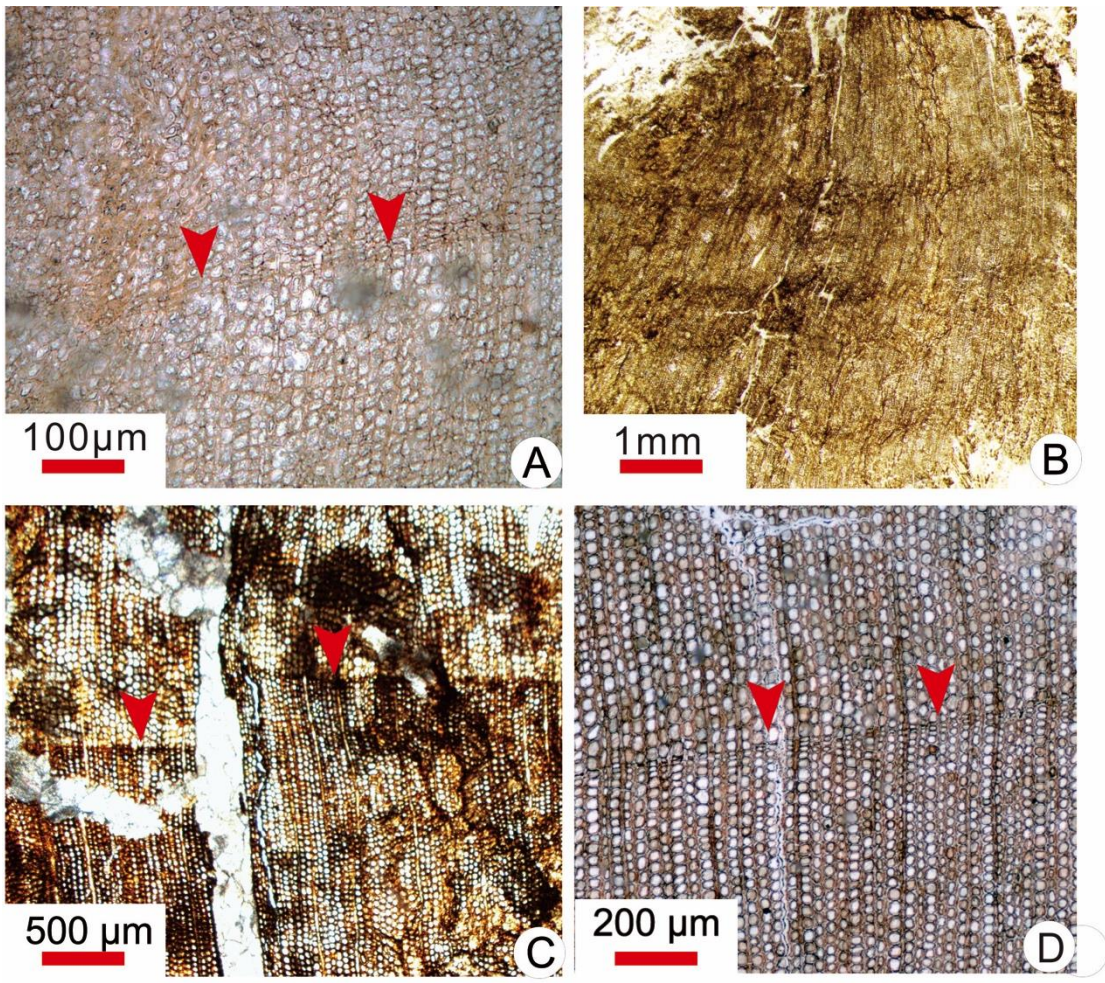

Figure 5-4 A. Growth ring boundary (arrows) of *Xinjiangoxylon turpanense*; B. The secondary xylem of XTT-C-11; C. Growth ring boundary (arrows) of XTT-C-6; D. Growth ring boundaries (arrows) of XTT-C-4 gen. nov. .

§5.2 Palaeobotany across the Permian-Triassic boundary

5.2.1 Plants in the Permian Junggar-Turpan Basin

China has a complex tectonic history. It consists of a number of amalgamated plates, microcontinent and terranes. The plant elements of the four major floras: Cathaysian, Angaran, Euramerican and Gondwanan can be found in the Late Permian of China. The Cathaysian flora occupied most area (Fig. 5-7) of China. The incoming of some elements of the Euramerican flora occurred mainly in the Late Permian of the Sino-Korean-Tarim (North China) Block. Some very rare suspect Gondwanan plant fragments, namely *Glossopterids,* have been mentioned in the Southern Tibet-Western Yunnan Region (Li, 1995). Typical Angaran elements were found in the Junggar-Hinggan Region. In the research area, typical Angaran and Cathaysian plants coexisted as this area

corresponding to the Subangara Realm.

As mentioned in Chapter 2, the present Junggar basin results from the amalgamation of Junggar, West Junggar and East Junggar terranes. The terranes of the Altai (East Junggar) and Junggar regions were fully amalgamated by orogeny acting during the end of Early Carboniferous to the Middle—Late Carboniferous. Since then, Junggar regions became a part of the Siberia Craton. Junggar terrane and West Junggar were amalgamated during Late Carboniferous to Late Permian times and accompanied by the closure of the Balkhash-Junggar Ocean. The Junggar terrane uplifted and became an intra-continental terrestrial basin in the latest Carboniferous (Yang et al., 2007).

The earliest flora in this area was found in the Wutulake Formation of West Junggar (Dou and Sun, 1983, 1985;). The Wutubulake Formation originally considered being entirely within the Devonian, the recent discovery of *Monograptus* in the Wutubulake Formation indicates that the collections of the algae *Cooksonella sphaerica* Senkevich and the Rhyniophyte *Salopella xinjiangensis* Dou**,** belong in fact to the Late Silurian Pridolian. Only the fossil plant *Zosterophyllum* sp. from the upper part of the Wutubulake Formation is regarded as Early Devonian in age.

The Early Permian flora of Xinjiang from the entirely terrestrial Lower Chichitsao Group in the western part of the Junggar-Hinggan Permian Angaran province is characterized by the occurrence of many *Zamiopteris* and *Neoggerathiopsis* taxa with large leaves, and some Euramerican and Cathaysian elements like *Taeniopteris* and *Sphenophyllum* cf. *thonii* (Dou and Sun, 1983). In the eastern part of the province, the intercalated marine and terrestrial Tatouhe Formation contains *Nephropsis*, *Crassinervia*, and *Zamiopteris* (Huang, 1982).

The Late Permian floras are much better developed than the Early Permian floras. The Late Permian flora from the Changfangkou Group in the Junggar Basin of Xinjiang is typically Angaran in composition (Sun, 1989). The Late Permian floras from Cangfanggou Group are dominated by pteridosperms followed by cordaites, cycads with Mesozoic characteristics, less abundant filicopsids, sphenopsids, and ginkgophytes, rare mosses and a questionable conifer fragments. 29 genera and 58 species were reported from the Changfanggou Group, e.g. *Annularia neuburgiana, "Callipteris" zeilleri, Comia major, Tatarina, Phylladoderma, Psygmophyllum demestrianum, Yavorskyia mungatica, Lepeophyllum mungatica, L. actaeonelloides, "Glossopteris" tunguskana,* and a variety of sulcial *Cordaites.* The flora contains a smaller number of Cathaysian elements such as *Taeniopteris densissima, T.* aff. *norinii* and other *Taeniopteris* species.

The age of the floristic mixing between Cathaysian and Angaran floras in northern China has generally been previously constrained to be Late Permian (Durante, 1983; Wu, 1993; Shi et al., 1995; Deng et al., 2009; Sun et al., 2010; Zhang et al., 2014). However, earlier floristic intermingling has also been reported, for example, in the Early Permian of Xinjiang (Dou and Sun, 1985; Wu et al., 1997). The recent researchs on the fossil plants imply that the mixing of Angaran and Cathaysian plants in eastern Xinjiang took place progressively during the middle to the late Middle Permian (Wordian to Capitanian) (Wei et al., 2015). Wei et al. (2015) discovered the common element of the

Cathaysian flora, *Cordaites permica*, together with Angaran plants. The convergence and intermingling elements of both Angaran and Cathaysian floras were triggered by the tectonic and palaeogeographical evolution of the Tianshan–Hingan fold belt in Northwest China.

During the Carboniferous to Early Permian, this fold belt existed as a shallow seaway as the western extension of the great Sino-Mongolian seaway that separated Siberia in the north from North China in the south (Zhang, 1988; Shi, 2006). At this time, the Junggar terrane was located on the southern fringe of Siberia, separated from North China by the Tianshan–Hingan seaway, and its floral content was strongly dominated by the Angaran flora. Then, in the beginning of late Early to early Middle Permian, strong and widespread tectonic movements occurred in eastern Xinjiang, resulting in the collision and amalgamation of Siberia with North China and the Tarim blocks during the final closure of the Tianshan–Hingan seaway (Shi et al., 1995; Wartes et al., 2002; Deng et al., 2009).

In the Early Permian, some elements of Euramerican floras and few elements of Cathaysian floras occurred in northwestern or western Xinjiang is Early Permian (Dou and Sun, 1985; Wu et al., 1997). The emergence of these Euramerican and Cathaysian elements may relate to the amalgamation of Junggar area and Tarim block where the Euramerican flora with few Cathaysian elements prevailed.

In the eastern Xinjiang, the Cathaysian elements appeared in the Middle Permian floras in eastern Xinjiang. While, the mixed of Cathaysian and Angaran floras was late Middle Permian floras in Qilian Mountains of Gansu province (Sun and Liu, 2010). That indicates the amalgamation of Junggar area and Northwest China blocks (Beishan and Alex blocks) in the Middle Permian.

Further east, mixed Angaran and Cathaysian floras have also been documented extensively in northeast China (eastern extension of the Tianshan–Hingan fold belt), but in these eastern areas they are Late Permian in age (Jin and Mi, 1993; Deng et al., 2009; Zhang et al., 2014), thus significantly later than their counterparts in the central (Gansu and eastern Xinjiang) and western (northwestern Xinjiang) parts of the Tianshan–Hingan fold belt.

The convergence and intermingling elements of Angaran, Cathaysian and Euramerican floras indicate the timing and the direction of how the Tianshan–Hingan seaway was closed through the Permian, it becomes apparent that the closure of the seaway and thus the collision of the North China and Tarim blocks with Siberia must have proceeded in a manner much like closing a pair of scissors in that the closure of the seaway proceeded gradually and progressively from west to the east (Wei et al., 2015).

The tectonic and palaeogeographical evolution played an important role for the mixing of floras. But, whether the climate drove the migration of the Angaran and Cathaysian floral elements in the Late Palaeozoic. Wei et al. (2015) reported fossil woods from the Middle Permian to the early Late Permian in the Hami area. In the Permian, the Hami and our research areas were in the same basin. These fossil woods from different levels of Middle Permian to the early Late Permian deposits provide key information to

understand the climate in the Junggar terrane during this period.

Five samples from Hami area show weakly developed growth rings. The latewood is 1-3 cells thick. Two samples even lack of growth rings. That indicates that the climate in the Middle Permian to the early Late Permian was similar to that during the Permian-Triassic transition: it was warm and humid with limited temperature and precipitation fluctuations.

During the whole Permian, the North China blocks drifted to the north, but the climate did not show significant change. It may relate to the global warming during the Late Permian.

5.2.2 Dramatic changes of the Permian phytogeoprovinces in North China

The Cathaysian flora might have an endemic, oriental origin from the Procathaysian flora, which perhaps existed mainly in Early Carboniferous in China (Li, 1995). This first occurrence of a Cathaysian flora was found in North and Northwest China and characterized by the "*Neuropteris ovate - Cathaysiodendron nanpiaoense"* assemblage discovered in the middle-upper part of the Taiyuan Formation. From the middle Early Permian, the Cathaysian flora showed a southward extension attested by its discovery in the South China Block and the Yangtze Platform besides in North and Northwest China, covering then almost the whole China (Fig. 5-6). Some others Cathaysian floral elements even migrated to the Arabian, in the North Gondwanan domain, during the Middle Permian (Guadalupian). Then from the Middle to the Late Permian, the various paleofloras on the Arabian plate were composed by a mixture of Gondwanan, Cathaysian, and euramerican elements. (Berthelin et al., 2003) (Fig. 5-5).

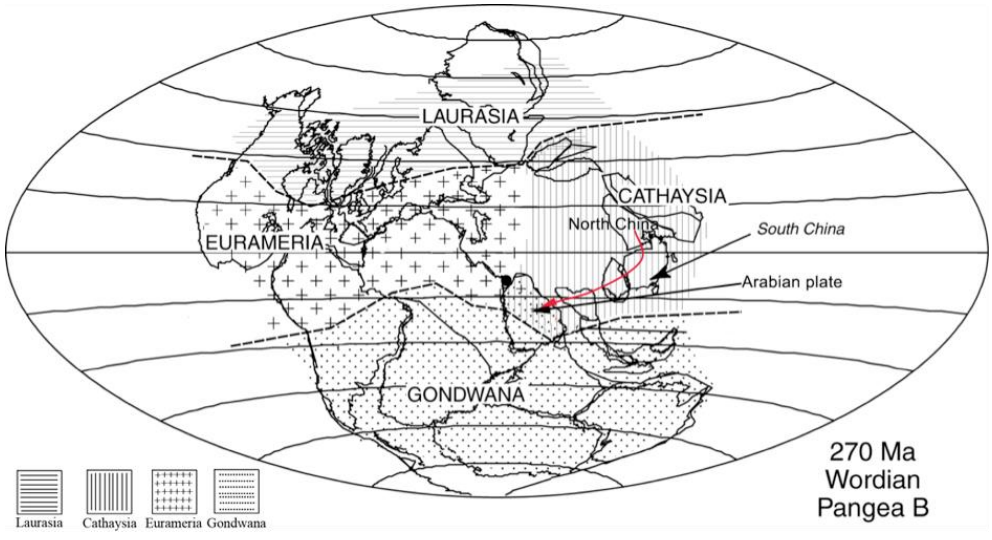

Fig. 5-5 The south migration path (red arrow) of the Cathaysian flora (according to Berthelin et al., 2003)

The decline and final disappearance of the Cathaysian flora in North China is caused chiefly by the Sino-Korean-Tarim (North China) Block drifting to the north and

the globally prevailing Permian hot and dry climate which migrated gradually from West to the East (Euramerica to Subangara) (Li, 1995).

As the North China blocks moved to the north with its Cathaysian vegetal cover, the convergence of Angaran and Cathaysian floras occured mainly in the Middle Permian in eastern Xinjiang and Qilian Mountains of Gansu province. (Fig. 5-8). The Angaran flora migrated to the south at the same time. Consequently, in the Late Permian, the subangara flora prevailed in the north North China blocks and Northwest China intermingling with the surviving Cathaysian plants. In the middle North China block, some representative members of the cathaysian flora were replaced by Zechstein migrating conifers of Western Europe in the Late Permian Shihchienfeng flora, in which only a small number of Cathaysian elements of relatively drought-enduring habit, e. g., *Yuania* and *Taeniopteris taiyuanensis* survived (Fig. 5-7).

The South China block remained in the equator area during the whole Permian. Most Cathaysian elements persisted to the end of the Permian**,** the succession of species driven by biologic evolutionary mechanisms, some taxa locally survived to the earliest Triassic, then completely vanished in the world.

Conversely, the disappearance of most of the Cathaysian elements in the North China blocks during the Late Permian result from the drifting of these blocks from equatorial or sub-equatorial location to north sub-tropical or warm temperate locations. It is noteworthy that many cathaysian elements migrated far to the north (Deng et al, 2009). This may relate to the global warming in the Late Permian.

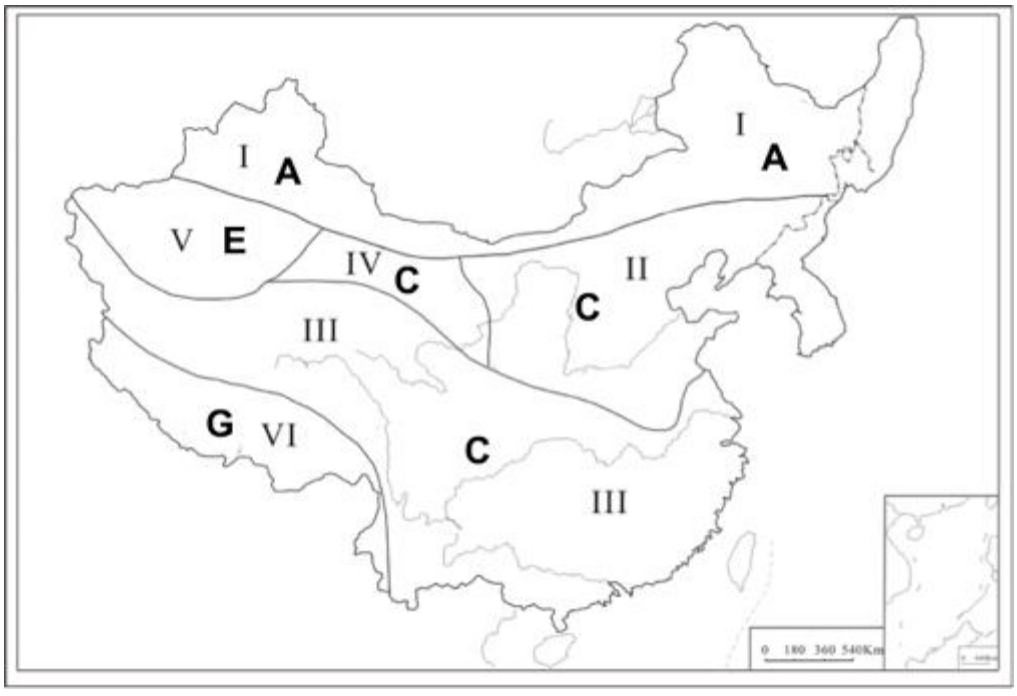

Figure 5-6 Phytogeoprovinces of the Early to Middle Permian floras in China (According to Li Xingxue, 1995). A: Angara flora; C: Cathaysian flora; E: Euramerian flora; G: Gondwana flora.
I. Junggar-Hingan Provinces; II. North China Province; III. South China Province; IV. Northwest China Province; V. Tarim Province; VI. southern Tibet and western Yunnan

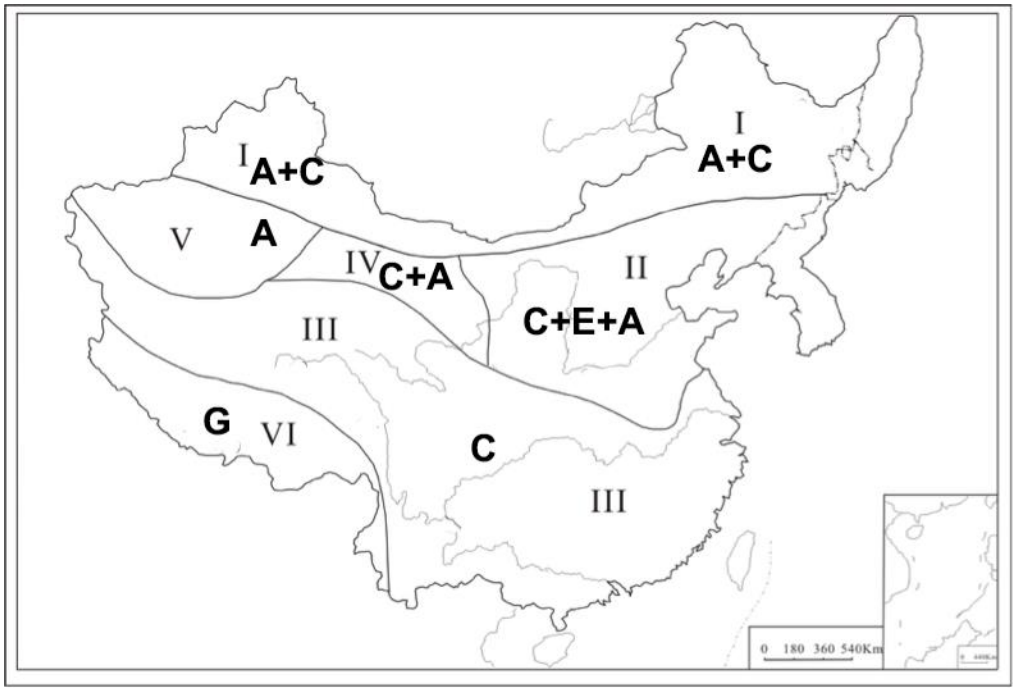

Figure 5-7 Phytogeoprovinces of the Late Permian floras in China (according to Li, 1995; Deng et al., 2009). A: Angara flora; C: Cathaysian flora; E: Euramerian flora; G: Gondwanan flora
I. Junggar-Hingan Provinces; II. North China Province; III. South China Province; IV. Northwest China Province; V. Tarim Province; VI. southern Tibet and western Yunnan

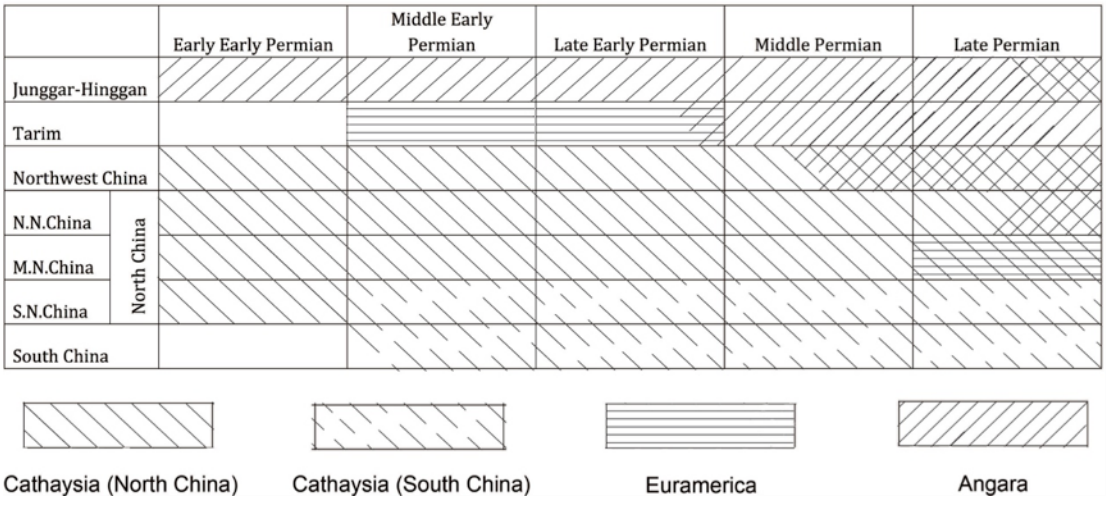

Figure 5-8 Distribution and mutation of Permian phytogeoprovinces in China. N. N. China: north North China subprovince; M. N. China: middle North China subprovince; S. N. China: south North China subprovince (modified after Li, 1995).

5.2.3 Plants across the Permian-Triassic boundary in the Junggar-Turpan Basin

During the field missions, more than one hundred forty plant impression and compression fossils were collected and most identified at the genus level. Each

stratigraphic occurrence of plant fossil debris is indicated on the logs.

1. Late Permian flora in the Junggar-Turpan Basin

The Cangfangou Group (including Quanzijie, Wutonggou and Guodikeng formations) is very rich in plant fossils (Fig. 5-9, 5-10, 5-11, 5-12). They represent the typical Late Permian "*Callipteris*"-*Comia*- sulcial *Cordaites* assemblage. This assemblage was extensively described by Sun (1989). Three subassemblages are recognized:

1. *Cordaites-Comia major* subassemblage. It is mainly distributed in the Quanzijie Formation. The floral subassemblages are dominated by Cordaitales (*Cordaites angustifolius*, *C. andalepensis*, and sulcial *C. adleri*, *C. clerii* and *C. insignis*), with secondary occurrence of pteridosperms ("*Callipteris*" cf. lanceolata, "*C.*" zeilleri, *Comia major, C.* aff. *dentata* and *Compsopteris* cf. *adzvensis*) and filicales (*Pecopteris anthriscifolia*, *Pecopteris* sp., *Sphenopteris yichunensis* and *Cladophlebis* sp.). Few mosses (Bryophyta sp. indet) and equisetales (*Paracalamites angustus*) were discovered. No ginkgoales, cycads and conifers were found.

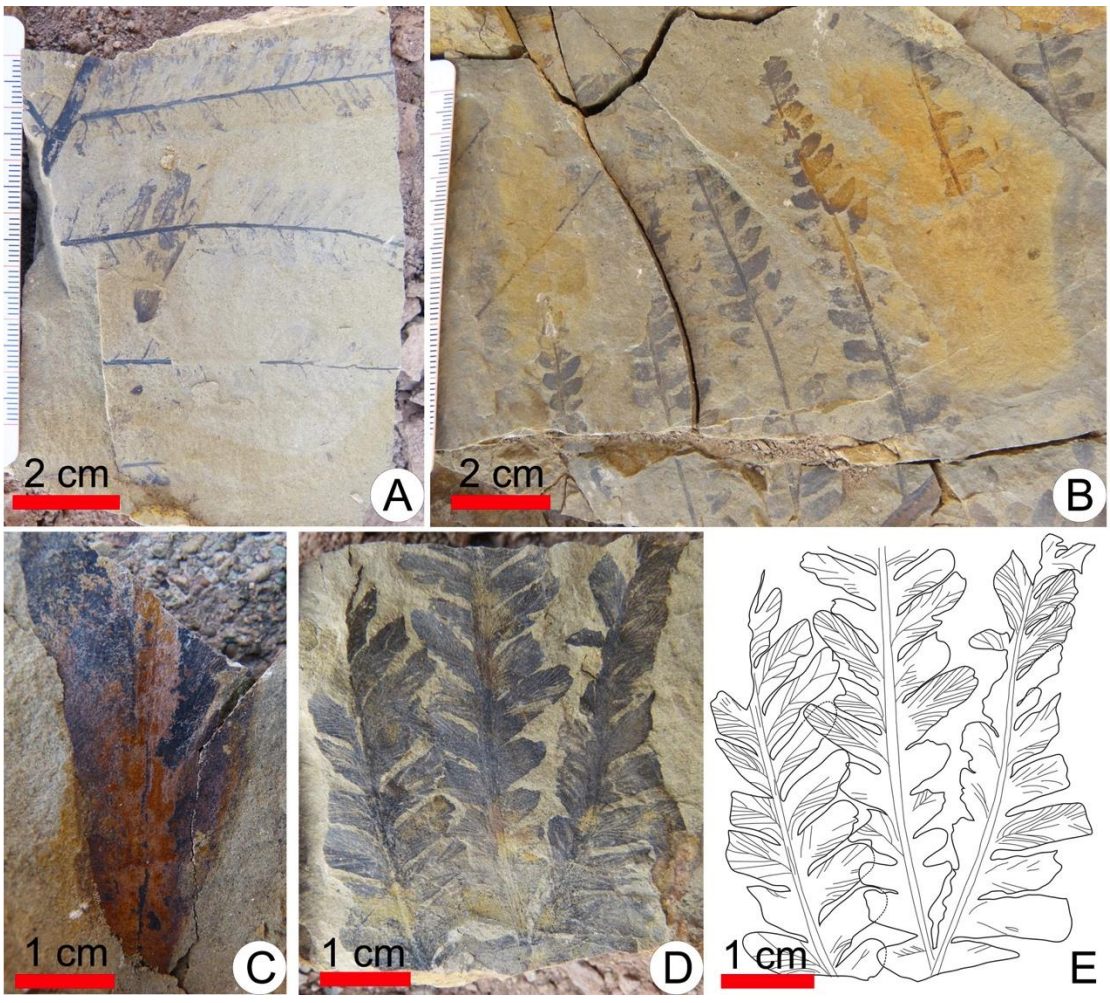

Figure 5-9 Fossil plants from Wutonggou Formation at Taoshuyuan C section. A, B. *Pecopteris* sp.; C. *Compsopteris* sp.; D. *"Callipteris"* sp. 1; E. Drawing of picture D.

2. *Taeniopteris-Psygmophyllum* subassemblage. This subassemblage occurs in the Wutonggou Formation and lower part of Guodikeng Formation. Pteridosperms

("*Callipteris*", *Comia* and *Psygmophyllum*) dominate this subassemblage. Cordaitales (*Cordaites andalepensis*, and sulcial *C. adleri*, *C.* aff. *clerii* and *C. insignis*) and equisetales (*Paracalamites angustus, P. tenuicostatus, Paraschizoneura* sp., *Annulina neuburgiana* and *Annularis* sp.) are secondary occurrence. Cycads (*Taeniopteris densissima, T.* aff. norinii, *Taeniopteris* sp. and *Yavorskyia mungatice*) are abundant. Among these, *Taeniopteris densissima* represents typical elements of the Cathaysian palaeobiogeographic province. Few moss (*Polyssaievia spinulifolia*) and ginkgoales (*Rhipidopsis hongshanensis* and *Rhipidopsis* sp.) are present.

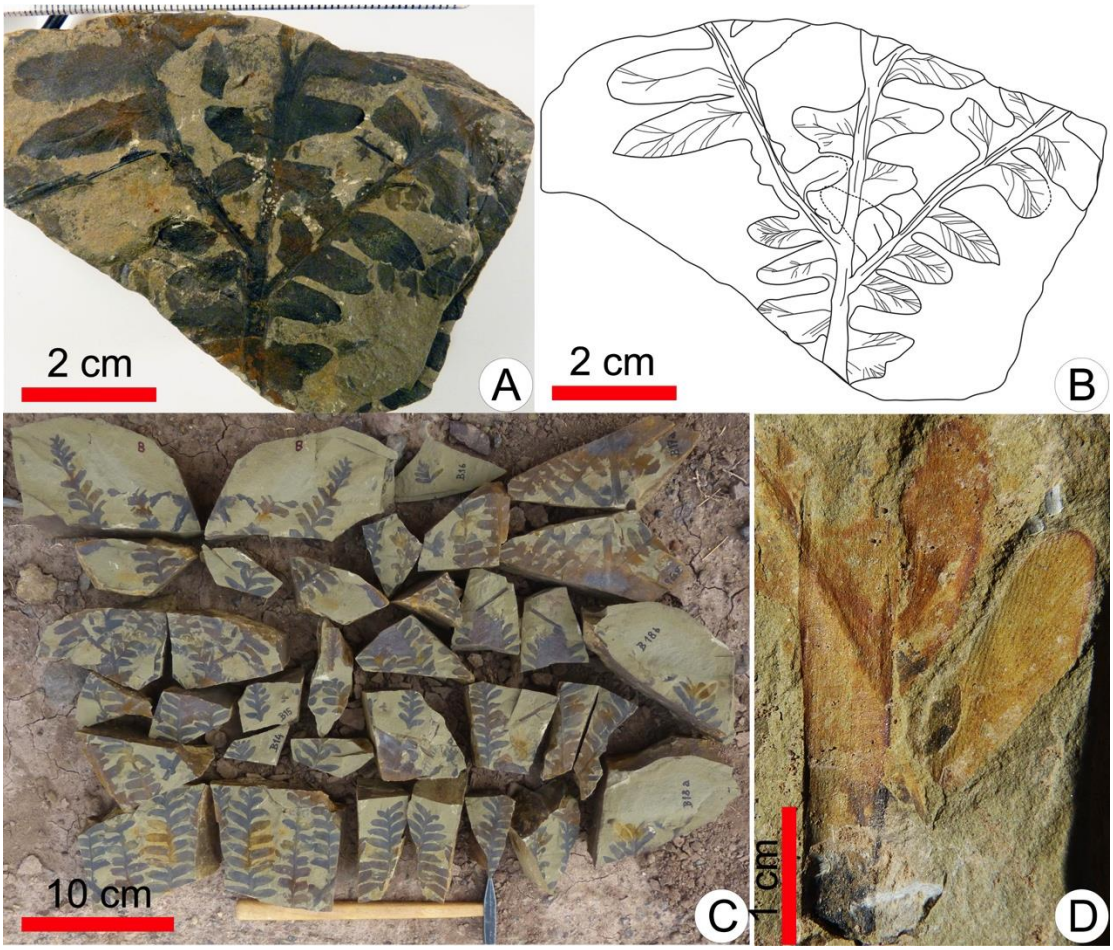

Figure 5-10 Fossil plants from Wutonggou Formation at Taoshuyuan C section. A. *Callipteris* sp. 2; B. Drawing of picture A; C. *Callipteris* sp. 2; D. *Cordaites* sp.

3. *Tatarina-Ctenis* subassemblage. This subassemblage is present in the middle part of Guodikeng Formation (upper part of Guodikeng Formation in Sun's). The floral subassemblages are dominated by pteridosperms *Tatarina,* but "*Callipteris*", *Comia* and *Psygmophyllum* are absent. Cycads (*Ctenis raritetinerris* and *Yavorskyia mungatice*) are common elements. Filicales (*Cladophlepis tenuiaxialis* and Pecopteris anthriscifolia) and Cordaitales (*Cordaites insignis*) are present. Equisetales (*Paracalamites tenuicostatus*) are much reduced.

   The fossil woods include equisetales (*Arthropitys* cf. *communis* and *Arthropitys* sp.)

and conifers (*Septomedullopitys szei* and *Agathoxylon* cf. *leei*).

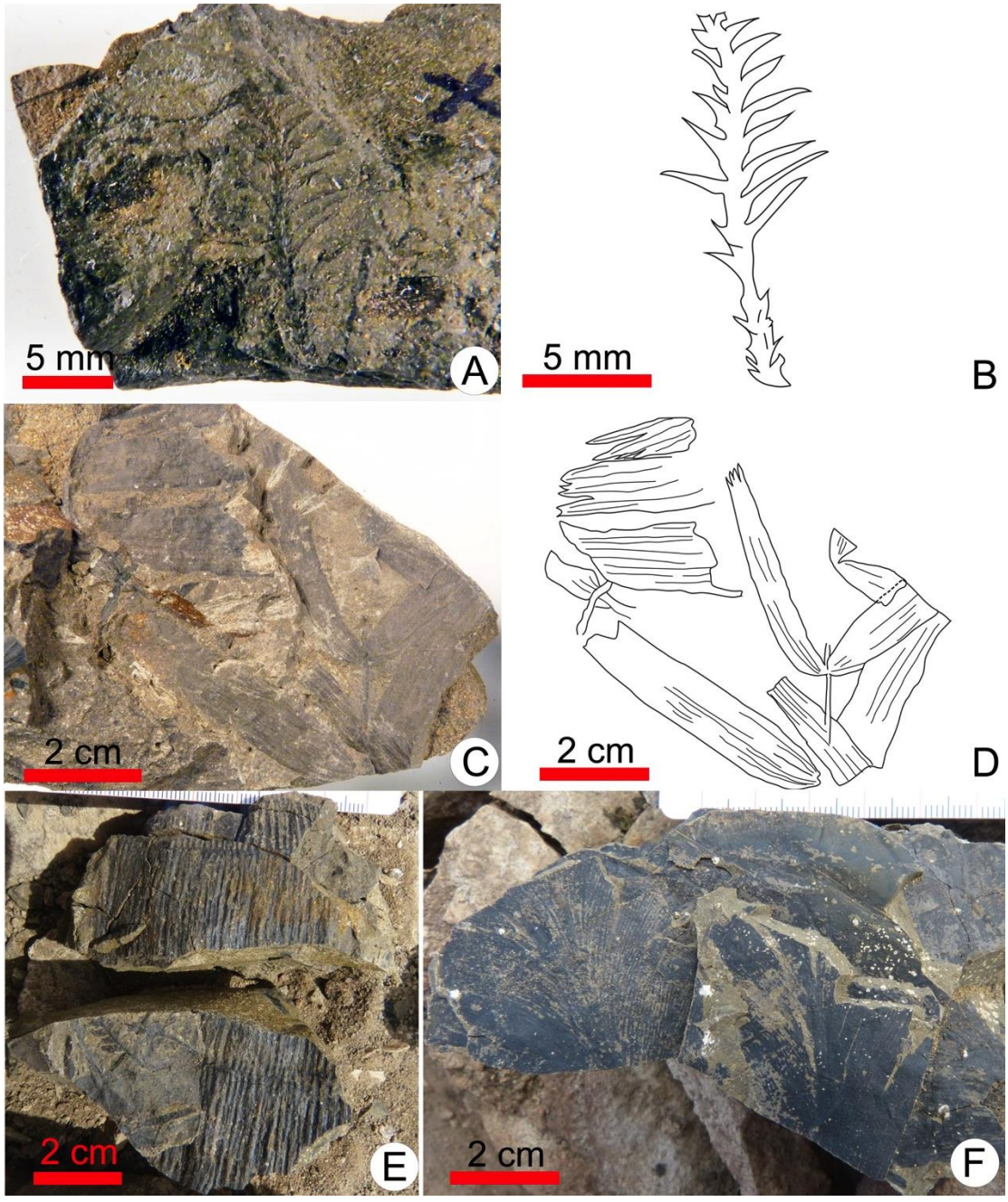

Figure 5-11 Fossil plants from Guodikeng Formation at Taoshuyuan A section. A. *Polyssaievia spinulifolia*; B. Drawing of picture A; C. *Schizoneura manchuriensis*; D. Drawing of picture C; E. *Paracalamites* sp.; F. *Psygmophyllum* sp.

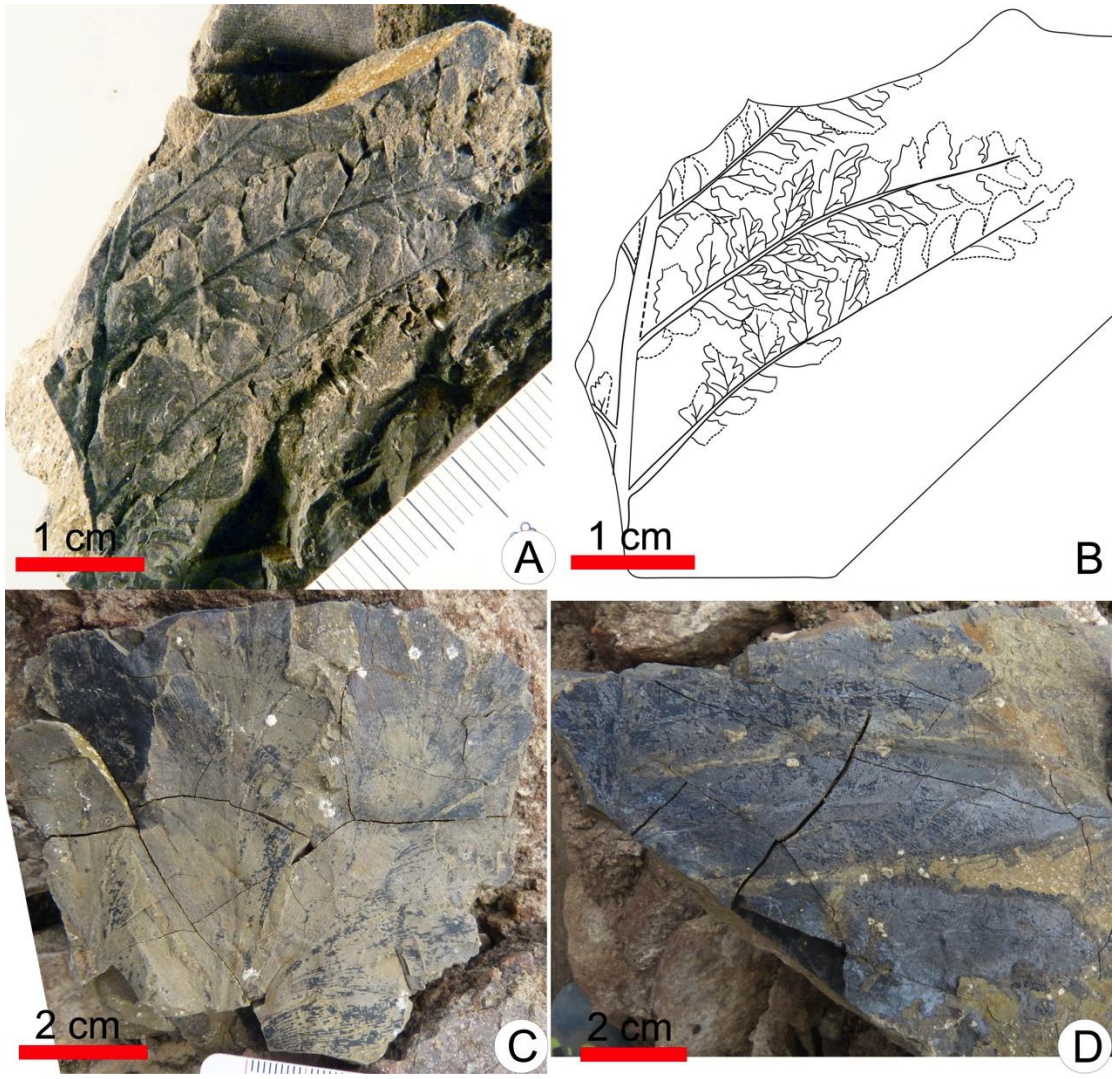

Figure 5-12 Late Permian fossil plants from Guodikeng Formation at Taoshuyuan A section. A. *Sphenopteris* sp.; B. Drawing of picture A; C. *Psygmophyllum* sp.; D. "*Callipteris*" sp.

2. Early Triassic flora in the Junggar-Turpan Basin

Early Triassic plant fossils are found in the upper part of Guodikeng Formation and the lowermost few meters of Jiucaiyuan Formation at the Dalongkou Section. Most plant fossils consist of scattered, comminuted debris. New plant taxon *Annalepis* appears in this flora (Fig. 5-13, A, B). *Annalepis* is a Triassic lycopsid that relates to *Isoetes*, with similar growth habit as *Pleuromeia* (Grauvogel-Stamm and Duringer, 1983; Naugolnykh, 2013). The genus *Annalepis* is based on isolated sporophylls that articulate in cones (Meng, 1998; Grauvogel-Stamm and Lugardon, 2001). In the early Early Triassic (Induan), *Tomiostrobus*, a subgenus of *Annalepis* (Dobruskina, 1995) or a synonymous genus of *Annalepis* (Meng et al., 2000) is widely spread in Siberia (Sadovinkow, 1982), *Cylostrobus* and *Skilliostrobus* in southeastern Australia (Retallack, 1975; Ash, 1979). Some plant stems belonging to equisetales (*Neocalamites* spp.) are found (Fig. 5-13, C, D). Few fragments of *Pecopteris* were reported in this area (Yang et al., 1989).

Abundant fossil woods were found in the Guodikeng Formation at the Taoshuyuan C

section. All the samples were identified as conifers (Fig. 5-13, E).

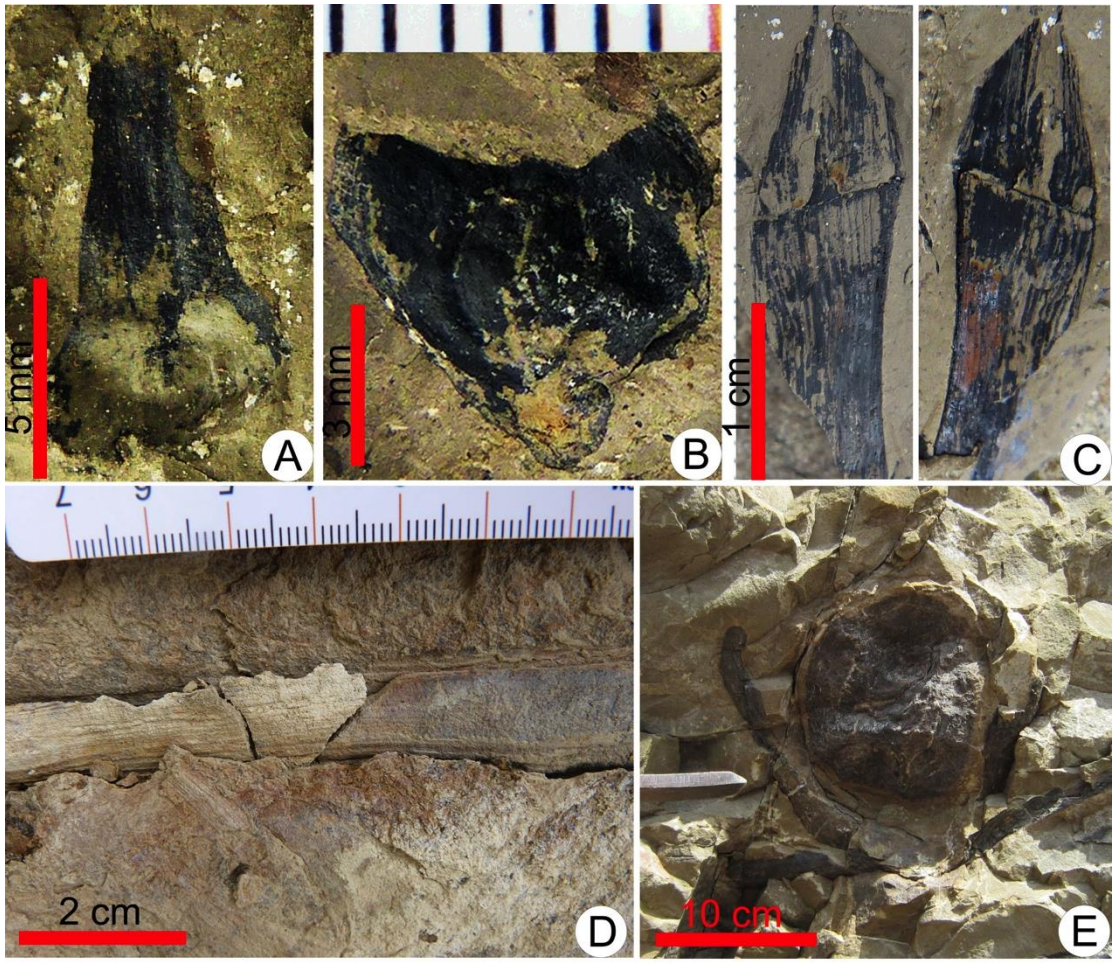

Figure 5-13 Early Triassic fossil plants from Guodikeng Formation (A, B, C and E) and Jiucaiyuan Formation (D). A, B. *Annalepis* sp.; C. *Neocalamites* sp. 1; D. *Neocalamites* sp. 2; E. Fossil woods. A-D are from Dalongkou area, E is from Taoshuyuan area.

Comparison with the *Annalepis-Peltaspermum* and the relicts of gigantopterids assemblage from Kayitou Formation, South China

The assemblage has been defined from the fossil plants content of the early Early Triassic Kaiyitou Formation of western Guizhou and eastern Yunnan (Yu, 2008). Lithologically, the formation is a set of non-marine clastic deposits which are compose of yellow fine-grained sandstone. This assemblage contains 17 species belonging to 10 genera: *Annalepis zeilleri*, *A. brevicystis*, *A. latiloba*, *A. furongqiaoensis* and *Annalepis* spp. in Isoetaceae genus *Annalepis*; ?*Lepidodendron* sp., *Stigmaria ficoides* and *Stigmaris* spp. in Lepidodendrales; *Paracalamites stenocostatus* in Arthrophytes; *Pecopteris* sp. and ?*Sphenopteris* sp. in Pteridophyta; aff. *Peltaspermum martinsii, P. lobulatum P.* spp. in Peltaspermaceae; ?*Sphenobaiera* sp. in Ginkgopsida; Gigantopteridales of *Giantonoclea* sp. and *Gigantopteris* sp.; and a few unidentified fossil plants.

Compared with the Kayitou Formation palaeofloral assemblage, the present flora is also dominated by lycopsids. The present flora differs from the Kayitou Formation palaeofloral assemblage by its abundant fossil woods of conifer affinities and the lack of

relic elements from the Cathaysian flora.

Comparison with the *Pleuromeia jiaochengensis* assemblage from Liujiagou Formation, North China

The assemblage is represented by the plants from Liujiagou Formation of Shihchienfeng Group (Wang and Wang, 1989). The formation is composed of a set of greyish purple and purple feldspathic sandstones intercalated with sandy shales and argillites, occasionally with the lenses of greyish green feldspathic sandstone, about 480m in thickness. Most of the fossil plants in the formation are autochthonous. The assemblage is composed of more than 16 species belonging to 12 genera (Wang and Wang., 1982; Wang and Wang, 1989): *Pleuromeia altinis*, *P*. *jiaochengensis*, *P. pateriformis, Macrrstachya gracilis*, *Phyllotheca yusheensis*, *Crematopteria brevipinnata*, *C*. *circinalis*, *Peltaspermum lobulatum*, *P. calycinum*, *Voltzia* sp., *Willsiostrobus* sp.etc. The assemblage is dominated by the Lycopsids (characterized by *Pleuromeia*) and subordinated by the horsetails (highlighting *Macrostachya gracilis* and *Phyllotheca yusheensis*) and ferns in which the *Crematopteris brevipinnata* and *C. circinalis* are the important elements of the Buntsandstein palaeoflora of Western Europe.

Our assemblage and the Liujiagou palaeofloral assemblage are both dominated by lycopsids. The difference is that lycopsid *Annalepis* is an abundant element in present our palaeofloral assemblage, while in the Liujiagou Formation, *Pleuromeia* dominates. The only species related to conifer in the Liujiagou Formation is *Voltzia* sp.

Comparison with Early Triassic Siberia floras

The Early Triassic Angara flora is represented by the plants from the Tunguss Basin, Russia which are dominated by ferns (Marattiaeeae, Osmundaceae, Dieksonlaceae and Schizeaeeae) and subordinated by seed ferns and conifers, according to the study of the previous workers. The flora is basically inherited from the Late Permian Angara flora.

Compared with the Early Triassic Siberia floras, our flora has also abundant conifers. The present flora differs from the Early Triassic Siberia floras in having lycopsids and lack of ferns.

3. End Permian extinction of flora

In the Junggar-Turpan Basin, the abundance and diversity of plants demonstrate deep changes across the PTB interval. Plant fossils are abundant in the Late Permian strata, with up to 32 genera and 60 species recorded. The most common plant genera found are typical of the Subangaran flora with some Angaran and Cathaysian elements. The most common plant species found are "*Callipteris*" cf. *lanceolata*, "*C.*" zeilleri, *Comia major, C.* aff. *dentate, Cordaites angustifolius*, *C. andalepensis*, and sulcial *C. adleri*, *C. clerii* and *C. insignis.*

In contrast, the earliest Triassic vegetation was poor in abundance and diversity, with only 6 genera and 7 species represented. In general, the Early Triassic vegetation was sparse and monotonous with lycopsids, equisetales, filicalesand conifers. Not any relict of the Late Permian Subangaran flora was found in the Early Triassic deposits. The Triassic newcomers include *Annalepis, Neocalamites* and fossil woods *Junggaropitys*

dalongkouensis, XTT-C-4 gen. nov. and *Xinjiangoxylon turpanense*.

However, the fossil plants preserved in the research area are not successive. Thus, temporal patterns of diversity changes are hard to recognise. There is no evidence that the regional disappearance of plants across the PTB in the study area was instantaneous.

For a longer timescale, we notice that plant genera and species gradually decreased from 26 genera and 53 known species in the Wuchiapingian, to 10 genera and 15 known species in the Changhsingian, and only 6 genera and 7 known species in the Induan (Sun, 1989 and our results). In other words, about 81 % of megaplant species were eliminated at the end-Wuchiapingian. Only about 47 % of species originated in the Changhsingian (Fig. 5-14). At the end of the Changhsingian, almost all of species vanished.

4. Recovery of the flora after the end-Permian biotic crisis

The end-Permian mass extinction is the only one joining terrestrial plants massive extinction and a major extinction in the marine realms (Cascales-Miñana and Cleal, 2013). Based on the palaeobotanical data for the end-Permian Northern China Block, several environmental stresses were identified, for instance, wind activity, fungal proliferation, water stress, elevated atmospheric CO_2 concentration and wildfire (Wang and Zhang, 1998). After this severest extinction, the physical environments became very poor over the next 5–6 Myr (Retallack et al., 2011; Chen and Benton, 2012; Sun et al., 2012; Retallack, 2013； Benton and Newell, 2014). Land plants are known to be particularly sensitive to environments and palaeoclimate. But the records of land plants in Early Triassic are not continuous, thus it is hard to recognise the details of the beginning of the post-crisis recovery of vegetation.

Wang (1991) is the first palaeobotanist who has thoroughly studied the land-plant recovery and noted its extinction at the Permian-Triassic transition and its subsequent recovery. He proposed a two-stage recovery model of Triassic land-flora from the end-Permian life crisis: the first was the Early Triassic *Pleuromeia* stage with three sub-zones, the first one dominated by the lycopsid *Pleuromeia*; the second being the Middle Triassic *Tongchuanophyllum* stage with two sub-zones (*Isoetes* and *Scytophyllum* sub-zones) characterized by the broad-leaved pteridosperm *Tongchuanophyllum* and the sphenopsids *Equisetites* and *Neocalamites*.

Yu (2008) found a similar recovery process in South China. The first stage was the expansion of the vegetation stage in the Early Triassic: in the early Early Triassic, the *Annalepis*-dominated flora covered the land; in the late Early Triassic, gymnosperm (e.g. *Albertia* and *Voltzia*) and pteridosperm (e.g. *Neuropteridium*) began to be flourishing. The second stage was the occurrence of riparian vegetation in shore-lagoon. It is represented by the *Pleuromeia-Annalepis* flora.

Grauvogel-Stamm and Ash (2005) researched on the Triassic fossil plants and found that the Triassic land-plant recovery also include two stages: a long survival interval in the Early Triassic, similarly dominated by the lycopsid *Pleuromeia* being the oldest Triassic land flora represented in Europe; and the early Middle Triassic floras correspond to the recovery interval itself, with the early Anisian flora of northeastern France (Grauvogel-Stamm, 1978) representing the first phase and the Upper Anisian flora of Italy

(Broglio et al., 2002) corresponding to the second phase.

In the research area, the middle and late Triassic, and early Middle Triassic plant fossils are very rare. Thus, it is impossible to recognise all the process of the recovery of vegetation.

But we found that in each area, after the end-Permian biotic crisis, the lycopsids and some other ferns played an important role in the vegetation recovery.

Looy et al. (1999) analysed the spores and pollen during the recuperation after the end-Permian crisis in the European part of the Pangea megacontinent. They found that the conifer forests were dominant after the latest Permian vanished during the crisis and the lycopsids experienced an adaptive radiation and dominated the landscapes for 4–5 million years. A similar fern-spike has been observed after the crisis at the Cretaceous-Tertiary boundary indicating that ferns took over after the extensive destruction of forests. In modern times, lycopsids and ferns are often the pioneer species that take over disturbed sites (Pfefferkorn, 1999). In the Junggar-Turpan Basin, we found that the lycopsids (*Annalepis*) and ferns (*Neocalamites* and *Pecopteris*) were also pioneer species after the end-Permian crisis. This result corresponds to our research on the spores and pollen (section 2.6.1).

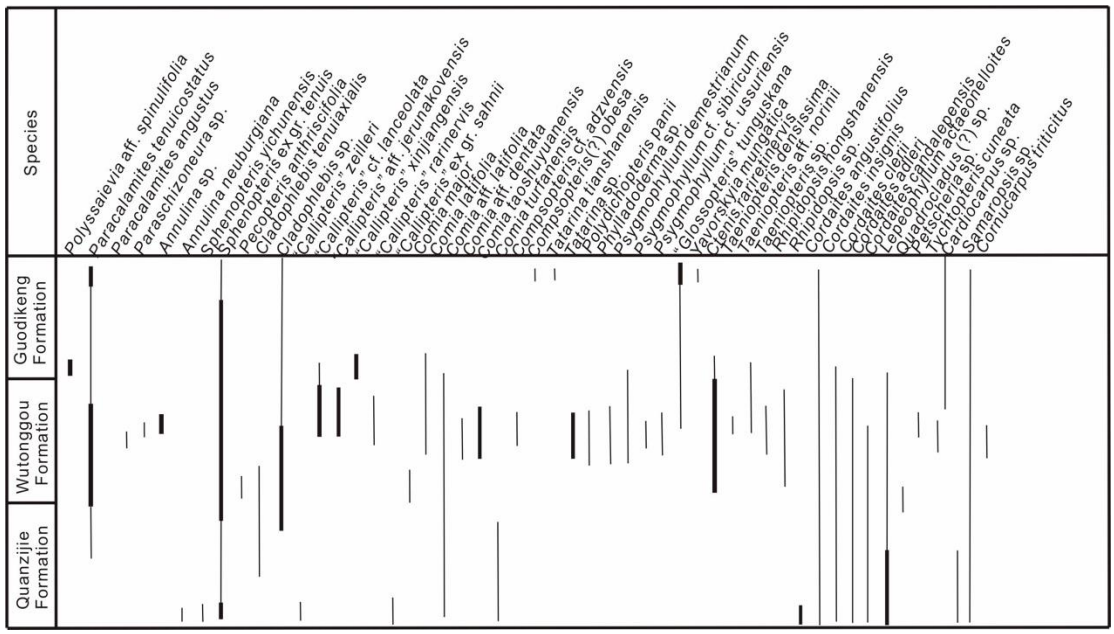

Figure 5-14 Distribution of fossil plants from Late Permian in the Taoshuyuan area (fossil plant data are from Sun, 1989).

5. Vegetation in the early Early Triassic in the Junggar-Turpan Basin

The beds yielding *Annalepis* and *Neocalamites* are found just above the PTB. The first conifer woods are found at least 37 m above the PTB. Some *Neocalamites* and *Pecopteris* were discovered in the lower part of Jiucaiyuan Formation.

Due to the preservation of fossils, we speculate that the lycopsids, equisetales and filicales are autochthonous burial or parautochthonous (burial over short distances). But some samples of wood fossils show wide space between the tracheids in their secondary

xylem. That means they had macerated in the water for a long time before they were buried. Hence, the fossil woods are allochthonous, transported by rivers may be from far of their burial site.

The early Early Triassic vegetation possibly covers two main ecosystems: (1) one characterized by lowland environments (flood plains and marshes) containing lycopods, equisetales and other filicales. (2) The second might have been in upland environments (upland levees, drier parts of floodplains, extrabasinal areas including mountainous regions) that were mainly inhabited by conifers. The upland ecosystem may develop relatively late.

§5.3 Sedimentary facies related to the plant extinction

In Austalia, India and the south Urals, the fluvial sequences across the PTB always show a marked increase in the sediment grain size (Newell et al., 1999; Ward et al., 2000; Chakraborty and Sarkar, 2005). In the Karoo basin of South Africa, the rivers changed from the highly bended river to lowly bended river (anomaly layer) in the Late Permian to braided river deposition in the Early Triassic (Smith, 1995; Ward et al., 2000). These changes were related to the weathering and erosion rates increasing after the vegetation vanished.

In the western Guizhou and eastern Yunnan, South China, the *Gigantopteris* flora has been replaced by the Annalepis-Peltspermum dominated flora in the earliest Triassic. The Early Triassic Kayitou Formation was represented by lagoon environments. While, deposits of the overlying Dongchuan Formation show a progressive change in depositional environment to braided river (Bercovici et al., 2015). Until now, no plant fossils nor spore and pollens were reported in the Dongchuan Formation.

In the Shaanxi, North China, the PTB were placed in the upper member of Sunjiagou Formation. The deposits across the PTB show a change from lagoon or lacustrine environment to braided rivers (lower member of Liujiagou Formation). Almost all the plants vanished at the end Permian (Chu et al., 2015).

In the Dalongkou area, the earliest Triassic deposits of upper part of Guodikeng Formation show lake or pond environments. The overlying Jiucaiyuan Formation was represented by unconfined flow within lakes or ponds, and alluvial plain environments. The numerous mud clasts occurring within the Sh facies of the basal of Jiucaiyuan Formation are interpreted to result from the reworking of mud chips produced by mud craks formation. The mud chips reflect a pulse of intense soil erosion (Retallack, 1999; Retallack and Krull, 1999; Thackerary et al., 1990; Stanley and Yang, 1994). Comparable features can be observed in the North China. The basal sandstones of the Liujiagou Formation contain numerous mud breccias.

As was demonstrated in Chapter 4, during the P-T interval, there is no record of major orogenic events in the basin that could have resulted in the striking sedimentological changeover from meandering to braided river systems. The changes may well be related

to the vegetation extinction. On the one hand, the die-off of plants decreased the strength of channel banks； on the other hand, it would increase sediment supply from hill slopes, and thereby would increase sediment loads in the channels (Ward et al., 2000).

In the Taoshuyuan area, comparable features were observed. At the lowermost of Guodikeng Formation, the deposits changed from the freshwater pond or lake, and flood plain environments to the braided river. The same change took place at the bottom of Jiucaiyuan Formation. The two changes may result from the die-off of plants.

Conclusions

This thesis work has been dedicated to the anatomical study of the fossil woods and the analysis of the fossil plants assemblages replaced in their sedimentary environments, to study the environmental changes during the Permian-Triassic transition in the Junggar and Turpan basins. Based on our results, the main conclusions are as follow:

Fossil woods:

We describe five genera and six species of fossil woods. Among them, three new genera are established (one new genus is still in review):

Junggaropitys dalongkouensis was collected from the Early Triassic sediments of the Guodikeng Formation in the Turpan Basin and the Middle–Late Triassic sediments of the Karamay Formation in the Junggar Basin. The new genus is based on the detailed description of permineralized woods is well characterized by these diagnostic characters: a small homogeneous pith, endarch primary xylem and *Protophyllocladoxylon*-type secondary xylem. The quantitative growth-ring analyses of *J. dalongkouensis* indicate that this species was evergreen, the leaf longevity being 3 to 6 years.

Xinjiangoxylon turpanense was collected from the Early Triassic sediments of the Guodikeng Formation in the Turpan Basin. It is characterized by a solid, nonseptate and heterocellular pith, endarch primary xylem and *Protophyllocladoxylon*-type secondary xylem.

XTT-C-4 fossil wood, genus and species novae, was collected from the Late Permian–Early Triassic Guodikeng Formation in the Turpan Basin, Northwest China. Its permineralized wood is characterized by a heterogeneous pith, endarch primary xylem and *Protophyllocladoxylon*-type secondary xylem. The pith consists of parenchyma cells and supporting diaphragms formed by brick-like sclerenchyma cells. The quantitative growth-ring analyses of *T. taoshuyuanensis* indicate that the species was evergreen, the leaf longevity being comprised between 3 to 15 years.

The tree collected species vascularised and supported by *Protophyllocladoxylon*-type woods were distributed mainly in the cool temperate climate zone of the southern hemisphere, various climate zones of northern hemisphere and equatorial zone during the Late Palaeozoic.

The samples recognised as *Arthropitys* cf. *communis* and *Agathoxylon* cf. *leei* represent new taxa, we will collect more materials and discuss the details of the taxon in the next stage.

Sedimentary paleoenvironments:

In the Dalongkou area, the successions show two prominent changes. In the Wutonggou Formation, the environments changed from braided river to ephemeral fluvial systems or ponds and alluvial plain deposits, forming several sedimentary cycles. The overlying Guodikeng Formation is characterized by the perennial freshwater lake or

ponds, associated with their flood-plain environments. The depositional environment changed to unconfined flow within lakes or ponds, and alluvial plains in the Jiucaiyuan Formation.

In the Taoshuyuan area, the studied interval spans parts of the Wutonggou, Guodikeng and Jiucaiyuan formations where four major types of depositional environments were identified based mainly on the sedimentological analyses. The vertical successions show changes, from ever-flooded lake or pond, or flood plain depositional environments to braided rivers depositional environment, then to alluvial plain environment, and finally to braided rivers depositional environment.

The petrographic analysis on detrital siliciclastic samples shows: (1) the sources of detrital particles remained, during the whole Permian Triassic transition, essentially the same; (2) the volcaniclasts originated from several distinct volcanic sources; (3) the sources are similar for the Dalongkou and the Taoshuyuan sections. During the Permian-Triassic transition, the presently separate Dalongkou and Taoshuyuan sections belonged to the same basins, therefore the Bogda Mountains might uplift not before the Middle-Late Triassic oe even during the early Jurassic. The limestone samples imply a quiet, low energetic depositional environment with a moderate to very limited siliciclastic detrital input (lacustrine environment).

Palaeoclimate and palaeoenvironmental reconstructions:

The study of the fossil woods growth-ring patterns from different species allowed us to deduce the palaoclimate during the Permian-Triassic transition. On these basis, the palaeoclimate reconstruction shows: (1) the climate in the Junggar terrane around the PTB was warm and humid with limited temperature and precipitation fluctuations; (2) The temperature and precipitation remained relatively stable during the P-T transition. (3) The Palaeo-Tethys megamonsoons did not influence the Junggar terrane along the east coast of mid-latitude Pangaea.

The previously reported five fossil woods from the Middle Permian to the early Late Permian deposits of Hami area show that the climate during this period was warm and humid with limited temperature and precipitation fluctuations as well. Thus, we speculate that although the North China blocks drifted to the north during the Permian, the global warming may diminish its impact on the climate and that induced no significant effect on the floristic exchanges between the Angaran and the northern edge of the Cathaysian domains.

In the Late Permian, the most Cathaysian elements disappeared on the North China blocks. That may result from the globally prevailing Permian hot and dry climate, which migrated gradually from the west to the orient.

Plant fossils, abundant in the Late Permian strata, became, dramatically, rare in the Early Triassic deposits. The Late Permian and Early Triassic macrofloral data that the previous authors provided and we worked on indicate that plant genera and species gradually decreased from 26 genera and 53 species in the Wuchiapingian, to 10 genera and 15 species in the Changhsingian, and only 6 genera and 7 species in the Induan. The temporal trend in the change of the flora living in the Junggar and Turpan basins appears

to be indicative of a long, protracted extinction process that may have started well before the Permian-Triassic boundary. Such a “drawn out” extinction process spanning the entire Late Permian and across the PTB therefore does not support a globally synchronous end-Permian catastrophic event such as meteor impacts.

After the end-Permian crisis, the lycopsids (*Annalepis*) and ferns (*Neocalamites* and *Pecopteris*) played roles of pioneer species. The early Early Triassic vegetation possibly covers two main ecosystems: (1) one characterized by lowland environments containing lycopods, equisetales and other filicales. (2) The other ecosystem might have been in the upland environments that were mainly inhabited by conifers. The upland ecosystem may develop relatively late.

The die-off of plants decreased strength of channel banks and increased sediment delivery from hill slopes, and thereby would increase sediment loads in channels. It may result in the depositonal environmental changes around the Wuchiapingian-Changhsingian boundary and in the Early Triassic in the research area.

References

Algeo, T.J., Chen, Z.Q., Fraiser, M.L., Twitchett, R.J., 2011. Terrestrial-marine teleconnections in the collapse and rebuilding of Early Triassic marine ecosystems. Palaeogeography, Palaeoclimatology, Palaeoecology 308, 1–11.

Algeo, T.J., Twitchett, R.J., 2010. Anomalous Early Triassic sediment fluxes due to elevated weathering rates and their biological consequences. Geology 38, 1023–1026.

Allen, M.B., Sengor, A.M.C., Natal'in, B.A., 1995. Junggar, Turfan and Alakol basins as Late Permian to ? Early Triassic extensional structures in a sinistral shear zone in the Altaid orogenic collage, Central Asia. Journal of the Geological Society 152 (2), 327–338.

Arche, A., López-Gómez, J., 2005. Sudden changes in fluvial style across the Permian– Triassic boundary in the eastern Iberian Ranges, Spain: analysis of possible causes. Palaeogeography, Palaeoclimatology, Palaeoecology 229, 104–126.

Ash, J., 1983. Growth rings in *Agathis robusta* and *Araucaria cunninghami* from tropical Australia. Aust. J. Bot. 31, 269–276.

Ashraf, A.R., Sun, G., Wang, Y.D., Uhl, D., Li, C., Mosbrugger, V., 1999. The Triassic-Jurassic boundary in the Junggar basin (NW-China)-Preliminary palynostratigraphic results. Acta Palaeobotanica Supplementum 2, 85-91.

Ash, S.R. 1979. Skilliostrobus , a new lycopsid cone from the Early Triassic of Australia. Alcheringa 3, 73–89.

Ash, S.R., Creber, G.T., 1992. Palaeoclimatic interpretation of the wood structures of the trees in the Chinle Formation (Upper Triassic), Petrified Forest National Park, Arizona, USA. Palaeogeogr. Palaeoclimatol. Palaeoecol. 96, 299–317.

Bambach, R.K., Knoll, A.H., Wang, S.C., 2004. Origination, extinction, and mass depletions of marine diversity. Palaeobiology 30(4), 522-542.

Benton, M.J., Newell, A.J., 2014. Impacts of global warming on Permo-Triassic terrestrial ecosystems. Gondwana Research 25 (4), 1308–1337.

Benton, M.J., Twitchett, R.J., 2003. How to kill (almost) all life: the end-Permian extinction event. Trends in Ecology & Evolution 18(7), 358-365.

Bercovici, A., Cui, Y., Forel, M.-B., Yu, J., Vajda, V., 2015. Terrestrial palaeoenvironment characterization across the Permian–Triassic boundary

in South China. J. Asian Earth Sci. 98, 225–246.
Bercovici, A., Vajda, V., 2016. Terrestrial Permian – Triassic boundary sections in South China. Glob. Planet. Chang. 143, 31-33.
Berthelin, M., Broutin, J., Kerp, H., Crasquin-Soleau, S., Platel, J. P., & Roger, J. (2003). The Oman Gharif mixed palaeoflora: a useful tool for testing Permian Pangea reconstructions. Palaeogeography, Palaeoclimatology, Palaeoecology, 196(1), 85-98.
Berthelin, M., Stolle, E., Kerp, H., Broutin, J., 2006. *Glossopteris anatolica* Archangelsky and Wagner 1983, in a mixed middle Permian flora from the Sultanate of Oman: Comments on the geographical and stratigraphical distribution. Review of Palaeobotany and Palynology 141(3), 313-317.
Bian, W., Hornung, J., Liu, Z., Wang, P., Hinderer, M., 2010. Sedimentary and palaeoenvironmental evolution of the Junggar Basin, Xinjiang, Northwest China. Palaeobiodiversity and Palaeoenvironments 90, 175–186.
Biggs, A.R., 1987. Occurrence and location of suberin in wound reaction zones in xylem of 17 tree species. Phytopathology 77 ,718-725.
Biradar, N.V., Bonde, S.D., 1981. *Nandorioxylon saksenae* gen. et sp. nov. — a new gymnospermous wood from the Kamthi Stage of Chandrapur District, Maharashtra State, India. Geophytology 11, 90–95.
Boucot, A.J., Chen, X., Scotese, C.R., Fan, J.X., 2009. Phanerozoic global climatic reconstruction. Science Press, Beijing, 173 pp. (In Chinese)
Brea, M., Césari, S.N., 1995. An anatomically preserved stem from the Carboniferous of Gondwana: *Phyllocladopitys petriellae* Brea and Césari, sp. nov. Review of Palaeobotany and Palynology 86 (3), 315-323.
Brea, M., Artabe, A, Spalletti, L.A., 2008. Ecological reconstruction of a mixed Middle Triassic forest from Argentina. Alcheringa 32 (4), 365-393.
Brea, M., Matheos, S.D., Raigemborn, M.S., Iglesias, A., Zucol, A.F., Prámparo, M.B., 2011. Palaeoecology and palaeoenvironments of Podocarp trees in the Ameghino Petrified forest (Golfo San Jorge Basin, Patagonia, Argentina): constraints for early Palaeogene palaeoclimate. Geologica acta 9 (1), 13-28.
Brison, A.L., Philippe, M., Thevenard, F., 2001. Are Mesozoic wood growth rings climate-induced? Palaeobiology 27, 531– 538.
Broglio, L.C., Fugagnioli A., Van Konijnenburg-Van Cittert J., Kustatscher E., Posenato R., . Wachtler, 2002. Anisian macroflora from the northern Dolomites (Monte Prà della Vacca/Kühwiesenkopf, Braies): a first report, Riv. Ital. Palaeontogr. Stratigr. 108, 1–390.
Cao, C., Wang, W., Liu, L., Shen, S., Summons, R.E., 2008. Two episodes of ^{13}C depletion in organic carbon in the latest Permian: Evidence from the

terrestrial sequences in northern Xinjiang, China. Journal of Asian Earth Sciences, 270(34), 251-257.

Carroll, A.R., Graham, S.A., Hendrix, M.S., Ying, D., Zhou, D., 1995. Late Paleozoic tectonic amalgamation of northwestern China: sedimentary record of the northern Tarim, northwestern Turpan, and southern Junggar Basins. Geological Society of America Bulletin 107, 571–594. doi:10.1130/0016-7606(1995)107<0571:LPTAON>2.3.CO;2

Cascales-Miñana, B., Cleal, C.J., 2013. The plant fossil record reflects just two great extinction events. Terra Nova 26 (3), 195–200.

Césari, S.N., Álvarez-Vázquez, C., Méndez-Bedia, I., Álvarez-Laó, D., Turrero, P., Arbizu, M., 2015. First report of permineralised plants in the Stephanian of Arnao (Asturias, northwestern Spain). Palaeogeography, Palaeoclimatology, Palaeoecology, 440, 475-486.

Chakraborty, T., Sarkar, S., 2005. Evidence of lacustrine sedimentation in the Upper Permian Bijori Formation, Satpura Gondwana basin: palaeogeographic and tectonic implications. Journal of Earth System Science 114, 303–323.

Chattaway, M.M., 1949. The development of tyloses and secretion of gum in heartwood formation. Australian Journal of Science Research Series B, Biological Science 2, 227 – 240.

Chen, Z.Q., Benton, M.J., 2012. The timing and pattern of biotic recovery following the end-Permian mass extinction. Nature Geoscience 5 (6), 375–383.

Chen, Zhong-Qiang, Algeo, T.J., Bottjer, D.J., 2014a. Global review on the Permian–Triassic mass extinction and subsequent recovery: Part I. Earth-Sci. Rev. 137, 1–5.

Chen, Zhong-Qiang, Yang, Hao, Luo, Mao, Benton, M.J., Kaiho, Kunio, Zhao, Laishi, Huang, Yuangeng, Zhang, Kexing, Fang, Yuheng, Jiang, Haishui, Qiu, Huan, Li, Yang, Tu, Chengyi, Shi, Lei, Zhang, Lei, Feng, Xueqian, Chen, Long, 2014b. Complete biotic and sedimentary records of the Permian–Triassic transition from Meishan section, South China: Ecologically assessing mass extinction and its aftermath. Earth-Sci. Rev.. 149, 67-107.

Cheng, Z., Lucas, S.G., 1993. A possible nonmarine GSSP for the Permian-Triassic boundary. Albertiana 12, 39-44.

Cheng, Z.W., Wu, S.Z., Fang, X.S., 1996. The Permian–Triassic sequences in the southern margin of the Junggar Basin and the Turpan Basin, Xinjiang, China. In: Hongfei, Hou, Jinsong, Zhou (Eds.), Field Trip Guide, Volume 1, Stratigraphy, Palaeontology, Sedimentology, Petroleum and Coal Geology. 30th International Geological Congress. Geological Publishing House, Beijing, China.

Cheng, Z.W., Wu, S.Z., Fang, X.S., 1997. The Permian–Triassic sequences in the southern margin of the Junggar Basin and the Turpan Basin, Xinjiang. Xinjiang Geol. 15 (2), 155–173.

Choulet, F., Faure, M., Cluzel, D., Chen, Y., Lin, W., Wang, B., 2012. From oblique accretion to transpression in the evolution of the Altaid collage: new insights from West Junggar, northwestern China. Gondwana Res. 21, 530–47.

Chrysler, M.A., 1908. Tyloses in tracheids of conifers. New Phytologist 7(8), 198-204.

Chu, D., Tong, J., Song, H., Benton, M. J., Bottjer, D.J., Song, H., Tian, L., Early Triassic wrinkle structures on land: stressed environments and oases for life. Sci. Rep. 5, 10109; doi: 10.1038/srep10109.

Crasquin, S., Forel, M.-B., 2014. Ostracods (Crustacea) though Permian–Triassic events. Earth-Sci. Rev. 137, 52–64.

Creber, G.T., Chaloner, W.G., 1984. Influence of environmental factors on the wood structure of living and fossil trees. The Botanical Review 50, 357–448. Crisafulli, A., 1998. Leños gimnospérmicos de la Formación Melo (Pérmico Inferior), Uruguay. Parte II. *Stiloxylon, Polysolenoxylon* y *Bageopitys*. Ameghiniana, 35 (2), 133-140.

Cochard, H., Tyree, M.T., 1990. Xylem dysfunction in *Quercus*: vessel sizes, tyloses, cavitation, and seasonal changes in embolism. Tree Physiology 6, 393 – 407.

Cui, Y., Bercovici, A., Yu, J.-X., Kump, L.R., Freeman, K.H., Su, S.-G., Vajda, V., 2016. Carbon cycle perturbation expressed in terrestrial Permian–Triassic boundary sections in South China. Glob. Planet. Chang. http://dx.doi.org/10.1016/j.gloplacha.2015.10.018.

Davison, E.M., Tay, F.C.S., 1985. The effect of waterlogging on seedlings of Eucalyptus marginata. New Phytologist 101, 743 – 753.

Davies, C., Allen, M.B., Busboy, M.M., Safonova, I., 2010. Deposition in the Kuznetsk Basin, Siberia: insights into the Permian–Triassic transition and the Mesozoic evolution of Central Asia. Palaeogeography, Palaeoclimatology, Palaeoecology 295, 307–322.

Dechamps, R., 1984. Evidence of bush fires during the Plio-Pleistocene of Africa (Omo and Sahabi) with aid of fossil woods. In: Coetzee, J.A., Van Zinderen Bakker, E.M. (Eds.), Palaeoecology of Africa and Surrounding Islands 16, Rotterdam.

Deng, S.H., Wan, C.B., Yang, J.G., 2009. Discovery of a Late Permian Angara–Cathaysia mixed flora from Acheng of Heilongjiang, China, with discussions on the closure of the Palaeoasian Ocean. Sci. China Earth Sci. 52 (11), 1746–1755.

DiMichele, W.A., Kerp, H., Tabor, N.J., Looy, C.V., 2008. The so-called "Palaeophytic–Mesophytic" transition in equatorial Pangea — multiple biomes and vegetational tracking of climate change through time. Palaeogeography,

Palaeoclimatology, Palaeoecology 268, 151–163.
DiMichele, W.A., Hook, R.W., 1992. Palaeozoic terrestrial ecosystems. In: Behrensmeyer A. K., Damuth J. D., DiMichele W. A., et al., eds., Terrestrial ecosystems through time. University of Chicago Press, Chicago and London. 204–325
DiMichele, W.A., Pfefferkorn, H.W., Gastaldo, R.A., 2001. Response of Late Carboniferous and Early Permian Plant Communities to Climate Change 1. *Annual Review of Earth and Planetary Sciences*, 29(1), 461–487
Dobruskina, I., 1995. Keuper (Triassic) flora from Middle Asia (Madygen, Southern Fergana), New Mexico Museum Nature History Science Bulletin, 5: 1-49.Dou, Y.W., Sun, Z.H., 1985. On the Late Palaeozoic plants in northern Xinjiang. Acta Geol. Sin. 59 (1), 1–11 (In Chinese with English summary).
Dou, Y.W., Sun, Z.H., 1983. Devonian plants. Palaeontological Atlas of Xinjiang, 2, 561-562.
Domeier, M., Torsvik, T.H., 2014. Plate tectonics in the late Palaeozoic. Geoscience Frontiers 5, 303–350. doi:10.1016/j.gsf.2014.01.002
Dute, R.R., Duncan, K.M., Duke, B., 1999. Tyloses in abscission scars of loblolly pine. IAWA Journal 20, 67 – 74.
Durante, M., 1983. Existence of an Upper Permian mixed Cathaysio–Angarian flora in Nanshan (North China). Geobios 16 (2), 241–242.
Eshet, Y., Rampino, M.R., Visscher, H., 1995. Fungal event and palynological record of ecological crisis and recovery across the Permian-Triassic boundary. Geology. 23(11), 967-970.
Erwin, D.H., 2000. The permo-triassic extinction. Shaking the Tree: Readings from Nature in the History of Life, pp.189.
Falcon-Lang, H.J., 1999. The Early Carboniferous (Courceyan– Arundian) monsoonal climate of the British Isles. Geol. Mag. 136, 177–187.
Falcon-Lang, H.J., 2000a. A method to distinguish between woods produced by evergreen and deciduous coniferopsids on the basis of growth ring anatomy: a new palaeoecological tool. Palaeontology 43 (4), 785-793.
Falcon-Lang, H.J., 2000b. The relationship between leaf longevity and growth ring markedness in modern conifer woods and its implications for palaeoclimatic studies. Palaeogeography, Palaeoclimatology, Palaeoecology 160 (3), 317-328.
Falcon-Lang, H.J., 2003. Growth interruptions in silicified conifer woods from the Upper Cretaceous Two Medicine Formation, Montana, USA: implications for palaeoclimate and dinosaur. Palaeogeography, Palaeoclimatology, Palaeoecology 199 (3), 299-314.
Feng, Qing-Lai, Algeo, T.J., 2014. Evolution of oceanic redox conditions during the

Permo-Triassic transition: evidence from deepwater radiolarian facies. Earth- Sci. Rev. 137, 34–51.

Feng, Z., Wang, J., Röβler, R., 2010. Palaeoginkgoxylon zhoui, a new ginkgophyte wood from the Guadalupian (Permian) of China and its evolutionary implications. Review of Palaeobotany and Palynology 162, 146-158.

Feng, Z.,Wang, J., Shen, G.L., 2008. Zalesskioxylon xiaheyanense sp. nov., a gymnospermous wood of the Stephanian (late Pennsylvanian) from Ningxia, northwestern China. Journal of Asian Earth Sciences, 33 (3/4), 219-228.

Feng, Z., 2012. *Ningxiaites specialis*, a new woody gymnosperm from the uppermost Permian of China. Review of Palaeobotany and Palynology 181 (1), 34-46.

Feng, Z.,Wang, J., Rößler, R., 2011. A unique gymnosperm from the latest Permian of China, and its ecophysiological implications. Review of Palaeobotany and Palynology 165 (1), 27-40.

Feng, Z., Wang, J., Liu, L. J., Rößler, R., 2012. A Novel Coniferous Tree Trunk with Septate Pith from the Guadalupian (Permian) of China: Ecological and Evolutionary Significance. International Journal of Plant Sciences 173 (7), 835-848.

Fluteau, F., Besse, J., Broutin, J., Ramstein, G., 2001. The Late Permian climate. What can be inferred from climate modelling concerning Pangea scenarios and Hercynian range altitude? Palaeogeography, Palaeoclimatology, Palaeoecology 167, 39–71. doi:10.1016/S0031-0182(00)00230-3

Foster, C.B., Afonin, S.A., 2005. Abnormal pollen grains: an outcome of deteriorating atmospheric conditions around the Permian–Triassic boundary. J. Geol. Soc. Lond. 162, 653–659.

Foster, C.B., Stephenson, M.H., Marshall, C, Logan, G.A., Greenwood, P.F., 2002. A revision of Reduviasporonites Wilson 1962: description, illustration, comparison and biological affinities. Palynology 26(1), 35-58.

Fritts, H.C., 1976. Tree Rings and Climate. Academic Press, New York.

Fritts, H.C., 1976. Tree Rings and Climate, Academic Press, London, pp. 1-576.

Fu, J., Deng, X., 1997. The Late Permian Bivalve Fossils and Their Ages in Taoshuyuan, Turpa, Xinjiang. Journal of Northwest University (Natural Science Edition), 27(2), 146-150. (In Chinese with English abstract)

Galfetti, T., Hochuli, P.A., Brayard, A., Bucher, H., Weissert, H., Vigran, J.O., 2007. Smithian/ Spathian boundary event: evidence for global climatic change in the wake of the end-Permian biotic crisis. Geology 35, 291–294.

Gastaldo, R.W., DiMichele, W.A., Pfefferkorn, H.W., 1996. Out of the Icehouse into the Greenhouse–A late Palaeozoic Analog for Modern Global Vegetational Change. GSA Today 6(10), 1–7.

Glasspool, I.J., Scott, A.C., 2010. Phanerozoic concentrations of atmospheric oxygen reconstructed from sedimentary charcoal. Nature Geoscience 3, 627–630.

Grauvogel-Stamm, L., Duringer, P., 1983. *Annalepis zeilleri* Fliche 1910 emend., un organe reproducteur de Lycophyte de la Lettenkohle de l′Est de la France. Morphologie, spores in situ et paléoécologie. Geologische Rundschau 72 (1) , 23-51.

Grauvogel-Stamm, L., Lugardon, B., 2001. The Triassic Lycopsids Pleuromeia and Annalepis: relationship, evolution and origin. American Fern Journal, 91 (3): 115-149.

Grauvogel-Stamm, L., Ash, S.R., 2005. Recovery of the Triassic land flora from the end-Permian life crisis. Comptes Rendus Palevol 4 (6), 593-608.

Greene, T.J., Carroll, A.R., Hendrix, M.S., Graham, S.A., Wartes, M.A., Abbink, O.A., 2001. Sedimentary record of Mesozoic deformation and inception of the Turpan-Hami basin, northwest China. Paleozoic and Mesozoic tectonic evolution of central and eastern Asia 194, 371-394.

Greene, T.J., Carroll, A.R., Wartes, M., Graham, S.A., Wooden, J.L., 2005. Integrated Provenance Analysis of a Complex Orogenic Terrane: Mesozoic Uplift of the Bogda Shan and Inception of the Turpan-Hami Basin, NW China. J. Sediment. Res. 75, 251–267. doi:10.2110/jsr.2005.019

Goddéris, Y., Roelandt, C., Schott, J., Pierret, M.-C., François, L.M., 2009. Towards an integrated model of weathering, climate, and biospheric processes. Reviews in Mineralogy and Geochemistry 70, 411–434.

Hallam, A., 1998. Mass extinctions in Phanerozoic time[J]. Geological Society, London, Special Publications 140(1), 259-274.

He, Bin, Xu, Yi-Gang, Huang, Xiao-Long, Luo, Zhen-Yu, Shi, Yu-Ruo, Yang, Qi.-Jun.,Yu, Song-Yue, 2007. Age and duration of the Emeishan flood volcanism, SW China: Geochemistry and SHRIMP zircon U–Pb dating of silicic ignimbrites, post-volcanic Xuanwei Formation and clay tuff at the Chaotian section. Earth Planet. Sci. Lett. 225, 306–323.

He, J., Wang, S.J., Hilton, J., Shao, L., 2013. *Xuanweioxylon scalariforme* gen. et sp. nov. Novel Permian coniferophyte stems with scalariform bordered pitting on secondary xylem tracheids. Review of Palaeobotany and Palynology 197 (15), 152-165.

Hendrix, M.S., 2000. Evolution of Mesozoic sandstone composition, southern Junggar, northern Tarim, and western Turpan basins, northwest China: a detrital record of the ancestral Tian Shan. Journal of Sedimentary Research 70, 520–532.

Hermann, E., Hochuli, P.A., Bucher, H., Brühwiler, T., Hautmann, M., Ware, D., Roohi, G., 2011. Terrestrial ecosystems on North Gondwana in the aftermath of the end- Permian mass extinction. Gondwana Research 20, 630–637.

Hiete, M., Berner, U., Heunisch, C., hling, H.-G., 2006. A high-resolution inorganic

geochemical profile across the Zechstein–Buntsandstein boundary in the North German Basin. Zeitschrift der Deutschen Gesellschaft für Geowissenschaften 157, 77–105.

Hilton, J., Wang, S. J., Galtier, J., Li, C.S., 2001. An Early Permian plant assemblage from the Taiyuan Formation of northern China with compression/impression and permineralized preservation. Review of Palaeobotany and Palynology, 114(3), 175–189.

Hilton, J., Wang, S.J., Zhu, W.Q., 2002. *Callospermarion* ovules from the Early Permian of northern China: palaeofloristic and palaeogeographic significance of callistophytalean seed-ferns in the Cathaysian flora. Review of Palaeobotany and Palynology 120(3–4), 301–314.

Hochuli, P.A., Vigran, J.O., Hermann, E., Bucher, H., 2010. Multiple climatic changes around the Permian-Triassic boundary event revealed by an expanded palynological record from mid-Norway. Geological Society of America Bulletin, 122(5-6), 884-896.

Hou, J.P., 2004. Two sporo-pollen assemblages of Guodikeng formation and discussion on the Permo-Triassic boundary in Junggar Basin, Xinjiang. In: Editorial Committee of Professional Papers of Stratigraphy and Palaeontology of Chinese Academy of Geological Sciences (Ed.), Professional papers of Stratigraphy and Palaeontology, vol. 28. Geological Publishing House, Beijing, pp. 177–204.

Jacoby, G.C., 1989. Overview of tree-ring analysis in tropical regions. IAWA Bull. 10, 99–108.

Jablonski, D., 1985. Extinctions in the fossil record. Philosophical Transactions: Biological Sciences 344 (1307), 11–16.

Jablonski, D., 1991. Extinctions: a palaeontological perspective[J]. Science (New York, NY) 253(5021), 754.

Jin, J.H., Mi, J.R., 1993. The Cathaysian–Angara mixed flora of Hongshan, Yichun of Heilongjiang. J. Changchun Univ. Earth Sci. 23 (3), 241–248 (In Chinese with English abstract).

Kiehl, J.T., Shields, C.A., 2005. Climate simulation of the latest Permian: Implications for mass extinction. Geology 33, 757–760. doi:10.1130/G21654.1

Knoll, A.H., Bambach, R.K., Payne, J.L., Pruss, S., Fischer, W.W., 2007. Palaeophysiology and end-Permian mass extinction. Earth and Planetary Science Letters 256, 295–313. doi:10.1016/j.epsl.2007.02.018

Knoll, A.H., 1984. Patterns of extinction in the fossil record of vascular plants. In: Nitecki, M. (Ed.), Extinctions. University of Chicago Press, Chicago, pp. 21–68.

Knoll, A.H., Niklas, K.J., 1987. Adaptation, plant evolution, and the fossil

record. Reviews in Palaeobotany and Palynology 50, 127–149.
Kräusel, R., 1928. Beiträge zur Kenntnis der Karruformation Deutsch-Südwest-Afrikas. Im Vertrieb bei der Preussischen Geologischen Landesanstalt.
Kräusel, R., 1928. Paläobotanische Notizen, X. Über ein Keuperholz mit cordaitem Mark. Senckenbergiana Lethaia 10, 247-250.
Kräusel, R., 1956. Hölzer aus dem Südlichen Gebiet der Karru-Schichten Südwest-Afrikas. Senckenbergiana Lethaia 37, 447-453.
Kräusel, R., Maithy, P.K., Maheshwari, H.K., 1961. Gymnospermous woods with primary structures from Gondwana rocks-a review. The Palaeobotanist 10, 97-107.
Lepekhina, V.G., 1969. Palaeoxylological characterization of the Upper Palaeozoic coal-bearing deposits of the Kuznetsk Basin. Translation Geological Institute Academy of Sciences USSR 130, 126-140 (In Russian).
Lepekhina, V.G., 1972. Woods of Palaeozoic pycnoxylic gymnosperms with special reference to North Eurasia representatives. Palaeontographica Abteilung B 138 (1-4), 44-106.
Leitch, M.A., Savidge, R.A., Downes, G.M., Hudson, T.L., 1999. Induction of tyloses in Eucalyptus globulues chips. IAWA Journal 20, 193 – 201.
Li, Y., Li, J., Cheng, Z., Sun, D., Liu, J., Zheng, J., 2004. Study on palaeomagnetism of Permian-Trassic in Pantaoyuan of Turpan, Xinjiang. Xinjiang Geology, 22(2): 136-142 (In Chinese).
Li, Y., Li, J., Cheng, Z., Sun, D., Liu, J., Zheng, J., 2004. Study on palaeomagnetism of Permian-Trassic in Pantaoyuan of Turpan, Xinjiang. Xinjiang Geology, 22(2): 136-142 (In Chinese with English abstract).
Li, Z.M., 1986. On the anatomy of *Dadoxylon taiyuanensis* sp. nov. Acta Botanica Sinica 28, 555-558 (In Chinese with English abstract).
Liao, Z., Lu, L., Jiang, N., Xia, F., Song, F., Zhou, Y., Li, S., Zhang, Z., 1987. Carboniferous and Permian in the western part of the east Tianshan Mountains. Eleventh Congress of Carboniferous Stratigraphy and Geology, Guidebook Excursion 4. Beijing, China, 50 pp.
Liu, Z., 2000. The Peimian-Triassic Boundary on the Northern Margin of the Turpan-Hami Basin of Xinjiang, NW China. Journal of Stratigraphy 24(4), 310-314 (In Chinese with English abstract).
Li X.X. Editor-in-Chief, 1995. Fossil floras of China through the geological ages. Guangzhou: Guangdong Science and technology Press, 1-695.
Looy, C.V., 2000. The Permian-Triassic biotic crisis: collapse and recovery of terrestrial ecosystems. LPP Foundation.
Looy, C.V., Brugman, W.A., Dilcher, D.L., Visscher, H., 1999. The delayed resurgence of forests after the Permian–Triassic ecologic crisis. Proceedings of the National Academy of Sciences of the United States of America 96, 13857–13862.
Lucas, S.G., 1998. Global Triassic tetrapod biostratigraphy and biochronology.

Palaeogeography, Palaeoclimatology, Palaeoecology 143, 347–384. doi:10.1016/S0031-0182(98)00117-5

Lucas, S.G., 2009. Timing and magnitude of tetrapod extinctions across the Permo-Triassic boundary. Journal of Asian Earth Sciences 36, 491–502. doi:10.1016/j.jseaes.2008.11.016

Maheshwari ,H.K., 1966. On some fossil woods from the Raniganj Stage of the Raniganj Coalfield, Bengal. 28 (Studies in the Glossopteris flora of India)[J]. Palaeobotanist 15(3), 243-257.

Maheshwari, H.K., 1972. Permian wood from Antarctica and revision of some Lower Gondwana wood taxa. Palaeontographica Abteilung B 138, 1-43.

Martin, E.E., MacDougall, J.D., 1995. Sr and Nd isotopes at the Permian/Triassic boundary: a record of climate change. Chemical Geology 125, 73–100.

McLoughlin, S., Lindström, S., Drinnan, A.N., 1997. Gondwanan floristic and sedimento- logical trends during the Permian–Triassic transition: new evidence from the Amery Group, northern Prince Charles Mountains, East Antarctica. Antarctic Science. 9, 281-298.

Metcalfe, I., Foster, C.B., Afonin, S.A., Nicoll, R.S., Mundil, R., Wang, X., Lucas, S.G., 2009. Stratigraphy, biostratigraphy and C-isotopes of the Permian–Triassic non-marine sequence at Dalongkou and Lucaogou, Xinjiang Province, China. J. Asian Earth Sci. 36, 503–520. doi:10.1016/j.jseaes.2008.06.005

Meyer, R.W., 1967. Tyloses development in White Oak. Forest Products Journal 17, 50 – 56.

McElhinny, M.W., Embleton, B.J.J., Ma, X.H., Zhang, Z.K., 1981. Fragmentation of Asia in the Permian. Nature 293, 212–216.

Miall, A.D., 1996. The geology of fluvial deposits. Springer, p. 582.

Michaelsen, P., 2002. Mass extinction of peat-forming plants and the effect on fluvial styles across the Permian–Triassic boundary, northern Bowen Basin, Australia. Palaeogeography, Palaeoclimatology, Palaeoecology 179, 173–188.

Mussa, D., 1958. Conifera fóssil do carbonifero superior de Santa Catarina. Boletim Departamento Nacional da Produção Mineral, Divisão de Geologia e Mineralogia 182, 1-23.

Mussa, D., de Carvalho. R.G., dos Santos, P.R., 1980. Estudo estratigráfico e palaeoecológico em ocorrências fossilíferas da Formação Irati, Estado de São Paulo, Brasil. Boletim IG-USP Instituto de Geociéncias da Universidade de São Paulo, 1, 142-149.

Mussa, D., 1986. Eustelos Gondwanicos de medullas diafragmadas e a sua posicão estratigrafica. Boletim IG-USP Instituto de Geociéncias da Universidade de São Paulo, 17, 11-26.

Naugolnykh S.V., Kerp, H., 1996. Aspects of Permian palaeobotany and palynology. XIV. On the oldest known peltasperms with radially symmetrical ovuliferous discs from the Kungurian (uppermost Lower

Permian) of the Fore-Urals (Russia). Rev. Palaeobot. Palynol. 91: 1–4, pp. 35–62.

Newell, A.J., Sennikov, A.G., Benton, M.J., Molostovskaya, I.I., Golubev, V.K., Minikh, A.V., Minikh, M.G., 2010. Disruption of playa-lacustrine depositional systems at the Permo-Triassic boundary: evidence from Vyazniki and Gorokhovets on the Russian Platform. Journal of the Geological Society 167, 695–716.

Newell, A.J., Tverdokhlebov, V.P., Benton, M.J., 1999. Interplay of tectonics and climate on a transverse fluvial system, Upper Permian, Southern Uralian Foreland Basin, Russia. Sedimentary Geology 127, 11–29.

Pang, Q.Q., Jin, X.C., 2004. Ostrocoda in the Guodikeng formation and continental Permo-Triassic boundary of Dalongkou section, Jimsar, Xinjiang. In: Editorial Committee of Professional Papers of Stratigraphy and Palaeontology of Chinese Academy of Geological Sciences (Ed.), Professional Papers of Stratigraphy and Palaeontology, vol. 28. Geological Publishing House, Beijing, pp. 205–246.

Panshin AI, DeZeeuw C. 1980. Textbook of wood technology, 4th edn. New York, NY: McGraw-Hill.

Pant, D.D., Singh, V.K., 1987. Xylotomy of some woods from Raniganj Formation (Permian), Raniganj Coalfield, India. Palaeontographica Abteilung B 203, 1-82.

Parameswaran, N, Knigge, H, Liese, W., 1985. Electron microscopic demonstration of a suberised layer in the tylosis wall of beech and oak. IAWA Bulletin NS 6, 269 – 271.

Parrish, J.T., 1993. Climate of the supercontinent Pangea. The Journal of Geology, 215-233.

Payne, J., Clapham, M., 2012. End-Permian mass extinction in the oceans: an ancient analog for the 21st century? Ann. Rev. Earth Planet. Sci. 40, 89–111.

Peng, Y., Yu, J., Gao, Y., yang, F., 2006. Palynological assemblages of non-marine rocks at the Permian–Triassic boundary, western Guizhou and eastern Yunnan, South China. Journal of Asian Earth Sciences 28(4), 291-305.

Pearce, R.B., 1990. Occurrence of decay-associated xylem suberization in a range of wood species. European Journal of Forest Pathology 20, 275 – 289.

Péron, S., Bourquin, S., Fluteau, F., Guillocheau, F., 2005. Palaeoenvironment reconstructions and climate simulations of the Early Triassic : Impact of the water and sediment supply on the preservation of fluvial systems. Geodinamica Acta 18, 431–446.

Petriella, B., 1982. *Medullopitys menendezii* n. sp., leño picnoxilico de gimnospermas del Palaeozóico Superior de Mendoza. Argentina. Ameghiniana 19 (3/4), 253–257.

Pfefferkorn, H.W., 1999. Recuperation from mass extinctions. Proceedings of the National Academy of Sciences, 96(24), 13597-13599.

Pfefferkorn, H.W., Archer, A. W., Zodrow, E. L., 2001. Modern Tropical Analogs for Carboniferous Standing Forests: Comparison of Extinct *Mesocalamites* with Extant *Montrichardia*. Historical Biology, 15, 235–250

Talboys, P.W., 1964. A concept of the host-parasite relationship in Verticillium wilt diseases. Nature. 361, 361 – 364.

Raup, D.M., Sepkoski, Jr.J.J., 1982. Mass extinctions in the marine fossil record. Science 215(4539), 1501-1503.

Raup D M., 1994. The role of extinction in evolution. Proceedings of the National Academy of Sciences 91(15), 6758-6763.

Retallack, G.J., 1975. The life and times of a Triassic lycopod. Alcheringa, 1, 3-29.

Retallack, G.J., 1995. Permian–Triassic life crisis on land. Science 267, 77–80.

Retallack, G.J., 1999. Postapocalyptic greenhouse paleoclimate revealed by earliest Triassic paleosols in the Sydney Basin, Australia. Geological Society of America Bulletin 111(1), 52-70.

Retallack, G.J., Krull, E.S., 1999. Landscape ecological shift at the Permian - Triassic boundary in Antarctica. Australian Journal of Earth Sciences 46(5), 785-812.

Retallack, G.J., Sheldon, N.D., Carr, P.F., Fanning, M., Thompson, C.A., Williams, M.L., Jones, B.G., Hutton, A., 2011. Multiple Early Triassic greenhouse crises impeded recovery from Late Permian mass extinction. Palaeogeography, Palaeoclimatology, Palaeoecology 308 (1), 233–251.

Retallack, G.J., 2012. Permian and Triassic greenhouse crises. Gondwana Research. http://dx.doi.org/10.1016/j.gr.2012.03.003 (online first).

Retallack, G.J., 2013. Permian and Triassic greenhouse crises. Gondwana Research 24, 90–103.

Romano, C., Goudemand, N., Vennemann, T.W., Ware, D., Schneebeli-Hermann, E., Hochuli, P.A., Brühwiler, T., Brinkmann, W., Bucher, H., 2012. Climatic and biotic upheavals following the end-Permian mass extinction. Nat. Geosci. 6, 57–60.

Royer, D.L., Wilf, P., Janesko, D., Kowalski, E., Dilcher, D., 2005. Correlations of climate and plant ecology to leaf size and shape: potential proxies for the fossil record. Am. J. Bot. 92, 1141–1151. doi:10.3732/ajb.92.7.1141

Sengor, A.M.C., Nat'lin, B.A., 1996. Palaeotectonics of Asia: fragments of a synthesis. In: Yin, A., Harrison, T.M. (Eds.). The Tectonic Evolution of Asia. Cambridge University Press, New York, pp. 486–640.

Schweingruber, F.H., 1992. Annual growth rings and growth zones in woody plants in southern Australia. IAWA Bulletin 13, 359-379.

Schweingruber, F.H., 1996. Tree Rings and Environment Dendroecology. Swiss Federal Institute for Forest, Berne, pp. 1- 609.

Schubert J K, Bottjer D J. Aftermath of the Permian-Triassic mass extinction event:

Palaeoecology of Lower Triassic carbonates in the western USA[J]. Palaeogeography, Palaeoclimatology, Palaeoecology, 1995, 116(1), 1-39.

Schultze-Motel, J., 1961. Gymnospermen-Hölzer aus dem Jura des Nördlichen Harzvorlandes: *Protophyllocladoxylon quedlinburgense* n. sp. Mber. Dtsch. Akad. Wiss, 3, 418-426.

Scotese, C.R., 2001. Atlas of Earth history, vol. 1. PALAEOMAP Project, Arlington, Texas.

Scott, A., 1979. The ecology of Coal Measure floras from northern Britain. *Proceedings of the Geologists' Association*, 90(3), 97–116

Sheldon, N.D., 2006. Abrupt chemical weathering increase across the Permian–Triassic boundary. Palaeogeography, Palaeoclimatology, Palaeoecology 231, 315–321.

Shi, X., Zhang, W., Yu, J.X., Chu, D.L., Huang, C., 2014. The flora from Karamay Formation in the south and north Tianshan Mountain, Xinjiang. Geological Science and Technology Information 33 (1), 55-61 (In Chinese with English abstract).

Shi, X., Yu, J.X., Li, H., Chi, H.F., Zhang, W., 2014. *Xinjiangoxylon* gen nov., a New Gymnosperm from the Latest Permian of China. Acta Geologica Sinica (English Edition) 88 (5), 1356-1363.

Shi, X., Yu, J., Broutin, J., Pons, D., 2015. *Junggaropitys*, a new gymnosperm stem from the Middle–Late Triassic of Junggar Basin, Northwest China, and its palaeoecological and palaeoclimatic implications. Review of Palaeobotany and Palynology 223, 10–20.

Shi, G.R., 2006. The marine Permian of East and Northeast Asia: an overview of biostratig- raphy, palaeobiogeography and palaeogeographical implications. J. Asian Earth Sci. 26 (3–4), 175–206.

Shi, G.R., Archbold, N.W., Zhan, L.P., 1995. Distribution and characteristics of mixed (transitional) mid-Permian (Late Artinskian–Ufimian) marine faunas in Asia and their palaeogeographical implications. Palaeogeogr. Palaeoclimatol. Palaeoecol. 114, 241–271.

Signor, P.W. Biodiversity in geological time[J]. American Zoologist, 1994, 34(1), 23-32.

Smith, R.M.H., Ward, P.D., 2001. Pattern of vertebrate extinctions across an event bed at the Permian-Triassic boundary in the Karoo Basin of South Africa. Geology 29, 1147–1150.

Smith, R.M.H., 1995. Changing fluvial environments across the Permian–Triassic boundary in the Karoo Basin, South Africa and possible causes of tetrapod extinctions. Palaeogeography, Palaeoclimatology, Palaeoecology 117, 81–104.

Stanley, S.M., Yang, X., 1994. A double mass extinction at the end of the Paleozoic

Era. Science, 266(5189), 1340.
Steiner M B, Eshet Y, Rampino M R, et al. Fungal abundance spike and the Permian–Triassic boundary in the Karoo Supergroup (South Africa)[J]. Palaeogeography, Palaeoclimatology, Palaeoecology, 2003, 194(4): 405-414.
Sun, F., 1989. On the Late Permian Angara flora of Turfan Basin, Xinjiang, with special reference to the subdivision of Angara Province. -M.Sc. thesis, Nanjing Institute of Geology and Palaeontology, Chinese Academy of Sciences. 1–192 (in Chinese with English abstract).
Sun, G., Mosbrugger, V., Li, J., Chen, X.S., 2001. Late Triassic flora of the Junggar Basin, Xinjiang, China. In: Sun, G., Mosbrugger, V., Ashraf, A.R., Wang, Y.D. (Eds), The advanced study of prehistory life and geology of Junggar Basin, Xinjiang, China. In: Proc Sino-German Cooperation Symp Prehistory Life and Geology of Junggar Basin, Xinjiang, China. Urumqi, pp 8-20.
Sun, G., Meng, F.S., Qian, L., Ouyang, S., 1995. Triassic floras. In: Li X.X. (Ed) Fossil plants of China through the geological ages. Guangdong Science and Technology Press, Guangzhou, pp 355–373.
Sun, G., Miao, Y.Y., Mosbrugger, V., Ashraf, A.R., 2010. The Upper Triassic to Middle Jurassic strata and floras of the Junggar Basin, Xinjiang, Northwest China. Palaeobiodiversity and Palaeoenvironments 90, 203-214.
Sun, K.Q., Liu, J., Liu, X.Y., Li, L., 2010. Discovery and significances of the mixed Cathaysian– Angaran flora in Yumen of Gansu Province. Geol. Rev. 56 (3), 305–311 (In Chinese with English abstract).
Sun, Y., Joachimski, M.M., Wignall, P.B., Yan, C., Chen, Y., Jiang, H., Wang, L., Lai, X., 2012. Lethally hot temperatures during the Early Triassic greenhouse. Science 338 (6105), 366–370.
Sze, H.C., 1934. On the occurrence of an interesting fossil wood from Urumqi (Tihua) in Sinkiang. Bulletin of Geological Society of China 13, 581-590.
Sze, H.C., 1956. Old Mesozoic plants from the Yenchang Formation, Northern Shaanxi. Palaeontologia Sinica New Series A 5 (Whole Number 139), 1-217.
Tang, W., Zhang, Z., Li, J., Li, K., Chen, Y., Guo, Z., 2014. Late Paleozoic to Jurassic tectonic evolution of the Bogda area (northwest China): Evidence from detrital zircon U-Pb geochronology. Tectonophysics 626, 144–156. doi:10.1016/j.tecto.2014.04.005
Taylor, E.L., Ryberg, P.E., 2007. Tree growth at polar latitudes based on fossil tree ring analysis. Palaeogeography, Palaeoclimatology, Palaeoecology, 255(3), 246-264.
Thackeray, J.F., Van der Merwe, N.J., Lee-Thorp, J.A., Sillen, A., Lanham, J.L., Smith, R., Keyser， A., Monteiro, P.M.S., 1990. Changes in carbon isotope ratios in the Late Permian recorded in therapsid tooth apatite. Nature 347, 751 - 753;

doi:10.1038/347751a0.

Thomas, S.G., Tabor, N.J., Yang, W., Myers, T.S., Yang, Y., Wang, D., 2011. Palaeosol stratigraphy across the Permian–Triassic boundary, Bogda Mountains, NW China: implications for palaeoenvironmental transition through earth's largest mass extinction. Palaeogeography, Palaeoclimatology, Palaeoecology 308 (1–2), 41–64.

Tian, B.L., Li, H.Q., 1992. A new special petrified stem, *Guizhouoxylon dahebianense* gen., sp. nov., from the Upper Permian in Shuicheng district, Guizhou, China. Acta Palaeontologica Sinica 27(1), 21-30 (In Chinese and English summary).

Tian, B.L., Hu, T., Zhao, H., 1996. The first discovery of *Walchiopremnon gaoi* sp. nov. in China. Geological Section of Beijing Graduate School, China University of Mining and Technology, Department of Geology, China University of Ming and Technology Selected papers on coal geology, celebrating Prof. Gao Wentai's eightieth birthday and his sixty-years career in geology. China Coal Industry Publishing House, Beijing, pp. 118-125 (In Chinese).

Traverse, A., 1988. Plant evolution dances to a different beat: plant and animal evolutionary mechanisms compared. Historical Biology 1, 277–301.

Twitchett, R.J., Looy, C.V., Morante, R., Visscher, H., Wignall, P.B., 2001. Rapid and synchronous collapse of marine and terrestrial ecosystems during the end-Permian biotic crisis. Geology 29, 351. doi:10.1130/0091-7613(2001)029<0351:RASCOM>2.0.CO;2

Veevers, J.J., Conaghan, P.J., Shaw, S.E., 1994. Turning point in Pangean environmental history at the Permian/Triassic (P/Tr) boundary. In: Klein, G.D. (Ed.), Pangea: Palaeoclimate, Tectonics, and Sedimentation During Accretion, Zenith, and Breakup of a Supercontinent: Geological Society of America Special Paper, 288, pp. 187–196.

Visscher, H., Brinkhuis, H., Dilcher, D.L., Elsik, W.C., Eshet, Y.,Looy, C.V., Rampino, M.R., Traverse, A., 1996. The terminal Palaeozoic fungal event: evidence of terrestrial ecosystem destabilization and collapse. Proc. Natl. Acad. Sci. U. S. A. 93, 2155–2158. Visscher, H., Sephton, M.A., Looy, C.V., 2011. Fungal virulence at the time of the end-Permian biosphere crisis?. Geology 39(9), 883-886.

Wan, M., Yang, W., Wang, J., 2014. *Septomedullopitys szei* sp. nov., a new gymnospermous wood from Lower Wuchiapingian (Upper Permian) continental deposits of NW China, and its implication for a weakly seasonal humid climate in mid-latitude NE Pangaea. Palaeogeography, Palaeoclimatology, Palaeoecology 407 (1), 1–13.

Wang, J., 2000. Permian wood from Inner Mongolia, North China: with special reference to Palaeozoic climate change of North China Block. The Palaeobotanist 49, 353-370.

Wang, J., 2010. Late Palaeozoic macrofloral assemblages from Weibei Coalfield, with reference to vegetational change through the Late Palaeozoic Ice-age in the North China Block. International Journal of Coal Geology 83(2), 292-317.

Wang, S.J., Hu, Y.F., Cui, J.Z., 2000. A new species of Araucarioxylon Kraus from the early Early Permian. Nei Mongol, China. Acta Botanica Sinica 42, 427-432.

Wang, S.J., Hilton, J., Galtier, J., Tian, B., 2006. A large anatomically preserved calamitean stem from the Upper Permian of southwest China and its implications for calamitean development and functional anatomy. Plant Systematics and Evolution, 261(1–4), 229–244

Wang, S.J., Li, S.S., Hilton, J., Galtier, J., 2003. A new species of the sphenopsid stem Arthropitys from Late Permian volcaniclastic sediments of China. Review of Palaeobotany and Palynology, 126(1–2), 65–81

Wang, S.J., 1991a. A new permineralized wood of the Late Triassic from northern Guangdong Province. Acta Scientiarum Naturalium Universitaitis Sunyatseni 30 (3), 66-69 (In Chinese with English abstract).

Wang, S.J., 1991b. The occurrence of the *Xenoxylon ellipticum* in the Late Triassic from North Guangdong, China. Acta Botanica Sinica 33 (10), 810-812.

Wang, Z.Q., 1991. Recovery of vegetation from the terminal Permian mass extinction in North China. Review of Palaeobotany and Palynology, 91, 121–142.

Wang, Z.Q., Wang, L.X., 1989. Earlier Early Triassic fossil plants in the Shiqianfeng Group in North China. Shanxi Geology, 14 (1): 23- 40 (in Chinese with English abstract).

Wang, Z.Q., Wang L.X., 1982. A new species of the lycopsid Pleuromeia from the Early Triassic of Shanxi, China and its ecology. Palaeontology, 25 (1), 215-225

Wang Z.Q., 1991. Recovery of vegetation from the terminal Permian mass extinction in North China. Review of Palaeobotany and Palynology, 91, 121–142.Wang, Z.Q., Zhang, Z.P., 1998. Gymnosperms on the eve of the terminal Permian mass extinction in North China and their survival strategies. Chinese Science Bulletin, 43 (11), 889-897.

Wang, Z.Q., 1996. Recovery of vegetation from the terminal Permian mass extinction in North China[J]. Review of Palaeobotany and Palynology 91(1): 121-142.

Ward, P.D., Montgomery, D.R., Smith, R., 2000. Altered river morphology in South Africa related to the Permian–Triassic extinction. Science 289, 1740–1743.

Wartes, M.A., Carroll, A.R., Greene, T.J., 2002. Permian sedimentary record of the Turpan–Hami Basin and adjacent regions, Northwest China; constraints on postamalgamation tectonic evolution. Geological Society of America Bulletin 114, 131–152.

Wei, X., Zhang, X., Shi, G. R., Zhao, X., Huang, X., & Luan, T. (2016). First report of a phytogeographically mixed (transitional) Middle–Late Permian fossil wood assemblage from the Hami area, northwest China, and implications for Permian phytogeographical, palaeogeographical and palaeoclimatic evolution in central Asia. Palaeogeography, Palaeoclimatology, Palaeoecology, 448, 125-140.

Winguth, C., Winguth, A.M.E., 2012. Simulating Permian–Triassic oceanic anoxia dis- tribution: implications for species extinction and recovery. Geology 40, 127–130.

Wilson, K., White, D.I.B., 1986. The anatomy of wood: its diversity and variability. London: Stobart & Sons.

Wu, S.Z., 1993. Formation and evolution of floristic provinces of Carboniferous and Permian in Xinjiang. Xinjiang Geol. 11 (1), 13–22 (In Chinese with English abstract).

Wu, X.Y., Sun, B.N., Sen, G.L., Wang, Y.D., 1997. Permian fossil plants from northern margin of Tarim basin, Xinjiang. Acta Palaeontol. Sin. 36, 1–22 (In Chinese with English abstract).

Xiao, W. J., Han, C. M., Yuan, C., Sun, M., Lin, S. F., Chen, H., Li, Z., Li, J., Sun, S., 2008. Middle Cambrian to Permian subduction-related accretionary orogenesis of North Xinjiang, NW China: implications for the tectonic evolution of Central Asia. J. Asian Earth Sci. 32, 102–17.

Xiao, W., Kröner, A., Windley, B.F., 2009. Geodynamic evolution of Central Asia in the Palaeozoic and Mesozoic. International Journal of Earth Sciences 98, 1185–1188. doi:10.1007/s00531-009-0418-4

Xiao, W.J., Windley, B., Sun, S., Li, J.L., Huang, B.C., Han, C.M., Yuan, C., Sun, M., Chen, H.L.,2015. A tale of amalgamation of three Permo-Triassic collage systems in Central Asia:oroclines, sutures, and terminal accretion. Annual Review of Earth and Planetary Sciences 43, 477–507.

Xie, Shu-Cheng, Pancost, R.D., Yin, Hong-Fu, Wang, Hong-Mei, Evershed, R.P., 2005. Two episodes of microbial change coupled with Permo/Triassic faunal mass extinction. Nature 434, 494–497.

Yamada T. 2001. Defense mechanisms in the sapwood of living trees against microbial infection. Journal of Forest Research. 6(3), 127-137.

Yang, J.D., Qu, L., Zhou, H., Cheng, Z., Zhou, T., Hou, J., Li, P., Sun, Su., Li, Y., Zhang, Y., Wu, X., Zhang Z., Wang, Z., 1986. Permian and Triassic strata and fossil assemblages in the Dalongkou area of Jimsar, Xinjiang. People's Republic of China, Institute of Geology, Chinese Academy of Geological Science,

Geological Memoirs Series 2 (3), 1-262 (In Chinese with English abstract).
Yang, G., Li, Y., Gu, P., Yang, B., Tong, L., Zhang, H., 2012. Geochronological and geochemical study of the Darbut Ophiolitic Complex in the West Junggar (NW China): implications for petrogenesis and tectonic evolution. Gondwana Res. 21, 1037–49.
Yang, W., Liu, Y., Feng, Q., Lin, J., Zhou, D., Wang, D., 2007. Sedimentary evidence of Early–Late Permian mid-latitude continental climate variability, southern Bogda Mountains, NW China. Palaeogeography, Palaeoclimatology, Palaeoecology 252, 239–258.
Yang, W., Feng, Q., Liu, Y., Tabor, N., Miggins, D., Crowley, J.L., Lin, J., Thomas, S., 2010. Depositional environments and cyclo- and chronostratigraphy of uppermost Carboniferous–Lower Triassic fluvial–lacustrine deposits, southern Bogda Mountains, NW China – a terrestrial palaeoclimatic record of mid-latitude NE Pangea. Global and Planetary Change 73, 15–113.
Yao, Z.Q., Liu, L.J., Zhang, S., 1994. Permian wood from western Henan, China: implications for palaeoclimatological interpretations. Review of Palaeobotany and Palynology 80 (3), 277-290.
Young, P.J., Megonigal, J.P., Sharitz, R.R., Dat, F.P., 1993. False ring formation in Baldcypress (Taxodium distichum) saplings under two flooding regimes. Wet- lands 13, 293–298.
Yu, Jian-Xin, Peng, Yuan-Qiao, Zhang, Su-Xin, Yang, Feng-Qing, Zhao, Quan-Ming, Huang, Qi-Sheng, 2007. Terrestrial events across the Permian–Triassic boundary along the Yunnan–Guizhou border, SW China. Global Planet. Change 55, 193–208.
Yu, Jian-Xin, Li, Hui-Min, Zhang, Su-Xin, Feng, Qing-Lai, 2008. Timing of the terrestrial Permian–Triassic boundary biotic crisis: implications from U–Pb dating of authigenic zircons. Sci. China Ser. D 51, 1633–1645.
Yu, Jian-Xin, Broutin, J., Huang, Qi-Sheng, Grauvogel-Stamm, L., 2010. *Annalepis*, a pioneering lycopsid genus in the recovery of the Triassic land flora in South China. Comptes Rendus Palévol 9, 479–486.
Yu, Jian-Xin, Broutin, J., Chen, Zhong-Qiang, Shi, Xiao, Li, Hui, Chu, Dao-Liang, & Huang, Qi-Sheng, 2015. Vegetation changeover across the Permian–Triassic Boundary in Southwest China: extinction, survival, recovery and palaeoclimate: a critical review. Earth-Science Reviews. 149, 203-224.
Zhang, H., 1988. The characters of the Late Permian mixed floras around Angara land and their formative mechanism. Geol. Rev. 34 (4), 343–350 (In Chinese with English abstract).
Zhang, H., Cao, C.-q., Liu, X.-l., Mu, L., Zheng, Q.-f., Liu, F., Xiang, L., Liu, L.-j., Shen, S.-z., 2015. The terrestrial end-Permian mass extinction in South China. Palaeogeogr. Palaeoclimatol. Palaeoecol.

http://dx.doi.org/10.1016/j.palaeo.2015.07.002 (in press).
Zhang, D.J., Sun, Y.W., Ding, H.S., Yang, Z.Y., Tang, L.J., 2014. Lopingian mixed floras from Linxi Formation in Soron area, Inner Mongolia. Global Geol. 17 (2), 67–77.
Zhang, L.C., Xu, X., 1995. Geological developing history. Xinjiang Uygur Autonomous Region Geological Publishing House, Beijing, China, pp. 742-759 (in Chinese).
Zhang, W., Zheng, S.L., 1984. Two new species of *Dadoxylon* from the Zhesi Formation in Xiwuzhumuqi of Inner Mongolia. Journal of Changchun College of Geology 4, 69-71 (In Chinese with English abstract).
Zhang, W., Li, Y., Zhen g, S.L., Li, N., Wan g, Y. D., Yang , X.J., Yi , T.M., Yan g, J.J., Fu, X.P., 2006. Fossil woods of China. China Forestry Publishing House, Beijing, pp. 1-356 (In Chinese) (English version: 2008).
Zhang, W., Wang, Y.D., Zheng, S.L., Yang, X.J., Li, Y., Fu, X.P., Li, N., 2007. Taxonomic investigations on permineralized conifer woods from the Late Palaeozoic Angaran deposits of northeastern Inner Mongolia, China and their palaeoclimatic significance. Review of Palaeobotany and Palynology, 144, 261-285.
Zhang, X., 1981. Regional Stratigraphic Chart of northwestern China, Branch of Xinjiang Uygur Autonomous Region. Geological Publishing House, Beijing. 496 pp. (in Chinese).
Zhang, Y., Wang, J., Liu, L., Li, N., 2010. *Protophyllocladoxylon jingyuanense* sp. nov., a gymnospermous wood of the Serpukhovian (Late Mississippian) from Gansu, Northwest China. Acta Geologica Sinica 84, 257–268.
Zhao, X.J., 1980. Mesozoic Vertebrata-bearing beds and stratigraphy of northern Xinjiang. Memoirs of the Institute of Vertebrate Palaeontology and Palaeoanthropology, Academia Sinica Series A 15, 1-119 (In Chinese).
Zhou, T.S., Li, P.X., Yang, J.D., Liu, S.W., Cheng, Z.W., Wu, S.Z., Li, Y.A., 1997. Stratotype section of non-marine of Permian–Triassic boundary in China. Xinjiang Geol. 15 (3), 211–226.
Zhu, H.C., Ouyang, S., Zhan, J.Z., Wang, Z., 2005. Comparison of Permian palynological assemblages from the Junggar and Tarim basins and their phytoprovincial significance. Review of Palaeobotany and Palynology 136, 181–207.
Ziegler, A.M., Hulver, M.L., Rowley, D.B., 1997. Permian world topography and climate. In: Martini, I.P. (Ed.), Late Glacial and Postglacial Environmental Changes: Pleistocene, Carboniferous–Permian, and Proterozoic. Oxford University Press, Oxford, pp. 111–146.
Zürcher E, Kucera LJ, Bosshard HH. 1985. Bildung und Morphologies der Thyllen: ein Literaturübersicht. *Vierteljahrschrift Naturforschung* Gesellschaft Zürich 130, 311 – 333.

ANNEXES

Annexe 1: Shi, X., Yu, J., Li, H., Chi, H., Zhang, W., 2014. *Xinjiangoxylon* Gen. Nov., a New Gymnosperm from the Latest Permian of China. *Acta Geologica Sinica (English Edition)*, *88*(5), 1356-1363

Annexe 2: Shi, X., Yu, J., Broutin, J., Pons, D., 2015. *Junggaropitys,* a new gymnosperm stem from the Late Triassic of Junggar Basin, Northwest China, and its palaeoclimatic implications. Review of Palaeobotany and Palynology, 223: 10-20.